Carbohydrate Systems for Biosensing, Imaging, and Medical Applications

Inaugural-Dissertation
to obtain the academic degree
Doctor rerum naturalium (Dr. rer. nat.)
submitted to the Department of Biology, Chemistry, and Pharmacy
of Free Universität Berlin

by
Dan Grünstein
from Mulhouse, France

2013

Doctoral studies were conducted from June 2009 to December 2012 under the supervision of Prof. Peter H. Seeberger at the Max Planck Institute of Colloids and Interfaces in the Department of Biomolecular Systems.

1st Reviewer: Prof. Peter H. Seeberger

2nd Reviewer: Prof. Rainer Haag

Date of defense: February 11, 2013

Table of Contents

Acknowledgments

First of all, I would like to express my sincere thankfulness to my committee chair, Professor Peter H. Seeberger for having given me the possibility of carrying my doctoral studies under his strong human support and scientific guidance. I place on record, my strong and sincere sense of gratitude for its openness towards my Jewish strict observance as well as the freedom I experienced to organize my own schedule.

I am also grateful to Professor Rainer Haag for generously agreeing to supervise and co-chair my doctoral examination.

I would like to thank Ms. Dorothee Böhme for her consistent and timely help and in the resolution of all administrative problems. Many thanks to the people from IT service, Alex Schetter, Marco Hennig, and Simon Bunte for having resolved many of software and computer issues.

I want to thank in particular my first labmate, Dr. Raghavendra Kikkeri, for having been my mentor during the first year of my doctoral work. I am indebted for all he taught me about organic chemistry but also for the creativity he rouses in me. It has been a great moment to spend time with him on discussions related to science, life, and philosophy.

I was fortunate also to share the laboratory during my second year with Dr. Sung-You Hong. We spent great time together trying to solve synthetic issues on fullerenes or nanoparticles and having nice pizza-lunch.

Last but not least, I wish to thank my third labmate, Dr. Ali Barandov, for having shared with me the laboratory and even the hood during my last year. I can’t forget our enthusiastic discussions, the music we listened together. I will never forget hints and laughs we shared.

I can’t forget Dr. Mattan Hurevich who has been a friend, a confident, and supporter during my stay in Professor Seeberger’s group.

A very special thanks to Dr. Claney Lebev Perreira for proof-reading all the chapters of my thesis as well as for their valuable comments, suggestions, and strong scientific insights. I would also like to thank Dr. Bernd Lepenies for the German translation of the summary.

Three and a half years of being with colleagues from different countries helped me to seize the nuances and the reasoning modalities expressed in such international settings. It has

expanded my vision in many aspects of my life. Dr. Davide Esposito, Ms. Chian-Hui Lai, Dr. Gianfranco Lopopolo, Dr. Faustin Kamena, Ms. Maha Maglinao, Dr. Bernd Lepenies, Bopanna Ponnappa Monnanda, Heung Sik Hahm, Dr. Steffen Eller, Dr. Daniele Leonori, Dr. Anish Chakkumkal, Ms. Oliviana Calin, Dr. David Kennedy, Christopher Martin, Dr. Nahid Azzouz, Dr. Cullen Klein, Dr. Jeyakumar Kandasamy have directly or indirectly participated to this valuable experience. Thank you to all of you.

I also would like to thank the Marie Curie Fellowship organization for providing me with the necessary funding during my doctoral studies.

Finally, I would like to express my deepest gratitude and my love to my family. To my wife and my son. To my father and my mother. To my brother and his wife.

Summary

In the following chapters, I will investigate the role of different carbohydrate constructs – from monovalent to polyvalent nanoscale materials– and their application in molecular diagnostics, biosensing, imaging, and medicine. New synthesis were established and exploited to understand and monitor interactions involved with carbohydrates. I have also developed carbohydrate-based novel therapeutic approaches that can intervene in important biomedical applications. The work is presented is a size-dependent manner starting with the smallest construct to bigger structures.

Chapter 1 summarizes different strategies for preparing multivalent carbohydrate probes and their major applications in biosensing, imaging, and other biological or medical applications. To address fundamental aspects of carbohydrate-based interactions that were developed in the Seeberger group, different types of multivalent systems ranging from dendrimers to supramolecular structures, and from fullerenes to nanoparticles in order to fine tune the spatial and the topology structures of the carbohydrate ligands required in such systems.

Chapter 2 describes the synthesis of a bifunctional chelator construct, that simultaneously coordinate ^{99m}Tc-metal cores and tether biomolecules for selective targeting and imaging of specific organs –a key feature in the development of modern radiodiagnostics. The chelator was successfully conjugated with the monosaccharides followed by efficient reaction with the organometallic precursor $[M(CO)_3]^+$ (M = Re, ^{99m}Tc) to generate the ^{99m}Tc-labeled glycoconjugates. Biodistribution of the radioactive-^{99m}Tc-labeled glycoconjugates was examined in mice. Noticeably, different biodistribution patterns were observed, reflecting trends in the uptake of carbohydrate analogues by various organs.

Chapter 3 deals with the development of a series of multivalent sensors that self-assemble *via* hydrophobic supramolecular interactions. The multivalent sensors are comprised of a fluorescent Ru(II) core surrounded by a heptamannosylated β-cyclodextrin scaffold. Photophysical and spectroscopic analyses confirmed that the three mannosylated sensors displayed 14, 28, and 42 sugar units, respectively. Each complex adopted original and unique spatial arrangements. The sensors were then used to investigate the influence of carbohydrate spatial arrangement and clustering upon lectin and bacterial binding.

Chapter 4 reports the design and synthesis of polyhydroxylated fullerenes and dodecavalent fullerene-based glycoclusters. The constructs were used as radical scavengers and anti-inflammatory agents in the treatment of ischemic stroke in rats subjected to transient middle cerebral artery occlusion. Magnetic resonance imaging was used to evaluate the infarct size reduction due to the treatment. Treated animals showed better neurological assessment compared to controls. Both agents, preserved neurons after ischemic stroke in the perilesional area and reduced the density of macrophags/microglia infiltration in rats. Reduction of cellular and humoral immune responses due to treatment may constitute an attractive therapeutic approach for ischemic stroke.

Chapter 5 presents the work the development of localized surface plasmon resonance transducers based on Au island films prepared by evaporation on glass and annealing were optimized for monitoring the specific interaction between Con A and mannose immobilized on Au islands. Sensing assays were performed under stationary and flow conditions, the latter providing kinetic parameters for protein binding and dissociation. Enhanced response and visual detection of protein binding was demonstrated using Au nanoparticles stabilized with mannose molecules.

Zusammenfassung

In den folgenden Kapiteln werden die Synthese und Anwendung verschiedener synthetischer Kohlenhydratstrukturen –von monovalenten bis hin zu polyvalenten Nanomaterialien– in der molekularen Diagnostik, Biosensorik, in bildgebenden Verfahren und der Medizin beschrieben. Im Rahmen dieser Arbeit wurden neue Systeme etabliert und dazu genutzt um molekulare Interaktionen, an denen Kohlenhydrate beteiligt sind, besser zu verstehen. Darüber hinaus wurden neue Kohlenhydrat-basierte Therapiestrategien für verschiedene biomedizinische Anwendungen entwickelt. Die Arbeiten werden im Folgenden der Größe der Konstrukte nach geordnet dargestellt (vom kleinsten zum größten Konstrukt).

Kapitel 1 fasst verschiedene Strategien zur Herstellung multivalenter Kohlenhydrat-Sonden und ihre Anwendungen in Biosensorik, Bildgebung sowie weiteren biologischen und medizinischen Anwendungen zusammen. Um grundlegende Aspekte von Kohlenhydrat-basierten Interaktionen eingehend zu untersuchen, wurden verschiedene Arten multivalenter Systeme entwickelt, von Dendrimeren bis hin zu supramolekularen Strukturen, von Fullerenen bis hin zu Nanopartikeln. Dabei wurden die verschiedenen Systeme gewählt um die räumliche Orientierung der jeweiligen Kohlenhydrat-Liganden den Anforderungen der Systeme entsprechend anzupassen.

Kapitel 2 beschreibt die Synthese eines bifunktionellen Chelators, der einen ^{99}Tc-Metallkern koordiniert und an den gleichzeitig Biomoleküle zum zellspezifischen Targeting und zur Bildgebung von Organen angebunden werden können –ein entscheidender Aspekt bei der Entwicklung moderner Radiodiagnostika. Der Chelator wurde erfolgreich mit Monosacchariden konjugiert, gefolgt von einer Reaktion mit dem organometallischen Vorläufer $[M(CO)_3]^+$ (M = Re, ^{99m}Tc) um ^{99m}Tc-markierte Glykokonjugate herzustellen. Die *in vivo*-Verteilung der ^{99m}Tc-markierten Glykokonjugate wurde im Mausmodell untersucht. Dabei wurden unterschiedliche Verteilungsmuster beobachtet, die eine spezifische Aufnahme der jeweiligen Kohlenhydrate in die unterschiedlichen Organe andeuten.

In Kapitel 3 wird die Entwicklung einer Reihe multivalenter Sensoren beschrieben, die aufgrund von hydrophoben supramolekularen Interaktionen selbst assemblieren. Diese multivalenten Sensoren bestehen aus einem fluoreszierenden Ru(II) Kern, umgeben von einem heptamannosylierten β-Cyclodextrin. Photophysikalische und spektroskopische Analysen bestätigten, dass die drei mannosylierten Sensoren 14, 28 bzw. 42 Zuckereinheiten aufwiesen. Jeder Sensor zeichnete sich dabei durch eine einzigartige Anordnung der

Zuckereinheiten aus. Die Sensoren wurden anschließend dazu genutzt, um den Einfluss der räumlichen Orientierung der Zuckerliganden auf die Bindung an Lektine und Bakterien zu untersuchen.

In Kapitel 4 ist die Planung und Synthese polyhydroxylierter Fullerene und dodekavalenter, Fulleren-basierter Glykocluster dargestellt. Die Konstrukte wurden als Radikalfänger und anti-inflammatorische Substanzen zur Therapie in einem Ratten-Schlaganfall-Modell genutzt. Mittels Magnetresonanztomographie wurde gezeigt, dass die Infarktgröße nach der Therapie reduziert war. Darüber hinaus zeigten die Tiere nach der Behandlung geringere neurologische Symptome. Die Konstrukte wirkten zudem schützend auf Nervenzellen in dem Infarkt benachbarten Hirnregionen und führten zu einer reduzierten Infiltration von Makrophagen/Mikroglia in Ratten. Die verringerte zelluläre und humorale Immunantwort nach der Behandlung könnte einen neuen Therapieansatz für Schlaganfall darstellen.

In Kapitel 5 wird die Entwicklung lokalisierten Oberflächenplasmonresonanz-Signalwandler basierend auf Gold-Inseln dargestellt, die durch Bedampfen auf Glas aufgebracht wurden. Hiermit wurde die Interaktion zwischen ConA und auf den Gold-Inseln immobilisierter Mannose gemessen. Die Biosensorik-Tests wurden unter stationären und kontinuierlichen Bedingungen durchgeführt; letztere dienten dazu die Kinetik der Proteinbindung und Dissoziation zu untersuchen. Eine verstärkte Antwort und visuelle Detektion der Proteinbindung konnte mit Hilfe von Mannose-funktionalisierten Goldnanopartikeln nachgewiesen werden.

Chapter 1

Multivalent Carbohydrate Systems: Support, Synthetic Strategies, and Applications

---

The results reported in this chapter have been partially published in:

(a) Kennedy, D. C.; Grünstein, D.; Lai, C.-H.; Seeberger, P. H. *Chem. Eur. J.* accepted.
(DOI: 10.1002/chem.201204155 – The original article is available at:
http://dx.doi.org/10.1002/chem.201204155)

(b) Kikkeri, R.; Hong, S. Y.; Grünstein, D.; Laurino, P.; Seeberger, P. H. *Beilstein-Institut: Functional Nanoscience* **2010**, 143.
(The original article is available at:
http://www.beilstein-institut.de/Bozen2010/ Proceedings/Seeberger/Seeberger.pdf)

(c) Kikkeri, R.; Grünstein, D.; Seeberger, P. H. *J. Am. Chem. Soc.* **2010**, *132*, 10230.
(DOI: 10.1021/ja103688s – The original article is available at:
http://pubs.acs.org/doi/abs/10.1021/ja103688s)

Table of Contents

Abstract

Different strategies for preparing multivalent carbohydrate probes and their major applications in biosensing, imaging, and other biological or medical applications are presented in this chapter.

To address fundamental aspects of carbohydrate-based interactions, the Seeberger laboratory developed previously different types of multivalent systems ranging from dendrimers to supramolecular structures, and from fullerenes to nanoparticles in order to fine tune the spatial and the topology structures of the carbohydrate ligands required in such systems.

Chapter 1 briefly introduces the work on multivalent tools that was reported by others before and describes how the Seeberger group contributed to this field. Modulating these platforms with carbohydrate ligands enabled their application in the areas of biosensing, imaging, and therapeutics.

1. Introduction

Multivalent binding events mediate many processes in biological systems. Interactions that are governed by such simultaneous and cooperative binding provide combined strength to the biological event. The term of avidity conceptualizes the main characteristic of the multivalent interactions. Indeed, cooperative interactivity is the combined synergistic strength of bond affinities rather than the sum of each defined individual ligand–receptor interaction.[1]

Throughout biology, cells, viruses, and bacteria have established natural and polyvalent architectures in the infinite diversity of interaction between two entities stemming out from a huge pool of components in the genomic, proteomic or glycomic in order to generate a fruitful ligand–receptor connection.

Carbohydrates are integral to biological signaling networks and cell–cell interactions, yet the detection of discrete carbohydrate interactions remains difficult since binding is generally weak. A large number of biological processes, such as cell adhesion and migration, phagocytosis, cell differentiation, and apoptosis call for carbohydrate-involved interaction.[2] In the last decades, significant insights into new carbohydrate-based interactions have been gained. New methodologies that can effectively probe these interactions remain a challenge for scientists.

Efforts made to capture the advantage of multivalent display for the generation of new strategies in the development of biochemistry led to the development of innovative multivalent scaffolds and platforms mimicking natural frameworks and providing the required avidity. [3] Multivalent carbohydrate ligands show great promise because of the strong chelating effects as well as the fine tuning of spatial and topological proximities.

The Seeberger laboratory has contributed to that field by focusing part of its work on the development of carbohydrate-based multivalent structures and in the investigation of their applications for biosensing, imaging, and drug development (Figure 1).

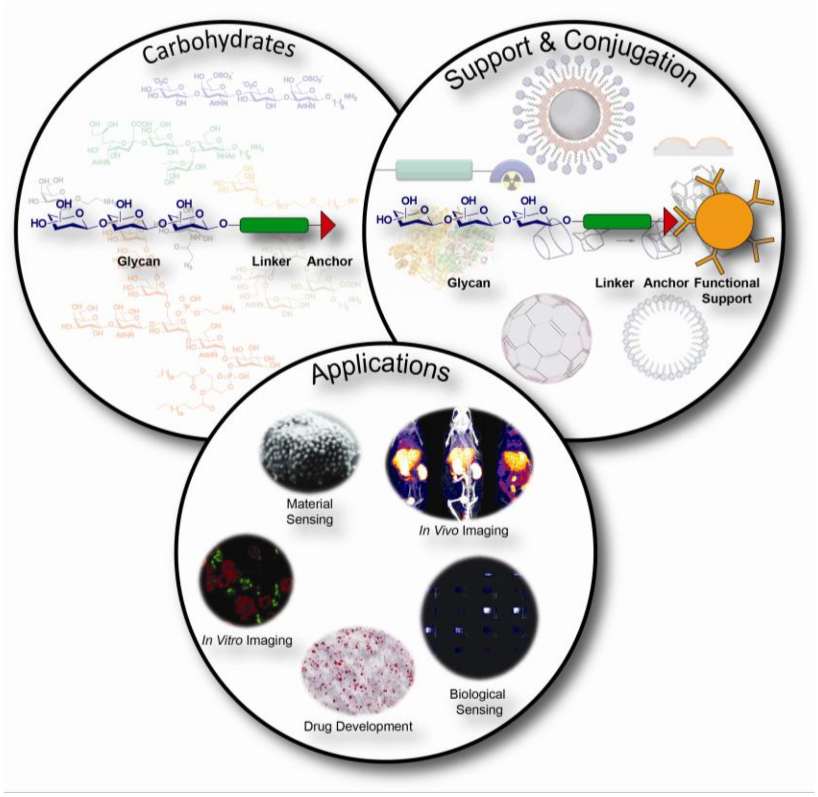

Figure 1. Multivalent systems and carbohydrates were combined to create new tools for biosensing, imaging, and therapeutics.

This introductory chapter discusses the strategies developed over the last five years in the Seeberger laboratory for preparing multivalent carbohydrate probes with platforms ranging from dendrimers to supramolecular structures, and from fullerene balls to nanoparticles and their major applications in biosensing, imaging, and medicine (Figure 2).

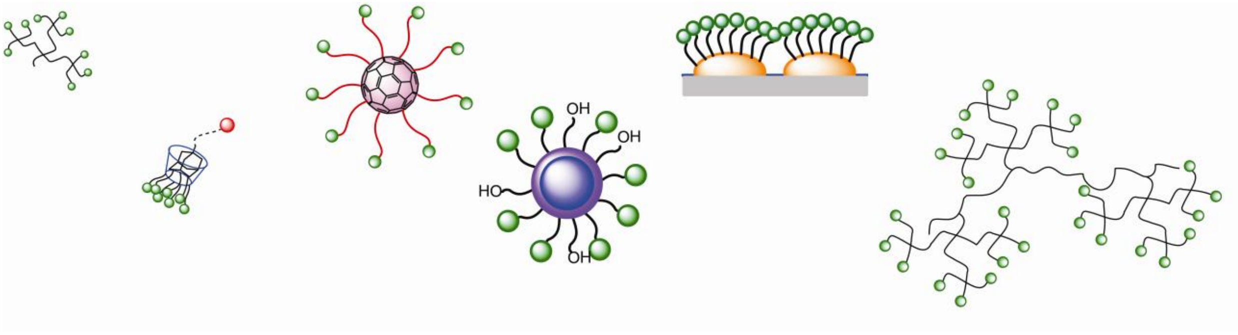

Figure 2. Various platforms were used as tools to create multivalent systems for further applications.

2. Development

2.1. Dendrimers

Dendrimers are repetitively assembled molecules that present a hyper-branched architecture emanating radially from a central core. Dendrimer morphology is similar to biological macromolecules of well-defined three-dimensional structure.[4] Dendrimer popularity greatly increased since their introduction in the early 1980s by Vögtle and Fréchet.[5]

The potential of dendrimer for material, optical, biomedical, electrical, as well as catalysts applications, have been exploited.[6] Dendrimers have been decorated with a large number of different molecules such as pharmaceutically active compounds, photosensitizers, redox units, carbohydrates, and other relevant organic molecules.[7] Multivalent dendrimer probes have been designed and used to increase binding avidity rather than affinity.

Sugar-adorned dendrimers also called glycodendrimers have been successfully introduced in different biomedical applications. They act as anti-cancer drugs, potent anti-viral, and anti-inflammatory agents.[8] Carbohydrate–lectin interactions are critical to many biological systems such as the inflammatory response, cell growth, viral infections, cell–cell adhesion and communication, host–pathogen interactions, fertility, development, and cancer. Lectins are sugar-binding proteins with defined glycan recognition domains on the surface of viruses and bacteria as well as of plant and animal cells. Therefore, methods are needed that can effectively probe weak carbohydrate–lectin interactions to improve the understanding of their role.[9]

In order to address fundamental aspects of the multivalent carbohydrate–protein interactions and to monitor binding events, metal-based glycodendrimer were developed using the metal core as read-out partner of the binding event. The Seeberger group has contributed to that field by developing different synthetic strategies of metal-based glycodendrimer and applied those dendrimers upon lectin sensing.

2.1.1. Synthetic Strategies

2.1.1.1. One-pot Approach to Fluorescent Glycodendrimers

Early work on metallo-glycodendrimers focused on Cu(II), Re(II), Re(I), and Tc(I) complexes, where the assembly of the dendron with the metal was controlled by non-covalent interactions (i.e. electrostatic forces, hydrogen bonding, metal coordination).[10]

In the Seeberger laboratory, initial work was based on a versatile chelator 8-hydroxyquinoline – frequently employed as a ligand in coordination chemistry– to support the dendrimer. First and second generation dendrimers were synthesized providing three and nine sugars on a single chelator unit, respectively.[11] The hydroxyquinoline-confined glycodendron then self-assembled around a transition or lanthanide metal core –enabling a fluorescent read-out– to obtain high nuclear glycodendrimers bearing up to 18 sugar units.[12] Mannose and galactose-capped dendrons were prepared using Zn(II), Al(III), and Gd(III) as metal core due to their non-bleaching fluorescence in the visible and near infrared region (NIR), and their potent use for NIR imaging as well as magnetic resonance imaging (MRI) agent in the case of Gd (Scheme 1).

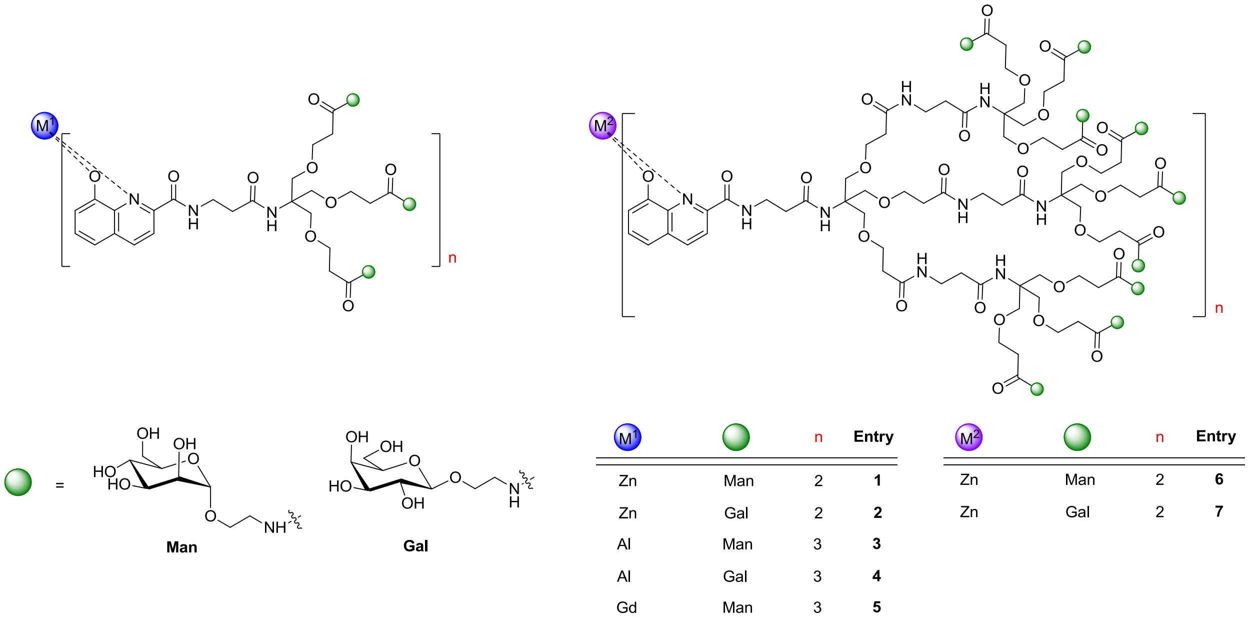

M^1	●	n	Entry
Zn	Man	2	**1**
Zn	Gal	2	**2**
Al	Man	3	**3**
Al	Gal	3	**4**
Gd	Man	3	**5**

M^2	●	n	Entry
Zn	Man	2	**6**
Zn	Gal	2	**7**

Scheme 1. Metallo-glycodendrimers **1–7**.

2.1.1.2. Ru(II) Glycodendrimers *via* Click Chemistry

Ru(II) dendrimers have been already successfully introduced in artificial photosynthesis, for light-emitting devices and molecular switches, electrochemical sensors for oxygen and DNA damage, as well as chemosensors for phosphate and glucose.[13] Among the metal cores used as support of the dendrimer framework, Ru(II)-based complexes are possibly most attractive. Indeed, the octahedral Ru(II) core is robust and exhibits a low-lying excited ligand to metal charge transfer (^{3}LMCT) state with lifetimes up to 1 μs. In addition to their strong oxidizing and reducing capabilities, Ru(II) complexes present also high-emission quantum yields, which render the read-out event more effective.[14]

We have developed new and easy approaches to access to size dependent Ru(II)-based carbohydrate dendrimers *via* copper-catalyzed azide–alkyne cycloaddition often referred to as "click chemistry". The Huisgen [2+3] dipolar cycloaddition has already been applied to the sugar functionalization of poly(amido amine) (PAMAM) dendrimers and nanoparticles. In order to reveal the carbohydrate–lectin interaction, we extended this approach by appending dendritic wedges to 2,2'-bipyridine (bipy) ligand **8** on a $[Ru(bipy)_3]^{2+}$-type fluorescent core (Scheme 2).[15]

Ru(II) alkynes **9** and **15** were then used as template basis prior to the conjugation with azide-containing molecules. Two strategies were used for the synthesis of the metallo-glycodendrimers. For one path, the dendritic synthon bearing the alkyne moieties was linked to the Ru(II) core affording **9** followed by further "click chemistry" with azido-modified carbohydrates such as mannose, galactose, glucose, di-mannose, and maltose, to furnish compounds **10–14**, respectively (Scheme 2).[16]

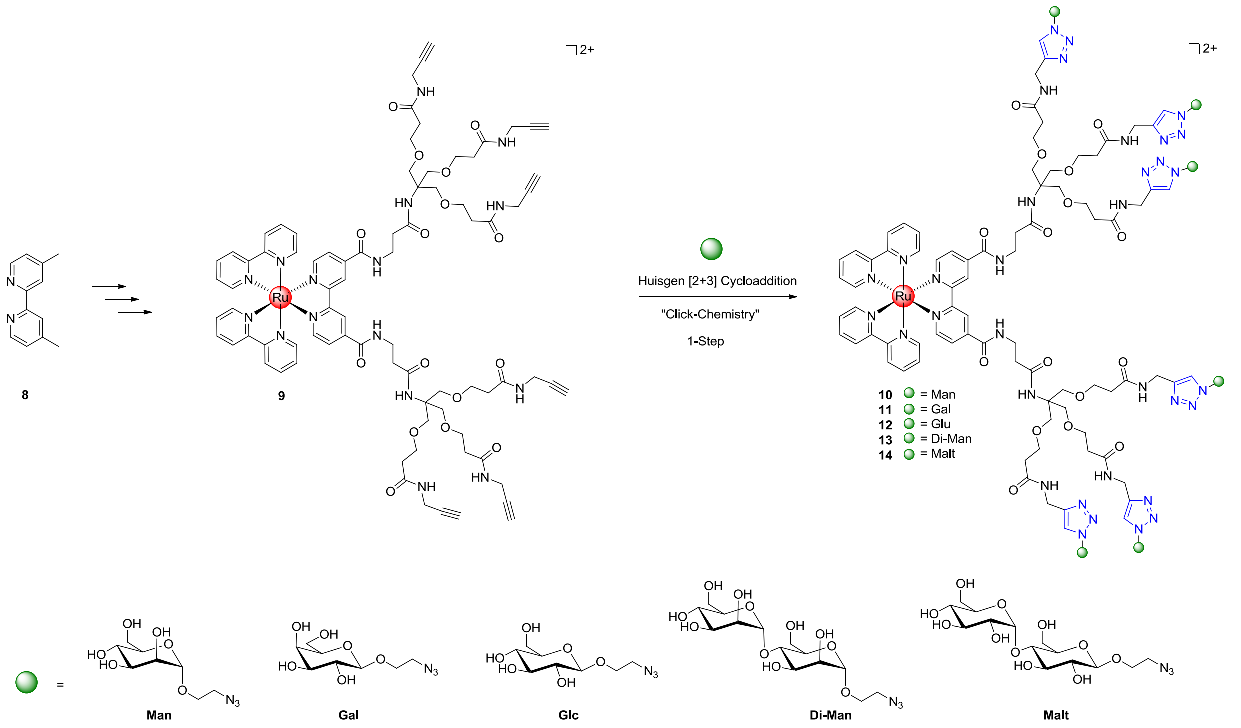

Scheme 2. Synthetic key step to generate metallo-glycodendrimers **10–14** with highlight of the resulting triazole (blue).

The second approach is based on the preparation of carbohydrate-containing dendron with a terminal azide that was subsequently coupled to the Ru(II) alkyne **15** to obtain **16** and **17** bearing up to 27 sugar units (Scheme 3).

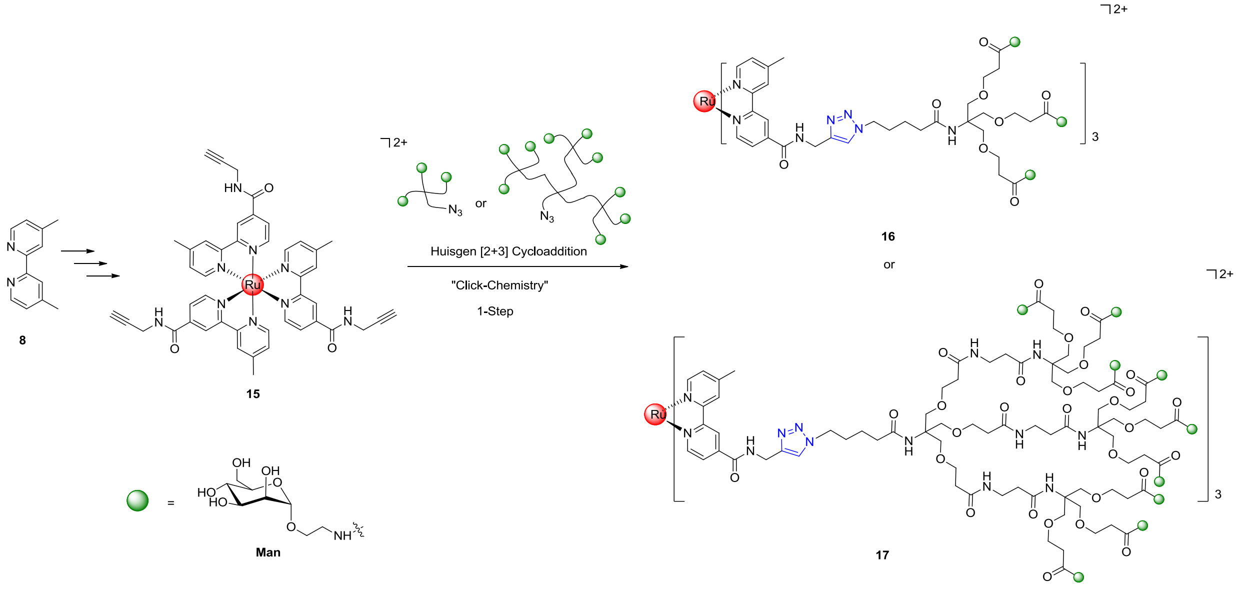

Scheme 3. Overview of the synthesis that produced **16** and **17** with highlight of the resulting triazole (blue).

The optical properties of the complexes **10–14**, **16**, and **17** were assessed by determining the quantum yield and their maximum emission at around 645 nm. It should be noticed that the quantum yield of **17** is almost twice greater than that of compounds **10–14**, indicative of the increasing carbohydrate density around the Ru(II) core that strongly influences its photophysical and colloidal aggregation properties.

2.1.1.3. Ru(II) Glycodendrimers *via* Amide Coupling

In order to fully harness the effect of homogeneous branching that encapsulates the Ru(II) core, another strategy to generate Ru(II) glycodendrimers based on a convergent series of amide couplings was harvested using $RuCl_3$ or *cis*-$[Ru(bipy)_2]Cl_2$ as starting material. Different dendrimer microenvironments surrounding the metal core were synthesized, and consequently modified the photochemical and electrochemical properties of the Ru(II) atom.

The first generation of Ru(II) glycodendrimer **18–23** was prepared through simple modification of the bipy-ligand with monovalent carbohydrate mannose and galactose. Addition of tripod units afforded to the second generation of the dendritic structures **24–27**, while addition of two ninepod units gave complexes **28** and **29** of the third generation bearing up to 18 sugar units (Scheme 4).[17]

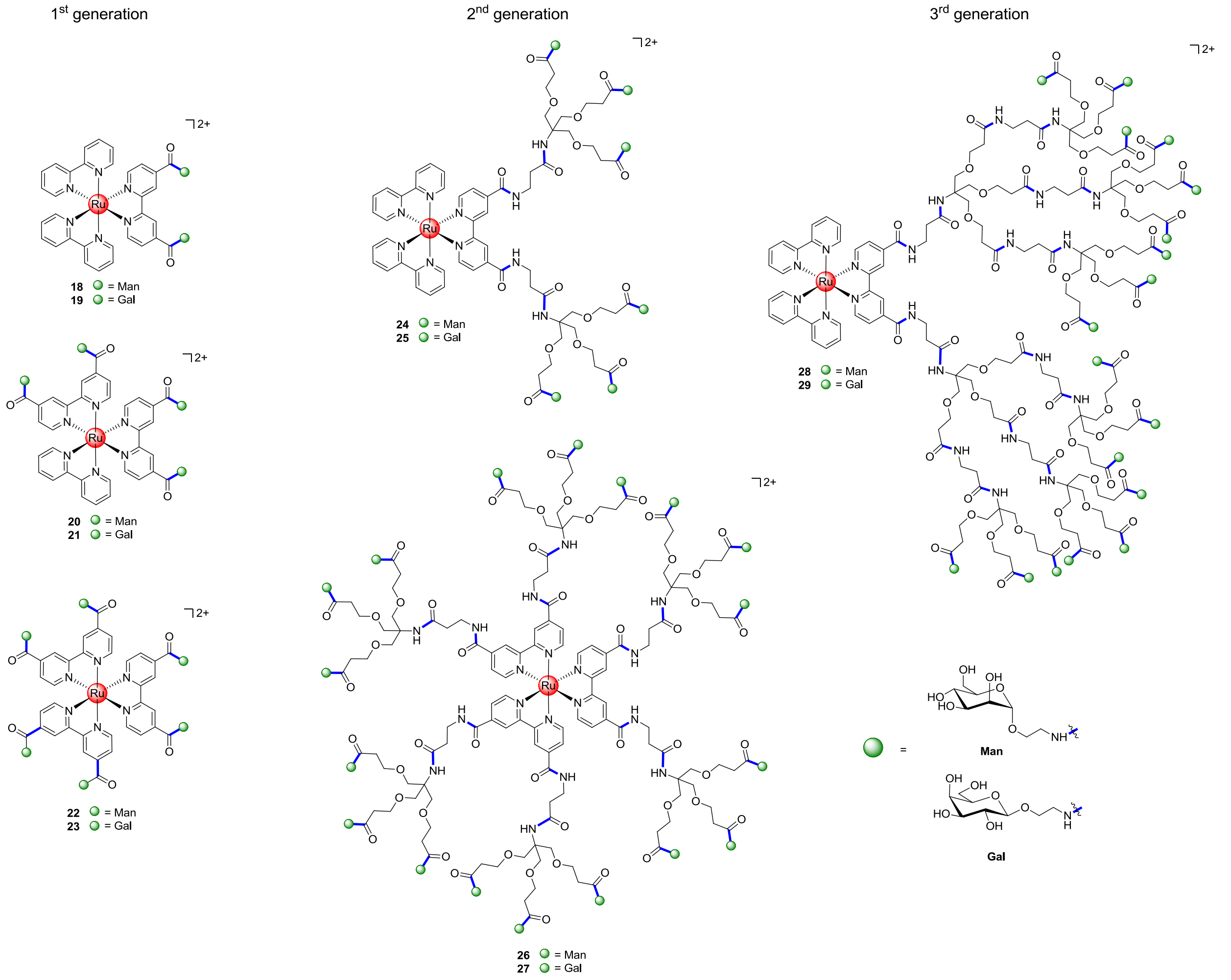

Scheme 4. Collection of Ru(II) glycodendrimers **18–29** with the amide bonds highlighted in blue.

2.1.2. Applications

2.1.2.1. Ru(II) Glycodendrimers as Lectin Biosensors

While many standard screening methods require a complex technical setup and significant expertise, the concept of molecular logic gate is based on a clear-cut binary output that defines the event providing a single-step method to analyze modification of properties.[18]

To exploit the potential of fluorescent glycodendrimers as screening tools, we studied the selectivity and sensitivity of the energy and photo-induced electron transfer (PET) process affected by the dendrimer architecture during the lectin sensing process. A molecular logic gate-based method was adapted to the analysis of the properties of diverse glycodendrimers involved in specific and selective carbohydrate–lectin interactions.

The glycodendrimer library **18–29** bearing two, four, six, or 18 sugar units (mannose or galactose) was used to support the molecular logic operations enabling the determination of the best dendrimer model for studying the carbohydrate–lectin interactions. Inputs for the analysis were pH, *N*,*N*'-4,4'-bis(benzyl-2-boronic acid)bipyridinium dibromide (BBV), and different lectins –Concanavalin A (Con A) and Aniara Galanthus nivalis (GNA)– that interact with mannose, and asialoglycoprotein (ASGPR) that recognizes galactose. The relative change in the fluorescent quantum yield of the metallo-glycodendrimers served as output. The optical event was generated by displacement and segregation of the quencher BBV from the Ru(II) complex sugar array by lectins, thus reconstituting the fluorescent signal (Figure 3).

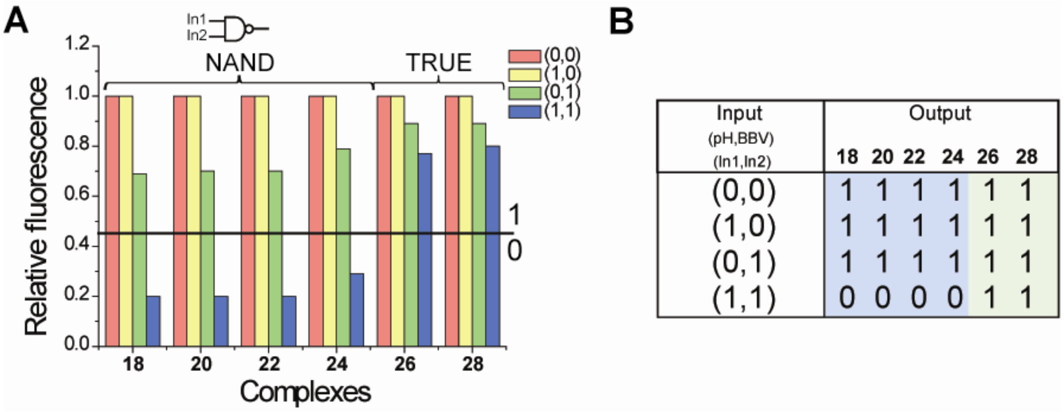

Input (pH,BBV) (In1,In2)	Output 18	20	22	24	26	28
(0,0)	1	1	1	1	1	1
(1,0)	1	1	1	1	1	1
(0,1)	1	1	1	1	1	1
(1,1)	0	0	0	0	1	1

Figure 3. (A) Schematic representation of relative fluorescence responses to pH and BBV as inputs. (B) Corresponding truth table.

Using a digital analytical method, glycodendrimers were found to behave in two different modes. Complexes **18–24** constitute a NAND gate based on effective PET and failed to display lectin binding, while for complexes **26** and **28** a weak PET was observed due to higher sugar density.

2.1.2.2. Incubation of Ru(II) Dendrimers with Protein Microarrays

Taking advantage of the strong optical advantage of Ru(II) complexes, microarrays based on direct optical readout for carbohydrate–protein interactions were developed. Con A was immobilized on a microarray prior to incubation with complexes **24**, **25**, **28**, and **29**. Strong fluorescent signals were observed on slides that were incubated with mannose complexes **24** and **28**. Therefore, using dendrimers **24** and **28** containing six and 18 mannose units respectively led us to detect Con A at the concentration level of 0.125 $\mu g \cdot mL^{-1}$ (620 nM) (Figure 4).[19]

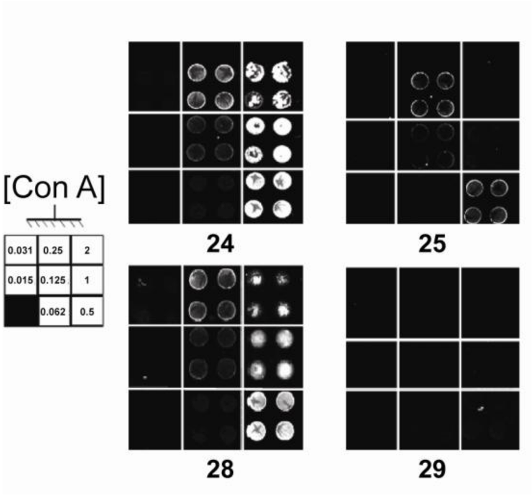

Figure 4. Incubation of Ru(II) glycodendrimers **24**, **25**, **28**, and **29** with Con A at different concentrations expressed in $mg \cdot mL^{-1}$.

2.1.2.3. Development of Sugar Sensor

After establishing that Ru(II) glycodendrimers are useful tools to detect carbohydrate–lectin interactions visually, the redox properties of the metal core were exploited to develop an electrochemical biosensor. Con A was immobilized on a gold surface prior to incubation of the chip with **24**. Following incubation, theses surfaces were transferred to an electrochemical cell and the square-wave voltametric (SWV) signals were recorded. The reusable sugar sensor was based on the displacement of the redox glycoprobe **24** interacting with the lectin-functionalized gold chip. Incubation of the chip with boronic acid substituted Merrifield resin (P-1) displaced any sugar interacting with Con A, and served as washing step. The Con A-functionalized chip containing **24** was immersed into solutions of varying concentrations of different glycans and SWV signals for Ru(II) were recorded. The current decreased in a concentration dependent manner, suggesting that the redox complex **24** was replaced in a competitive manner by preferentially binding sugars for Con A. The detection limit for glucose (7 μM) compares favorably to detection limits for other methods. Figure 5 illustrates the mechanism of the redox sensor. The washing step using P-1 allowed for the regeneration of the system enabling an iterative process.

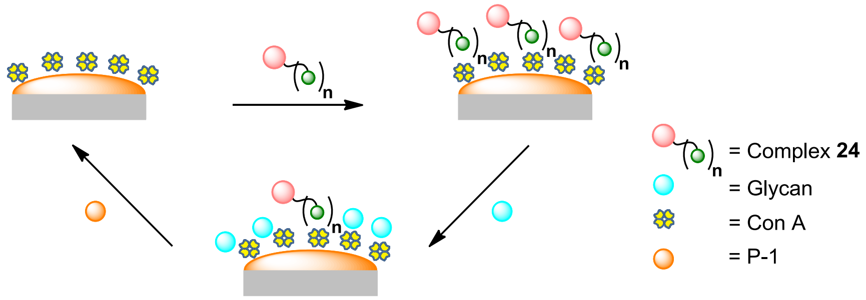

Figure 5. Schematic representation of the redox biosensor.

Different strategies have been exploited to generate a multivalent carbohydrate display. Dendrimer-based structures have been shown to be a successful candidate. Conjugation of the dendrimer with a fluorescent metal core enabled the read-out of the binding event opening new insights for the combination of the recognition step –using the multivalent component– with additional functionality.

2.2. Supramolecules

Supramolecular chemistry refers to the area of chemistry beyond that of single molecules and focuses on chemical systems made up of a discrete number of assembled molecular subunits. The development by Jean-Marie Lehn, Donald J. Cram, and Charles J. Pedersen, of defined host–guest complexes in which a host molecule recognizes and selectively binds a certain guest, contributed to this new field and was awarded the Nobel prize in 1987.[20]

Supramolecular chemistry evolved in the 1990s as Stoddart and Willner developed molecular machines and chemical biosensors integrating supramolecular systems in order to increase functionality of the systems.[21]

The Seeberger laboratory has utilized supramolecular chemistry to generate multivalent system with additional functionality for specific targeting drug delivery or as support for the creation of new carbohydrate-multivalent systems using capped cyclodextrins (CD).[22]

2.2.1. Carbohydrate-functionalized Cyclodextrins for Specific Targeting

Targeting specific cell lines is a challenging issue in the development of new drug delivery systems. Cell-specific binding and uptake can be achieved using the right ligand for the specific receptor (i.e. endogenous lectins expressed on cell-specific surfaces). Carbohydrate-based systems show great promise for cell-specific drug delivery. As specificity drivers, glycodendrimers are attractive for their potential use as multivalent systems.[23]

In addition to the ligand system, the construct should also contain a delivery unit enabling the release of the drug at a specific site. Such chemical systems can be constructed *via* supramolecular self-assembly of defined components providing the required multimodal characteristic to the overall structure: the multivalent targeting unit and the delivery unit.[24]

For the purpose of our research, the delivery unit –alkyne β-cyclodextrin (Alkyne-βCD)– was functionalized with a ninepod galactose dendrimer bearing an azido-end using a Huisgen [2+3] dipolar cycloaddition to form **32**. Galactose residues recognize ASGPR, a C-type lectin expressed on parenchymal hepatocytes (HepG2 cells) in the liver. Mannose dendrimers were prepared for control experiments. The β-cyclodextrin (βCD) was then equipped with rhodamine B (RhB), a fluorescent dye, to allow for visualization of the binding event between the chemical construct **34** and HepG2 cells and for further uptake *in vitro*. The delivery subunit βCD was also used as a molecular vector for drug delivery. In this respect, βCD was then loaded with doxorubicin, a potent chemotherapy drug, affording **36** to induce apoptosis in HepG2 cells (Scheme 5).[25]

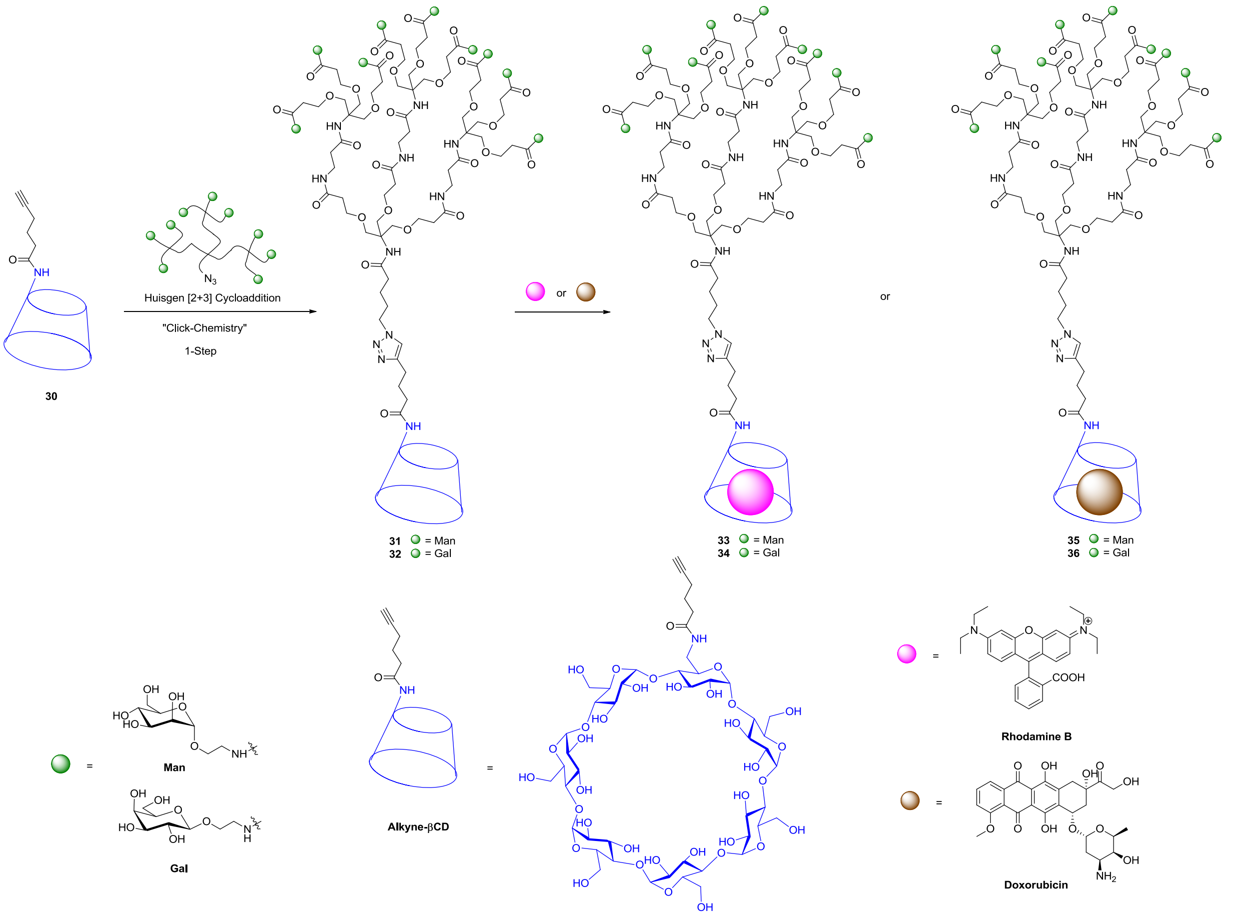

Scheme 5. Synthesis of the rhodamine- or doxorubicin-loaded βCDMan and βCDGal.

Galactose adorned dendrimers induced ASGPR-mediated endocytosis into HepG2 cells. The uptake was quantitatively analyzed by flow cytometry. Incubation of HepG2 cells with the mannose dendron **33** or with Rhb non-functionalized βCD showed only marginal unspecific uptake (Figure 6A). Apoptosis of targeted HepG2 cell was detected by staining with Annexin V-APC and subsequent measurement by flow cytometry showed that highest degree of apoptosis was observed in HepG2 cells incubated with doxorubicin loaded heptagalactosylated β-cyclodextrin (βCDGal) **36** (Figure 6B).

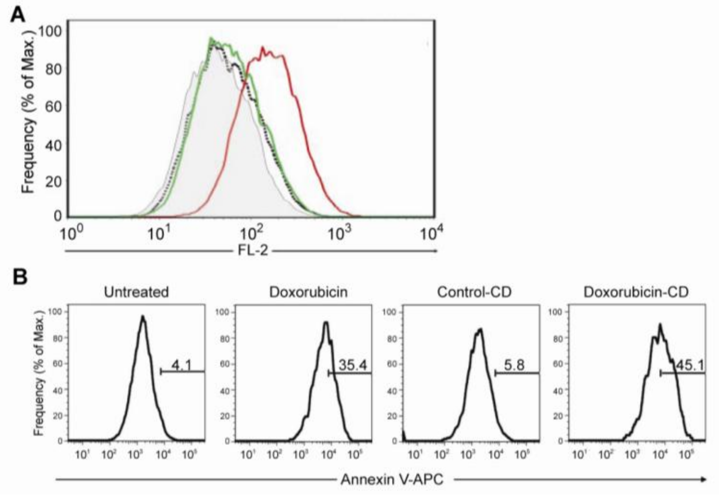

Figure 6. (A) Targeting of the hepatocellular carcinoma cell line HepG2 with βCD glycodendrimers. HepG2 cells were left untreated (grey area), incubated with rhodamine B-labeled βCD (dotted line) or labeled βCD glycodendrimers containing terminal Man (green line) or Gal residues (red line). Uptake was measured by flow cytometry. (B) Induction of apoptosis in HepG2 cells treated with doxorubicin-loaded βCDGal. Cells were left untreated or were treated with doxorubicin only, βCDGal or doxorubicin-loaded βCDGal. Apoptosis was detected by Annexin-V-APC staining and subsequent measurement by flow cytometry. Bars indicate the frequency of apoptotic cells present in the whole HepG2 cell population.

The delivery system based on a carbohydrate multivalent platform enabled specific targeting of ASGPR lectins on hepatocytes, followed by further release of doxorubicin inducing apoptosis *in vitro*. This organization enjoyed multimodal properties: targeting *via* carbohydrate dendrimer and delivery *via* supramolecular assembly.

2.2.2. Single Supramolecular Scaffold Orients Carbohydrates to Sense Bacteria

There is no ideal scaffold for multivalent display, as the design of multivalent probes has to consider many aspects. Among them, the valency (i.e. the number of carbohydrate ligands) and the spatial arrangement of the lectin target's multiple binding sites are relevant features to consider. C_5-symmetrical glycoconjugates orienting five ganglioside GM1 pentasaccharides for the neutralization of the pentameric cholera toxin, and C_3-symmetrical ganglioside GM3 trisaccharide that inhibit the influenza virus hemaglutination are wonderful examples of well-designed structures.[26]

With the aim of creating new architectures for multivalent display of carbohydrates, we designed a small-molecule with a Ru(II) fluorescent core –for the read-out– with tunable symmetry that can support two, four or six heptamannosylated βCD (βCDMan) *via* supramolecular assembly leading to exposure of 14, 28, or 42 mannose units on the core periphery, respectively (Scheme 6).[27]

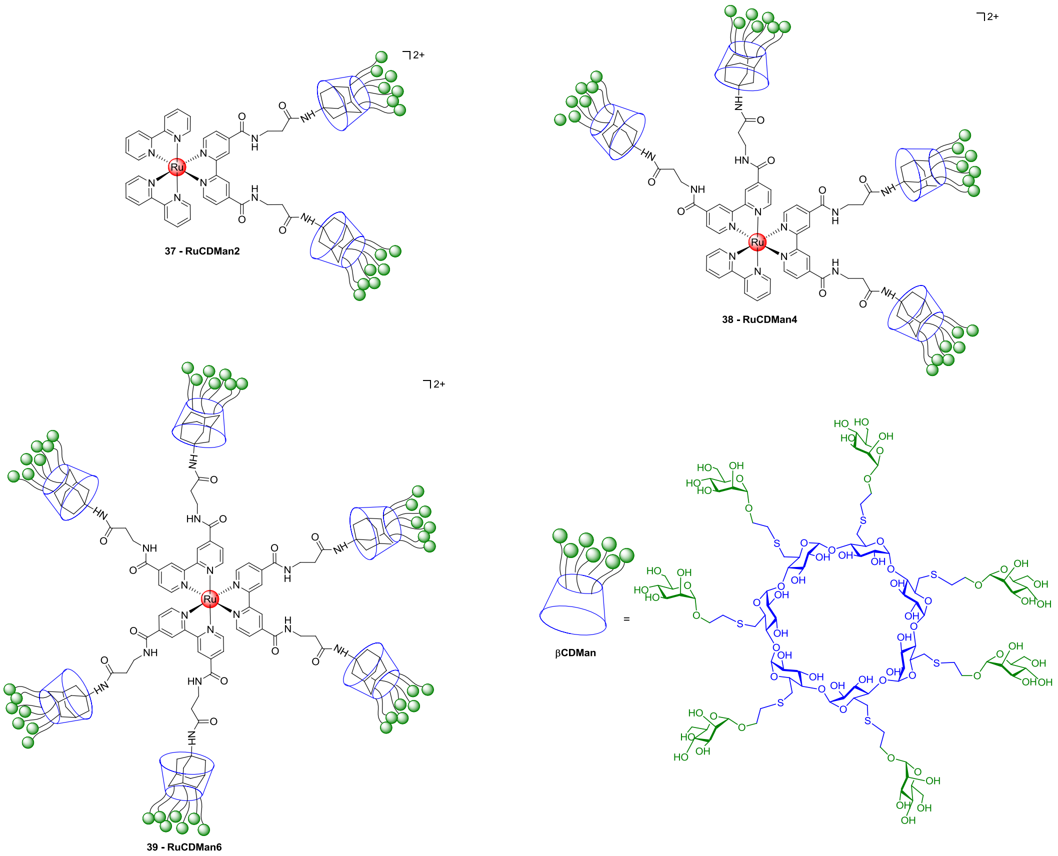

Scheme 6. Structure of the supramolecular assemblies **37–39**.

Modification of the photophysical properties was examined in order to determine the effects of covering the Ru(II) core with different numbers of βCDMan. An increase in quantum yield correlated with the increasing complexity of the structures as more units of βCD assembled around the metal core. The physical shielding of the core prevented effective fluorescence quenching. Nano-ESI mass spectrometry was used to confirm the existence of complete supramolecular assembly. The results of Nuclear Overhauser effect spectroscopy study (NOESY) indicated that the specific inner βCD protons were involved in the interaction with the adamantyl moieties.

In order to analyze the kinetics and mechanism of carbohydrate–lectin complex formation in real time, surface plasmon resonance (SPR) was used as tool to understand the influence of mannose density on lectin binding. Different concentrations of complexes **37–39** were sputtered on two Con A sensor chips [low-(LD) and high-(HD) Con A density] with the intention of distinguishing whether the presence of more mannose-binding sites would stabilize bound complexes, or whether binding site clustering would inhibit the interaction. It was found that high Con A concentrations stabilized the binding since complexes **37** and **38** strongly prefer to bind Con A-HD over Con A-LD. Moreover, we found that **38** with 28 sugar units binds to Con A-HD more efficiently and dissociate much slower that **37** which presents fewer sugar on its periphery. Surprisingly, complex **39** with 42 mannose units did not bind both Con A chips. Indeed, the greater number of mannose residues impacted on the bulkiness impeding the formation of stable complex with the lectin. This result indicated that there is an upper limit in the number of carbohydrates to achieve binding and that the arrangement modality of the structure is another factor to consider when contemplating binding efficiency (Figure 7).[28]

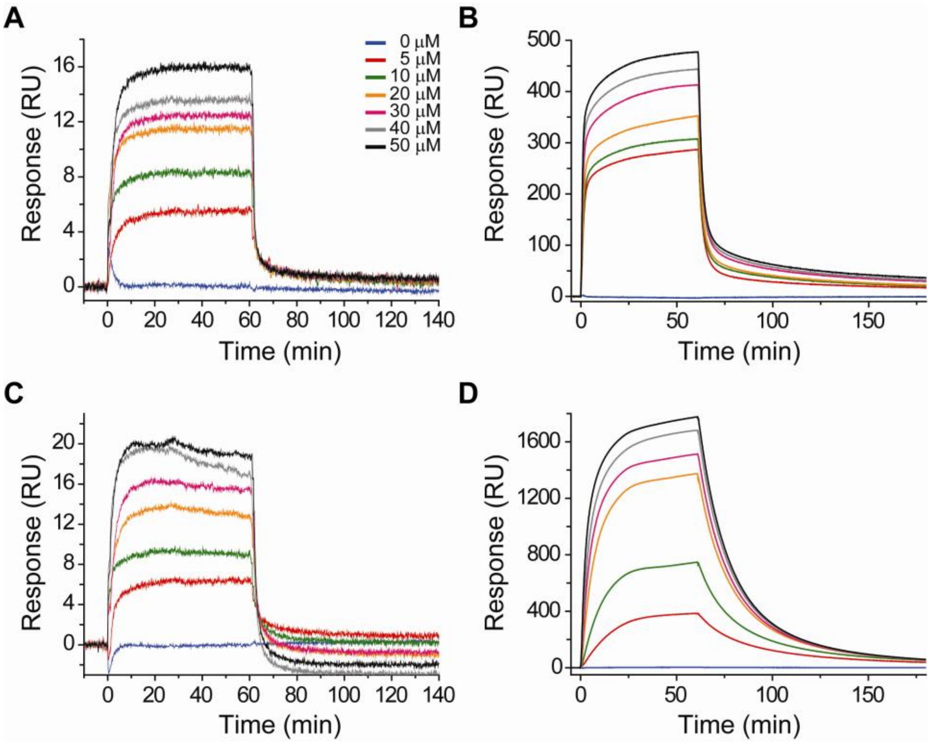

Figure 7. SPR sensorgrams of RuCDMan2 **37** and RuCDMan4 **38** at different concentrations (indicated). Graphs (A) and (B) show binding of RuCDMan2 **37** to Con A-LD and Con A-HD, respectively. Graphs (C) and (D) show binding of RuCDMan4 **38** to Con A-LD and Con A-HD, respectively.

The binding capacity of complex **39** was assessed using the mannose-specific adhesin FimH as receptor. This protein is located on the pili of *Escherichia coli* (*E. coli*) strain ORN178. The bacterial strain was incubated with **39**, and confocal microscopy was used to visualize the interaction between the complexes and the bacterial pili. Binding was evident due to the inherent fluorescence of the Ru(II) core and the specificity was controlled using a different strain (ORN 208) with a mutation in the fimH gene that renders the pili unable to bind mannose.[29]

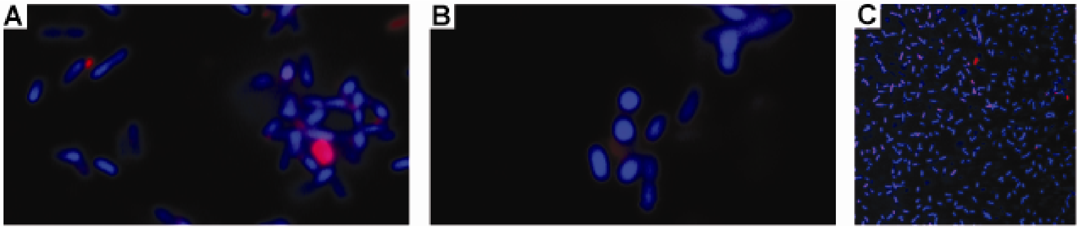

Figure 8. Confocal laser scanning microscopy images for (A), (B) the incubation of bacteria *E. coli* strain ORN178 with RuCDMan6 **39**. Incubation of (C) ORN208 with RuCDMan6 **39** as negative control.

The multivalent system could be used for the investigation of other carbohydrate–lectin interactions since the glycosylated βCD are easily interchangeable. This approach is a new route for the generations of libraries of novel multivalent probes.

2.3. Fullerenes

C_{60} fullerenes, molecules in the shape of a hollow sphere of 60 carbon atoms, exhibit properties that render them promising candidates for biomedical and controlled drug delivery applications. When appropriately modified, fullerenes can migrate through the blood brain barrier and can be applied for biomedical purposes.[30]

In this respect, modified fullerenes have been used as an efficient platform for the globular, multivalent presentation of targeting biomolecules. In particular, the C_{60} hexakis adducts initially developed by Hirsch and co-workers are unique organic molecules with an appealing compact spherical scaffold for the construction of multifunctional nanomaterials. C_{60} hexakisadducts are molecules with a spherical architecture and have the ability to present multiple copies of ligands around the C_{60} surface.[31]

Nierengarten *et al.* have reported pioneering work in the design and synthesis of dodecavalent fullerene-based glycoclusters as well as their application to bacterial sensing.[32] Fullerene hexakis-adducts bearing peripheral carbohydrate moieties can be efficiently prepared by grafting unprotected sugar derivatives onto the fullerene core using “click chemistry”.[33]

The design and synthesis of multivalent structures should involve a rationale whereby the multivalent framework identity as well as the template support should be taken into account considering potential applications.[34] In an effort to design and create a new drug for ischemic stroke, we have synthesized a C_{60} hexakisadduct derivative bearing twelve alkyne groups and used the copper-mediated Huisgen 1,3-dipolar cycloaddition to append the twelve GlcN moieties on the C_{60} periphery (Scheme 7).

To evaluate a possible anti-inflammatory effect of fullerene, glucosamine (GlcN) was covalently attached to the C_{60} core. Since GlcN inhibits the nuclear factor-κB (NF-κB) to reduce the humoral and cellular immune response and it has a beneficial effect on cerebral inflammation after ischemic stroke, we prepared a fullerene decorated with twelve GlcN epitopes.[35]

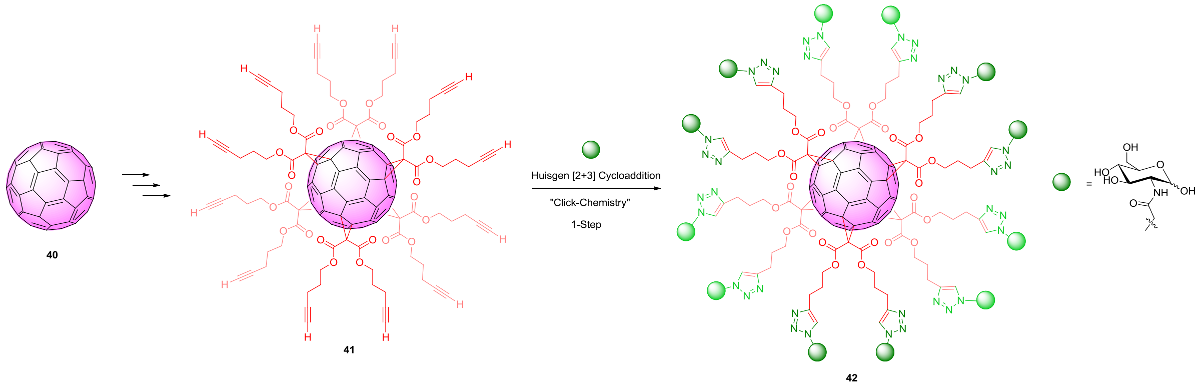

Scheme 7. Schematic overview of the synthesis of $C_{60}(GlcN)_{12}$ **42** bearing 12 sugar units.

We demonstrated that cerebral infarct volume and post-stroke inflammation are reduced in spontaneously hypertensive rats (SHR) treated with $C_{60}(GlcN)_{12}$ compared to controls after transient middle cerebral artery occlusion (tMCAO) –a model for ischemic stroke. Infarct volume was determined by T2 weighted (T2w) MRI 5 days after tMCAO (Figure 9). In all SHR treated with either 0.5 or 5.0 mg·kg^{-1} $C_{60}(GlcN)_{12}$, infarction was observed both in the left caudoputamen and partly in the cortex. Compared to placebo (0.9% NaCl), 0.5 and 5.0 mg·kg^{-1} $C_{60}(GlcN)_{12}$ led to a dose-dependent reduction of infarct volume.[36]

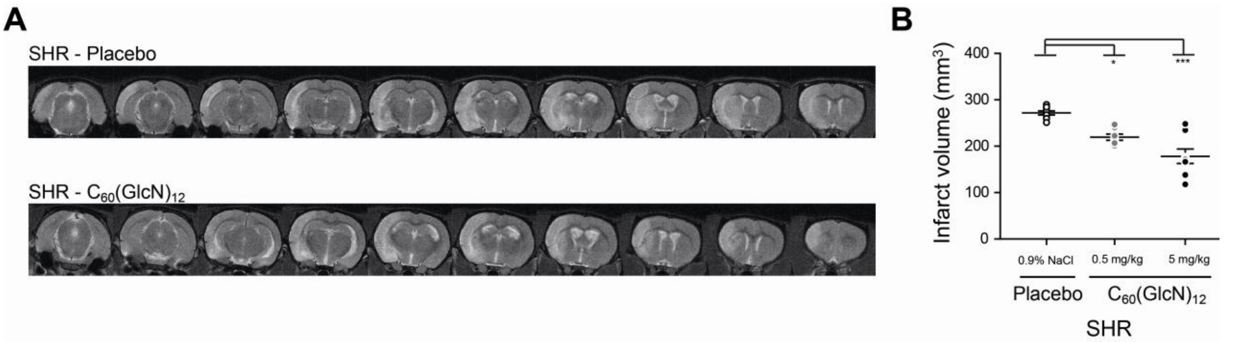

Figure 9. Treatment with $C_{60}(OH)_{34-36}$ or $C_{60}(GlcN)_{12}$ attenuates infarct volume in SHR subjected to tMCAO. (A) Representative T2w images of strokes incurred in placebos (0.9% NaCl) and treated animals with $C_{60}(GlcN)_{12}$ 5 days after tMCAO. (B) Quantitative analysis of infarct volumes 5 days after tMCAO in SHR rats. Different dosages were used in SHR strain. Aligned dot plot of values. Bars and error bars in indicate means of N = 9 [SHR; Placebo], N = 7 [SHR; 0.5 $mg \cdot kg^{-1}$ $C_{60}(GlcN)_{12}$], N = 8 [SHR; 5.0 $mg \cdot kg^{-1}$ $C_{60}(GlcN)_{12}$] per group ± standard error of mean (S.E.M.). (B) Kruskall-Wallis statistic. $^{*}P < 0.05$; $^{***}P < 0.001$.

Treatment with $C_{60}(GlcN)_{12}$ also reduced $CD68^+$ cells (marker for inflammation) expressed on monocytes and macrophages in the subcortical region. Treatment with functionalized fullerenes was also associated with an increase of neurons, thus indicating that the compound is not neuronotoxic, even when the cells are in vulnerable state as is the case under ischemic conditions. $C_{60}(GlcN)_{12}$ also improved cells proliferation compared to placebo.

These finding, in addition to improved neurological score, demonstrated that multivalent expression of GlcN on fullerene is promising in the development of new drug candidate for ischemic stroke.

2.4. Iron Oxide Nanoparticles

The synthesis and functionalization of water-soluble iron oxide magnetic nanoparticles (MNP) as imaging agents has become of particular interest due to the emergence and success of MRI in hospitals for biomedical research and diagnostics. In this respect, the unique physical and super paramagnetic properties as well as the overall structural robustness of magnetite (Fe_3O_4) MNP enable its use as good magnetic resonance contrast imaging agent and has been extensively studied over the past 20 years.[37]

In order to further exploit the potential of Fe_3O_4 MNP, efforts are made to add functionalities on the MNP surface that would allow for active and specific targeting of specific cells. Among biocompatible ligands and specific targeting agents, carbohydrates are promising candidates since they contribute to signaling, adhesion, and recognitions processes of the extra-cellular domain.[38] Moreover, the high surface-to-volume ratio presented by these nanoparticles offers the opportunity for MNP as a good multivalent carrier reinforcing the relatively weak binding of a single sugar with its corresponding receptor (i.e. lectins, antibodies, or enzymes).

MRI is widely used as imaging tool in the study of neurological disease. The Davis group has shown *in vivo* imaging of artificial brain disease using carbohydrate coated MNP. Host response to injury or disease induces up-regulation of the carbohydrate-binding transmembrane proteins CD62E (E-selectin) and CD62P (P-selectin) in the sites of inflammation in the brain, offering the opportunity to act as ideal diagnostic marker.[39] MNP were coated with Sialyl Lewis^x (SiaLe^x) –a targeting vector for CD62– followed by intravenous injection in the tail vein to visualize inflammation in the brain. In this work, selectin expression on activated endothelium in the brain was induced by microinjection of interleukin-1β (IL-1β) into the left striatum of the rat. Since artificial inflammation were used it is unclear if one can extrapolate to concrete disease (i.e. ischemic stroke).

In the Seeberger group, MNP nanoparticles presenting amine functionalities at the outer surface (NH$_2$@MNP) were prepared following earlier reports (Scheme 8).[40] Superconducting quantum interference device (SQUID) data showed that the field-dependent magnetization did not present hysteresis loops, indicating that these water soluble MNP were superparamagnetic and ready for MRI purpose. The diameter of NH$_2$@MNP was around 10 ± 2 nm. MNP were then subjected to functionalization with SiaLe^x for specific targeting, Lewis^x (Le^x) for unspecific control, and ethanolamine for negative control to get SiaLe^x@MNP, Le^x@MNP, and OH@MNP, respectively. Enzymatic sialic acid quantification around the SiaLe^x@MNP surface gave about 10.4 ± 1.2 nmol·mg^{-1} of SiaLe^x on the MNP surface.

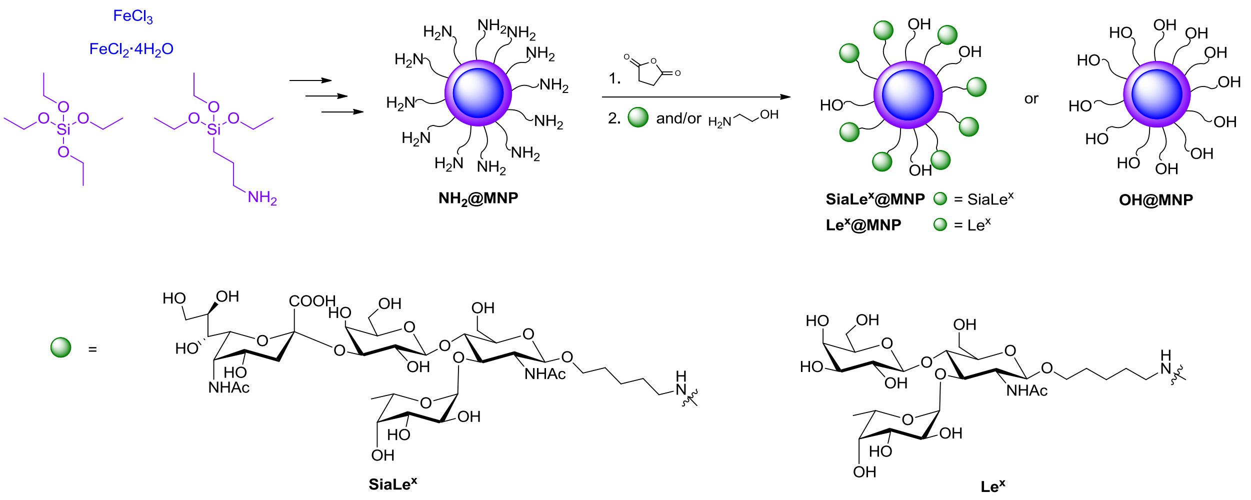

Scheme 8. Synthetic route for the preparation of SiaLe^x@MNP, Le^x@MNP, and OH@MNP.

The most popular model of ischemic stroke is the intraluminal thread (ILT) technique that lead to MCAO.[41] This involved the insertion of an occluding device into the internal carotid of the mice (C57/BL6 mice). The thread was removed for a tMCAO after 60 min. Depending on the length of occlusion, the severity of the reduction in blood flow, and the collateral supply resulting infarcts was located either in subcortical or cortical and subcortical regions. After 5 h, the contrast agent were injected and MNP uptake in the brain was determined using T2* MRI 24 h after tMCAO. (Figure 10)

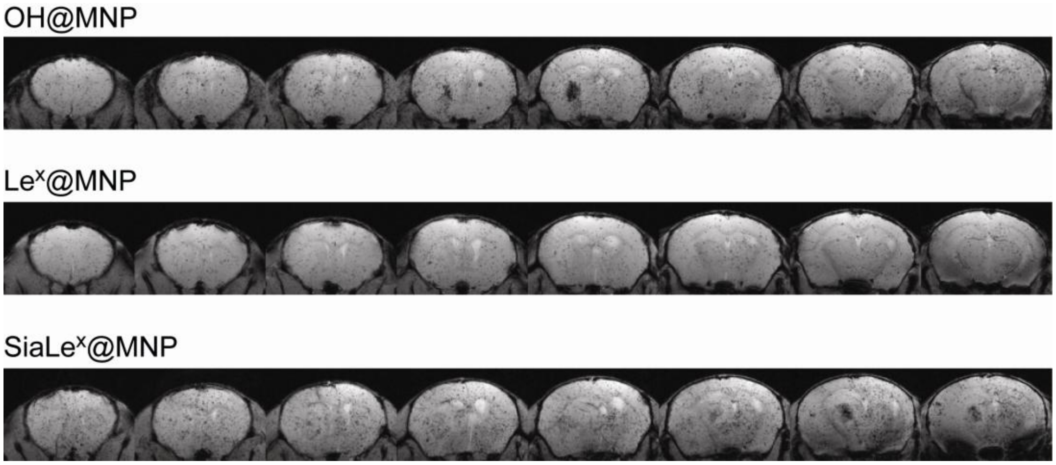

Figure 10. Representative T2* images of strokes incurred in OH@MNP, Le^x@MNP,and SiaLe^x@MNP treated animals 24 h after tMCAO. A single dosage of 1 mmol·kg^{-1} was used in the mice with N = 6 [OH@MNP, Le^x@MNP,and SiaLe^x@MNP].

In the OH@MNP group, all animals exhibited punctate regions of contrast accumulation all over the brain. In 4/5 animals, the hypo-intensity in T2* images appears to be more profound in the ischemic territory. Furthermore, 3 of those 4 animals exhibited a strong focal region of high particle accumulation in the striatum. In the Le^x@MNP group, all animals exhibited punctate regions of contrast accumulation all over the brain. There did not appear to be any regions of strong accumulation. Finally in the $SiaLe^x$@MNP, all animals exhibited punctate regions of contrast accumulation all over the brain but in 2/5 animals there were regions of higher contrast accumulation in the striatum and thalamus.[42]

In vivo experiments are ongoing to determine the specificity of the MNP binding or cell uptake in the sites of inflammation in the brain.

2.5. Quantum Dots

Quantum dots (QDs) are semiconductor nanoparticles that have attracted widespread interest in biology and medicine due to their unique optical and electronic properties. The QD core consists of CdSe, CdTe, CdS, ZnSe, InP, InAs or PbSe. Among them, CdSe and CdFe cores are the most used. Their stability can be improved by using a core-shell-shell arrangement, where the outer shell provides resistance to the environment through effective isolation of the inner core (CdSe-CdS-ZnS- or CdSe-ZnSe-ZnS-model).[43]

QDs exhibit unique optical properties that offer significant advantages over the commonly used fluorophores. They are characterized by wide excitation and narrow emission spectra, high fluorescence quantum yield, and great photostability. The ability to control their luminescence properties by size adjustments and the reduced tendency to photobleach renders QDs suitable for fluorescence-probing applications in the detection of specific biological interactions *in vitro* and *in vivo* in cells, tissues and in the entire body.[44]

To make QDs more useful for probing living cells and other biological applications, these semiconductor nanocrystals need to be conjugated to biomolecules such as carbohydrates (Carb@QDs) far away from the QDs surfaces and without disturbing the biological function of these molecules. In this respect, we are interested in developing and optimizing methods for preparing multivalent Carb@QDs. Such multivalent nanoparticles hold several advantages over free carbohydrates and may improve targeting by combining lower affinity carbohydrates on the particle surface to increase binding avidity. In addition, different glycan sequences or other compounds can be combined to improve selectivity and customize therapy. Other potential applications include cell labeling and use as glyconanosensors.[45]

2.5.1. Continuous-flow Reactor-based Synthesis of Carbohydrate-capped QDs

Various aspects of QD synthesis and functionalization have been harvested. We adopted both batch and continuous-flow methods to synthesize and functionalize QDs with sugars. QDs are mostly synthesized in nonpolar organic solvents and hydrophobic surface ligands such as trioctylphosphine oxide (TOPO), trioctylphosphine (TOP), tetradecylphosphonic acid (TDPA), oleic acid or amines. However, traditional batch processes are of limited utility for the large production of QDs due to limited temperature control and lack of homogeneous mixing. Continuous-flow microreactors provided precise control over reaction conditions, including temperature. Moreover, the production time was independent of the process scale. The high surface-to-volume ratio of the microreactor channels enables precise temperature control as well as efficient mixing, allowing for the production of large quantities of monodisperse QDs needed for life science applications.[46]

The Seeberger group developed a protocol for a three-step synthesis of Carb@QDs using three sequential continuous-flow reactors (Figure 11).[47]

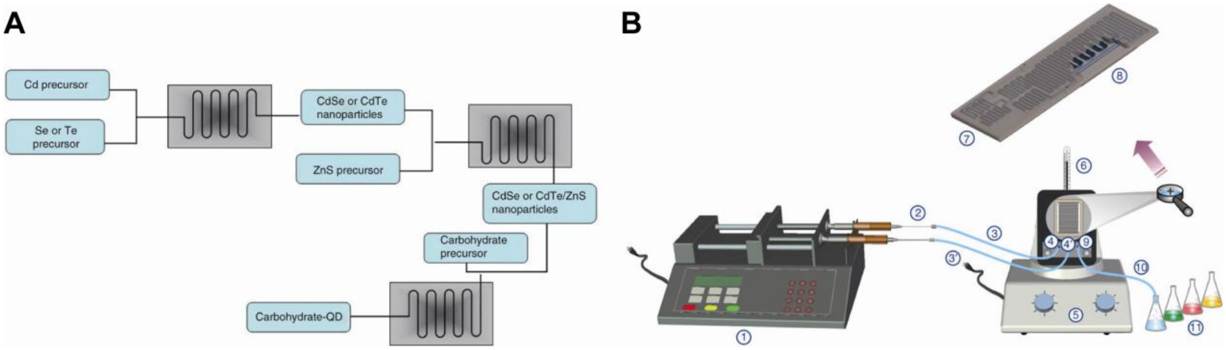

Figure 11. Schematic overview of (A) the continuous flow synthesis and (B) the continuous flow system used carbohydrate-functionalized QDs. (1) Syringe pump; (2) gas-tight syringes; (3 and 3′) PTFE tubing; (4 and 4′) inlets; (5) hot plate; (6) thermo couple; (7) mixing system; (8) microreactor; (9) outlet; (10) PTFE tubing with back-pressure regulator; (11) collection vials.

Firstly, CdSe and CdTe nanoparticles with different emission maxima were prepared by injection of a 1:1 mixture of Cd precursor and Se or Te precursor. The Cd precursor was prepared upon addition of oleic acid and oleyamine to a solution of cadmium oxide dissolved in lauric acid. The Se and Te precursors were prepared by dissolving elemental Se or Te powder with TOP in a glass microreactor. Reaction times ranged from 3 to 30 min at different temperatures. The average size distribution of each sample was calculated from the extinction spectra. The optical properties of the QDs show a time-dependent bathochromic shift in the band-edge emission as well as an enhancement of luminescence intensity. Nanocrystals collected 1 min after injection are relatively small and exhibit fluorescence in the far UV-visible region. Longer reaction times lead to an increase in size and show a bathochromic fluorescence shift. The photoluminescence peaks of CdSe QDs are sharp, with full width at half maximum (FWMH) values of the band-edge luminescence between 30 and 50 nm, indicating the narrow size distribution of the QDs. The second step consisted of a further modification by introducing a secondary shell in a continuous process. A mixture of hexamethyl disilathiane, TOP, diethylzinc in toluene and zinc sulfide were injected separately from the QD solution into the microreactor. Transmission electron microscopy (TEM) images revealed highly crystalline, monodisperse and cubic nanoparticles. Different QD solubilization and surface functionalization have been devised over the past years. Exchange of hydrophobic surfactant molecules with bifunctional molecules that are hydrophilic on one side and hydrophobic on the side that binds to the ZnS shell facilitates this process. Most often, thiols have been used as anchoring groups on the ZnS surface. Accordingly, the previous ZnS-coated CdTe quantum dots were functionalized by ligand exchange with pyridine in continuous flow. Freshly prepared oleic acid-coated CdTe-ZnS QDs were dissolved in pyridine and injected into the microreactor. The resulting pyridine coating was then exchanged with carbohydrates. A mixture of freshly prepared dihydrolipoic acid and mercapto-polyethylene glycol (PEG) mannose or galactose and QD solutions were simultaneously injected into the microreactor. The UV-vis and fluorescent spectra of the quantum dots did not change following sugar coating (Figure 12).

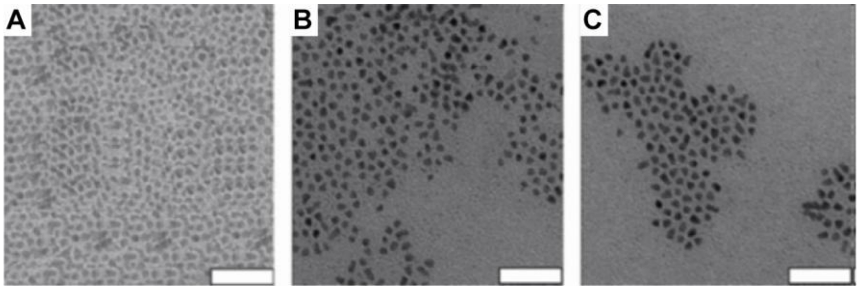

Figure 12. TEM images of (A) CdSe QDs, (B) CdTe/ZnS nanoparticles, and (C) CdTe/ZnS/mannose nanoparticles. Scale bars: 50 nm.

2.5.2. *In vitro* Imaging and *in vivo* Liver Targeting using Carbohydrate-capped QDs

While the use of Carb@QDs for *in vitro* applications has been described before, we exploited Carb@QDs for *in vivo* targeting as well. HepG2 cells that ASGPR and bind to galactose-terminal glycoproteins were used. HepG2 cells clustered in presence of galactose-coated QDs (Gal@QDs). Flow cytometry after 2 h incubation with cells revealed that Gal@QDs were taken up by HepG2 cells preferentially over polyethylene glycol QDs (PEG@QDs) (Figure 13).[48]

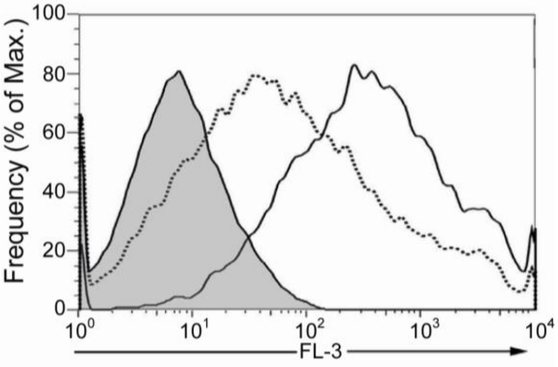

Figure 13. Specific uptake of Gal@QDs by HepG2 cells. HepG2 cells were incubated with either 20 nmol of PEG@QDs or Gal@QDs. For inhibition of Gal@QDs binding and receptor-mediated uptake, HepG2 cells were preincubated with a galactose-polymer before adding Gal@QDs. Compared to the PEG@QDs (gray area), Gal@QDs were preferentially taken up by the HepG2 cells (solid line). Uptake was partially inhibited by preincubating cells with galactose-polymer (dotted line).

After demonstrating the specific uptake of Gal-QDs *in vitro*, *in vivo* liver targeting was studied. For this purpose, mice received either PEG@QDs or QDs capped with mannose (Man@QDs) or galactosamine (GalNAc@QDs) by intravenous injection. A low level of unspecific sequestration was observed in the liver 2 h after injection of PEG@QDs. In contrast, injection of Man@QDs or GalNAc@QDs resulted in a high number of QDs sequestering in the liver (Figure 14). This finding suggested binding and/or endocytosis of the QDs mediated by the mannose receptor and ASGPR. The latter lectin is expressed predominately on hepatocytes, while the mannose receptor is strongly expressed on Kupffer cells and sinusoidal endothelial cells in the liver. Carbohydrate–protein interactions are specific and may be exploited for targeted drug delivery *in vivo*.

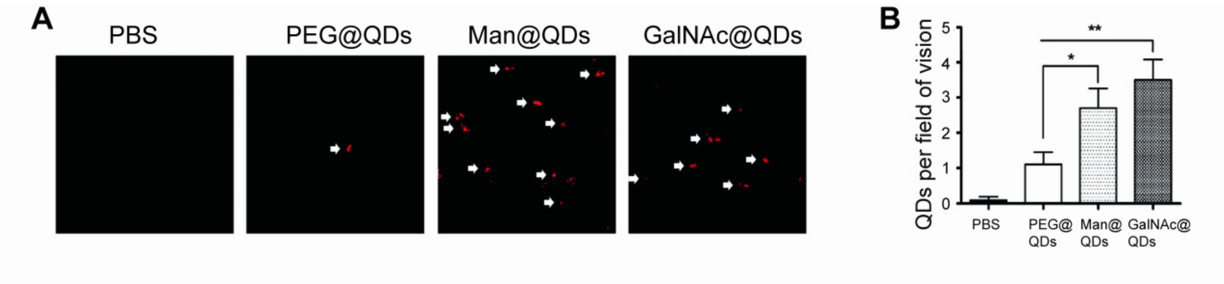

Figure 14. Specific liver sequestration of Man@QDs and GalNAc@QDs in liver. Mice were injected with PBS or PEG@QDs or Man@QDs or GalNAc@QDs. 2 h after injection mice were sacrificed and livers were perfused. (A) Paraffin sections of the livers were prepared, and QD sequestration in the liver was visualized by fluorescence microscopy. Arrows indicate QDs sequestered to liver tissue. (B) Statistical analysis of QD sequestration in the liver was performed by counting 10 microscopic fields of vision for each mouse. Data are presented as mean ± S.E.M. for each group.*$P < 0.05$; **$P < 0.01$.

2.6. Gold Islands

In material chemistry, the development of biosensors to study interactions between biological molecules (i.e. carbohydrate–protein interactions) is generating increasing interest. Currently, surface plasmon resonance (SPR) plays a central role in monitoring such events. Nevertheless, the number of applications of localized surface plasmon resonance (LSPR) is increasing due to the lower cost and higher flexibility with respect to SPR.[49]

The common experimental scheme for LSPR sensing consists of immobilization of a receptor layer on the nanostructured metal surface of the transducer. Monitoring variations in the optical response results from local changes in the refractive index occurring upon the binding event with the biological analyte.[50]

Accordingly, LSPR transducers based on random discontinuous (island-type) gold films were prepared, in a collaboration with the Rubinstein group, to support as multivalent system a self-assembled monolayer (SAM) of carbohydrates. The specific recognition between the mannose-binding lectin Con A with the mannose SAM or with controls (galactose- or linker-SAM) was investigated to determine the selectivity and sensitivity of the LSPR system. Mannose coated Au nanoparticles (Man@AuNPs) were then used to interact with Con A immobilized on the Au island surface, thus providing an enhancement of the LSPR signal as well as convenient imaging of the Con A recognition event (Figure 15).[51]

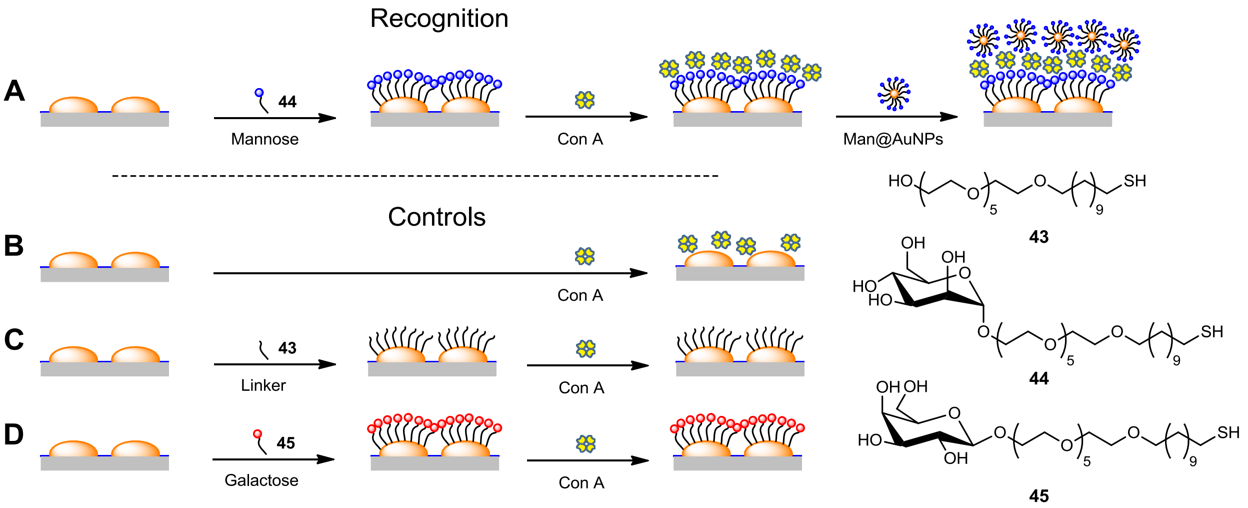

Figure 15. Left: schematic presentation of the recognition and control experiments with Au island transducers. (A) Specific binding of Con A to a SAM of **44** (mannose) followed by binding of Man@AuNPs; (B) non-specific adsorption of Con A on bare Au; (C), (D) non-specific interaction of Con A with SAMs of **43** (linker) and **45** (galactose), respectively. Right: Molecules used for the formation of the self-assembled monolayers on the gold surfaces: linker **1**, linker-modified mannose **44**, and linker-modified galactose **45**.

Transmission spectra for the series of experiments described in Figure 15 are shown for 5.0 nm Au island films (Figure 16). An increase in intensity and a red-shift of the surface plasmon band indicated the formation of the respective SAMs. The specific binding of Con A to the mannose SAM was marked by an increase in the maximum intensity and a red-shift of the plasmon band position. When Au island transducers were coated with a linker SAM or the non-specific galactose SAM, no response to Con A was observed. Control experiments with no SAM showed adsorption of Con A on the bare Au.

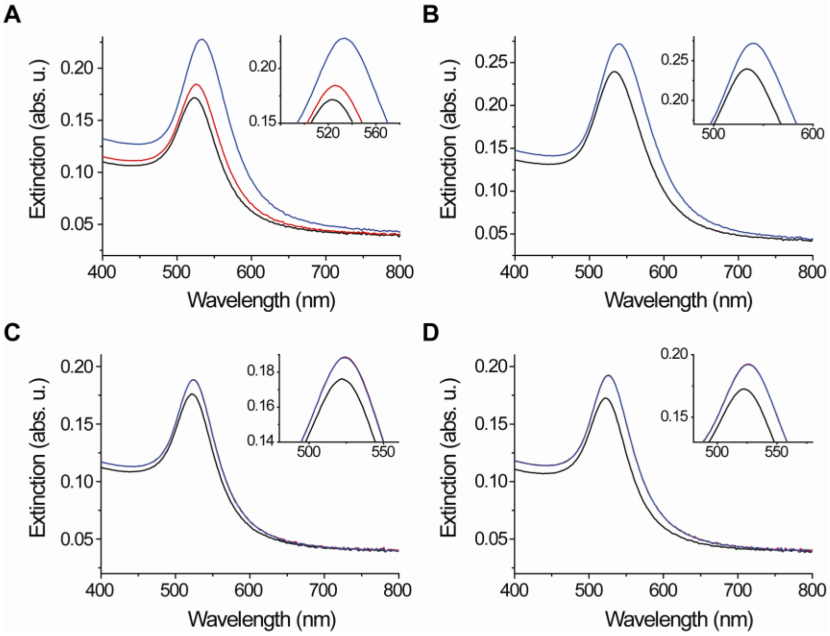

Figure 16. LSPR spectra of 5.0 nm (nominal thickness) Au island films. (A)–(D) correspond to the experiments depicted in Figure 15. The different spectra were recorded after PEG-silane modification (black lines), formation of a carbohydrate or linker SAM (red lines), and incubation with Con A (blue lines). Note that in (C) and (D) the red and blue lines coincide.

The kinetics of Con A binding to the different SAMs were monitored in a flow configuration using 5.0 nm Au island films at a constant wavelength of 545 nm (Figure 17). A solution of Con A was pumped through the cell, and the LSPR transducer response was measured. A sizeable extinction increase, indicating specific binding, was recorded when Con A was injected over the mannose-coated LSPR transducer, followed by a slow release upon change to buffer solution. On the other hand, essentially no response was detected upon injection of Con A over the linker-coated transducer, while a weak response was observed for the non-specific binding of Con A to the galactose-coated transducer.

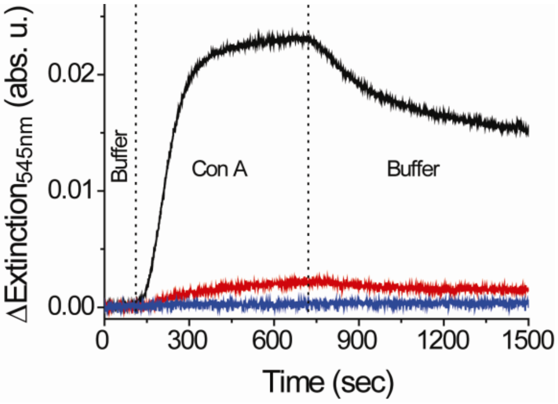

Figure 17. Con A association and dissociation kinetics measured with 5 nm Au island transducers. The transducers were modified with SAMs of **44** (black line), **43** (blue line), and **45** (red line).

Binding of Man@AuNPs was assayed using 15 nm Au island films. UV-vis spectra corresponding to the preparation of the recognition interface and the binding of Con A followed by Man@AuNPs were recorded. Binding of the multivalent Man@AuNPs was evident as a major change in the spectra of the Au film studied (Figure 18, left panel) as well as on the high-resolution scanning electron microscopy (HRSEM) images (Figure 18, right panel).

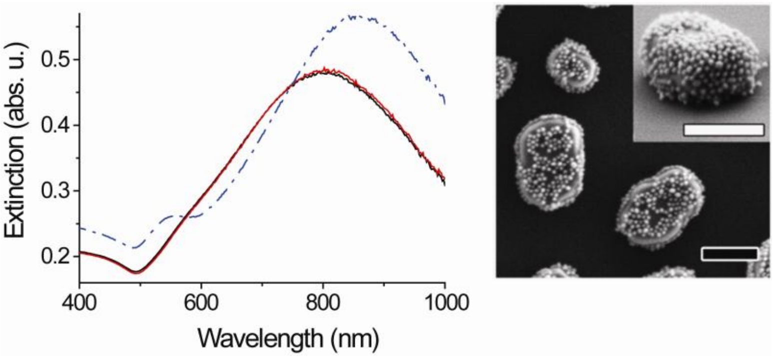

Figure 18. UV-vis spectra (left) and HRSEM images (right) corresponding to the binding of Man@AuNPs to Con A bound to mannose-modified 15 nm Au film. Spectra were recorded in solution after formation of a mannose SAM (black lines), binding of Con A from a Con A solution (1 μM) (red lines), and incubation with Man@AuNPs (blue dashed-dotted lines). Inset: tilted projection of a single island coated with Man@AuNPs. Scale bars: 200 nm.

The use of ultrathin gold island films as platform for multivalent presentation of carbohydrates allowed for the monitoring and imaging of carbohydrate–protein interactions. The system was adapted to enable characterization in a flow mode in order to determine the association and dissociation constants of the interaction event.

2.7. Polymers

2.7.1. Detection of Bacteria Using Glyco-dendronized Polylysine

Many multivalent probes have structures that do not allow for proper adjustment of the carbohydrate ligand position in order to achieve optimal binding with the receptors. Glyco-dendronized polymers exhibit a double framework based the two-dimensional structure of the polymer and the three-dimensional structure of the dendrimers that synergistically create a flexible multivalent system integrating a capacity to bend and adapt to the existing environment of the carbohydrate receptors on the pathogen surface. Thus, the resulting polyvalent systems can adjust the carbohydrate units for the most efficient binding interaction with the lectins.[52]

Poly-L-lysine (PLL) –extensively used for the design of diverse multivalent structures– was chosen as polymer backbone for its biocompatibility, biodegradability, availability in a range of molecular weights, and the lateral free amino chain that allows for further functionalization. Polymer functionalization is challenging since it has to proceed selectively, in high yield, and without further additional purification steps.[53]

A previously explored [2+2] cycloaddition method for polymer functionalization using the energy of light that avoids metal contamination, takes place in water, and circumvents the use of carbohydrate protecting groups was explored for gylco-dendrimers generation. To enhance the scalability of the photochemical reaction, a continuous-flow photochemical reactor was exploited for its high surface-to-volume ratio that provides precise control over reaction conditions, efficient and homogeneous mixing, easy conjugation with minimum side reactions. Two sets of dendrons with three or nine carbohydrates units were synthesized bearing either mannose or galactose. The first- and second-generation dendrons were subsequently attached to the PLL polymer backbone to furnish the glyco-dendronized polymers **48–51** using photochemical [2+2] cycloaddition in a continuous-flow reactor (Scheme 9).[54]

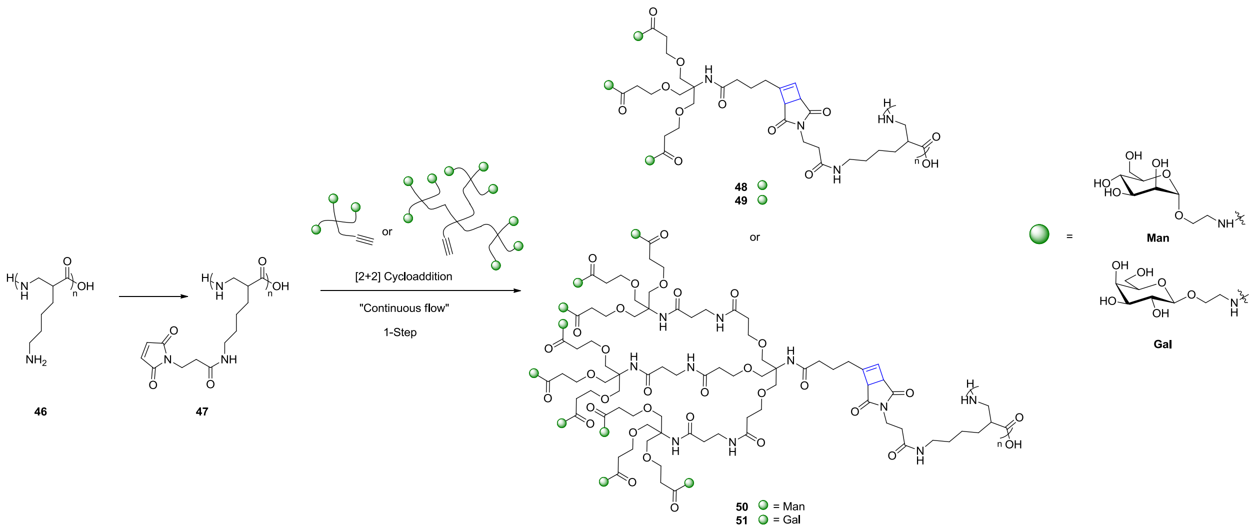

Scheme 9. Functionalization of PLL with first- and second generation dendrons with highlight in blue of the four-membered rings formed upon cycloaddition.

Bacterial detection assays were performed to demonstrate the detection capabilities of the glyco-dendronized polymers. For this purpose, polymer **50** bearing ninepod mannose units was incubated with mannose-binding ORN178 bacterial strain of *E. coli*. Clustering was detected by confocal microscopy using 4',6-diamidino-2-phenylindole (DAPI), a fluorescent dye that stains bacterial DNA (Figure 19A). In the case of a single mannose polymer, no aggregation was observed pointing to relevance of multivalent carbohydrate presentation through the dendrons. The incubation of polymer **50** with the mutant *E. coli* strain ORN208 devoid of mannose receptors did not show any aggregation (Figure 19C). The specific interaction between the glyco-dendronized polymers and the bacteria was further confirmed upon addition of fluorescent Con A-FITC, a mannose-binding lectin. Solutions of different bacterial concentrations (10^5–10^7) were incubated with mannose polymer **50**, followed by the addition of Con A-FITC to enable the localization of the polymer. In the case of ORN178, ConA-FITC staining successfully localized the polymer (Figure 19B), while for ORN208 neither clustering not Con A-FITC labeling could be observed (Figure 19D).

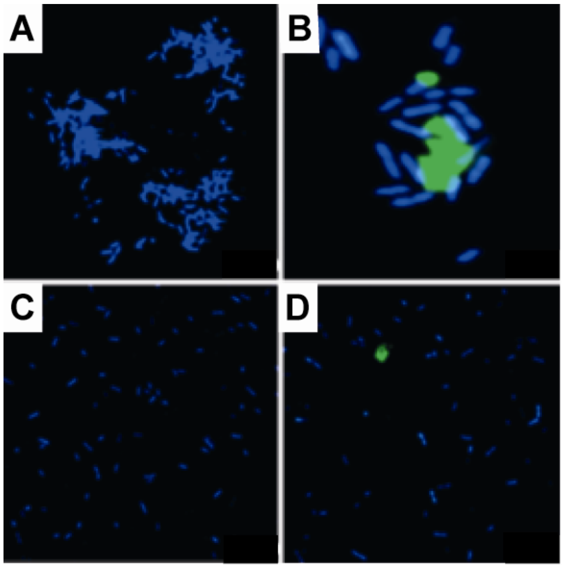

Figure 19. Confocal laser scanning microscope images for the incubation of bacteria *E. coli* strain ORN178 and dendronized polymer **50** (A); and ConA-FITC (B). Strain ORN208 (negative control) in the presence of **50** (C) and ConA-FITC (D).

2.7.2. Modular Approach Towards Bioactive Fiber Meshes Carrying Oligosaccharides

The design and fabrication of three-dimensional polymer integrating biological activity are key issues in the development of biomedicine. Biofunctional polymer nanofiber meshes could meet structural and functional aspects required for the generation of such materials.[55]

In this respect, nanofiber meshes constructed *via* electrospinning could be attractive due to the versatility and simplicity of the method. These polymer mesh scaffolds have been successfully introduced in biological systems.[56]

In order to establish a multivalent system for the manufacture of biologically active material, post-functionalization of fiber meshes involving spinning of a mesh-forming polymer followed by introduction of carbohydrates onto the mesh surfaces has been utilized. Accordingly, nanofiber meshes composed of poly(ε-caprolactone) (PCL) and poly-pentafluorophenolmethacrylate (PPfpMa) blends (for further functionalization) have been obtained by cospinning of PCL with the poly-methacrylate derivative. The introduction of the biofunctional carbohydrates was done *via* amide coupling and monitored by means of UV-vis spectroscopy as the amine-terminated functional molecule releases detectable pentafluorophenol (Figure 20).[57]

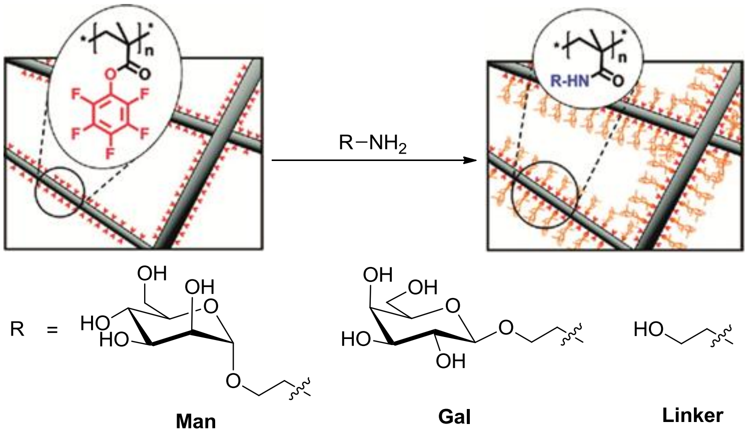

Figure 20. Functionalization of fiber meshes bearing activated esters at the surface allows for the introduction of different amino-functionalized molecules [2-aminoethyl-mannopyranoside (Man), 2-aminoethyl-galactopyranoside (Gal), or 2-aminoethanol (linker)]. Introduction of functional molecules is accompanied by the release of a pentafluorophenol reporter that can be monitored by UV-vis spectroscopy.

Carbohydrate structures on pathogens have been recognized as highly relevant in the induction of the host immune response. The recognition of microorganism-specific saccharides by innate immune receptors is significant in the detection mechanisms of bacterial pathogens by the immune system. The mammalian Toll-like receptor 4 (TLR4) interacts with the bacterial lipopolysaccharides (LPS) inducing recognition followed by activation of the immune response by producing antibacterial substances and macrophage recruitment. Mannose-containing oligosaccharides contribute to the latter process upon interaction with macrophages *via* the mannose receptor which mediates endocytosis and cytokine production. The immune reaction is then triggered by these signaling molecules.[58]

Mannose-functionalized fiber meshes were investigated to elucidate whether LPS-mediated stimulation of antigen-presenting cells (APCs) –macrophages– could be enhanced in their presence. Tumor necrosis factor-α (TNF-α), a pro-inflammatory cytokine released by APCs upon stimulation, was used as read-out parameter to monitor the stimulation. Galactose- and aminoethanol-functionalized meshes were then used as specificity controls as well as negative controls. Peritoneal macrophages from mouse were seeded on the meshes and stimulated with LPS. Co-stimulation of mannose meshes with LPS induced significantly increase of TNF-α (< 30%) compared to galactose- or aminoethanol-functionalized meshes. In the absence of LPS, no cytokines were produced (Figure 21).

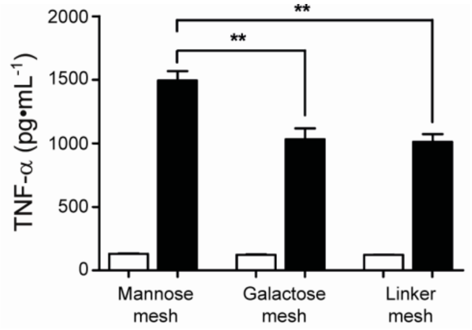

Figure 21. TNF-α production by peritoneal exudate cells after stimulation with LPS in combination with the functionalized meshes. PECs were seeded on the meshes and stimulated in the presence (black bars) or absence (white bars) of 10 ng·mL^{-1} LPS overnight. TNF-α was measured in supernatants of stimulated macrophages. Measurements were performed in triplicates. Data are expressed as mean ± S.E.M. for each group. $^{**}P < 0.01$.

PCL/PPfpMA blends were successfully prepared and prone to react with amine-terminated molecules and to present in a multivalent form biological active carbohydrate. The meshes were used as platform to trigger macrophages stimulation opening new routes for the generation of healing-supported material.

3. Conclusion

The development of novel multivalent carbohydrate scaffolds for the understanding, recognition, and modulation of biological processes as well as for their role in elucidation of new interactions or biomedical applications continues to be an attractive target for research.

The Seeberger group has developed a myriad of different polyvalent systems with the aim of direct application. This chemistry is at the interface with other disciplines. Therefore, rational design of the chemical structures should be linked with future potent use.

4. Abbreviations

abs. u.	absorbance unit
Al	aluminium
APC	antigen-presenting cells
Au	gold
AuNP	gold nanoparticle
BBV	*N*,*N*'-4,4'-bis(benzyl-2-boronic acid)bipyridinium dibromide
bipy	bipyridine
C_{60}	fullerene
Carb@QD	carbohydrate-coated gold nanoparticle
Con A	Concanavalin A
Cu	copper
DAPI	4',6-diamidino-2-phenylindole
Di-man	dimannose
DNA	deoxyribonucleic acid
E. coli	*Escherichia coli*
Fe_3O_4	iron oxide
FITC	fluorescein isothiocyanate
FWMH	full width at half maximum
Gal	galactose
Gal@QD	galactose-coated quantum dot
GalNAc	*N*-acetyl glucosamine
GalNAc@QD	*N*-acetyl glucosamine-coated quantum dot
Gd	gadolinium
Glc	glucose
GlcN	glucosamine
GNA	Aniara Galanthus nivalis
HD	high density
HepG2	parenchymal hepatocytes

HOMO	highest occupied molecular orbital
HRSEM	high-resolution mass spectrometry
IL-1β	interleukin-1β
LD	low density
Le^x	Lewis^x
Le^x@MNP	Lewis^x-coated magnetic nanoparticle
LMCT	ligand to metal charge transfer
LSPR	localized surface plasmon resonance
LUMO	lowest unoccupied molecular orbital
Malt	maltose
Man	mannose
Man@AuNP	mannose-coated gold nanoparticle
Man@QD	mannose-coated quantum dot
MNP	magnetic nanoparticle
MRI	magnetic resonance imaging
NF-κB	nuclear factor-κB
NIR	near infrared region
NOESY	Nuclear Overhauser effect spectroscopy
OH@MNP	hydroxyl-coated magnetic nanoparticle
P-1	boronic acid substituted Merrifield resin
PAMAM	poly(amido amine)
PCL	poly(ε-caprolactone)
PEG	polyethylene glycol
PEG@QD	polyethylene glycol-coated quantum dot
PET	photo-induced electron transfer
PLL	poly-L-lysine
PPfpMA	poly-pentafluorophenolmethacrylate
QD	quantum dot
Re	rhenium

Rhb	rhodamine B
rtPA	recombinant tissue plasminogen activator
RU	response unit
Ru	ruthenium
SAM	self-assembled monolayer
SEM	scanning electron microscope
SHR	spontaneously hypertensive rats
SiaLe^x	sialyl Lewis^x
SiaLe^x@MNP	sialyl Lewis^x-coated magnetic nanoparticle
SPR	surface plasmon resonance
SQUID	superconducting quantum interference device
SWV	square-wave voltametric
T2w	T2 weighted
Tc	technetium
TDPA	tetradecylphosphonic acid
TEM	transmission electron microscope
tMCAO	transient middle cerebral artery occlusion
TNF-α	tumor necrosis factor-α
TOP	trioctylphosphine
TOPO	trioctylphosphine oxide
Zn	zinc
βCD	native β-cyclodextrin
βCDGal	heptagalactosylated β-cyclodextrin
βCDMan	heptamannosylated β-cyclodextrin

5. References

---

[1] (a) Fasting, C.; Schalley, C. A.; Weber, M.; Seitz, O.; Hecht, S.; Koksch, B.; Dernedde, J.; Graf, C.; Knapp, E.-W.; Haag, R. *Angew. Chem.-Int. Edit.* **2012**, *51*, 10472. (b) Connors, K. A. *Binding Constants: The Measurement of Molecular Complex Stability*, Wiley, New York, **1987**. (c) Koshland, D. E.; Neet, K. E. *Annu. Rev. Biochem.* **1968**, *37*, 359. (d) Perlmutter-Hayman, B. *Acc. Chem. Res.* **1986**, *19*, 90.

[2] (a) Liang, R.; Yan, L.; Loebach, J.; Ge, M.; Uozumi, Y.; Sekanina, K.; Horan, N.; Gildersleeve, J.; Thompson, C.; Smith, A.; Biswas, K.; Still, W. C.; Kahne, D. *Science* **1996**, *274*, 1520. (b) Liang, R.; Loebach, J.; Horan, N.; Ge, M.; Thompson, C.; Yan, L.; Kahne, D. *Proc. Natl. Acad. Sci. U. S. A.* **1997**, *94*, 10554.

[3] Mammen, M.; Choi, S. K.; Whitesides, G. M. *Angew. Chem.-Int. Edit.* **1998**, *37*, 2755.

[4] (a) Marcos, M.; Martin-Rapun, R.; Omenat, A.; Serrano, J. L. *Chem. Soc. Rev.* **2007**, *36*, 1889. (b) Lo, S. C.; Burn, P. L. *Chem. Rev.* **2007**, *107*, 1097. (c) Euliss, L. E.; DuPont, J. A.; Gratton, S.; DeSimone, J. M. *Chem. Soc. Rev.* **2006**, *35*, 1095. (d) Twyman, L. J.; King, A. S. H.; Martin, I. K. *Chem. Soc. Rev.* **2002**, *31*, 69. (e) Serroni, S.; Campagna, S.; Puntoriero, F.; Di Pietro, C.; McClenaghan, N. D.; Loiseau, F. *Chem. Soc. Rev.* **2001**, *30*, 367.

[5] (a) Buhleier, E.; Wehner, W.; Vögtle, F. *Synthesis* **1978**, 155. (b) Hawker, C. J.; Frechet, J. M. J. *J. Am. Chem. Soc.* **1990**, *112*, 7638.

[6] (a) Khandare, J.; Calderon, M.; Dagia, N. M.; Haag, R. *Chem. Soc. Rev.* **2012**, *41*, 2824. (b) Ofek, P.; Fischer, W.; Calderon, M.; Haag, R.; Satchi-Fainaro, R. *Faseb J.* **2010**, *24*, 3122. (c) Xu, S. J.; Luo, Y.; Haag, R. *Macromol. Rapid Commun.* **2008**, *29*, 171. (d) Roller, S.; Siegers, C.; Haag, R. *Tetrahedron* **2004**, *60*, 8711. (e) Stiriba, S. E.; Frey, H.; Haag, R. *Angew. Chem.-Int. Edit.* **2002**, *41*, 1329.

[7] (a) Metullio, L.; Ferrone, M.; Coslanich, A.; Fuchs, S.; Fermeglia, M.; Paneni, M. S.; Pricl, S. *Biomacromol.* **2004**, *5*, 1371 (b) de Paz, J. L.; Noti, C.; Bohm, F.; Werner, S.; Seeberger, P. H. *Chem. & Biol.* **2007**, *14*, 879. (c) Andre, J. P.; Geraldes, C.; Martins, J. A.; Merbach, A. E.; Prata, M. I. M.; Santos, A. C.; de Lima, J. J. P.; Toth, E. *Chem. Eur. J.* **2004**, *10*, 5804. (d) Benito, J. M.; Gomez-Garcia, M.; Mellet, C. O.; Baussanne, I.; Defaye, J.; Fernandez, J. M. G. *J. Am. Chem. Soc.* **2004**, *126*, 10355. (e) Turnbull, W. B.; Kalovidouris, S. A.; Stoddart, J. F. *Chem. Eur. J.* **2002**, *8*, 2988. (f) Ashton, P. R.; Boyd, S. E.; Brown, C. L.; Nepogodiev, S. A.; Meijer, E. W.; Peerlings, H. W. I.; Stoddart, J. F. *Chem. Eur. J.* **1997**, *3*, 974. (g) Li, Y.; Jang, W. D.; Nishiyama, N.; Kishimura, A.; Kawauchi, S.; Morimoto, Y.; Miake, S.; Yamashita, T.; Kikuchi, M.; Aida, T.; Kataoka, K. *Chem. Mat.* **2007**, *19*, 5557-5562. (h) Chavan, S. A.; Maes, W.; Gevers, L. E. M.; Wahlen, J.; Vankelecom, I. F. J.; Jacobs, P. A.; Dehaen, W.; De Vos, D. E. *Chem. Eur. J.* **2005**, *11*, 6754. (i) Battah, S. H.; Chee, C. E.; Nakanishi, H.; Gerscher, S.; MacRobert, A. J.; Edwards, C. *Bioconjugate Chem.* **2001**, *12*, 980. (j) Nishiyama, N.; Stapert, H. R.; Zhang, G. D.; Takasu, D.; Jiang, D. L.; Nagano, T.; Aida, T.; Kataoka, K. *Bioconjugate Chem.* **2003**, *14*, 58. (k) Ornelas, C.; Aranzaes, J. R.; Cloutet, E.; Alves, S.; Astruc, D. *Angew. Chem.-Int. Edit.* **2007**, *46*, 872. (l) Perez, L.; Garcia-Martinez, J. C.; Diez-Barra, E.; Atienzar, P.; Garcia, H.; Rodriguez-Lopez, J.; Langa, F. *Chem. Eur. J.* **2006**, *12*, 5149. (m) Krishnamoorthy, K.; Dasari, R. R.; Nantalaksakul, A.; Thayumanavan, S. *Chem. Commun.* **2007**, 739.

---

[8] (a) Landers, J. J.; Cao, Z. Y.; Lee, I.; Piehler, L. T.; Myc, P. P.; Myc, A.; Hamouda, T.; Galecki, A. T.; Baker, J. R. *J. Infect. Dis.s* **2002**, *186*, 1222. (b) Heidecke, C. D.; Lindhorst, T. K. *Chem. Eur. J.* **2007**, *13*, 9056. (c) Heidecke, C. D.; Lindhorst, T. K. *Chem. Eur. J.* **2007**, *13*, 9056.

[9] (a) Bertozzi, C. R.; Kiessling, L. L. *Science* **2001**, *291*, 2357. (b) Pilcibello, K. T.; Slawek, D. E.; Mahal, L. K. *Proc. Natl. Acad. Sci. U. S. A.* **2007**, *104*, 11534. (c) Mann, D. A.; Kanai, M.; Maly, D. J.; Kiessling, L. L. *J. Am. Chem. Soc.* **1998**, *120*, 10575. (d) Rhodes, J. M.; Campbell, B. J.; Yu, L. G. *Biochem. Soc. Trans.* **2008**, *36*, 1482. (e) Sarter, K.; Mierke, C.; Beer, A.; Frey, B.; Fuhrnrohr, B. G.; Schulze, C.; Franz, S. *Autoimmunity* **2007**, *40*, 345. (f) Lloyd, D. H.; Viac, J.; Werling, D.; Reme, C. A.; Gatto, H. *Vet. Derm.* **2007**, *18*, 197. (g) Howes, L.; Jones, R. J. *Reprod. Immun.* **2002**, *53*, 181. (h) Stringer, S. E. *Biochem. Soc. Trans.* **2006**, *34*, 451. (i) Yu, L. G. *Glycoconjug. J.* **2007**, *24*, 411.

[10] (a) Gottschaldt, M.; Koth, D.; Muller, D.; Klette, I.; Rau, S.; Gorls, H.; Schafer, B.; Baum, R. P.; Yano, S. *Chem. Eur. J.* **2007**, *13*, 10273. (b) Roy, R.; Kim, J. M. *Tetrahedron* **2003**, *59*, 3881. (c) Constable, E. C.; Kariuki, B.; Mahmood, A. *Polyhedron* **2003**, *22*, 687. (d) Kojima, S.; Hasegawa, T.; Yonemura, T.; Sasaki, K.; Yamamoto, K.; Makimura, Y.; Takahashi, T.; Suzuki, T.; Suzuki, Y.; Kobayashi, K. *Chem. Commun.* **2003**, 1250. (e) Hasegawa, T.; Yonemura, T.; Matsuura, K.; Kobayashi, K. *Bioconjugate Chem.* **2003**, *14*, 728.

[11] (a) Balzani, V.; Bergamini, G.; Ceroni, P.; Vogtle, F. *Coordin. Chem. Rev.* **2007**, *251*, 525. (b) Albrecht, M.; Witt, K.; Weiss, P.; Wegelius, E.; Frohlich, R. *Inorg. Chim. Acta* **2002**, *341*, 25. (c) Shen, L.; Li, F. Y.; Sha, Y. W.; Hong, X. Y.; Huang, C. H. *Tetrahedron Lett.* **2004**, *45*, 3961. (d) Albrecht, M.; Osetska, O.; Klankermayer, J.; Frohlich, R.; Gumy, F.; Bunzli, J. C. G. *Chem. Commun.* **2007**, 1834. (e) Van Deun, R.; Fias, P.; Nockemann, P.; Schepers, A.; Parac-Vogt, T. N.; Van Hecke, K.; Van Meervelt, L.; Binnemans, K. *Inorg. Chem.* **2004**, *43*, 8461. (f) Comby, S.; Imbert, D.; Chauvin, A. S.; Bunzli, J. C. G. *Inorg. Chem.* **2006**, *45*, 732. (g) Imbert, D.; Comby, S.; Chauvin, A. S.; Bunzli, J. C. G. *Chem. Commun.* **2005**, 1432.

[12] (a) Cross, J. P.; Lauz, M.; Badger, P. D.; Petoud, S. *J. Am. Chem. Soc.* **2004**, *126*, 16278. (b) Vicinelli, V.; Ceroni, P.; Maestri, M.; Balzani, V.; Gorka, M.; Vogtle, F. *J. Am. Chem. Soc.* **2002**, *124*, 6461.

[13] (a) Rusak, D. A.; James, W. H.; Ferzola, M. J.; Stefanski, M. J. *J. Chem. Ed.* **2006**, *83*, 1857. (b) Hu, Y. Z.; Tsukiji, S.; Shinkai, S.; Oishi, S.; Hamachi, I. *J. Am. Chem. Soc.* **2000**, *122*, 241. (c) Weh, J.; Duerkop, A.; Wolfbeis, O. S. *ChemBioChem* **2007**, *8*, 122. (d) Aoki, S.; Zulkefeli, M.; Shiro, M.; Kohsako, M.; Takeda, K.; Kimura, E. *J. Am. Chem. Soc.* **2005**, *127*, 9129. (e) Lei, B. F.; Li, B.; Zhang, H. R.; Lu, S. Z.; Zheng, Z. H.; Li, W. L.; Wang, Y. *Adv. Funct. Mater.* **2006**, *16*, 1883. (f) Murtaza, Z.; Tolosa, L.; Harms, P.; Lakowicz, J. R. *J. Fluoresc.* **2002**, *12*, 187. (g) Shukla, A. D.; Das, A.; van der Boom, M. E. *Angew. Chem.-Int. Edit.* **2005**, *44*, 3237. (h) Gupta, T.; van der Boom, M. E. *Angew. Chem.-Int. Edit.* **2008**, *47*, 2260. (i) Gulino, A.; Gupta, T.; Mineo, P. G.; van der Boom, M. E. *Chem. Commun.* **2007**, 4878. (j) Mugweru, A.; Wang, B. Q.; Rusling, J. *Anal. Chem.* **2004**, *76*, 5557. (k) Janata, J.; Josowicz, M. *Nat. Mater.* **2003**, *2*, 19. (l) Drummond, T. G.; Hill, M. G.; Barton, J. K. *Nat. Biotech.* **2003**, *21*, 1192. (m) Lei, B. F.; Li, B.; Zhang, H.; Zhang, L. M.; Li, W. L. *J. Phys. Chem. C* **2007**, *111*, 11291. (n) Aoki, S.; Zulkefeli, M.; Shiro, M.; Kohsako, M.; Takeda, K.; Kimura, E. *J. Am. Chem. Soc.* **2005**, *127*, 9129.

[14] (a) Vogtle, F.; Plevoets, M.; Nieger, M.; Azzellini, G. C.; Credi, A.; De Cola, L.; De Marchis, V.; Venturi, M.; Balzani, V. *J. Am. Chem. Soc.* **1999**, *121*, 6290. (b) Takashima, H.; Shinkai, S.;

Hamachi, I. *Chem. Commun.* **1999**, 2345. (c) Wang, J. H.; Fang, Y. Q.; Bourget-Merie, L.; Polson, M. I. J.; Hanan, G. S.; Juris, A.; Loiseau, F.; Campagna, S. *Chem. Eur. J.* **2006**, *12*, 8539.

[15] (a) Fernandez-Megia, E.; Correa, J.; Rodriguez-Meizoso, I.; Riguera, R. *Macromol.* **2006**, *39*, 2113. (b) Wu, P.; Malkoch, M.; Hunt, J. N.; Vestberg, R.; Kaltgrad, E.; Finn, M. G.; Fokin, V. V.; Sharpless, K. B.; Hawker, C. J. *Chem. Commun.* **2005**, 5775. (c) Wu, P.; Feldman, A. K.; Nugent, A. K.; Hawker, C. J.; Scheel, A.; Voit, B.; Pyun, J.; Frechet, J. M. J.; Sharpless, K. B.; Fokin, V. V. *Angew. Chem.-Int. Edit.* **2004**, *43*, 3928. (d) Fernandez-Megia, E.; Correa, J.; Riguera, R. *Biomacromol.* **2006**, *7*, 3104. (e) Munoz, E. M.; Correa, J.; Fernandez-Megia, E.; Riguera, R. *J. Am. Chem. Soc.* **2009**, *131*, 17765. (f) Camponovo, J.; Hadad, C.; Ruiz, J.; Cloutet, E.; Gatard, S.; Muzart, J.; Bouquillon, S.; Astruc, D. *J. Org. Chem.* **2009**, *74*, 5071. (g) Touaibia, M.; Roy, R. *J. Org. Chem.* **2008**, *73*, 9292. (h) Branderhorst, H. M.; Ruijtenbeek, R.; Liskamp, R. M. J.; Pieters, R. J. *ChemBioChem* **2008**, *9*, 1836. (i) De la Fuente, J. M.; Penades, S. *Biochim. Biophys. Acta-Gen. Subj.* **2006**, *1760*, 636. (j) Earhart, C.; Jana, N. R.; Erathodiyil, N.; Ying, J. Y. *Langmuir* **2008**, *24*, 6215. (k) Babu, P.; Sinha, S.; Surolia, A. *Bioconjugate Chem.* **2007**, *18*, 146. (l) Oh, E.; Lee, D.; Kim, Y. P.; Cha, S. Y.; Oh, D. B.; Kang, H. A.; Kim, J.; Kim, H. S. *Angew. Chem.-Int. Edit.* **2006**, *45*, 7959.

[16] Kikkeri, R.; Liu, X. Y.; Adibekian, A.; Tsai, Y. H.; Seeberger, P. H. *Chem. Commun.* **2010**, *46*, 2197.

[17] (a) Kikkeri, R.; Hossain, L. H.; Seeberger, P. H. *Chem. Commun.* **2008**, 2127. (b) Kikkeri, R.; Garcia-Rubio, I.; Seeberger, P. H. *Chem. Commun.* **2009**, 235.

[18] (a) Horlacher, T.; Seeberger, P. H. *Chem. Soc. Rev.* **2008**, *37*, 1414. (b) Chen, S. M.; LaRoche, T.; Hamelinck, D.; Bergsma, D.; Brenner, D.; Simeone, D.; Brand, R. E.; Haab, B. B. *Nat. Methods* **2007**, *4*, 437. (c) Chen, S; Haab, B. B. *Clin. Prot.* **2008**, 101. (d) Lekka, M.; Laidler, P.; Labedz, M.; Kulik, A. J.; Lekki, J.; Zajac, W.; Stachura, Z. *Chem. & Biol.* **2006**, *13*, 505. (e) Dai, Z.; Kawde, A. N.; Xiang, Y.; La Belle, J. T.; Gerlach, J.; Bhavanandan, V. P.; Joshi, L.; Wang, J. *J. Am. Chem. Soc.* **2006**, *128*, 10018. (f) Kikkeri, R.; Grünstein, D.; Seeberger, P. H. *J. Am. Chem. Soc.* **2010**, *132*, 10230.

[19] Kikkeri, R.; Kamena, F.; Gupta, T.; Hossain, L. H.; Boonyarattanakalin, S.; Gorodyska, G.; Beurer, E.; Coullerez, G.; Textor, M.; Seeberger, P. H. *Langmuir* **2010**, *26*, 1520.

[20] Lehn, J. M. *Angew. Chem.-Int. Edit. Engl.* **1988**, *27*, 89.

[21] (a) Coskun, A.; Spruell, J. M.; Barin, G.; Dichtel, W. R.; Flood, A. H.; Botros, Y. Y.; Stoddart, J. F. *Chem. Soc. Rev.* **2012**, *41*, 4827. (b) Badjic, J. D.; Nelson, A.; Cantrill, S. J.; Turnbull, W. B.; Stoddart, J. F. *Accounts Chem. Res.* **2005**, *38*, 723. (c) Coskun, A.; Banaszak, M.; Astumian, R. D.; Stoddart, J. F.; Grzybowski, B. A. *Chem. Soc. Rev.* **2012**, *41*, 19.

[22] Engeldinger, E.; Armspach, D.; Matt, D. *Chem. Rev.* **2003**, *103*, 4147.

[23] (a) Courtney, A. H.; Puffer, E. B.; Pontrello, J. K.; Yang, Z. Q.; Kiessling, L. L. *Proc. Natl. Acad. Sci. U. S. A.* **2009**, *106*, 2500. (b) O'Reilly, M. K.; Collins, B. E.; Han, S.; Liao, L.; Rillahan, C.; Kitov, P. I.; Bundle, D. R.; Paulson, J. C. *J. Am. Chem. Soc.* **2008**, *130*, 7736. (c) Wang, S. K.; Liang, P. H.; Astronomo, R. D.; Hsu, T. L.; Hsieh, S. L.; Burton, D. R.; Wong, C. H. *Proc. Natl. Acad. Sci. U. S. A.* **2008**, *105*, 3690. (d) Arima, H.; Motoyama, K. *Sensors* **2009**, *9*, 6346. (e) Wada, K.; Arima, H.; Tsutsumi, T.; Hirayama, F.; Uekama, K. *Biol. Pharm. Bull.* **2005**, *28*, 500.

---

[24] (a) Haba, K.; Popkov, M.; Shamis, M.; Lerner, R. A.; Barbas, C. F.; Shabat, D. *Angew. Chem.-Int. Edit.* **2005**, *44*, 716. (b) Amir, R. J.; Shabat, D. *Chem. Commun.* **2004**, 1614. (c) Sagi, A.; Segal, E.; Satchi-Fainaro, R.; Shabat, D. *Bioorg. Med. Chem.* **2007**, *15*, 3720.

[25] (a) Ferreira, J. A. B.; Costa, S. M. B. *J. Photochem. Photobiol. A-Chem.* **2005**, *173*, 309. (b) Tornoe, C. W.; Christensen, C.; Meldal, M. *J. Org. Chem.* **2002**, *67*, 3057. (c) Rostovtsev, V. V.; Green, L. G.; Fokin, V. V.; Sharpless, K. B. *Angew. Chem.-Int. Edit.* **2002**, *41*, 2596. (d) Bernardes, G. J. L.; Kikkeri, R.; Maglinao, M.; Laurino, P.; Collot, M.; Hong, S. Y.; Lepenies, B.; Seeberger, P. H. *Org. Biomol. Chem.* **2010**, *8*, 4987.

[26] (a) Rosenzweig, B. A.; Ross, N. T.; Tagore, D. M.; Jayawickramarajah, J.; Saraogi, I.; Hamilton, A. D. *J. Am. Chem. Soc.* **2009**, *131*, 5020. (b) Fan, E. K.; Zhang, Z. S.; Minke, W. E.; Hou, Z.; Verlinde, C.; Hol, W. G. J. *J. Am. Chem. Soc.* **2000**, *122*, 2663. (c) Zhang, Z. S.; Merritt, E. A.; Ahn, M.; Roach, C.; Hou, Z.; Verlinde, C.; Hol, W. G. J.; Fan, E. *J. Am. Chem. Soc.* **2002**, *124*, 12991. (d) Ohta, T.; Miura, N.; Fujitani, N.; Nakajima, F.; Niikura, K.; Sadamoto, R.; Guo, C. T.; Suzuki, T.; Suzuki, Y.; Monde, K.; Nishimura, S. I. *Angew. Chem.-Int. Edit.* **2003**, *42*, 5186.

[27] Grünstein, D.; Maglinao, M.; Kikkeri, R.; Collot, M.; Barylyuk, K.; Lepenies, B.; Kamena, F.; Zenobi, R.; Seeberger, P. H. *J. Am. Chem. Soc.* **2011**, *133*, 13957.

[28] (a) Rich, R. L.; Myszka, D. G. *J. Mol. Recognit.* **2006**, *19*, 478. (b) Hardman, K. D.; Ainswort.Cf *Biochemistry* **1972**, *11*, 4910. (c) Dhayal, M.; Ratner, D. A. *Langmuir* **2009**, *25*, 2181. (d) Schlick, K. H.; Cloninger, M. J. *Tetrahedron* **2010**, *66*, 5305.

[29] (a) Kim, B. S.; Hong, D. J.; Bae, J.; Lee, M. *J. Am. Chem. Soc.* **2005**, *127*, 16333. (b) Jones, C. H.; Pinkner, J. S.; Roth, R.; Heuser, J.; Nicholes, A. V.; Abraham, S. N.; Hultgren, S. J. *Proc. Natl. Acad. Sci. U. S. A.* **1995**, *92*, 2081. (c) Choudhury, D.; Thompson, A.; Stojanoff, V.; Langermann, S.; Pinkner, J.; Hultgren, S. J.; Knight, S. D. *Science* **1999**, *285*, 1061. (e) Harris, S. L.; Spears, P. A.; Havell, E. A.; Hamrick, T. S.; Horton, J. R.; Orndorff, P. E. *J. Bacteriol.* **2001**, *183*, 4099.

[30] (a) Bosi, S.; Da Ros, T.; Spalluto, G.; Prato, M. *Eur. J. Med. Chem.* **2003**, *38*, 913. (b) Partha, R.; Conyers, J. L. *Int. J. Nanomed.* **2009**, *4*, 261. (c) Satoh, M.; Takayanag, I. *J. Pharmacol. Sci.* **2006**, *100*, 513. (d) Bakry, R.; Vallant, R. M.; Najam-Ul-Haq, M.; Rainer, M.; Szabo, Z.; Huck, C. W.; Bonn, G. K. *Int. J. Nanomed.* **2007**, *2*, 639. (e) Yamago, S.; Tokuyama, H.; Nakamura, E.; Kikuchi, K.; Kananishi, S.; Sueki, K.; Nakahara, H.; Enomoto, S.; Ambe, F. *Chem. Biol.* **1995**, *2*, 385.

[31] (a) Hirsch, A.; Lamparth, I.; Grosser, T.; Karfunkel, H. R. *J. Am. Chem. Soc.* **1994**, *116*, 9385. (b) Hirsch, A.; Vostrowsky, O. *Eur. J. Org. Chem.* **2001**, 829.

[32] (a) Iehl, J.; Nierengarten, J. F. *Chem.-Eur. J.* **2009**, *15*, 7306. (b) Iehl, J.; de Freitas, R. P.; Delavaux-Nicot, B.; Nierengarten, J. F. *Chem. Commun.* **2008**, 2450. (c) Compain, P.; Decroocq, C.; Iehl, J.; Holler, M.; Hazelard, D.; Barragan, T. M.; Mellet, C. O.; Nierengarten, J. F. *Angew. Chem.-Int. Edit.* **2010**, *49*, 5753. (d) Sigwalt, D.; Holler, M.; Iehl, J.; Nierengarten, J. F.; Nothisen, M.; Morin, E.; Remy, J. S. *Chem. Commun.* **2011**, *47*, 4640.

[33] (a) Cecioni, S.; Oerthel, V.; Iehl, J.; Holler, M.; Goyard, D.; Praly, J. P.; Imberty, A.; Nierengarten, J. F.; Vidal, S. *Chem.-Eur. J.* **2011**, *17*, 3252. (b) Nierengarten, J. F.; Iehl, J.; Oerthel, V.; Holler, M.; Illescas, B. M.; Munoz, A.; Martin, N.; Rojo, J.; Sanchez-Navarro, M.; Cecioni, S.; Vidal, S.; Buffet, K.; Durka, M.; Vincent, S. P. *Chem. Commun.* **2010**, *46*, 3860. (c) Compain, P.; Decroocq, C.; Iehl, J.; Holler, M.; Hazelard, D.; Barragan, T. M.; Mellet, C. O.; Nierengarten, J. F. *Angew. Chem.-Int. Edit.* **2010**, *49*, 5753.

---

[34] (a) Lis, H.; Sharon, N. *Chem. Rev.* **1998**, *98*, 637. (b) Sharon, N.; Lis, H. *Glycobiology* **2004**, *14*, 53R. (c) Lee, R. T.; Ichikawa, Y.; Kawasaki, T.; Drickamer, K.; Lee, Y. C. *Arch. Biochem. Biophys.* **1992**, *299*, 129. (d) Lee, Y. C.; Lee, R. T. *Accounts Chem. Res.* **1995**, *28*, 321. (e) Lundquist, J. J.; Toone, E. J. *Chem. Rev.* **2002**, *102*, 555. (f) Kitov, P. I.; Bundle, D. R. *J. Am. Chem. Soc.* **2003**, *125*, 16271.

[35] Hwang, S. Y.; Shin, J. H.; Hwang, J. S.; Kim, S. Y.; Shin, J. A.; Oh, E. S.; Oh, S.; Kim, J. B.; Lee, J. K.; Han, I. O. *Glia* **2010**, *58*, 1881.

[36] Fluri, F.; Grünstein, D.; Cam, E.; Ungethuem, U.; Hatz, F.; Schäfer, J.; Moch, H.; Schaeren-Wiemers, N.; Zeis, T.; Seeberger, P.H. *submitted*.

[37] (a) Laurent, S.; Forge, D.; Port, M.; Roch, A.; Robic, C.; Elst, L. V.; Muller, R. N. *Chem. Rev.* **2008**, *108*, 2064. (b) Mahmoudi, M.; Hofmann, H.; Rothen-Rutishauser, B.; Petri-Fink, A. *Chem. Rev.* **2012**, *112*, 2323.

[38] (a) De la Fuente, J. M.; Penades, S. *Biochim. Biophys. Acta-Gen. Subj.* **2006**, *1760*, 636. (b) Lartigue, L.; Oumzil, K.; Guari, Y.; Larionova, J.; Guerin, C.; Montero, J. L.; Barragan-Montero, V.; Sangregorio, C.; Caneschi, A.; Innocenti, C.; Kalaivani, T.; Arosio, P.; Lascialfari, A. *Org. Lett.* **2009**, *11*, 2992. (c) Earhart, C.; Jana, N. R.; Erathodiyil, N.; Ying, J. Y. *Langmuir* **2008**, *24*, 6215. (d) El-Boubbou, K.; Gruden, C.; Huang, X. *J. Am. Chem. Soc.* **2007**, *129*, 13392. (e) Liu, L. H.; Dietsch, H.; Schurtenberger, P.; Yan, M. D. *Bioconjugate Chem.* **2009**, *20*, 1349. (f) Liang, C. H.; Wang, C. C.; Lin, Y. C.; Chen, C. H.; Wong, C. H.; Wu, C. Y. *Anal. Chem.* **2009**, *81*, 7750.

[39] van Kasteren, S. I.; Campbell, S. J.; Serres, S.; Anthony, D. C.; Sibson, N. R.; Davis, B. G. *Proc. Natl. Acad. Sci. U. S. A.* **2009**, *106*, 18.

[40] Lai, C. H.; Lin, C. Y.; Wu, H. T.; Chan, H. S.; Chuang, Y. J.; Chen, C. T.; Lin, C. C. *Adv. Funct. Mater.* **2010**, *20*, 3948.

[41] Koizumi, J.; Yoshida, Y.; Nakazawa, T.; Ooneda, G.; *Jap. J. of Stroke.* **1986**, *8*, 1.

[42] Farr, T.; Grünstein, D.; Lai, C. H., Laettig, G.; Wang, C. C.; Harms, C.; Seeberger, P. H. *in preparation*.

[43] (a) Costa-Fernandez, J. M.; Pereiro, R.; Sanz-Medel, A. *Trac-Trends Anal. Chem.* **2006**, *25*, 207. (b) Xie, R. G.; Kolb, U.; Li, J. X.; Basche, T.; Mews, A. *J. Am. Chem. Soc.* **2005**, *127*, 7480. (c) Weiss, E. A.; Chiechi, R. C.; Geyer, S. M.; Porter, V. J.; Bell, D. C.; Bawendi, M. G.; Whitesides, G. M. *J. Am. Chem. Soc.* **2008**, *130*, 74. (d) Weiss, E. A.; Porter, V. J.; Chiechi, R. C.; Geyer, S. M.; Bell, D. C.; Bawendi, M. G.; Whitesides, G. M. *J. Am. Chem. Soc.* **2008**, *130*, 83. (e) Talapin, D. V.; Mekis, I.; Gotzinger, S.; Kornowski, A.; Benson, O.; Weller, H. *J. Phys. Chem. B* **2004**, *108*, 18826. (f) Jasieniak, J.; Mulvaney, P. *J. Am. Chem. Soc.* **2007**, *129*, 2841.

[44] (a) Carrillo-Carrion, C.; Cardenas, S.; Simonet, B. M.; Valcarcel, M. *Chem. Commun.* **2009**, 5214. (b) Giepmans, B. N. G.; Adams, S. R.; Ellisman, M. H.; Tsien, R. Y. *Science* **2006**, *312*, 217. (c) Liu, W. H.; Choi, H. S.; Zimmer, J. P.; Tanaka, E.; Frangioni, J. V.; Bawendi, M. *J. Am. Chem. Soc.* **2007**, *129*, 14530. (d) Clapp, A. R.; Medintz, I. L.; Mauro, J. M.; Fisher, B. R.; Bawendi, M. G.; Mattoussi, H. *J. Am. Chem. Soc.* **2004**, *126*, 301.

[45] (a) Howarth, M.; Liu, W. H.; Puthenveetil, S.; Zheng, Y.; Marshall, L. F.; Schmidt, M. M.; Wittrup, K. D.; Bawendi, M. G.; Ting, A. Y. *Nat. Methods* **2008**, *5*, 397. (b) Liu, W.; Howarth, M.; Greytak, A. B.; Zheng, Y.; Nocera, D. G.; Ting, A. Y.; Bawendi, M. G. *J. Am. Chem. Soc.* **2008**, *130*, 1274. (c) Howarth, M.; Takao, K.; Hayashi, Y.; Ting, A. Y. *Proc. Natl. Acad. Sci. U. S. A.* **2005**, *102*, 7583. (d) Stroh, M.; Zimmer, J. P.; Duda, D. G.; Levchenko, T. S.; Cohen, K. S.; Brown, E. B.;

Scadden, D. T.; Torchilin, V. P.; Bawendi, M. G.; Fukumura, D.; Jain, R. K. *Nat. Med.* **2005**, *11*, 678. (e) Robinson, A.; Fang, J. M.; Chou, P. T.; Liao, K. W.; Chu, R. M.; Lee, S. J. *ChemBioChem* **2005**, *6*, 1899. (f) Niikura, K.; Sekiguchi, S.; Nishio, T.; Masuda, T.; Akita, H.; Matsuo, Y.; Kogure, K.; Harashima, H.; Ijiro, K. *ChemBioChem* **2008**, *9*, 2623. (f) Higuchi, Y.; Oka, M.; Kawakami, S.; Hashida, M. *J. Control. Release* **2008**, *125*, 131.

[46] (a) Murray, C. B.; Norris, D. J.; Bawendi, M. G. *J. Am. Chem. Soc.* **1993**, *115*, 8706. (b) Peng, X. G.; Wickham, J.; Alivisatos, A. P. *J. Am. Chem. Soc.* **1998**, *120*, 5343. (c) William Yu, W.; Lianhua, Q.; Wenzhuo, G.; Xiaogang, P. *Chem. Mat.* **2003**, *15*, 2854. (d) Yu, W. W.; Wang, Y. A.; Peng, X. G. *Chem. Mat.* **2003**, *15*, 4300. (e) Yu, W. W.; Falkner, J. C.; Shih, B. S.; Colvin, V. L. *Chem. Mat.* **2004**, *16*, 3318. (f) Geyer, K.; Codee, J. D. C.; Seeberger, P. H. *Chem.-Eur. J.* **2006**, *12*, 8434. (g) Brivio, M.; Verboom, W.; Reinhoudt, D. N. *Lab Chip* **2006**, *6*, 329. (h) Mason, B. P.; Price, K. E.; Steinbacher, J. L.; Bogdan, A. R.; McQuade, D. T. *Chem. Rev.* **2007**, *107*, 2300.

[47] (a) Laurino, P.; Kikkeri, R.; Seeberger, P. H. *Nat. Protoc.* **2011**, *6*, 1209. (b) Kikkeri, R.; Laurino, P.; Odedra, A.; Seeberger, P. H. *Angew. Chem.-Int. Edit.* **2010**, *49*, 2054.

[48] (a) Kikkeri, R.; Lepenies, B.; Adibekian, A.; Laurino, P.; Seeberger, P. H. *J. Am. Chem. Soc.* **2009**, *131*, 2110. (b) Khorev, O.; Stokmaier, D.; Schwardt, O.; Cutting, B.; Ernst, B. *Bioorg. Med. Chem.* **2008**, *16*, 5216. (c) Babu, P.; Sinha, S.; Surolia, A. *Bioconjugate Chem.* **2007**, *18*, 146.

[49] (a) Jason-Moller, L.; Murphy, M.; Bruno, J. *Curr. Prot. Prot. Sci.*; John Wiley & Sons, Inc.: New York, **2006**; Chapter 19, Unit 19.13. (b) Homola, J. *Chem. Rev.* **2008**, *108*, 462. (c) Piliarik, M.; Vaisocherova, H.; Homola, *J. Methods Mol. Biol.* **2009**, 65. (d) Homola, J. *Anal. Bioanal. Chem.* **2003**, *377*, 528. (e) Hutter, E.; Fendler, J. H. *Adv. Mater.* **2004**, *16*, 1685. (f) Zhao, J.; Zhang, X. Y.; Yonzon, C. R.; Haes, A. J.; Van Duyne, R. P. *Nanomedicine* **2006**, *1*, 219.

[50] (a) Karakouz, T.; Vaskevich, A.; Rubinstein, I. *J. Phys. Chem. B* **2008**, *112*, 14530. (b) Vaskevich, A.; Rubinstein, I. *In Handbook of Biosensors and Biochips*; Marks, R., Cullen, D., Lowe, C., Weetall, H. H., Karube, I., Eds.; Wiley: Chichester, U.K., **2007**; Vol. 1. (c) Willets, K. A.; Van Duyne, R. P. *Annu. Rev. Phys. Chem.* **2007**, *58*, 267.

[51] (a) Bellapadrona, G.; Tesler, A. B.; Grünstein, D.; Hossain, L. H.; Kikkeri, R.; Seeberger, P. H.; Vaskevich, A.; Rubinstein, I. *Anal. Chem.* **2012**, *84*, 232. (b) Min, I. H.; Choi, L.; Ahn, K. S.; Kim, B. K.; Lee, B. Y.; Kim, K. S.; Choi, H. N.; Lee, W. Y. *Biosens. Bioelectron.* **2010**, *26*, 1326.

[52] (a) Ting, S. R. S.; Chen, G. J.; Stenzel, M. H. *Polym. Chem.* **2010**, *1*, 1392. (b) Marcos, M.; Martin-Rapun, R.; Omenat, A.; Serrano, J. L. *Chem. Soc. Rev.* **2007**, *36*, 1889. (c) Helms, B.; Mynar, J. L.; Hawker, C. J.; Frechet, J. M. J. *J. Am. Chem. Soc.* **2004**, *126*, 15020. (d) Zhang, A. F.; Zhang, B.; Wachtersbach, E.; Schmidt, M.; Schluter, A. D. *Chem.-Eur. J.* **2003**, *9*, 6083. (e) Chow, H. F.; Leung, C. F.; Li, W.; Wong, K. W.; Xi, L. *Angew. Chem.-Int. Edit.* **2003**, *42*, 4919. (f) Guo, Y. F.; van Beek, J. D.; Zhang, B. Z.; Colussi, M.; Walde, P.; Zhang, A.; Kroger, M.; Halperin, A.; Schluter, A. D. *J. Am. Chem. Soc.* **2009**, *131*, 11841. (g) Lau, K. N.; Chow, H. F.; Chan, M. C.; Wong, K. W. *Angew. Chem.-Int. Edit.* **2008**, *47*, 6912.

[53] (a) Mynar, J. L.; Choi, T. L.; Yoshida, M.; Kim, V.; Hawker, C. J.; Frechet, J. M. J. *Chem. Commun.* **2005**, 5169. (b) Lee, C. C.; Frechet, J. M. J. *Macromol.* **2006**, *39*, 476. (c) Hein, C. D.; Liu, X. M.; Wang, D. *Pharm. Res.* **2008**, *25*, 2216. (d) Fournier, D.; Hoogenboom, R.; Schubert, U. S. *Chem. Soc. Rev.* **2007**, *36*, 1369. (e) Soares, E. V.; Hebbelinck, K.; Soares, H. *Can. J. Microbiol.* **2003**, *49*, 336. (f) Chen, Z.; Meng, H. A.; Xing, G. M.; Chen, C. Y.; Zhao, Y. L.; Jia, G. A.; Wang, T. C.; Yuan, H.; Ye, C.; Zhao, F.; Chai, Z. F.; Zhu, C. F.; Fang, X. H.; Ma, B. C.; Wan, L. J. *Toxicol. Lett.*

2006, *163*, 109. (g) Campos, L. M.; Killops, K. L.; Sakai, R.; Paulusse, J. M. J.; Damiron, D.; Drockenmuller, E.; Messmore, B. W.; Hawker, C. J. *Macromol.* **2008**, *41*, 7063. (h) Connal, L. A.; Kinnane, C. R.; Zelikin, A. N.; Caruso, F. *Chem. Mat.* **2009**, *21*, 576.

[54] (a) Laurino, P.; Kikkeri, R.; Azzouz, N.; Seeberger, P. H. *Nano Lett.* **2011**, *11*, 73. (b) Booker-Milburn, K. I.; Anson, C. E.; Clissold, C.; Costin, N. J.; Dainty, R. F.; Murray, M.; Patel, D.; Sharpe, A. *Eur. J. Org. Chem.* **2001**, 1473. (c) Hook, B. D. A.; Dohle, W.; Hirst, P. R.; Pickworth, M.; Berry, M. B.; Booker-Milburn, K. I. *J. Org. Chem.* **2005**, *70*, 7558. (d) Ehrfeld, W.; Hessel, V.; Löwe, H. *Microreactors: New Technology for Modern Chemistry*; Wiley-VCH: Weinheim, **2000**. (e) *Microreactors in Organic Synthesis and Catalysis*; Wirth, T., Ed.; Wiley-VCH: Weinheim, **2008**; (f) *Chemical Reactions and Processes under Flow Conditions*; Luis, S. V., Garcia-Verdugo, E., Eds.; RSC Publishing: London, **2010**.

[55] (a) Stevens, M. M.; George, J. H. *Science* **2005**, *310*, 1135. (b) Langer, R.; Tirrell, D. A. *Nature* **2004**, *428*, 487. (c) Hutmacher, D. W. *J. Biomater. Sci.-Polym. Ed.* **2001**, *12*, 107. (d) Vogel, V.; Baneyx, G. *Annu. Rev. Biomed. Eng.* **2003**, *5*, 441. (e) Gentsch, R.; Börner, H. G. In *Bioactive Surfaces*; Borner, H. G., Lutz, J. F., Eds.; Springer-Verlag Berlin: Berlin, **2011**, *240*, 163.

[56] (a) Liang, D.; Hsiao, B. S.; Chu, B. *Adv. Drug Deliv. Rev.* **2007**, *59*, 1392. (b) Li, D.; Xia, Y. *Adv. Mater.* **2004**, *16*, 1151. (c) Gentsch, R.; Boysen, B.; Lankenau, A.; Börner, H. G. *Macromol. Rapid Commun.* **2010**, *31*, 59.

[57] (a) Ma, Z. W.; He, W.; Yong, T.; Ramakrishna, S. *Tissue Eng.* **2005**, *11*, 1149. (b) Kim, T. G.; Park, T. G. *Tissue Eng.* **2006**, *12*, 221.

[58] (a) Lepenies, B.; Seeberger, P. H. *Immunopharmacol. Immunotoxicol.* **2010**, *32*, 196. (b) Lepenies, B.; Yin, J. A.; Seeberger, P. H. *Curr. Opin. Chem. Biol.* **2010**, *14*, 404. (c) Miller, S. I.; Ernst, R. K.; Bader, M. W. *Nat. Rev. Microbiol.* **2005**, *3*, 36. (d) Taylor, M. E.; Conary, J. T.; Lennartz, M. R.; Stahl, P. D.; Drickamer, K. *J. Biol. Chem.* **1990**, *265*, 12156.

Chapter 2

A New Bifunctional Chelator for [$^{99m}Tc(CO)_3$]$^+$-Based Radiolabeling of Biomolecules and *In Vivo* Evaluation with Carbohydrates

---

The results reported in this chapter have been partially published in:

Barandov, A.; Grünstein, D.; Apostolova, I.; Roger, M.; Buchert, R.; Abram, U.; Brenner, W.; Seeberger, P.H. in preparation. A.B. and D.G. contributed equally to this work.

Table of Contents

Abstract

Bifunctional chelators, that simultaneously coordinate technetium-99m-metal (^{99m}Tc) cores and tether biomolecules for selective targeting and imaging of specific organs, are keys to developing modern radiodiagnostics.

Described is the synthesis of a new bifunctional tridentate chelator that is prepared in two steps. The chelator was successfully conjugated with the monosaccharides galactose, glucose, and mannose. Each conjugate reacted efficiently with the organometallic precursor $[M(CO)_3]^+$ [M = rhenium (Re), ^{99m}Tc] to selectively form neutral metal(I) tricarbonyl complexes. The electronically-equivalent, non-radioactive metal Re was used to confirm the tridentate coordination mode of the ligand by spectroscopic means and single crystal X-ray analyses.

The ^{99m}Tc-labeled chelator and glycoconjugates were efficiently prepared by efficient and straight forward labeling at moderate temperatures and with short reaction times.

Biodistribution of the radioactive-^{99m}Tc-labeled glycoconjugates was examined in mice. Noticeably different biodistribution patterns were observed, reflecting trends in the uptake of carbohydrate analogues by various organs.

1. Introduction

Carbohydrates are involved in numerous processes vital to living organisms including structure, metabolism, and communication. The breadth of cellular functions such as fertility and development, molecular recognition and surface adhesion, cell signaling, and inflammatory responses regulated by these biomolecules renders glycan-based tools important for biomedical research and drug development.[1]

The emergence of the radiolabeled glycan, 2-^{18}F-fluoro-2-deoxyglucose (^{18}FDG), was a breakthrough in mapping glucose metabolism *in vivo*.[2] ^{18}FDG is now a preeminent radiotracer for positron emission tomography, and is currently used for lung cancer diagnostics, as well as heart and brain imaging.[3] However, despite an overall good clinical performance as a radiopharmaceutical, ^{18}FDG has generated both false positive and negative results when used in cancer-imaging, limiting its use to some clinical settings.[4] Moreover, the cyclotron-produced fluorine-18 (^{18}F) isotope has a short half-life ($t_{1/2}$ = 1.8 h) significantly restricting its distribution range and availability. Accordingly, there is a growing need to develop new glycoconjugates containing more stable radioactive isotopes.

The ^{99m}Tc isotope, readily generated by relatively inexpensive ^{99m}Tc-nuclide generators with a half-life of six hours and $E\gamma$ = 140.5 KeV, possesses near-ideal nuclear properties for an isotope used in single photon emission computed tomography (SPECT). Consequently, as the "work horse" of the field it is used in more than 80% of all diagnostic examinations carried out worldwide.[5] However, designing the architecture of a suitable metalloradionuclide-based targeting agent requires special consideration. In contrast to the integrative radiotracers, where the addition of conventional isotopes such as ^{18}F, carbon-11 (^{11}C), and nitrogen-13 (^{13}N) does not impose drastic structural or electronic changes to the biomolecule, it is a substantial challenge to insert a radioactive metal isotope while retaining the targeting vector's affinity.[6]

Most often, bifunctional chelators (BFCs) are employed as the scaffold to simultaneously bind the biologically-relevant targeting molecule and the metalloradionuclide in radiolabelling assays.[7] The chelator alone can dramatically influence biodistribution of the final ^{99m}Tc-complex as proven during the development of second generation of ^{99m}Tc-diagnostic agents.[8] For instance, the moderately lipophilic chelator hexamethylpropyleneamineoxime (HMPAO) forms a neutral Tc(V) complex that is successfully utilized for brain imaging, while the positively charged complexes of multidentate phosphines such as ^{99m}Tc-Tetrofosmin and ^{99m}Tc-TechneCard are currently used as myocardial perfusion agents for heart imaging.[9]

Chelators to stabilize technetium ions in various oxidation states have been designed and synthesized.[10] The organometallic *fac*-[^{99m}Tc(CO)$_3$]$^+$ moiety is a remarkable core for developing new target-specific radiopharmaceuticals.[11] This precursor relies on a straightforward aqueous synthesis, is stable over a wide pH range, and reactive with various types of chelators upon substitution of coordinated water molecules. Despite the interest in developing new bifunctional tridentate ligands for this versatile technetium core, most chelators to date have been picolylamine or histidine derivatives. These compounds are generally comprised of tertiary amine and/or carboxylic acid residues at the chelating sites, which are considered to be hard bases for a soft metal ion like Tc(I).[12] Moreover, dipicolylaminealkylcarboxylates have been used for ^{99m}Tc-labeling of various peptides and carbohydrates; they impose formal positive charges of the metal ion to the resulting radiotracer. Chelator which can form neutral complexes with the *fac*-[^{99m}Tc(CO)$_3$]$^+$ moiety are rare.[13]

In this chapter, I describe the synthesis and characterization of a bifunctional tridentate chelator 2-[[(2-hydroxy-5-carboxyphenyl)amino]methyl]pyridin (HCPAMP) with an unprecedented molecular structure. HCPAMP forms well-defined neutral complexes with both Re and ^{99m}Tc. To illustrate the potential of the system, galactose, glucose, and mannose ^{99m}Tc-HCPAMP glycoconjugates were prepared. *In vivo* biodistribution of the resulting radiotracers was examined and revealed significant differences in organ uptake, likely a consequence of the biological activities of the three different targeting glycans.

2. Results and Discussion

2.1. Ligand Synthesis and Characterization

The bifunctional tridentate ligand HCPAMP **3** was synthesized in two steps (Scheme 1). Firstly, 3-amino-4-hydroxybenzoic acid **1** and excess 2-formylpyridine were reacted to afford (2-[[(2-hydroxy-5-carboxyphenyl)imino]methyl]pyridin) HCPIMP **2** as a yellow solid. Previous studies showed that the imine is potentially subject to unwanted dissociative or rearrangement reactions, such as solvolysis or metal-induced dissociation, over the desired chelation.[14] To avoid such side reactions, and at the same time enhance the chemical stability and physical flexibility of the final ligand system, the imine residue of **2** was reduced using sodium borohydride ($NaBH_4$) to furnish the desired ligand HCPAMP **3**.[15] Since hydroxyl residues are prone to react with carbodiimides that are used as carboxylic acid-activating agents, the hydroxyl group of **3** was protected by reacting it with *tert*-butyldimethylsilylchloride (TBDMSCl), prior to coupling with the glycan building blocks to form **4**.[16]

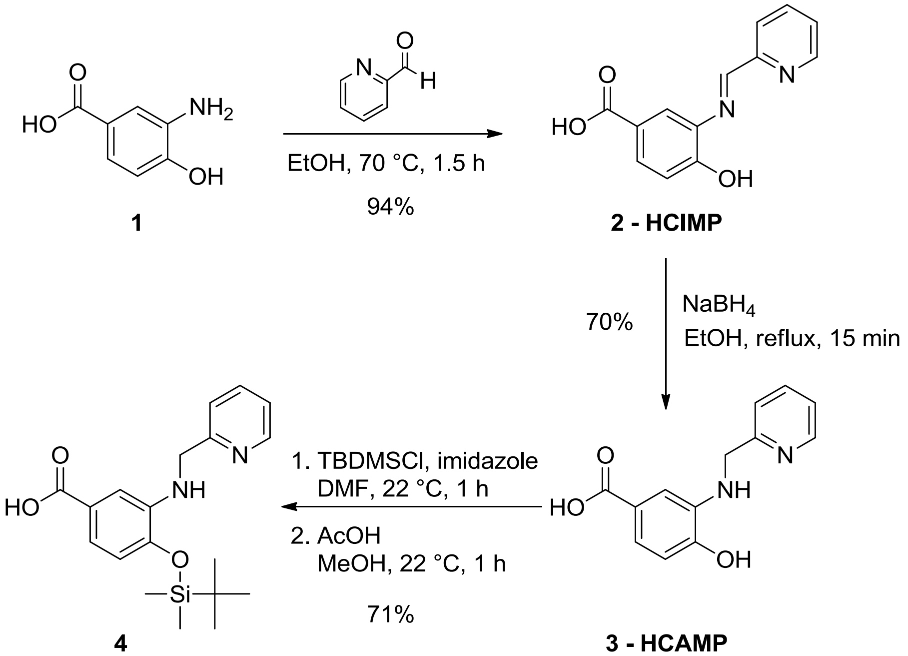

Scheme 1. Synthesis of tridentate bifunctional ligand HCPAMP **3** and protection of the hydroxyl group to form protected chelator **4**.

The azomethine proton (–C(*H*)=N) resonance of **2** –a singlet at δ 8.70 ppm– is absent from the ^{1}H NMR spectrum of **3**. Compound **4** shows three singlets at δ 4.54, 1.06, and 0.30 ppm corresponding to methylene [–N(H)–CH_2], *tert*-butyl [–Si–C–(CH_3)$_3$] and methyl [–Si–(CH_3)$_2$] protons, where the later protons are shifted due to their proximity to the silicium (Si) atom.[17] Moreover, the ^{13}C NMR spectrum of **4** confirms the presence of the hydroxyl protecting group with a high-field shifted singlet at δ -4.07 ppm associated with the methyl carbon of the silylated residue [O–Si–(CH_3)$_2$].[18]

Prior to conjugation to HCPAMP, an amine linker was installed at the anomeric position of galactose, glucose, and mannose using standard glycosylation chemistry to afford compounds **5–7**.[19] Carbohydrate-HCPAMP conjugates **8–10** were synthesized by the reaction of **4** with **5–7** in the presence of dicyclohexylcarbodiimide (DCC) and hydroxybenzotriazole (HOBt). Finally, all actetyl and *tert*-butyldimethylsilyl groups were cleaved using sodium hydroxide (NaOH) to afford glycoconjugates Gal-HCPAMP **11**, Glc-HCPAMP **12**, and Man-HCPAMP **13** (Scheme 2).[20]

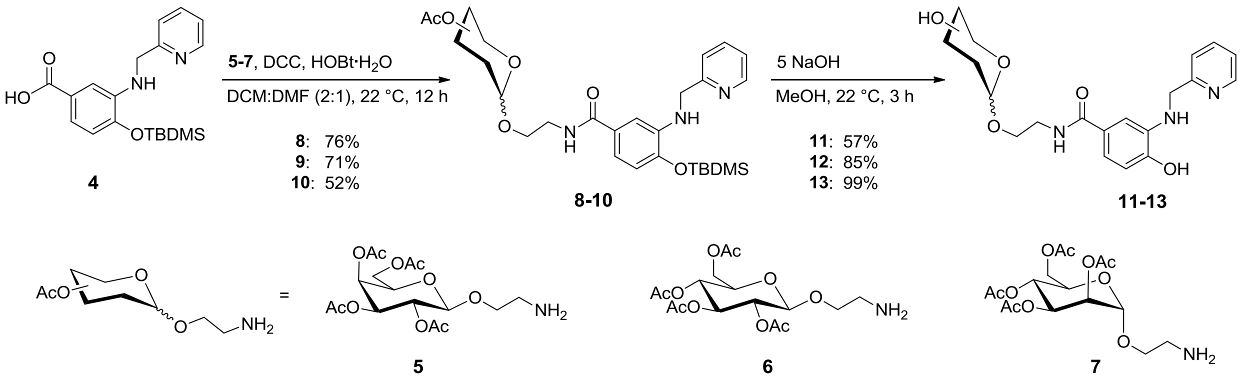

Scheme 2. Synthesis of glycoconjugates **11–13**.

2.2. Syntheses and Characterization of Re Complexes

HCPAMP **3** was designed to simultaneously stabilize the *fac*-[M(CO)$_3$]$^+$ (M = Re, ^{99m}Tc) moiety, while allowing for conjugation with biomolecules. The multidentate ligand **3** was designed to bind the metal core with a higher binding affinity than the competing conjugated carbohydrates. The specific mode of HCPAMP-metal binding was assessed by spectroscopic analysis using the electronically-equivalent, non-radioactive metal Re(I) tricarbonyl synthon [ReBr$_3$(CO)$_3$]$^{2-}$, because ^{99m}Tc is available only in radiotracer concentrations (nM to pM).

The HCPAMP-metal complex **14** was synthesized by reacting [NEt$_4$]$_2$[ReBr$_3$(CO)$_3$] with HCPAMP **3** in the presence of triethylamine (Et$_3$N) at 50 °C to afford the neutral complex **14** as a microcrystalline solid (Scheme 4). To characterize the molecular structure of the radiolabeled HCPAMP-carbohydrate (HCPAMP-carb) and investigate the selectivity of the labeling process, the galactose glycoconjugate **11** was reacted with $[NEt_4]_2[ReBr_3(CO)_3]$ under conditions similar to those applied to the synthesis of **14**. Reaction progress was monitored by *in situ* mass spectrometry, where completion was indicated by detection of **15** [*m/z* = 720 ($[M+H]^+$)] as the only Re-containing compound. After purification of the crude mixture, **15** was isolated as a pale yellow solid (Scheme 4).

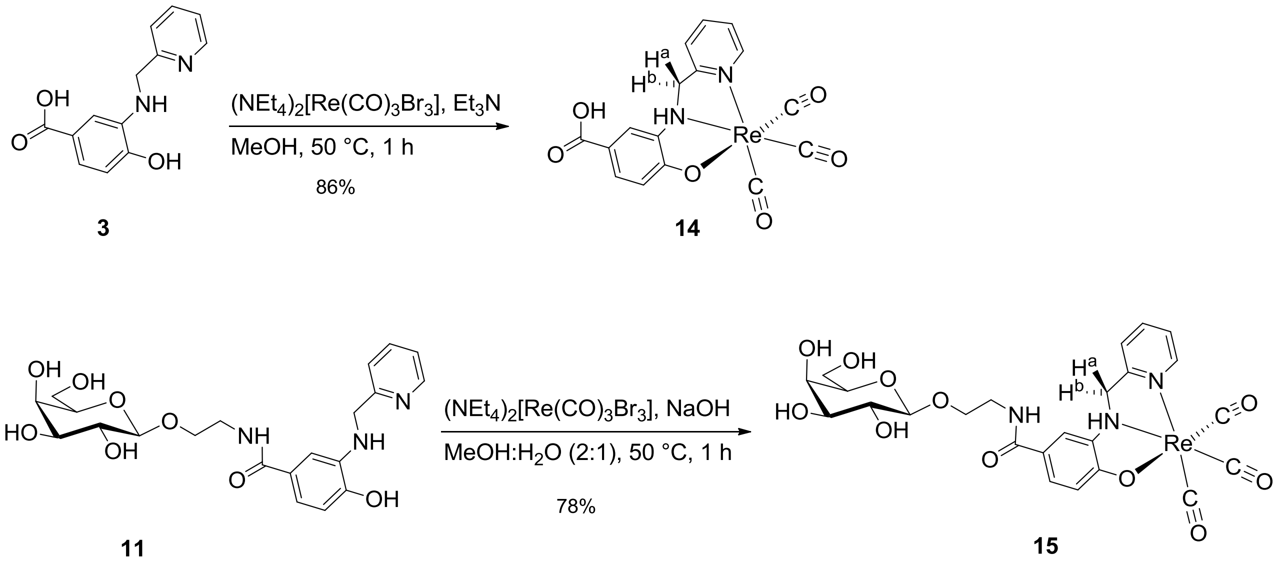

Scheme 3. Synthesis of Re complexes **14** and **15**.

The ^1H NMR spectra of both complexes **14** and **15** exhibited two doublets between δ 4.80 and 5.0 ppm with coupling constants of *J* = 15.7 and 15.8 Hz, respectively, which are consistent with the geminal coupling of a methylene residue in a five-membered ring (Table 1, Figure 1A).[21] Both nitrogen atoms of HCPAMP **3** are coordinated with Re to form a five-membered chelate ring. It should be noted that the hydroxyl groups of the galactose residue in **15** do not participate in the coordination sphere proving that HCPAMP has a higher affinity for the metal core and that the sugar subunit remains intact upon labeling. As expected for Re(I) tricarbonyl complexes, three down-field shifted signals between δ 196 and 199 ppm in ^{13}C NMR spectra of **14** and **15** are assigned to the three magnetically non-equivalent terminal tricarbonyls.[22]

The IR spectra of **14** and **15** exhibit a sharp, strong band in the range of 2010–2030 cm^{-1}, and a broad, intense absorption in the range of 1870–1890 cm^{-1}, attributed to ν(C–O) of the *fac*-$[Re(CO)_3]^+$ unit (Figure 1B).[23]

Table 1. Chemical shifts (δ) and coupling constants (J) of the geminal protons H^a and H^b of [–N(H)–CH_2] in **14** and **15**.

Compound	H^a δ (ppm)	J (Hz)	H^b δ (ppm)	J (Hz)
14	4.96	15.7	4.90	15.7
15	5.00	15.8	4.97	15.8

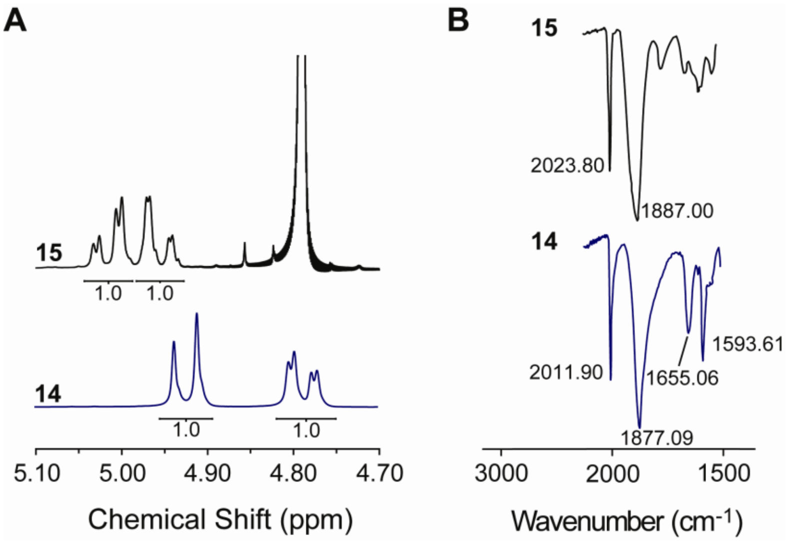

Figure 1. (A) ^1H NMR spectra (region enlarged) for **14** (in DMSO) and **15** (in D_2O). (B) IR spectra (region enlarged) of **14** and **15**.

For single-crystal X-ray diffraction, $[Re(CO)_3(HCPAMP)]$ **14** was recrystallized by cooling a saturated methanol solution to -25 °C and produced colorless needles of **14·MeOH**. The solid state molecular structure of **14** was determined by single-crystal X-ray diffraction and confirmed the spectroscopic analyses (Figure 2). The Re atom is six-coordinated, displaying a distorted octahedral coordination geometry. Negatively charged $[HCPAMP]^-$ coordinates the triangular face of the polyhedron with [*N*,*N*',*O*] atoms and the three remaining coordination sites are occupied by the terminal carbonyl ligands. The N1–Re bond length [2.222(5) Å] is within the expected range, based on reports of similar complexes containing 2-

aminomethylpyridine residues.[24] The carboxylic residue is exposed, lying outside the coordination sphere, and consequently has an ideal configuration for bioconjugation purposes. Together, these analyses demonstrate that HCPAMP is an ideal bifunctional ligand system for $[M(CO)_3]^+$ moieties, forming neutral complexes in solution and solid state. In contrast to previously reported bifunctional chelators that form complexes with $[M(CO)_3]^+$, the coordination site of the ligand system does not contain carboxylic acid or tertiary amine residues that are relatively hard bases for the soft Re(I) and Tc(I) metal ions.[25]

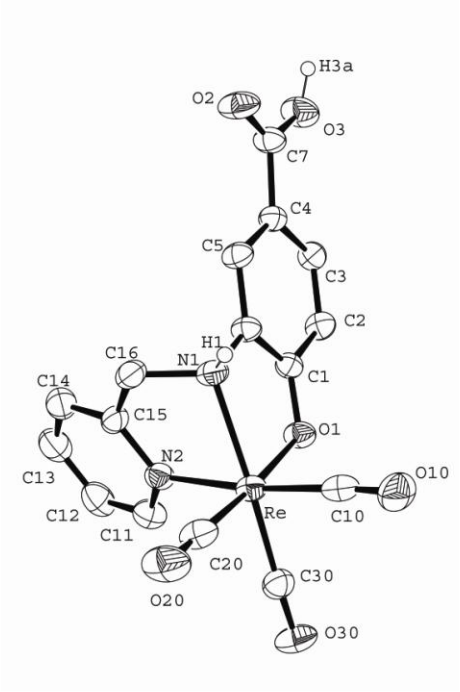

Figure 2. ORTEP plot of the molecular structure of **14** in the solid state. Thermal ellipsoids are set at the 40% probability level. Hydrogen atoms bonded to carbon atoms are omitted for clarity. Selected bond lengths [Å] and angles [°] of **14**: Re–C10 1.918(8), Re–C20 1.910(7), Re–C30 1.919(7), Re–O1 2.131(4), Re–N1 2.222(5), Re–N2 2.172(6), C10–Re–N1 100.3(3), C20–Re–O1 175.7(2), C30–Re–N2 96.7(3), C10–Re–C20 87.8(3), C10–Re–C30 87.7(3).

2.3. ^{99m}Tc-labeling of HCPAMP and Glycoconjugates

In anticipation of potential clinical applications, radiolabeling of HCPAMP and glycoconjugates was performed in a single step, using a "kit-like" approach, by adapting the procedure for the synthesis of the $[^{99m}Tc(H_2O)_3(CO)_3]^+$ precursor developed by Alberto *et al.*[26] A solution of $[^{99m}Tc(H_2O)_3(CO)_3]^+$ was adjusted to pH 7–8 by dropwise addition of aqueous hydrochloric acid (HCl) and phosphate buffered saline (PBS) solutions prior to the radiolabeling processes.[27] The

^{99m}Tc-labeled compounds [^{99m}Tc(CO)$_3$(HCPAMP)] **16** and [^{99m}Tc(CO)$_3$(HCPAMP-carb)] (Carb = Gal **17**; Glc **18**; Man **19**) were synthesized by the reaction of [^{99m}Tc(H$_2$O)$_3$(CO)$_3$]$^+$ with an aqueous solutions of HCPAMP or HCPAMP-carb **11–13** at pH 7–8 and 45 °C (Scheme 4). Radiochemical yield and purity of [^{99m}Tc(H$_2$O)$_3$(CO)$_3$]$^+$ as well as of **16–19** were verified by HPLC analysis.

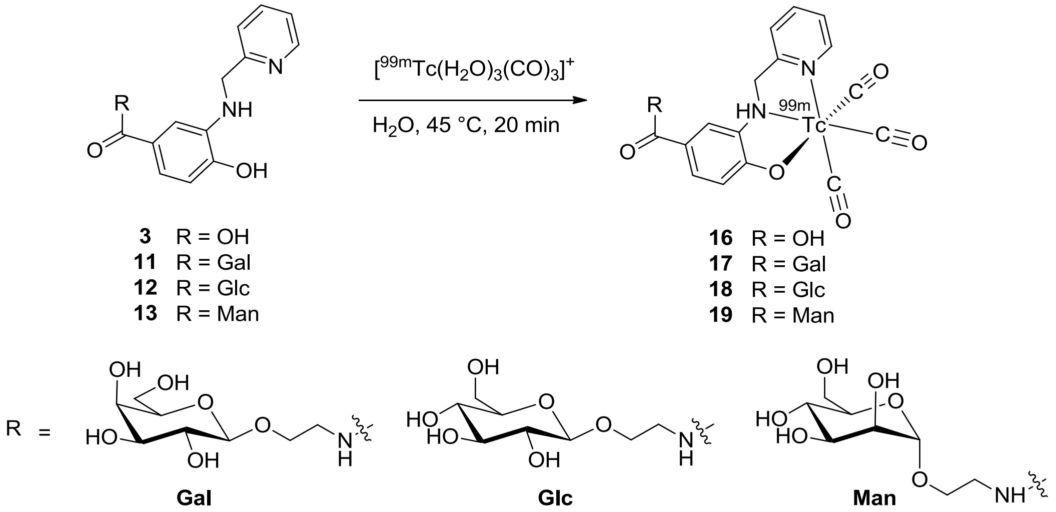

Scheme 4. ^{99m}Tc-radiolabeling of HCPAMP **3** and its glycoconjugates **14–16** to form the radiolabelled compounds **16–19**.

The labeled derivatives **16** and **17** were characterized by comparing the radioactive and UV traces of the isostructural Re and ^{99m}Tc complexes. In all cases, the retention times of the congener Re and Tc complexes were comparable (Table 2, Figure 3). The structures of the compounds are identical whether characterized at the tracer level (^{99m}Tc complexes) or macroscopic scale (Re complexes).

Table 2. HPLC retention times and radiochemical yields of the Re and ^{99m}Tc complexes detected with UV-detector at 230 nm or γ-detector.

Compound	**Retention time t$_R$ (min)**	**Radiochemical yield (%)**
14; **16**	17.48 (M = Re); 17.80 (M = ^{99m}Tc)	99.6
15; **17**	18.83 (M = Re); 19.05 (M = ^{99m}Tc)	98.1

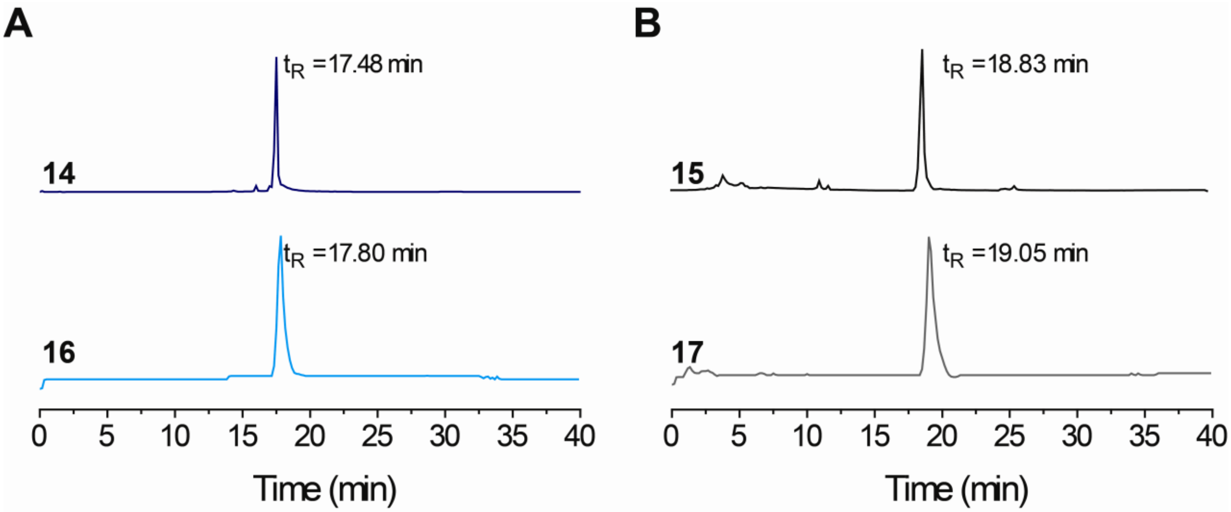

Figure 3. HPLC traces (A) for the complexes **14** (top) and **16** (bottom) and (B) for the complexes **15** (top) and **17** bottom). Re complexes **14** and **15** were detected with an UV-detector at 230 nm. ^{99m}Tc complexes **16** and **17** were detected using a γ-detector.

All three ^{99m}Tc-labeled glycoconjugates exhibited comparable radioactive traces in HPLC analyses confirming the expected structures (Table 3, Figure 4). Radiochemical yields (> 96%) of all the ^{99m}Tc-labeling products were ideal for *in vivo* applications.

Table 3. HPLC retention times and radiochemical yields of ^{99m}Tc complexes **17–19** detected using a γ-detector.

Compound	**Retention time t_R (min)**	**Radiochemical yield (%)**
17	19.05	98.1
18	19.41	96.1
19	19.29	96.1

19

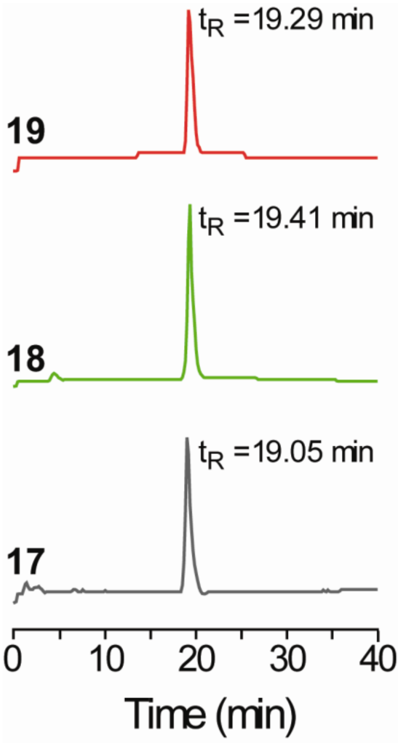

Figure 4. HPLC traces for the complexes **17–19** detected using a γ-detector.

2.4. Octanol-water Partition Coefficients

The octanol-water partition coefficients (log $P_{o/w}$ values) of complexes **16–19** are listed in Table 4. Compound **16** shows higher hydrophilicity compared to the glycan-conjugated analogs **17–19** at physiological pH. This trend can be explained by the presence of the negatively charged carboxylate group in **16** at pH 7.4 ($4 < pK_a < 5$).[28]

Table 4. Log $P_{o/w}$ values of complexes **16–19**.

Compound	**log $P_{o/w}$**
16	-0.416 ± 0.002
17	-0.270 ± 0.001
18	-0.239 ± 0.000
19	-0.012 ± 0.000

2.5. *In vivo* SPECT Imaging and *ex vivo* Biodistribution Studies

Using the kit approach and $[^{99m}Tc(CO)_3]^+$, compounds **3** and **11–13** were ^{99m}Tc-radiolabeled. Radiolabeled compounds **16–19** were obtained by incubating HCPAMP or the HCPAMP-carb with a solution of $[^{99m}Tc(H_2O)(CO)_3]^+$. The reproducibility of this process *via* a single step was compared by HPLC analysis in multiple trials. The radiochemical purity of the tracers was assessed by radio-TLC prior to injection.

Radiotracers **16–19** were individually injected into healthy mice and their biodistribution was investigated at 0.5 h, 1.3 h and 4.0 h after injection using SPECT/CT imaging (Figure 5). The early SPECT scan at 0.5 h after tracer post injection (p.i.) revealed organ uptake of the radio-labeled sugar analogues **17–19** in the following order: bladder (urine) > bowel > liver > spleen >kidneys >heart ≈ lungs (Figure 5). The high uptake in the bowel and the bladder suggests excretion of the tracers *via* both the gastrointestinal tract and the kidneys.

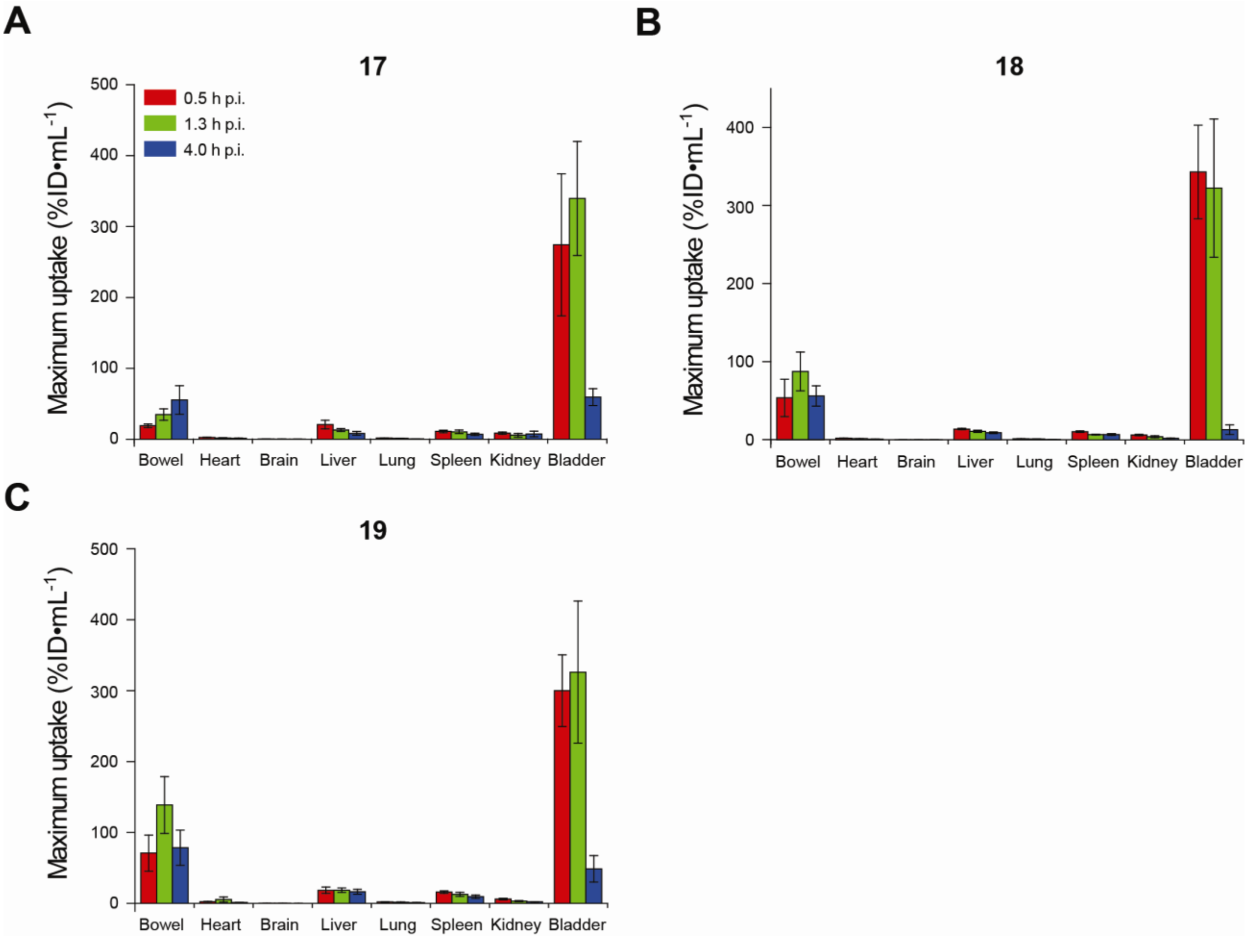

Figure 5. Biodistribution of ^{99m}Tc-labeled glycoconjugates (A) **17** Gal-, (B) **18** Glc-, and (C) **19** Man-HCPAMP in healthy mice (%ID·mL^{-1}). The biodistribution was measured at different time points (indicated). Bars and error bars indicate means of N = 5 [**17** and **18**] and N = 6 [**19**] per group ± standard error (S.E.).

The radiolabeled chelator [^{99m}Tc(CO)$_3$(HCPAMP)] **16** showed significantly lower uptake than the sugar analogues in heart, liver, lungs, spleen and kidneys suggesting specific uptake of the sugar analogues in these organs (Figure 6). Large concentration of **16** was observed in the bowel and the bladder indicating excretion *via* the gastrointestinal tract and the kidneys similar to the sugar analogues.

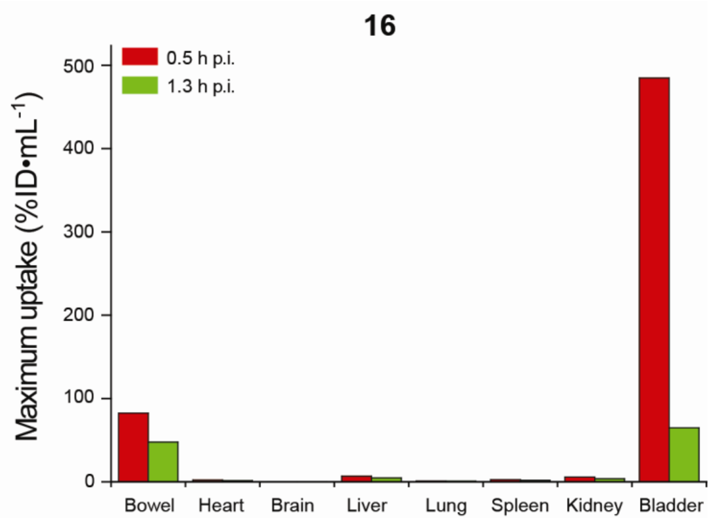

Figure 6. Biodistribution of control ^{99m}Tc(CO)$_3$(HCPAMP)] **16** in healthy mice (%ID·mL^{-1}). The biodistribution was measured at different time points (indicated). Bars indicate means of N = 1 per measurement.

The four SPECT images of the conjugate-injected mice acquired at 1 h p.i. illustrate subtle specific differences between the radiotracers (Figure 7). The striking difference in the biodistribution of the radiolabelled glycoconjugates **17–19** in contrast to **16**, strongly suggests that organ uptake is mainly determined by specific activity of the attached glycan residues.

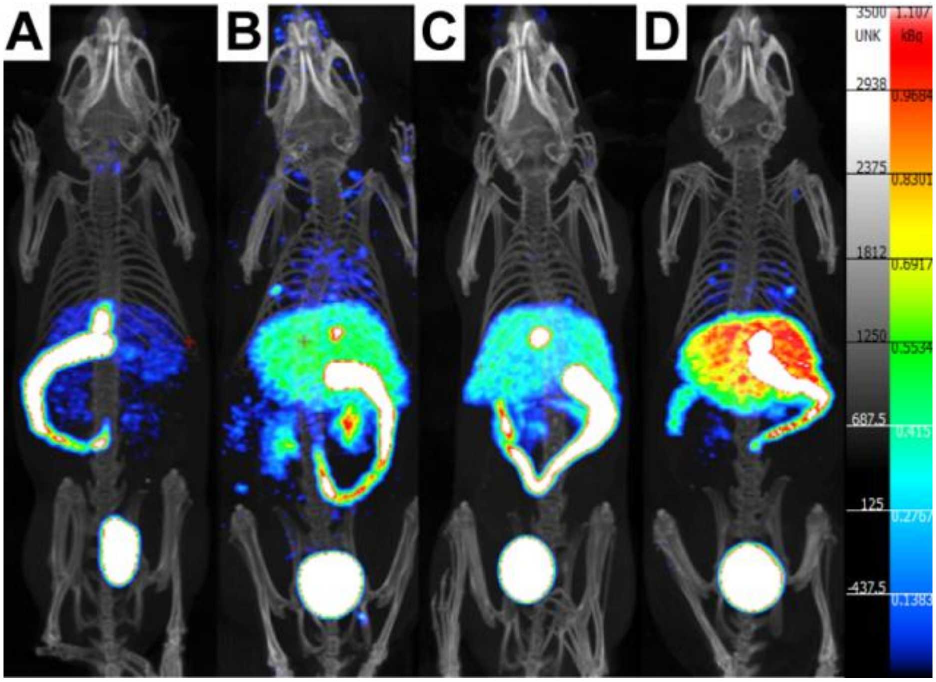

Figure 7. *In vivo* whole body SPECT/CT projection of mice injected with either (A) **16**, (B) **17**, (C) **18**, and (D) **19** 1 h p.i. Intensity levels are market on the right.

Ex vivo direct measurements of radioactivity levels in the organ tissues were performed after sacrificing the mice at 4.5 h p.i and the values correlated with the SPECT acquisition data (Figure 8). Overall, the highest organ uptake and retention was seen with mannose conjugate **19** in the liver. Mannose receptors are strongly expressed on Kupffer and sinusoidal endothelial cells in the liver, facilitating preferential and selective uptake of mannose derivatives.[29] Compound **17** had the second highest retention time in the liver, possibly because of interactions between galactose and asialoglycoproteins, lectins that are expressed exclusively in hepatic parenchymal cells in the liver.[30] Trace amounts were measured in the brain, however this observation most likely represents radiotracer activity in the fractional blood volume of the brain rather than specific uptake into brain tissue.

In clear contrast to ^{18}FDG, the blood brain barrier is impermeable to the radiolabeled glycoconjugates, which was anticipated due to hydrophilicity of the compounds **17–19** (log $P_{o/w} < 0$). This system was not designed to be a metabolism imaging agent as it is for ^{18}FDG, but instead a means to image carbohydrate–receptor interactions.[31]

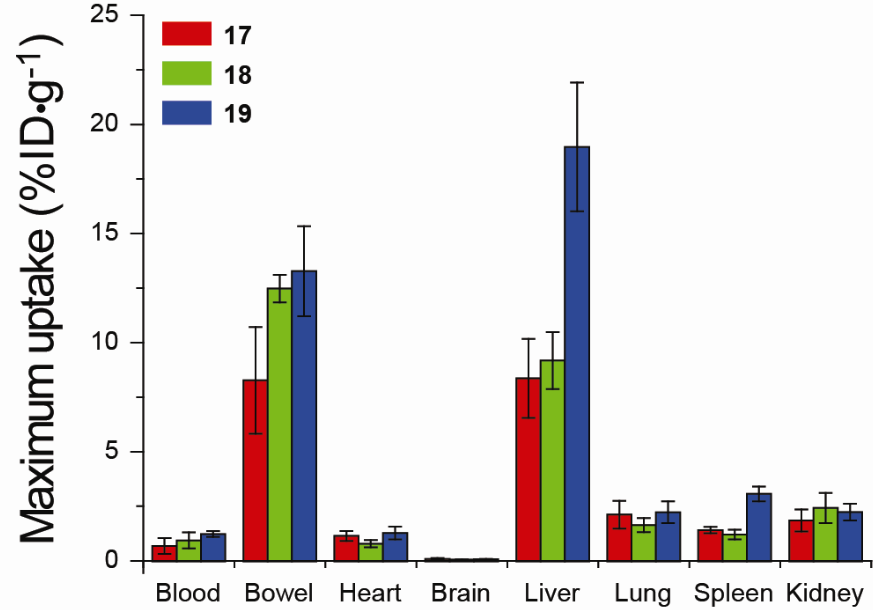

Figure 8. Post-mortem biodistribution of the ^{99m}Tc-labelled glycoconjugates **17**, **18** and **19** in organs extracted from healthy mice (%ID·g^{-1}) after 4.5 h. Bars and error bars indicate means of N = 5 [**17** and **18**] and N = 6 [**19**] per group ± S.E.

3. Conclusion

Chapter 2 described the synthesis and characterization of a novel tridentate bifunctional chelator HCPAMP, that forms well-defined neutral complexes with $[M(CO)_3]^+$ (M = Re, ^{99m}Tc) moieties. In contrast to previously reported chelators designed for Re and Tc tricarbonyl cores, the coordination site of HCPAMP does not include either tertiary amine or carboxylic acid residues, and does not impose positive or negative formal charges to the final radioactive tracer.

The carbohydrate conjugates of the chelator were obtained by conventional amide coupling with different sugars (galactose, glucose and mannose). The galactose complex HCPAMP-Gal reacted with Re(I) tricarbonyl by forming $[Re(CO)_3(HCPAMP\text{-}Gal)]$. The ^{99m}Tc-radiolabeling of HCPAMP as well as its monosaccharide conjugates were performed in a single step using a ^{99m}Tc tricarbonyl labeling kit. The high radiochemical yield (> 96%) of the labeling reactions as well as the radio-purity of the products $[^{99m}Tc(CO)_3(HCPAMP\text{-}carb)]$ were assessed by HPLC analysis.

The radioactive tracers **16–19** showed significant differences in their biodistribution patterns and body clearance times, despite the relatively minor structural variations of the monosaccharides.

Synthesis and subsequent investigation of the *in vivo* characteristics of this novel class of compounds is the focus of ongoing studies. Ultimately, the full potential of this new bifunctional chelator will be realized through conjugation with complex oligosaccharides to take advantage of the high binding affinities of those molecules for certain organ or tumor-specific lectins. Exploring the physiological functioning and biodistribution of more complex carbohydrates by radiolabelling their conjugates of the chelator HCPAMP is the subject of our current studies.

4. Experimental Part

4.1. Chemical Synthesis

4.1.1. General Experimental Details

Commercial grade reagents and solvents were used without further purification except as indicated below. Deionized water was obtained from an in-house purification system (Millipore). The term "concentrated under reduced pressure" refers to the removal of solvents and other volatile material using a rotary evaporator while maintaining a water bath temperature around 40 °C. The compounds purified by flash chromatography are further concentrated by the removal of residual solvent under high vacuum (< 0.2 mbar). Room temperature (r.t.) refers to the ambient temperature (20–25 °C).

4.1.2. Physical Properties and Spectroscopic Measurements

^{1}H NMR and ^{13}C NMR spectra were measured with a Varian 400-MR, Varian 600-MR, Bruker ECP 400, Bruker AC 500, or Bruker AC 700 spectrometer. The residual proton signal of solvent at δ 7.26 ppm for $CDCl_3$, 2.50 ppm for DMSO, and 4.79 ppm for D_2O was used as an internal reference for ^{1}H spectra. For ^{13}C spectra, the chemical shifts are reported relative to the δ 77.36 ppm for $CDCl_3$ and 39.51 ppm for DMSO. Coupling constants (J) are reported in Hertz (Hz). Multiplicities are given as: *s* (singlet); *d* (doublet); *t* (triplet); *dd* (doublets of doublet); *ddd* (doublets of doublets of doublet); *q* (quartet); *m* (multiplet); *dt* (doublets of triplet) or *td* (triplets of doublet). High-resolution mass spectra (HRMS) analyses were performed by the mass service of the Free University Berlin. ESI mass spectra were run on an Agilent 6210 ESI-TOF mass spectrometer. Infrared (IR) spectra were recorded on a Spectrum 100 FTIR spectrophotometer (Perkin-Elmer). Bands are described as: m (medium); s (sharp); w (wide) or vs (very sharp). Analytical thin layer chromatography (TLC) was performed on Kieselgel 60 F_{254} glass plates precoated with a 0.25 mm thickness of silica gel. The TLC plates were visualized with UV light and by staining with Hanessian solution (ceric sulfate and ammonium molybdate in aqueous sulfuric acid) or potassium permanganate solution (potassium permanganate in basic aqueous solution). Column chromatography was performed using Kieselgel 60 (230–400 mesh) silica gel with a typical 50–100:1 weight ratio of silica gel to crude product.

4.1.3. Analytical Purification

Analytical HPLC analyses were carried out on a Merck-Hitachi L6200 system equipped with an UV-detector (Merck Hitachi L-4250) and γ radiation-detector (Beckmann, 171 radioisotope detector). The separation was performed on a C-18 (AA 137) column (Knauer GmbH, Berlin, Germany) and all compounds were eluted with a linear gradient of water:MeCN:0.1% TFA. Preparative HPLC was performed using an Agilent 1200 HPLC apparatus with Prep C-18 column, and a mixture of water:MeCN:0.1% TFA. UV signals were detected at wavelengths of 220, 230, 245 and 280 nm.

4.1.4. Synthesis

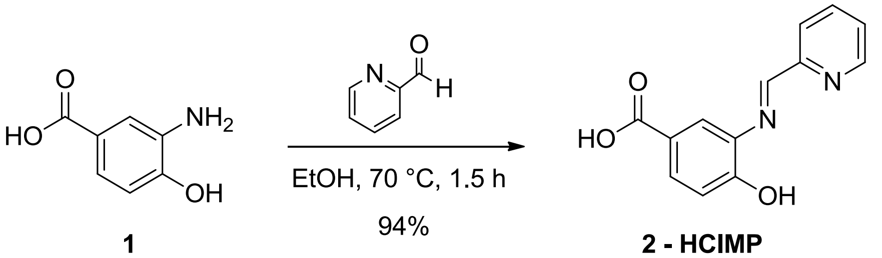

HCPIMP (2)

3-Amino-4-hydroxybenzoic acid **1** (5 g, 32.7 mmol) was dissolved in EtOH (30 mL) at 70 °C. 2-Formylpyridine (3.85 g, 35.9 mmol) was added dropwise, and the resulting suspension was stirred at 70 °C for 1.5 h. The precipitated yellow solid was filtered, washed with EtOH (3×10 mL), and dried under *high vacuo* to give HCPIMP **2** (7.4 g, 94%).

^{1}H NMR (400 MHz, DMSO) δ 12.61 (*s*, 1H), 10.15 (*s*, 1H), 8.81–8.51 (*m*, 1H), 8.70 (*s*, 1H), 8.34 (*d*, *J* = 7.9 Hz, 1H), 8.01–7.87 (*m*, 1H), 7.81–7.65 (*m*, 2H), 7.53 (*dd*, *J* = 6.4, 5.0 Hz, 1H), 7.00 (*d*, *J* = 8.2 Hz, 1H). ^{13}C NMR (100 MHz, DMSO) δ 167.0, 161.0, 155.2, 154.2, 149.6, 137.1, 136.9, 129.5, 125.6, 122.1, 121.7, 121.4, 116.2. IR (cm^{-1}) 3329 (m), 1681 (m), 1607 (m), 1592 (m), 1504 (m), 1379 (w), 1278 (s), 1227 (m), 1189 (s), 1155 (m), 1003 (m), 900 (m), 882 (m), 767 (m), 743 (vs), 686 (s). HRMS (ESI, positive mode) calcd. for $C_{13}H_{10}N_2NaO_3$ [M+Na]$^+$: 265.06, found: 265.05.

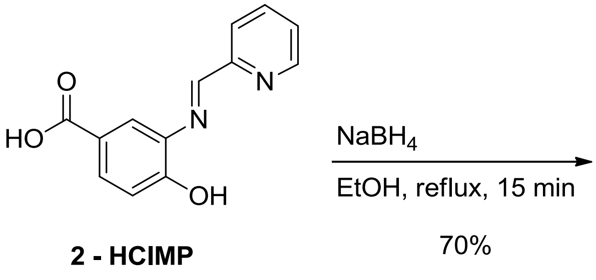

HCPAMP (3)

HCPIMP **2** (5 g, 20.6 mmol) and NaBH$_4$ (2.34 g, 61.9 mmol) were suspended in EtOH (20 mL) and heated under reflux for 15 min. After cooling the resulting clear solution to 40 °C, the solvent was removed under reduced pressure to dryness. The residue was treated with an aqueous solution (50 mL) of AcOH (3.72 g, 61.9 mmol). The product was then extracted with a mixture of THF:EtOAc (2:1, 3×100 mL). After drying the organic phase over MgSO$_4$, all volatiles were removed under vacuum and the resulting beige residue was washed with EtOH (2×10 mL) and dried under reduced pressure to afford HCPAMP **3** (3.54 g, 70%) as a beige solid.

^{1}H NMR (400 MHz, DMSO) δ 12.11 (*s*, 1H), 10.24 (*s*, 1H), 8.55 (*ddd*, *J* = 4.8, 1.8, 0.9 Hz, 1H), 7.74 (*td*, *J* = 7.7, 1.8 Hz, 1H), 7.35 (*d*, *J* = 7.8 Hz, 1H), 7.26 (*ddd*, *J* = 7.4, 4.9, 1.1 Hz, 1H), 7.13 (*dd*, *J* = 8.1, 2.0 Hz, 1H), 6.96 (*d*, *J* = 2.0 Hz, 1H), 6.74 (*d*, *J* = 8.1 Hz, 1H), 5.74 (*s*, 1H), 4.41 (*s*, 2H). ^{13}C NMR (100 MHz, DMSO) δ 167.7, 158.8, 148.8, 148.6, 136.7, 136.64, 122.0, 121.9, 121.1, 118.9, 112.6, 110.3, 56.0, 48.0, 39.5, 21.0, 18.5. IR (cm^{-1}) 3425 (m), 1653 (m), 1592 (vs), 1532 (s), 1490 (m), 1435 (w), 1399 (m), 1362 (m), 1328 (m), 1278 (vs), 1247 (vs), 1215 (s), 1203 (s), 1136 (m), 1054 (m), 1005 (s), 920 (w), 862 (w), 828 (w), 767 (vs), 733 (s). HRMS (ESI, positive mode) calcd. for $C_{13}H_{13}N_2O_3$ [M+H]$^+$: 245.09, found: 245.09.

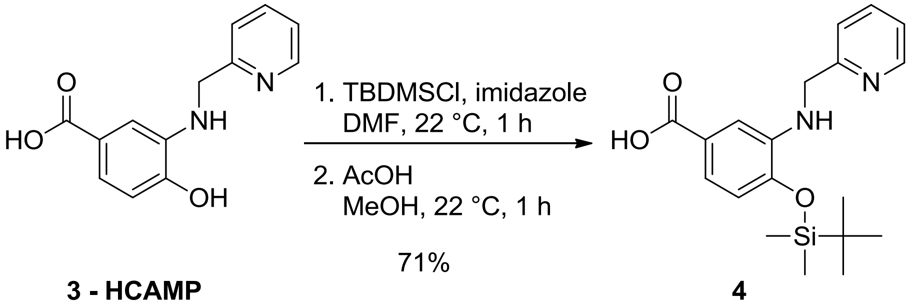

4-((tert-Butyldimethylsilyl)oxy)-3-((pyridin-2-ylmethyl)amino)benzoic acid (4)

HCPAMP **3** (2.0 g, 6.14 mmol), imidazole (2.3 g, 49.10 mmol) and TBDMSCl (2.9 g, 24.50 mmol) were dissolved in DMF (2 mL), and stirred at 22 °C under N_2 atmosphere for 1 h. MeOH (5 mL) was then added and the reaction mixture was stirred for another hour. This mixture was then diluted with 25% AcOH (20 mL), and extracted with EtOAc (3×50 mL). The organic phase was washed with water (3×20 mL), dried over $MgSO_4$, filtered, and removal of all volatiles under reduced pressure afforded a pale yellow residue that was washed with *n*-hexane (3×20 mL) and dried for 10 min under vacuum. The resulting solid was washed with water (3×5 mL) and dissolved in EtOAc (200 mL), then dried over $MgSO_4$, and filtered. The remaining solvent was removed under reduced pressure to yield **4** (2.1 g, 71%) as a white solid.

^{1}H NMR (600 MHz, $CDCl_3$) δ 8.61–8.59 (*m*, 1H), 7.67 (*td*, *J* = 7.7, 1.8 Hz, 1H), 7.43 (*dd*, *J* = 8.2, 2.1 Hz, 1H), 7.34 (*d*, *J* = 2.0 Hz, 1H), 7.32 (*s*, 1H), 7.22–7.19 (*m*, 1H), 6.79 (*d*, *J* = 8.2 Hz, 1H), 4.54 (*s*, 2H), 1.06 (*s*, 9H), 0.30 (*s*, 6H). ^{13}C NMR (150 MHz, $CDCl_3$) δ 171.8, 157.9, 149.0, 147.8, 139.9, 136.9, 123.1, 122.3, 121.7, 120.3, 111.9, 48.7, 25.9, 18.4, -4.1. HRMS (ESI, positive mode) calcd. for $C_{19}H_{27}N_2O_3Si$ $[M+H]^+$: 359.18, found: 359.17.

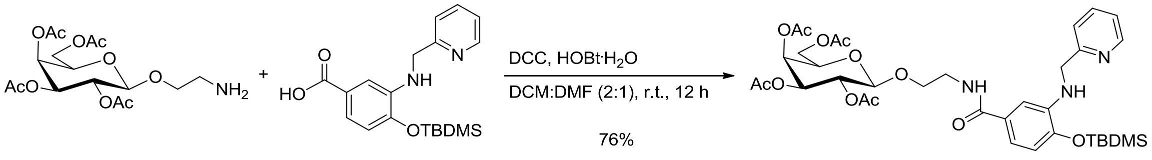

5 4 8

Gal-HCPAMP-TBDMS (8)

Compound **4** (55 mg, 0.14 mmol), HOBt·H_2O (21 mg, 0.14 mmol), and DCC (18 mg, 0.14 mmol) were dissolved in DCM:DMF (2:1, 4 mL). The reaction solution was stirred at 22 °C for 2 h, followed by the addition of **5** (50 mg, 0.14 mmol). After stirring the reaction mixture at 22 °C for another 20 h, the solvents were removed under vacuum. The crude was dissolved in DCM (20 mL) and washed with water (2×10 mL). The organic phase was dried over $MgSO_4$, filtered, and concentrated. The crude was then purified over flash column chromatography (SiO_2, DCM:MeOH; 98:2) to afford **8** (78 mg, 76%) as a white solid.

R_f 0.20 (DCM:MeOH 98:2). ^{1}H NMR (600 MHz, $CDCl_3$) δ 8.55 (*d*, *J* = 3.7 Hz, 1H), 7.75 (*t*, *J* = 7.6 Hz, 1H), 7.40 (*d*, *J* = 7.8 Hz, 1H), 7.27 (*dd*, *J* = 8.9, 3.0 Hz, 1H), 7.11 (*d*, *J* = 1.3 Hz, 1H), 6.99 (*dd*, *J* = 8.2, 1.8 Hz, 1H), 6.72 (*d*, *J* = 8.1 Hz, 1H), 6.62 (*s*, 1H), 5.38–5.33 (*m*, 1H), 5.16 (*dd*, *J* = 10.5, 7.9 Hz, 1H), 4.99 (*dd*, *J* = 10.5, 3.4 Hz, 1H), 4.60 (*s*, 2H), 4.48 (*d*, *J* = 7.9 Hz, 1H), 4.10 (*d*, *J* = 6.7 Hz, 2H), 3.95 (*dt*, *J* = 9.1, 4.6 Hz, 1H), 3.90 (*t*, *J* = 6.7 Hz, 1H), 3.79–3.66 (*m*, 2H), 3.54-3.46 (*m*, 1H), 2.12 (*s*, 3H), 1.99 (*s*, 3H), 1.95 (*s*, 3H), 1.84 (*s*, 3H), 1.01 (*s*, 9H), 0.24 (*s*, 6H). ^{13}C NMR (150 MHz, $CDCl_3$) *δ* 170.4, 170.2, 170.1, 169.8, 167.7, 157.36, 147.38, 145.8, 139.7, 138.4, 127.9, 122.8, 122.5, 116.9, 115.8, 109.6, 100.4, 77.5, 70.81, 70.80, 69.1, 69.0, 67.0, 61.3, 47.8, 39.6, 25.8, 20.7, 20.7, 20.67, 20.62, 18.3, -4.2. HRMS (ESI, positive mode) calcd. for $C_{35}H_{50}N_3O_{12}Si$ $[M+H]^+$: 732.316, found: 732.315.

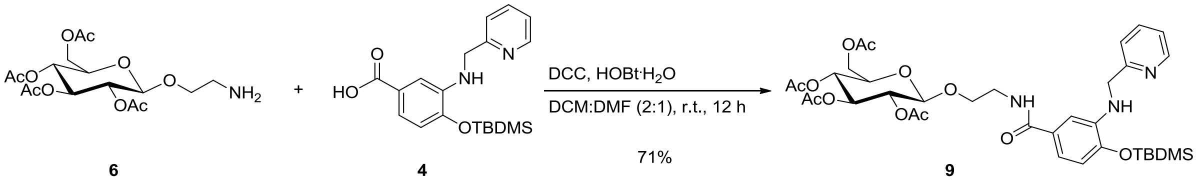

Glc-HCPAMP-TBDMS (9)

Compound **4** (28 mg, 0.08 mmol), HOBt·H_2O (14 mg, 0.09 mmol), and DCC (16 mg, 0.08 mmol) were dissolved in DCM:DMF (2:1; 4 mL). The reaction solution was stirred at 22 °C for 2 h, followed by the addition of **6** (30 mg, 0.08 mmol). After stirring the reaction mixture at 22 °C for another 20 h, the solvents were removed under vacuum. The crude was dissolved in DCM (20 mL) and washed with water (2×10 mL). The organic phase was dried over $MgSO_4$, filtered, and concentrated. The crude was then purified over flash column chromatography (SiO_2, DCM:MeOH; 98:2) to afford **9** (40 mg, 71%).

R_f 0.21 (DCM:MeOH 98:2). ^{1}H NMR (400 MHz, $CDCl_3$) *δ* 8.67 (*d*, *J* = 4.7 Hz, 1H), 8.24 (*t*, *J* = 7.5 Hz, 1H), 7.84 (*d*, *J* = 7.9 Hz, 1H), 7.74–7.68 (*m*, 1H), 7.18–7.11 (*m*, 2H), 7.04–6.98 (m, 1H), 6.76 (*d*, *J* = 8.5 Hz, 1H), 5.19 (*t*, *J* = 9.5 Hz, 1H), 5.07 (*d*, *J* = 9.8 Hz, 1H), 5.03 (*s*, 2H), 4.94 (*dd*, *J* = 9.7, 8.0 Hz, 1H), 4.57 (*d*, *J* = 8.0 Hz, 1H), 4.24 (*dd*, *J* = 12.3, 4.8 Hz, 1H), 4.17–4.06 (*m*, 2H), 4.03–3.93 (*m*, 1H), 3.86–3.51 (*m*, 5H), 2.02 (*s*, 3H), 2.00 (*s*, 3H), 1.87 (*s*, 3H), 1.03 (*s*, 9H), 0.29 (*s*, 6H). ^{13}C NMR (150 MHz, $CDCl_3$) *δ* 170.7, 170.7, 169.7, 169.6, 167.1, 156.5, 145.9, 145.7, 140.7, 137.7, 127.9, 125.9, 125.3, 118.5, 117.4, 109.5, 100.9, 77.2, 72.8, 72.7, 72.1, 71.9, 71.4, 69.4, 68.8, 68.5, 61.9, 44.5, 39.6, 29.8, 26.0, 20.9, 20.7, 20.7, 20.7, 18.5, -3.9. HRMS (ESI, positive mode) calcd. for $C_{35}H_{50}N_3O_{12}Si$ $[M+H]^+$: 732.315, found: 732.315.

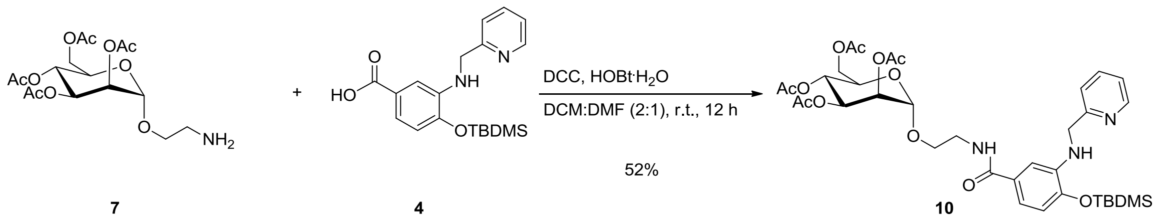

Man-HCPAMP-TBDMS (10)

Compound **4** (275 mg, 0.77 mmol), $HOBt{\cdot}H_2O$ (141 mg, 0.92 mmol), and DCC (158 mg, 0.77 mmol) were dissolved in DCM:DMF (2:1; 4 mL). The reaction solution was stirred at 22 °C for 2 h, followed by the addition of **7** (300 mg, 0.77 mmol). After stirring the reaction mixture at 22 °C for another 20 h, the solvents were removed under vacuum. The crude was dissolved in DCM (20 mL), and washed with water (2×10 mL). The organic phase was dried over $MgSO_4$, filtered and concentrated. The crude was then purified by flash column chromatography (SiO_2, DCM:MeOH; 98:2) to afford **10** (143 mg, 52%).

R_f 0.18 (DCM:MeOH 98:2). ^1H NMR (400 MHz, $CDCl_3$) δ 8.57 (*d*, *J* = 3.6, 1H), 7.71 (*t*, *J* = 7.6, 1H), 7.37 (*d*, *J* = 7.7, 1H), 7.23 (*d*, *J* = 5.6, 1H), 7.10 (*s*, 1H), 7.01 (*d*, *J* = 7.7, 1H), 6.75 (*d*, *J* = 8.1, 1H), 6.66 (*s*, 1H), 5.37–5.21 (*m*, 4H), 4.85 (*d*, *J* = 1.0, 1H), 4.55 (*s*, 2H), 4.23 (*dd*, *J* = 12.2, 5.7, 1H), 4.07 (*dd*, *J* = 12.2, 2.2, 1H), 3.99 (*ddd*, *J* = 9.5, 5.6, 2.2, 1H), 3.90–3.83 (*m*, 1H), 3.68–3.63 (*m*, 2H), 2.14 (*s*, 3H), 2.04 (*s*, 3H), 2.01 (*s*, 3H), 1.98 (*s*, 3H), 1.04 (*s*, 9H), 0.27 (s, 6H). ^{13}C NMR (100 MHz, $CDCl_3$) δ 170.7, 170.2, 170.1, 169.8, 167.9, 157.5, 148.2, 145.9, 139.9, 137.6, 127.9, 122.6, 122.2, 116.9, 115.8, 109.5, 97.8, 69.5, 69.2, 68.8, 67.7, 66.2, 62.6, 39.6, 29.8, 25.9, 20.9, 20.8, 20.8, 20.7, 18.4, -4.1. HRMS (ESI, positive mode) calcd. for $C_{35}H_{50}N_3O_{12}Si$ $[M+H]^+$: 732.315, found: 732.315.

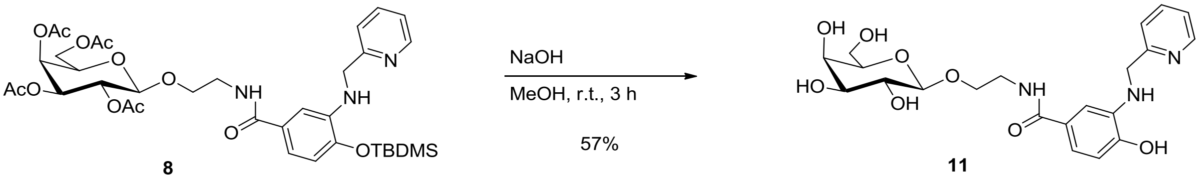

Gal-HCPAMP (11)

Compound **8** (140 mg, 0.19 mmol) was dissolved in MeOH (1 mL) and a NaOH (38 mg, 0.96 mmol) solution in water (1 mL) was added. The reaction solution was stirred at 22 °C for 30 min and neutralized by addition of aqueous solution of HCl (0.96 mmol, 956 µL, 1 M). After removal of solvent under reduced pressure, the residue was purified by HPLC C-18 (Water:MeCN:0.1% TFA) and lyophilized to give **11** (49 mg, 57%) as a pale yellow powder.

^{1}H NMR (600 MHz, D$_2$O) δ 8.66 (*d*, *J* = 5.8 Hz, 1H), 8.54 (*t*, *J* = 8.0 Hz, 1H), 8.07 (*d*, *J* = 8.1 Hz, 1H), 7.94 (*t*, *J* = 6.7 Hz, 1H), 7.18 (*dd*, *J* = 8.2, 2.0 Hz, 1H), 6.95 (*dd*, *J* = 8.2, 1.1 Hz, 1H), 6.87 (*s*, 1H), 4.90 (*s*, 3H), 4.40 (*d*, *J* = 7.9 Hz, 2H), 4.05–3.99 (*m*, 2H), 3.92 (*d*, *J* = 3.2 Hz, 1H), 3.87–3.81 (*m*, 2H), 3.71 (*d*, *J* = 6.0 Hz, 3H), 3.68–3.47 (*m*, 8H). ^{13}C NMR (150 MHz, D$_2$O) δ 170.5, 154.8, 147.6, 146.8, 140.9, 135.3, 125.8, 125.6, 125.5, 118.64, 114.0, 110.2, 103.0, 75.0, 72.6, 70.7, 68.5, 60.8, 44.8, 39.8. HRMS (ESI, positive mode) calcd. for $C_{21}H_{27}N_3NaO_8$ [M+Na]$^+$: 472.169, found: 472.174.

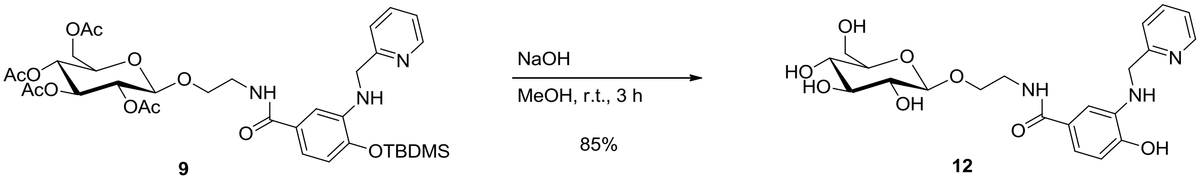

Glc-HCPAMP (12)

Compound **9** (86 mg, 0.12 mmol) was dissolved in MeOH (1 mL) and NaOH (23 mg, 0.59 mmol) solution in water (1 mL) was added. The reaction solution was stirred at 22 °C for 30 min and neutralized by addition of an aqueous solution of HCl (0.59 mmol, 588 µL, 1 M). After removal of solvent under reduced pressure, the residue was purified by HPLC C-18 (Water:MeCN:0.1% TFA) and lyophilized to give **12** (45 mg, 85%) as a pale yellow solid.

^{1}H NMR (600 MHz, D$_2$O) δ 8.66 (*d*, *J* = 5.9 Hz, 1H), 8.55 (*td*, *J* = 8.0, 1.5 Hz, 1H), 8.08 (*d*, *J* = 8.1 Hz, 1H), 7.95 (*t*, *J* = 6.8 Hz, 1H), 7.18 (*dd*, *J* = 8.2, 2.1 Hz, 1H), 6.95 (*d*, *J* = 8.2 Hz, 1H), 6.87 (*d*, *J* = 2.1 Hz, 1H), 4.91 (*s*, 2H), 4.46 (*d*, *J* = 8.0 Hz, 1H), 4.02 (*ddd*, *J* = 10.9, 6.6, 4.2 Hz, 1H), 3.88–3.81 (*m*, 2H), 3.66 (*dd*, *J* = 12.3, 5.9 Hz, 1H), 3.63–3.33 (*m*, 6H), 3.25 (*dd*, *J* = 9.4, 8.0 Hz, 1H). ^{13}C NMR (150 MHz, D$_2$O) δ 170.5, 154.7, 147.6, 146.9, 140.7, 135.3, 125.8, 125.7, 125.6, 118.6, 114.0, 110.2, 102.4, 75.8, 75.6, 73.0, 69.5, 68.5, 60.6, 44.7, 39.7. HRMS (ESI, positive mode) calcd. for $C_{21}H_{28}N_3O_8$ $[M+H]^+$: 450.187, found: 450.192.

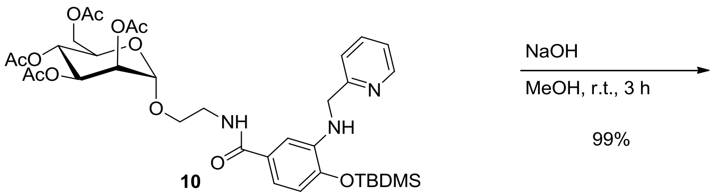

Man-HCPAMP (13)

Compound **10** (38 mg, 0.05 mmol) was dissolved in MeOH (1 mL) and NaOH (10 mg, 0.26 mmol) solution in water (1 mL) was added. The reaction solution was stirred at 22 °C for 30 min and neutralized by addition of aqueous solution of HCl (0.26 mmol, 250 µL, 1 M). After removal of solvent under reduced pressure, the residue was purified by HPLC C-18 (Water:MeCN:0.1% TFA) and lyophilized to give **13** (23 mg, 99%) as a pale yellow powder.

^{1}H NMR (600 MHz, D_2O) δ 8.66 (*dd*, *J* = 3.6, 3.0 Hz, 1H), 8.58–8.53 (*m*, 1H), 8.08 (*d*, *J* = 8.2 Hz, 1H), 7.97–7.93 (*m*, 1H), 7.18–7.13 (*m*, 1H), 6.95 (*dd*, *J* = 8.2, 0.7 Hz, 1H), 6.87–6.84 (*m*, 1H), 4.90 (*s*, 2H), 4.84 (*s*, 1H), 3.89 (*dd*, *J* = 3.2, 1.6 Hz, 1H), 3.86–3.80 (*m*, 1H), 3.77–3.47 (*m*, 10H). ^{13}C NMR (150 MHz, D_2O) δ 170.3, 154.7, 147.6, 140.8, 135.3, 125.8, 125.7, 125.5, 118.5, 114.0, 110.1, 99.6, 72.7, 70.4, 69.9, 66.4, 65.9, 60.6, 44.7, 39.3. HRMS (ESI, positive mode) calcd. for $C_{21}H_{28}N_3O_8$ $[M+H]^+$: 450.187, found: 450.192.

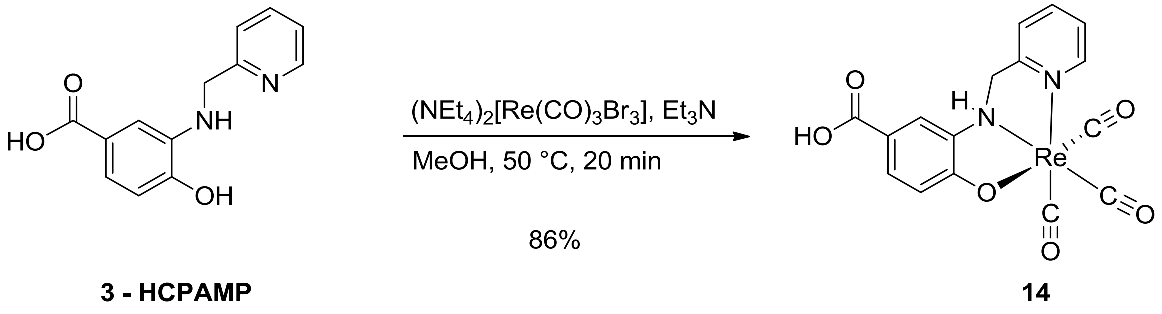

[Re(CO)$_3$(HCPAMP)] (14)

$(NEt_4)_2[Re(CO)_3Br_3]$ (77 mg, 0.1 mmol) and HCPAMP **3** (24 mg, 0.1 mmol) were suspended in MeOH (10 mL) and heated at 50°C for 30 min. Et_3N (28 µL, 0.2 mmol) was then added and the reaction solution was stirred for another 30 min. The reaction solution was concentrated to 2 mL under reduced pressure and cooled to -10 °C for 2 h. The obtained colorless microcrystalline solid was filtered and washed with pre-cooled methanol (2×1 mL), and dried under reduced pressure to afford **14** (44 mg, 86%).

^{1}H NMR (600 MHz, DMSO) *δ* 12.15 (*s*, 1H), 8.80 (*d*, *J* = 5.2 Hz, 1H), 8.62 (*d*, *J* = 3.9 Hz, 1H), 8.00 (*q*, *J* = 7.3 Hz, 1H), 7.80 (*d*, *J* = 1.8 Hz, 1H), 7.66 (*d*, *J* = 7.8 Hz, 1H), 7.54–7.47 (*m*, 1H), 7.42 (*dd*, *J* = 8.5 Hz, 1.8, 1H), 6.38 (*d*, *J* = 8.6 Hz, 1H), 4.96 (*d*, *J* = 16.0 Hz, 1H), 4.82 (*dd*, *J* = 15.9, 3.9 Hz, 1H). ^{13}C NMR (150 MHz, DMSO) *δ* 198.5, 198.3, 197.3, 171.8, 166.9, 159.2, 152.1, 140.1, 134.2, 130.4, 127.3, 125.6, 123.6, 118.7, 116.1, 64.3. IR (cm^{-1}) 2016 (s), 1877 (vs), 1657 (s), 1594 (s), 1506 (m), 1452 (w), 1405 (w), 1318 (s), 1282 (s), 1254 (s), 1237 (s), 1127 (m), 1031 (w), 842 (w), 765 (s). HRMS (ESI, positive mode) calcd. for $C_{16}H_{12}N_2O_6Re$ [M+H]$^+$: 515.025, found: 515.027.

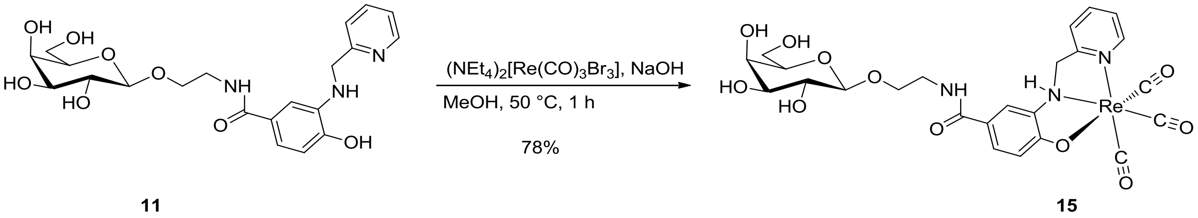

[Re(CO)$_3$(Gal-HCPAMP)] (15)

(NEt$_4$)$_2$[Re(CO)$_3$Br$_3$] (38.6 mg, 0.05 mmol) and **11** (22.5 mg, 0.05 mmol) were dissolved in MeOH:H$_2$O (2:1, 10 mL) and stirred at r.t. for 30 min. The pH of the reaction mixture was adjusted to about pH 8 by dropwise addition of an aqueous solution of NaOH (1 M), and stirred for 30 min. Thereafter, solvents were removed under reduced pressure and the resulting crude extract was dissolved in warm EtOH (1 mL) at 50 °C and stored at -10 °C for 3 h. The precipitated solid was filtered and washed with cold EtOH (2×0.2 mL), and dried under *high vacuo* to afford **15** (28 mg, 78%) as a pale yellow solid.

^{1}H NMR (600 MHz, D$_2$O) *δ* 8.85 (*d*, *J* = 5.5 Hz, 1H), 8.19 (*d*, *J* = 3.9 Hz, 1H), 7.88 (*d*, *J* = 2.3 Hz, 1H), 7.87 (*dd*, *J* = 7.8, 1.2 Hz, 1H), 7.48–7.43 (*m*, 2H), 7.42–7.39 (*m*, 1H), 6.59 (*d*, *J* = 8.7 Hz, 1H), 4.99 (*dd*, *J* = 15.8, 3.2 Hz, 2H), 4.43 (*dd*, *J* = 16.1, 2.6 Hz, 1H), 4.06 (*ddd*, *J* = 10.7, 6.4, 4.4 Hz, 1H), 3.92 (*d*, *J* = 3.2 Hz, 1H), 3.88 (*ddd*, *J* = 10.7, 6.4, 4.2 Hz, 1H), 3.75–3.48 (*m*, 9H). ^{13}C NMR (150 MHz, D$_2$O) *δ* 169.6, 167.6, 158.5, 152.3, 139.9, 134.0, 128.4, 125.5, 125.2, 123.1, 122.0, 118.7, 103.1, 75.0, 72.6, 70.7, 68.5, 64.3, 60.8, 48.8, 39.8. IR (cm^{-1}) 3349 (w), 2928 (w), 2848 (w), 2024 (vs), 1887 (vs), 1782 (m), 1675 (m), 1631 (m), 1613 (m), 1603 (m), 1554 (m), 1490 (m), 1310 (m), 1292 (m), 1197 (s), 1144 (s), 1066 (s), 1040 (s), 763 (m), 705 (m). HRMS (ESI, positive mode) calcd. for $C_{24}H_{27}N_3O_{11}Re$ $[M+H]^+$: 720.120, found: 720.205.

4.2. Materials and Methods

4.2.1. Octanol-water Partition Coefficients

Log $P_{o/w}$ values of the complexes **16–19** were determined applying the multiple back extraction method described by Troutner *et al.*[32]

4.2.2. *In vivo* SPECT/CT Imaging and *ex vivo* Biodistribution Studies

22 female wild type C57Bl/6 mice (10–12 weeks old) were purchased from the Central Animal Facility of the University Medical Center Charité (Berlin, Berlin). The animals were kept under standardized environmental conditions (20 ± 2 °C temperature, 50% ± 10% relative humidity, 12 h light-dark rhythm) and had access to water and food *ad libitum*. All experiments were performed according to the German Animal Protection Law with permission from the responsible local authorities.

In vivo single photon emission computed tomography (SPECT/CT) imaging was performed with a nanoSPECT/CT plus 4-head system (Bioscan, Paris, France) equipped with general purpose mouse apertures, each with 9 pinholes of 1 mm diameter.[33] This configuration provides a sensitivity of 1.2 $cps \cdot kBq^{-1}$ and spatial resolution in reconstructed images of about 0.7 mm full-width-at-half-maximum. The SPECT/CT system was calibrated for ^{99m}Tc so that local concentration of ^{99m}Tc-labelled tracers in different organs could be measured quantitatively (in $MBq \cdot mL^{-1}$). The animals were anesthetized i.p. with 200 $mg \cdot kg^{-1}$ ketamine plus 10 $mg \cdot kg^{-1}$ xylazine prior to injection of 39–100 MBq of the tracer via a lateral tail vein (0.15–0.2 mL injected volume). One mouse was injected with the complex $[^{99m}Tc(CO)_3(HCPAMP)]$ **16**. The ^{99m}Tc-labeled glycoconjugates **17** and **18** were evaluated in five mice each and **19** was evaluated in six mice. Each mouse was positioned on the mouse bed of the Minerve Small-Animal Environment System (Bioscan Europe, Paris, France) and kept at physiological temperature during imaging.[34] For each animal, 30 min duration static whole-body images were obtained by

SPECT at different time points after tracer injection, creating a time course of tracer concentration in the organs of interest.[35] In addition, whole-body CT was performed for anatomical localization. The *in vivo* Scope software package (Bioscan Europe) was used to manually draw regions of interest (ROI) in the following organs: bowel, heart, brain, liver, lungs, spleen and kidneys. The total concentration of tracer uptake by each organ was corrected for radioactive decay and was characterized by the maximum within each ROI, to minimize rater-dependence *via* the manual ROI definition.

After the last SPECT scan, the animals were sacrificed by cervical dislocation under deep anesthesia and dissected. Organs were removed, and radioactivity was measured in a well counter (Wallac wizard gamma-counter, Turku, Finland) also calibrated for ^{99m}Tc. The results were corrected for radioactive decay and expressed as percentage injected dose (%ID) per gram of tissue. The *ex vivo* measurements included a blood sample in addition to the organs analyzed in the SPECT data.

4.2.3. Preparation of the Radiolabeling Precursor $[^{99m}Tc(CO)_3(H_2O)_3]^+$ and General Radiolabeling Method for Synthesis of 16–19

$[^{99m}TcO_4]^-$ generator eluated in saline (300–700 MBq, 1 mL) was added to a mixture of sodium-boranocarbonate (4.5 mg), borax (7 mg), sodium tartrate tetrahydrate (7 mg).[36] The solution was heated for 20 min at 100 °C to afford $[^{99m}Tc(CO)_3(H_2O)_3]^+$ with a radiochemical yield of > 95%. The Tc(I) tricarbonyl solution was adjusted to around pH 7–8 with a mixture of HCl and PBS before further use in labeling.

4.2.4. General Radiolabeling Method

An aqueous solution of $[^{99m}Tc(CO)_3(H_2O)_3]^+$ (0.7–1 mL, 300-700 MBq) was added to a solution (0.1 mL) of HCPAMP **3** (0.1 mg, H_2O:DMSO, 100:1) or HCPAMP-carb (0.1 mg, H_2O, Carb = Gal **11**, Glc **12**, Man **13**). The resulting solution was heated to 45–50 °C for 20 min and the radiochemical yield and purity of the resulting compounds **16** to **19** were analyzed by means of HPLC.

4.2.5. X-ray Structure Determinations

The intensities for the X-ray determinations were collected on a STOE IPDS with Mo Kα radiation. The structures were solved by direct methods using *SHELXS-86* or *SHELXS-97*.[37] Subsequent Fourier-difference map analyses yielded the positions of the nonhydrogen atoms. Refinement was performed using *SHELXL-97*. Hydrogen atom positions were calculated for idealized positions and treated with the 'riding model' option of *SHELXL*. Crystal data and more details of the data collections and refinements are contained in Table 5.

Table 5. X-ray structure data collection and refinement parameters.

	[Re(CO)$_3$(HCPAMP)]·MeOH 14
Formula	$C_{17}H_{15}N_2O_7Re$
M_w (g·mol^{-1})	545.51
Crystal system	Monoclinic
a (Å)	7.213(1)
b (Å)	13.656(1)
c (Å)	18.437(2)
α (°)	90.00
b (°)	97.54(1)
γ (°)	90.00
V (Å^3)	1800.2(3)
Space group	P21/c
Z	4
$D_{calc.}$(g·cm^{-3})	2.013
μ (mm^{-1})	6.793
Absorption correction	integration
T_{min}/T_{max}	0.2224/0.5178
Number of reflections	11813
Number of independent [R(int)]	4126
Number parameters	238
R1/wR2	0.0442/0.0612
GOF	0.863

5. Abbreviations

AcOH	acetic acid
BFC	bifunctional chelator
C	carbon
calcd.	calculated
carb	carbohydrate
cps	counts per second
CT	computed tomography
d	day(s)
d	doublet
DCC	dicyclohexylcarbodiimide
DCM	dichloromethan
dd	doublets of doublet
ddd	doublets of doublets of doublet
DMF	*N*,*N*'-dimethylformamide
DMSO	dimethyl sulfoxide
dt	doublets of triplet
Et_3N	triethylamine
EtOAc	ethyl acetate
EtOH	ethanol
F	fluorine
FDG	2-F-fluoro-2-deoxyglucose
Gal	galactose
Glc	glucose
h	hour(s)
HCl	hydrochloric acid
HCPAMP	2-[[(2-hydroxy-5-carboxyphenyl)amino]methyl]pyridin
HCPIMP	(2-[[(2-hydroxy-5-carboxyphenyl)imino]methyl]pyridin)
HMPAO	hexamethylpropyleneamineoxime

HOBt	hydroxybenzotriazole
HPLC	high-performance liquid chromatography
HRMS	high-resolution mass spectrometry
Hz	Hertz
ID	infectious dosage
IR	infrared
J	coupling constant
m	multiplet
m	medium
Man	mannose
MeCN	acetonitrile
MeOH	methanol
min	minute(s)
N	number of experiment(s)
$NaBH_4$	sodium borohydride
NaOH	sodium hydroxide
NMR	nuclear magnetic resonance
ORTEP	Oak Ridge thermal-ellipsoid plot program
p.i.	post injection
PBS	phosphate buffered saline
$P_{o/w}$	octanol-water partition
ppm	parts-per-million
q	quartet
Re	rhenium
ROI	region of interest
s	singlet
s	sharp
s	second(s)
S.E.	standard error

Si	silicium
SPECT	single photon emission computed tomography
$t_{1/2}$	half-life
TBDMSCl	*tert*-butyldimethylsilylchloride
Tc	technetium
td	triplets of doublet
TFA	trifluoroacetic acid
THF	tetrahydrofuran
TLC	thin layer chromatography
t_R	retention time
vs	very sharp
w	wide
δ	chemical shift

6. Acknowledgments

I would like to express my gratitude to Dr. Ali Barandov for the precious help he delivered in the outcome of the project. I would like to thank him for the intensive assistance in the synthesis of the compounds. His scientific knowledge in radiochemistry as well as his ability to work with radioactive material enabled the right progress of the project.

I place on record my sincere gratitude to Prof. Ulrich Abram from the Free University (Berlin, Germany) for providing all the necessary facilities and equipment for the analysis of the radioactive compounds. I also thank his group members: Dr. Adelheid Hagenbach for X-ray analysis and Ms. Jacqueline Grewe for her permanent support in supplying ^{99m}Tc generator.

Finally, I take also the opportunity to thank Dr. Ivayla Apostolova and Dr. Ralph Butcher from Charité Hospital (Berlin, Germany) for their role in the *in vivo* imaging, analysis and interpretation of the results. Part of the work presented in this chapter would have not been possible without their relevant contribution.

7. References

---

[1] (a) Howes, L.; Jones, R. J. *Reprod. Immunol.* **2002**, *53*, 181. b) Stringer, S. E. *Biochem. Soc. Trans.* **2006**, *34*, 451. (b) Rhodes, J. M.; Campbell, B. J.; Yu, L. G. *Biochem. Soc. Trans.* **2008**, *36*, 1482. b) Sarter, K.; Mierke, C.; Beer, A.; Frey, B.; Fuhrnrohr, B. G.; Schulze, C.; Franz, S. *Autoimmunity* **2007**, *40*, 345. (c) Grünstein, D.; Maglinao, M.; Kikkeri, R.; Collot, M.; Barylyuk, K.; Lepenies, B.; Kamena, F.; Zenobi, R.; Seeberger, P. H. *J. Am. Chem. Soc.* **2011**, *133*, 13957. (d) Chen, C.-C.; Llado, V.; Eurich, K.; Tran, H. T.; Mizoguchi E. *Clinical Immunol.* **2011**, *140*, 268. (e) Pighon, A.; Gutkowska, J.; Jankowski, M.; Rabasa-Lhoret, R.; Lavoie, J.-M. *Metabolism Clinical and Experimental* **2011**, *60*, 629. (f) Ellis, C.L.; Edirisinghe, I.; Kappagoda, T.; Burton-Freeman, B. *J. Atherosclerosis Thrombosis* **2011**, *18*, 318. (g) Ulbrich, H. K.; Luxenburger, A.; Prech, P.; Eriksson, E. E.; Soehnlein, O.; Rotzius, P.; Lindbom, L.; Dannhardt, G. *J. Med. Chem.* **2006**, *49*, 5988.

[2] (a) Fowler, J. S.; Ido, T. *Seminars in Nuclear Medicine* **2002**, *32*, 6. (b) Ido, T.; Wan, C.-N. *J. Label Compounds Radiopharm* **1978**, *14*, 171.

[3] (a) Fowler, J. S.; Wolf, A. P. *Acc. Chem. Res*. **1997**, *30*, 181. (b) Gilman, M. D.; Aguino, S. L. *Semin. Roentgenol.* **2005**, *40*, 143. (c) B. Beuthien-Baumann, K. Hamacher, F. Oberdorfer, J. Steinbach, *Carbohydr. Res.* **2000** *327*, 1107.

[4] Hicks, R. J. *Cancer Imaging* **2004**, *4*, 22.

[5] Roesch, F.; Knapp, F. F. *Radionuclide Generators*: *Handbook of Nuclear Chemistry*, Kluewer Academic, New York, **2003**, 81.

[6] Braband, H.; Tooyama, Y.; Fox, T.; Simms, R.; Forbes, J.; Valliant, J. F.; Alberto, R. *Chem. Eur. J.* **2011**, *17*, 12967.

[7] Blower, P. *Dalton Trans.* **2006**, 1705.

[8] Dilworth, J. R.; Parrott, S. J. *Chem. Soc. Rev.* **1998**, *27*, 43.

[9] (a) Leonard, J. P.; Novotnik, D. P.; Neirinckx, R. D. *J. Nucl. Med.* **1986**, *27*, 1819. (b) Cheesman, E. H.; Blanchette, M. A.; Ganey, M. V.; Maheu, L. J.; Miller, S. J.; Watson, A. D. *J. Nucl. Med.* **1986**, *29*, 288. (c) Kelly, J. D.; Forster, A. M.; Higley, B.; Archer, C. M.; Booker, F. S.; Canning, L. R.; Chiu, K. W.; Edwards, B.; Gill, H. K.; McPartlin, M.; Nagle, K. R.; Latham, I. A.; Pickett, R. D.; Storey, A. E.; Webbon, P. M. *J. Nucl. Med.* **1993**, *34*, 222. (d) Deutsch, E.; Vanderheyden, J. L.; Gerundini, P.; Lisbon, K.; Hirth, W.; Colombo, F.; Zecca, L.; Savi, L.; Fazio, F. *J. Nucl. Med.* **1987**, *12*, 1870.

[10] Bowen, M. L.; Orvig, C. *Chem. Comm*. **2008**, 5077.

[11] (a) Liu, S.; Chakraborty, S. *Dalton Trans.* **2011**, *40*, 6077. (b) Lahorte, C. M. M.; Vanderheyden, J-L; Steinmetz, N.; Van de Wiele, C.; Dierck, R. A.; Slegers, G. *Eur. J. Nucl. Med. Mol. Imaging* **2004**, *31*, 887. (c) Schibli, R.; Schubiger, P. A. *Eur. J. Nucl Med* **2002**, 29, 1529.

[12] (a) Huheey, J. E. *Inorganic Chemistry: Principles of Structure and Reactivity* (3rd. ed. chapter 7) Ed. Wasserman, M., Harper & Row Publishers, Inc. New York **1983**, 286. (b) Liu, S.; Chakraborty, S. *Dalton Trans.*, **2011**, *40*, 6077.

[13] (a) Stephenson, K. A.; Banerjee, S. R.; Sogbein, O. O.; Levadala, M. K.; McFarlane, N.; Boreham, D. R.; Maresca, K. P.; Babich, J. W.; Zubieta, J.; Valliant, J. F. *Bioconjugate Chem.* **2005**, *16*, 1189. (b) Gasser, G.; Jaeger, K.; Zenker, M.; Bergmann, R.; Steinbach, J.; Stephan, H.; Metzler-Nolte, N. *J. Inorg. Biochem.* **2010**, *104*, 1133. (c) Xiong, C.; Lu, W.; Zhang, R.; Tian, M.;

Tong, W.; Gelovani, J.; Li, C. *Chem. Eur. J.* **2009**, *15*, 8979. (d) Ferreira, C. L.; Marques, F. L. N.; Okamoto, M. R. Y.; Otake, A. H.; Sugai, Y.; Mikata, Y.; Storr, T.; Bowen, M.; Yano, S.; Adam, M. J. *Applied Radiation and Isotopes* **2010**, *68*, 1087. (e) Morais, M.; Subramanian, S.; Pandey, U.; Samuel, G.; Venkatesh, M.; Martins, M.; Pereira, S.; Correia, J. D. G.; Santos, I. *Mol. Pharmaceutics* **2011**, *8*, 609. (f) Levadala, M. K.; Banerjee, S. R.; Maresca, K. P.; Babich, J. W.; Zubieta, J. *Synthesis* **2004**, 1759. (g) Banerjee, S. R.; Levadala, M. K.; Lazarova, N.; Wei, L. H.; Valliant, J. F.; Stephenson, K. A.; Babich, J. W.; Maresca, K. P.; Zubieta, J. *Inorg. Chem.* **2002**, *41*, 6417. (h) Banerjee, S. R.; Maresca, K. P.; Francesconi, L.; Valliant, J.; Babich, J. W.; Zubieta, J. *Nucl. Med. Biol.* **2005**, *32*, 1.

[14] Barandov, A.; Abram, U. *Inorg. Chem.* **2009**, *48*, 8072.

[15] Barandov, A.; Abram, U. *Polyhedron* **2009**, *28*, 1155.

[16] (a) Vowinkel, E.; Wolf, C. *Chem. Ber.* **1974**, *107*, 907. (b) Sheehan, J. C.; Hess, G. P. *J. Am. Chem. Soc.* **1955**, *77*, 1067. (c) Rebeck, J.; Feiler, D. *J. Am. Chem. Soc.* **1973**, *95*, 4052. (d) Bhatt, R. K.; Chauhan, K.; Wheelan, P.; Murphy, R. C.; Falk, J. R. *J. Am. Chem. Soc.*, **1994**, *116*, 5050.

[17] (a) Pauling, L. *J. Am. Chem. Soc.* **1932**, *54*, 3570. (b) Kita, Y.; Haruta, J.; Takehiko, F.; Segawa, J.; Tamura, Y. *Synthesis* **1981**, 451.

[18] Sykora, J.; Blechta, V.; Sychrovsky, V.; Hetflejs, J.; Sabata, S.; Soukupova, L.; Schraml, J. *Magn. Reson. Chem.* **2006**, *44*, 669.

[19] (a) R. Pragani, R; Stallforth, P; Seeberger, P. H. *Org. Lett.* 2010, 12, 1624. (b) Broddefalk, J.; Nilsson, U.; Kihlberg, J. *J. Carbohydr. Chem.* **1994**, *13*, 129.

[20] (a) Quagliotto, P.; Viscardi, G.; Barolo, C.; D'Angelo, D.; Barni, E.; Compari, C.; Duce, E.; Fisicaro, E. *J. Org. Chem.* **2005**, *70*, 9857. b) Patel, A.; Lindhorst, T. K. *Eur. J. Org. Chem.* **2002**, 79.

[21] Cookson, R. C.; Crabb, T. A. *Tetrahedron* **1972**, *28*, 2139.

[22] (a) Edwards, P. G.; Newman, P. D.; Stasch, A. *J. Organomet. Chem.* **2011**, *696*, 1652. (b) Costaa, R.; Baronea, N.; Gorczyckab, C.; Powersb, E. F.; Cupelob, W.; Lopezb, J.; Herrickb, R. S.; Ziegler, C. J. *J. Organomet. Chem.* **2009**, *694*, 2163. (c) Chen, Y.; Liu, W.; Jin, J.-S.; Liu , B.; Zou, Z.-G.; Zuo, J.-L.; You, X.-Z. *J. Organomet Chem.* **2009**, *694*, 763.

[23] (a) Wei, L.; Babich, J. W.; Ouellette, W.; Zubieta, J. *Inorg. Chem.* **2006**, *45*, 3057. (b) Anderson, P. A.; Keene, F. R.; Horn, E.; Tiekink, E. R. T. *Appl. Organomet. Chem*. **1990**, *4*, 523. (c) Gamelin, D. R.; George, M. W.; Glyn, P.; Grevek, F. W.; Schaffner, K.; Turner, J. J. *Inorg. Chem*. **1995**, *33*, 3246. (d) Granifo, J. *Polyhedron* **1999**, *18*, 1061.

[24] (a) Lazarova, N.; Babich, J.; Valliant, J.; Schaffer, P.; James, S.; Zubieta, J. *Inorg. Chem.* **2005**, *44*, 6763. (b) Storr, T.; Sugai, Y.; Barta, C. A.; Mikata, Y.; Adam, M. J.; Yano, S.; Orvig, C. *Inorg. Chem.* **2005**, *44*, 2698.

[25] Schibli, R; La Bella, R.; Alberto, R; Garcia-Garayoa, E.; Ortner, K.; Abram, U.; Schubiger, P. A. *Bioconjugate Chem*. **2000**, *11*, 345.

[26] Alberto, R.; Ortner, K.; Wheatley, N.; Schibli, R.; Schubiger, P. A. *J. Am. Chem. Soc.* **2001**, *123*, 3135.

[27] Garayoa, E. G.; Ruegg, D.; Blauenstein, P.; Zwimpfer, M.; Khan, I. U.; Maes, V.; Blanc, A.; Beck-Sickinger, A. G.; Tourwe, D. A.; Schubiger, P. A. *Nucl. Med. Biol.* **2007**, *34*, 17.

[28] Böhme, C.; Schmidt, T. C.; Löw, E.;·Stork, G. *Fresenius J. Anal. Chem.* **1998**, 360, 805.

[29] Malovic, I.; Sorensen, K. K.; Elvevold, K. H.; Nedredal, G. I.; Paulsen, S.; Erofeev, A. V.; Smedsrod, B. H.; McCourt, P. A. G. *Hepatology* **2007**, *45*, 1454.

---

[30] Roos, P. H.; Kolb-Bachofen, V.; Schlepper-Schafer, J.; Monsigny, M.; Stockert, R. J.; Kolb, H. *FEBS Lett.* **1983**, *157*, 253.

[31] (a) Tatsumi, M.; Nakamoto, Y.; Traughber, B.; Marshall, L. T.; Geschwind, J-F. H.; Wahl, R. L. *Cancer Res.* **2003**, *63*, 6252. (b) Yu, A.S.; Lin, H-D.; Huang, S-C.; Phelps, M. E.; Wu H-M. *J. Nucl. Med.* **2009**, *50*, 966.

[32] Troutner, D. E.; Volkert, W. A.; Hoffman, T. J.; Holmes, R. A. *Int. J. Appl. Radiat. Isot.* **1984**, *35*, 467.

[33] (a) Meikle, S. R.; Kench, P.; Kassiou, M.; Banati, R. B. *Phys. Med. Biol.* **2005**, *50*, R45. (b) Schramm, N. U.; Ebel, G.; Engeland, U.; Schurrat, T.; Behe, M.; Behr, T. M. *Ieee Trans. on Nucl. Sci.* **2003**, *50*, 315.

[34] Fueger, B. J.; Czernin, J.; Hildebrandt, I.; Tran, C.; Halpern, B. S.; Stout, D.; Phelps, M. E.; Weber, W. A. *J. Nucl. Med.* **2006**, *47*, 999.

[35] Pissarek, M.; Meyer-Kirchrath, J.; Hohlfeld, T.; Vollmar, S.; Oros-Peusquens, A. M.; Flogel, U.; Jacoby, C.; Krugel, U.; Schramm, N. *Eur. J. Nucl. Med. Mol. Imaging* **2009**, *36*, 1495.

[36] Alberto, R.; Ortner, K.; Wheatley, N.; Schibli, R.; Schubiger, P. A. *J. Am. Chem. Soc.* **2001**, *123*, 3135.

[37] (a) Sheldrick, G.M. *Acta Crystallogr.* **1990**, *46*, 467. (b) Sheldrick, G.M. SHELX97 – A Program Package for the Solution and Refinement of Crystal Structures, University of Göttingen, Germany, **1997**.

Chapter 3

Hexameric Supramolecular Scaffold Orients Carbohydrates to Sense Bacteria

---

The results reported in this chapter have been partially published in:

(a) Grünstein, D.; Maglinao, M.; Kikkeri, R.; Collot, M.; Barylyuk, K.; Lepenies, B.; Kamena, F.; Zenobi, R.; Seeberger, P. H. *J. Am. Chem. Soc.* **2011**, *133*, 13957.
(DOI: 10.1021/ja2036767 – The original article is available at:
http://pubs.acs.org/doi/abs/10.1021/ja2036767)

(b) Barylyuk, K.; Balabin, R. M.; Grünstein, D.; Kikkeri, R.; Frankevich, V.; Seeberger, P. H. and Zenobi, R. *J. Am. Soc. Mass Spectrom.* **2011**, *22*, 1167.
(DOI: 10.1007/s13361-011-0118-8 – The original article is available at:
http://link.springer.com/article/10.1007%2Fs13361-011-0118-8)

Table of Contents

Abstract

Carbohydrates are integral to biological signaling networks and cell–cell interactions, yet the detection of discrete carbohydrate–lectin interactions remains difficult since binding is generally weak. A strategy to overcome this problem is to create multivalent sensors, where the avidity rather than the affinity of the interaction is taking into account.

Chapter 3 describes the development of a series of multivalent sensors that self-assemble *via* hydrophobic supramolecular interactions. The multivalent sensors are comprised of a fluorescent ruthenium (Ru) core surrounded by a heptamannosylated β-cyclodextrin (βCDMan) scaffold. Two additional series of sensors were synthesized, the fluorescent core alone, and the core plus β-cyclodextrin (βCD) as proof-of-principle of the supramolecular self-assembly.

Photophysical and spectroscopic analyses confirmed the formation of the three mannosylated sensors displaying 14, 28, and 42 sugar units. Each complex adopted original and unique spatial arrangements.

The sensors were used to investigate the influence of carbohydrate spatial arrangement and clustering on the mechanistic and qualitative properties upon lectin binding. Simple visualization of binding between a fluorescent, multivalent mannose complex and the *Escherichia coli* (*E. coli*) strain ORN178 that possesses mannose-specific receptor sites, illustrates the potential for these complexes as biosensors.

1. Introduction

Carbohydrate–lectin interactions are critical to many biological systems.[1] Consequently, a better understanding of their interplay will provide important insights into specific biological processes. The weak affinities of carbohydrate–protein binding require improved tools to analyze carbohydrate–lectin complexes. Detection and read-out of binding can be improved by multivalent probes since they amplify the weak interactions and enhance the potency of carbohydrate ligands.

Many multivalent carbohydrate-based tools such as dendrimers, polymers, micelles and nanoparticles, as well as carbohydrates built on templates of cyclodextrins and calixarenes have been synthesized to monitor glycan-lectin recognition and binding events by electronic, optical, or microgravimetric methods.[2] These multivalent probes can be functionalized with carbohydrates either through linear synthesis where the sugar building blocks are incorporated during the synthetic process ("building-with-a-template"), or *via* convergent synthesis where sugar functionalization takes place as a discrete, final step ("building-on-a-template"). "Building-on-a-template" is advantageous for generating libraries of multivalent carbohydrate-based probes as different carbohydrate groups can be displayed by a variety of synthetic methods on a "fixed" core structure.

Important considerations for designing multivalent probes are valency, the spatial arrangement of the lectin target's multiple binding sites, and the response to external stimuli, such as biological or chemical triggering by carbohydrate–lectin binding.[3] No ideal scaffold for multivalent carbohydrate presentation exists, even though a myriad of systems have been described. For instance, C_5-symmetrical glycoconjugates that orient five ganglioside GM1 pentasaccharides can neutralize the pentameric Cholera toxin *via* a specific and multivalent interaction.[4] Similarly, a multivalent C_3-symmetrical ganglioside GM3 trisaccharide is a potent inhibitor of influenza virus hemagglutination.[5]

With the goal of creating a new architecture for multivalent sugar presentation using the "building-on-a-template" strategy, I developed three small-molecule scaffolds that are synthetically facile, robust, with tunable symmetry, and can accommodate different carbohydrate ligand functionalization with distinct optical and electrochemical properties. This platform is based on hydrophobic supramolecular interactions that allow for the self-assembly of a fluorescent scaffold with a multivalent system generating fluorescent, multivalent sensors.

The fluorescent core –the template– is derived from cis-bis(2,2'-bipyridine)dichlororuthenium(II) ($[Ru(bipy)_2]Cl_2$) or trichlororuthenium(III) ($RuCl_3$) to afford a di-adamantyl- (Ru2 **2**), a tetra-adamantyl- (Ru4 **3**), or a hexa-adamantyl-ruthenium(II) complex (Ru6 **4**). Around this core, βCDs, each equipped with seven mannose units to form βCDMan, self-assemble around the template as the the adamantyl "host" the CDs "guests" around the template.[6] Two different series of fluorescent compounds were produced by the host-guest interaction. One group of molecules contains only unmodified βCD (RuCD2 **5**, RuCD4 **6** and RuCD6 **7**). The second group of molecules consists of RuCDMan2 **8**, RuCDMan4 **9** and RuCDMan6 **10** bearing 14, 28 or 42 mannose units, respectively.

Multivalent carbohydrate presentation and lectin binding were examined using the RuCDMan complexes (**8–10**) and the lectin Concanavalin A (Con A). Surface plasmon resonance (SPR) measurements provided mechanistic, qualitative, and quantitative insights into the role of cluster arrangement. The fluorescence emission of the Ru(II) core was employed to visualize specific and shape-dependent interactions of **10** with *E. coli* strain ORN178 that exhibits mannose-specific receptor sites for recognition and binding to hosts cells.

2. Results and Discussion

2.1. Chemical Synthesis

Three variants of fluorescent templates were synthesized using common ligand **1** to afford the three scaffolds with distinct architectures for supporting the multivalent presentation of carbohydrate ligands.

Ligand **1** was obtained *via* a convergent synthesis using boc-protected β-alanine **11** and 4,4'-dimethyl-2,2'-bipyridine **14** as starting materials. **12** was obtained using water-soluble coupling reagent *N*-ethyl-*N*'-(diethylaminopropyl)-carbodiimide (EDC) and 1-adamantanamine in the presence of triethylamine (Et_3N), followed by deprotection of the amine using trifluoroacetic acid (TFA) to afford the amine **13**. In parallel, **14** was oxidized with chromium trioxide (CrO_3) in sulfuric acid (H_2SO_4) to afford the dicarboxylic acid **15** which was then converted to the activated diacid chloride before amide coupling with **13** to afford the ligand **1** (Scheme 1).

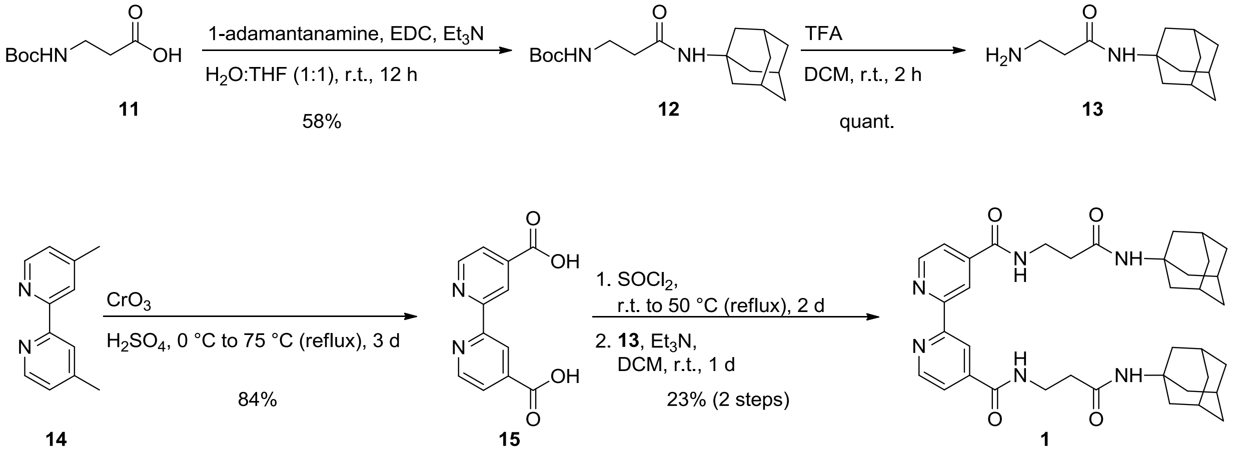

Scheme 1. Schematic overview of the synthetic procedure for ligand **1**.

The scaffolds were comprised of a central Ru(II) core that was equipped with either two (Ru2 **2**), four (Ru4 **3**) or six (Ru6 **4**) adamantyl groups. The di-adamantyl complex **2** was assembled by ligand complexation of **1** with $[Ru(bipy)_2]Cl_2$. Treatment of **1** with $RuCl_3$ using acetic acid (AcOH) as a reducing agent followed by bipyridine (bipy) as quenching agent, resulted in a mixture of tetra-adamantyl **3** and hexa-adamantyl **4**. The compounds were purified and separated by column chromatography (Scheme 2).

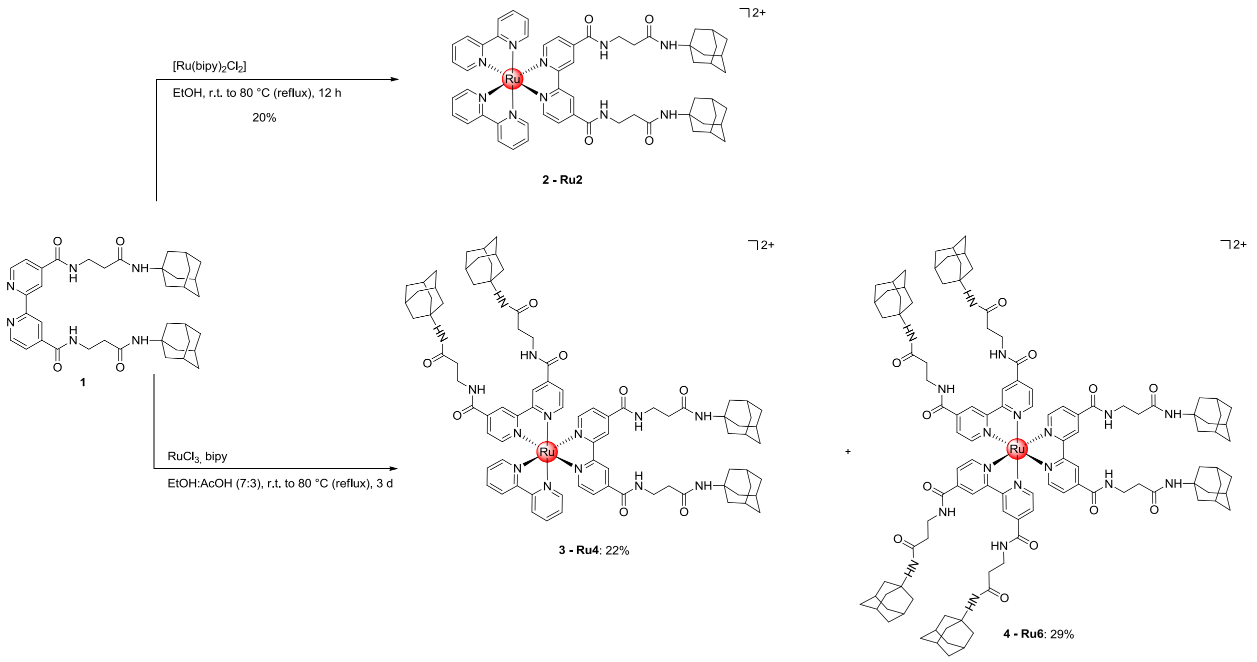

Scheme 2. Schematic overview of the synthetic procedure for the Ru-series **2–4**.

To demonstrate the supramolecular interaction between cyclodextrin derivatives and the adamantyl Ru(II) cores, complexes **2–4** were mixed with stoichiometric amounts (two, four and six equivalents) of native βCD mannosylated βCDMan (Scheme 3).

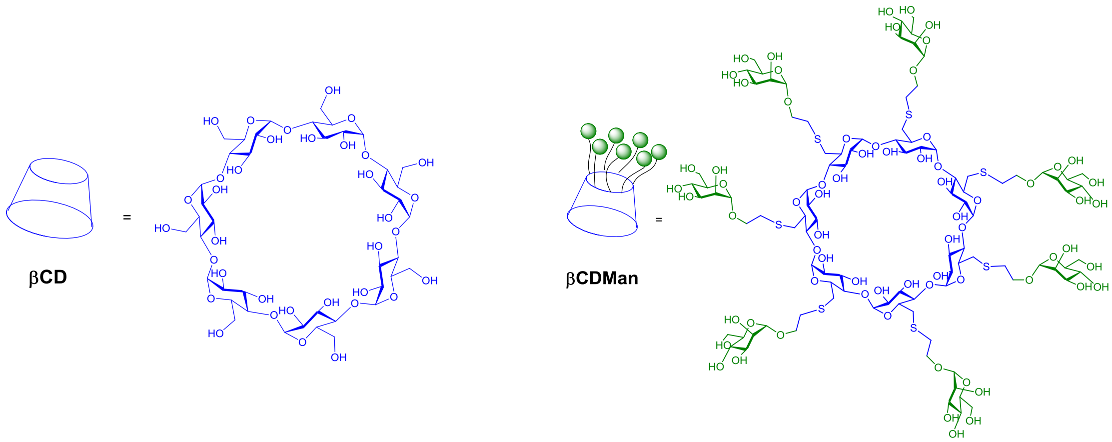

Scheme 3. βCD and βCDMan.

The complexes of the Ru-series **2–4** were only soluble in methanol. After mixing them with stochiometric amounts of native βCD, the different complexes of the RuCD-series **5–7** were obtained and were found to be soluble in water (Scheme 4).

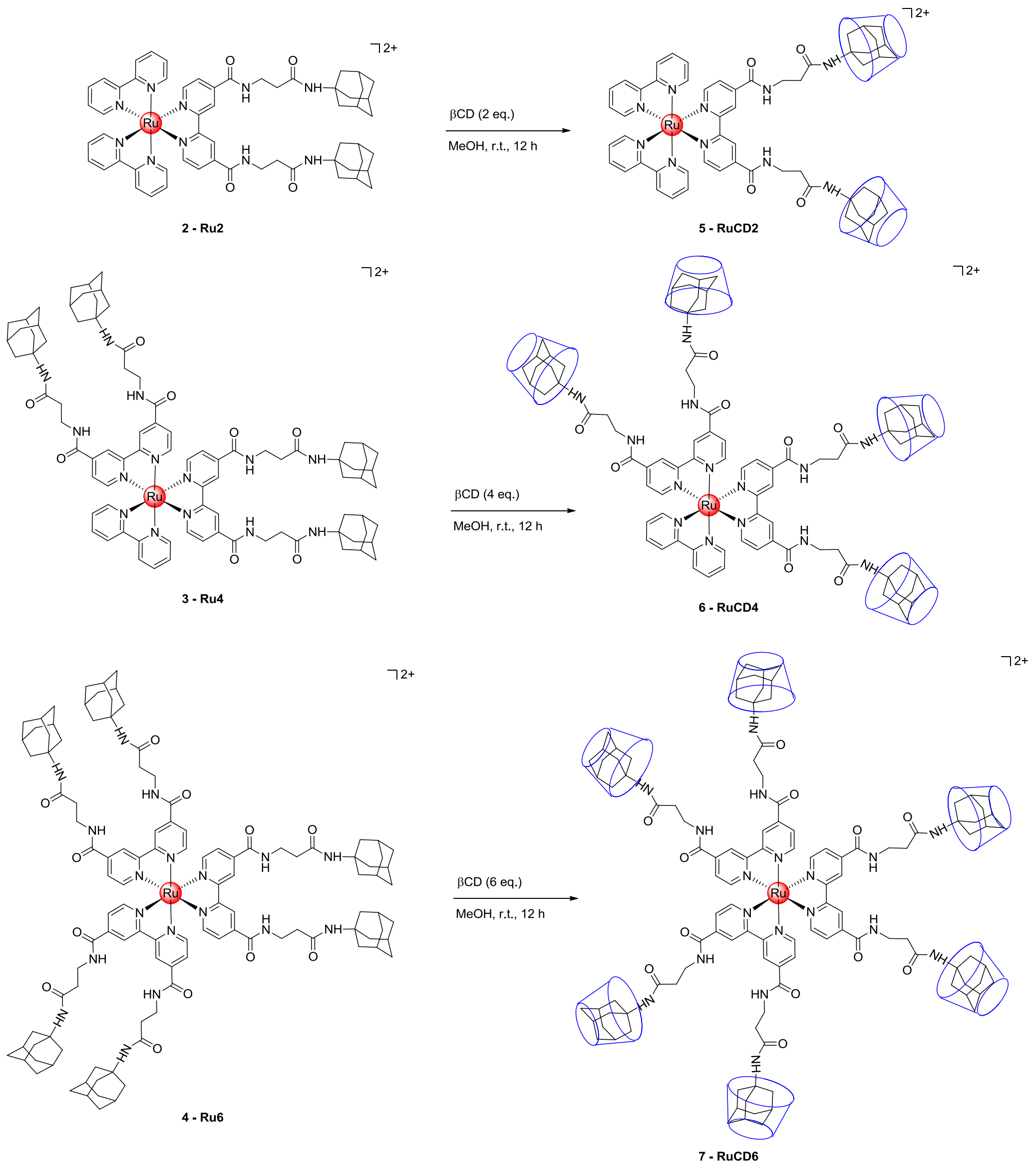

Scheme 4. Schematic overview of the synthetic procedure for the RuCD-series **5–7**.

Finally, a series of multivalent mannosylated structures was generated by mixing complexes **2–4** with βCDMan in water, using different mixing times and temperature, in stoichiometric amounts respective to the number of adamantyl units to afford RuCDMan2 **8**, RuCDMan4 **9** and RuCDMan6 **10**. These multivalent complexes expose 14, 28 or 42 mannose units on their periphery (Scheme 5).

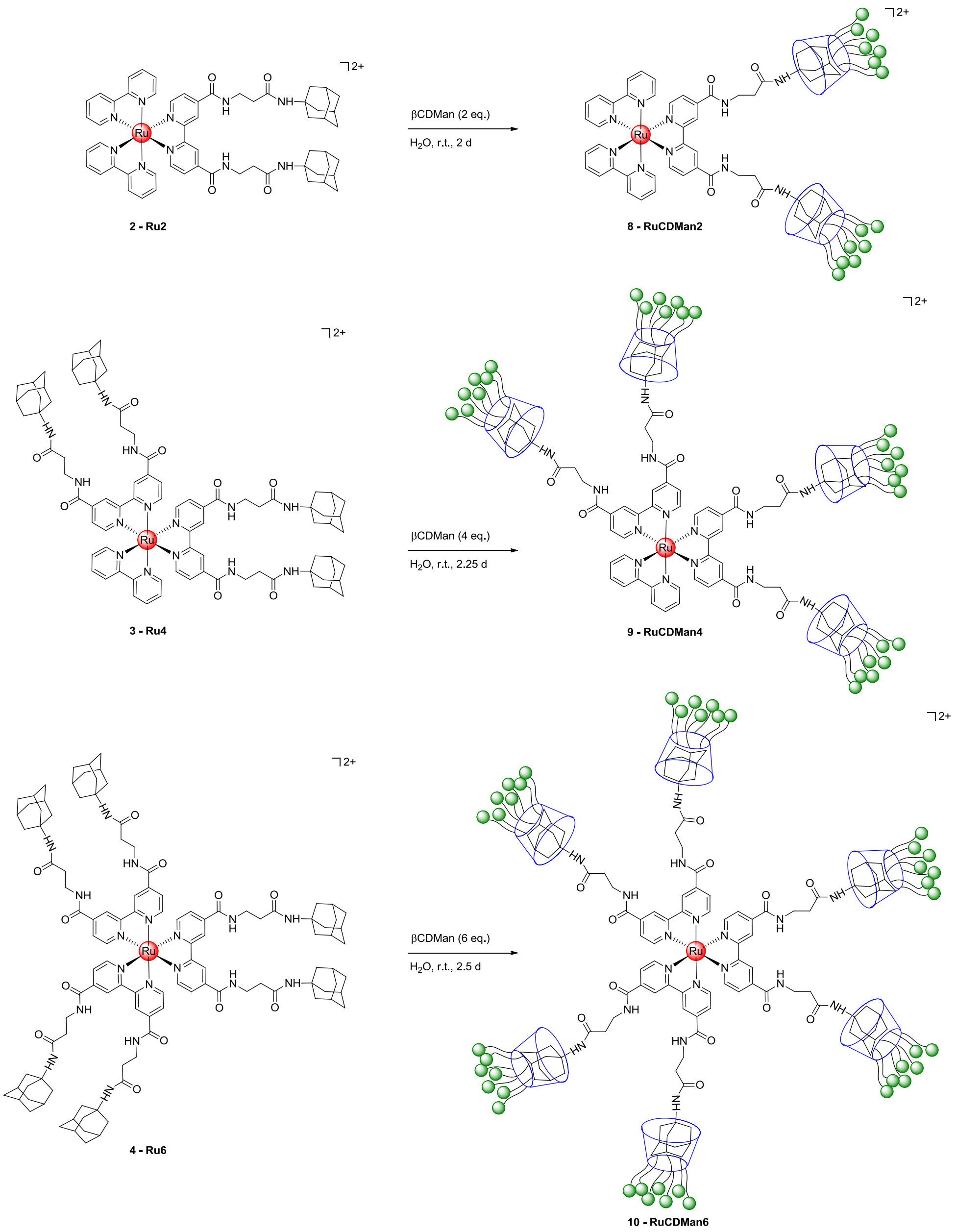

Scheme 5. Schematic overview of the synthetic procedure for the RuCDMan-series **8–10**.

It should be noted that complexes **2–4** can self-assemble with βCD carrying diverse glycosylation patterns thereby facilitating production of a collection of new multivalent systems.

2.2. Photophysical Properties

Ru(II) complexes have octahedral core symmetry, robustness, as well as strong oxidizing and reducing properties, thus rendering them attractive for use as sensors.[7] The photophysical properties of the Ru-series **2–4** were examined and compared with the properties of the RuCD-series **5–7** to determine the effects of covering the Ru core with βCD (Figure 1A, B and Table 1).

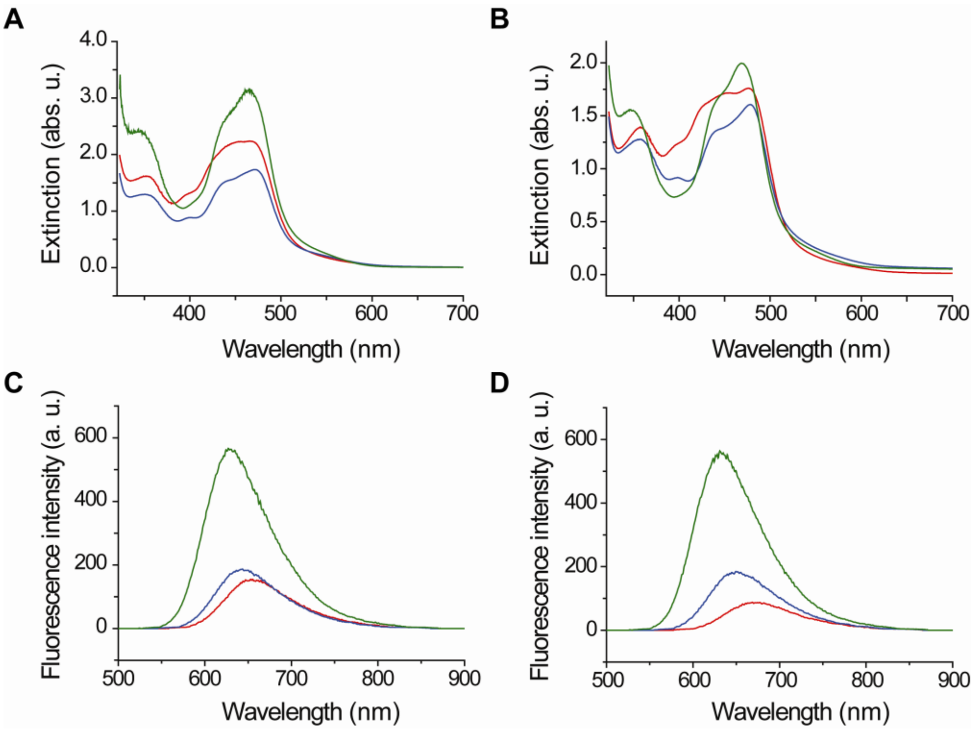

Figure 1. Absorption UV-vis spectra of (A) the Ru-series Ru2 **2** (red line), Ru4 **3** (blue line) and Ru6 **4** (green line) in MeOH and (B) the RuCD-series RuCD2 **5** (red line), RuCD4 **6** (blue line) and RuCD6 **7** (green line) in H_2O. Fluorescence emission spectra of (C) the Ru-series **2–4** in MeOH upon excitation at 475 nm and (D) the RuCD-series **5–7** in H_2O upon excitation at 475 nm.

The molar absorption coefficient $\varepsilon_{\lambda_{\max}^{\text{abs.}}}$, or molar absorptivity, is a measurement of how strongly a chemical species absorbs light at a given wavelength λ. The wavelength $\lambda_{\max}^{\text{abs.}}$ for which we got the maximal absorption in the UV spectra was chosen. This intrinsic property of the species was calculated from the maximal absorbance $A_{\max}$ at $\lambda_{\max}^{\text{abs.}}$ of each sample and is related to the pathlength l of the cell and to the concentration c of the different species *via* the Beer-Lambert law:

$$A_{\max} = \varepsilon_{\lambda_{\max}^{\text{abs.}}} \times c \times l \qquad (1)$$

From here, the molar absorption coefficient $\varepsilon_{\lambda_{\max}^{\text{abs.}}}$ could be calculated and the resultant values are listed in Table 1.

$$\varepsilon_{\lambda_{\mathrm{max}}^{\mathrm{abs.}}} = \frac{\mathrm{A_{max}}}{\mathrm{c} \times \mathrm{l}} \tag{2}$$

From these data, the relative fluorescence quantum yields could be also determined by measuring the fluorescence of a reference fluorophore (in this case, rhodamine) of known quantum yield Φ_{ref}. The quantum yield Φ of the different complexes was then calculated by:

$$\Phi = \Phi_{\mathrm{ref}} \times \frac{\mathrm{c}}{\mathrm{c_{ref}}} \times \frac{\mathrm{S_{ref}}}{\mathrm{S}} \tag{3}$$

where $\Phi_{ref} = 0.31$ (quantum yield of the reference), $c_{ref} = 1.67 \cdot 10^{-5}\ mol \cdot L^{-1}$ (concentration of the reference), and S, S_{ref} express the area under the emission peak. The results are listed in Table 1.

All spectra contain a first transition band (^{1}IL), located at around 350 nm, that is assigned to metal-centered d-d transitions.[8] An intense absorption band at about $\lambda_{\mathrm{max}}^{\mathrm{abs.}} \approx 475$ nm, and a shoulder at 450 nm dominate the spectra and originate from the splitting of the energy level of the first excited state caused by the trigonal symmetry of the complex. Both bands are assigned to a t_{2g}(Ru) → π^*(bipy) metal-to-ligand-charge transfer (^{1}MLCT).[9] The emission spectra of the Ru-series and the RuCD-series exhibited an emission band at around $\lambda_{\mathrm{max}}^{\mathrm{em.}} \approx 640$ nm. An increase in emission intensity and calculated quantum yield Φ directly correlates with the increasing complexity of the structures as more units of ligand **1** and βCDs are assembled around the Ru(II) core (Figure 1C, D and Table 1).[10]

Table 1. Photophysical data for ruthenium complexes **2–4** (in MeOH) and complexes **5–7** (in H_2O).

Entry	$\lambda_{\mathrm{max}}^{\mathrm{abs.}}$(nm)	$\mathrm{A_{max}}$	$\varepsilon_{\lambda_{\mathrm{max}}^{\mathrm{abs.}}}$(L·mol^{-1}·cm^{-1})	$\lambda_{\mathrm{max}}^{\mathrm{em.}}$(nm)	Φ
2	466.0	2.38	4760	668.5	0.14
3	471.0	1.73	3460	644.5	0.16
4	460.5	3.15	6300	631.0	0.48
5	477.0	1.76	5189	655.0	0.12
6	478.0	1.61	4586	641.5	0.23
7	468.5	1.99	5836	627.0	0.70

Physical shielding of the core by the surrounding scaffold prevents effective fluorescence quenching by dioxygen and solvent. Comparison of the quantum yields Φ within the Ru-series (complexes **2**, **3**, and **4**) illustrates the influence of the number of adamantyl ligands **1** on the fluorescence intensity. The consequences of forming supramolecular assemblies however are highlighted by direct comparison of a Ru-series complex and its RuCD equivalent such as comparing **3** and **6**, or **4** and **7**. Interestingly, no difference was observed when **2** and **5** were compared. This is likely because complexes **2** and **5** differ by the addition of only two βCDs, a minor structural difference, whereas an additional four βCD molecules have been incorporated into complex **6**, and six βCD molecules into complex **7**. While the bulky βCDs in **6** and **7** efficiently shield the fluorescent core from the environment, the two βCDs in complex **5** are not sufficient and consequently the fluorescent chromophore is easily quenched. Fluorescence peak analysis indicated a blue or hypsochromic shift, from 668.5 nm to 631.0 nm in the Ru-series, and from 655.0 nm to 627.0 nm in the RuCD-series occurs as more adamantyl ligand **1** or more βCD is added to the Ru(II) core. The observed hypsochromic shift of luminescence is possibly a consequence of so-called rigidochromism described in highly-hindered complexes.[11]

To summarize, an increasing number of adamantyl ligands **1** and, consequently, βCD units around the metal center strongly influenced the photophysical and colloidal properties of the Ru(II) core. Encapsulation of the core with βCDs led to an increase in fluorescence intensity through protection of the core properties.

2.3. Mass Spectrometric Analysis of the Supramolecular Complexes

The RuCD complexes **5–7** were analyzed by mass spectrometry to determine their stoichiometry and to analyze the supramolecular assembly.[12] Only small amounts of the RuCDMan complexes **8–10** were available and therefore these larger and heavier structures were not investigated. Electrospray ionization (ESI) is recognized as a soft ionization method that accommodates the generation of intact molecular ions from different species, including large non-volatile organic molecules and biopolymers.[13] On the other hand, the detection of non-covalent assemblies by ESI mass spectromethy remains challenging since supramolecular interactions are often disrupted during the electrospray process. To keep non-covalent complexes intact during the ionization and ion transmission processes, nano-ESI technique was employed.[14]

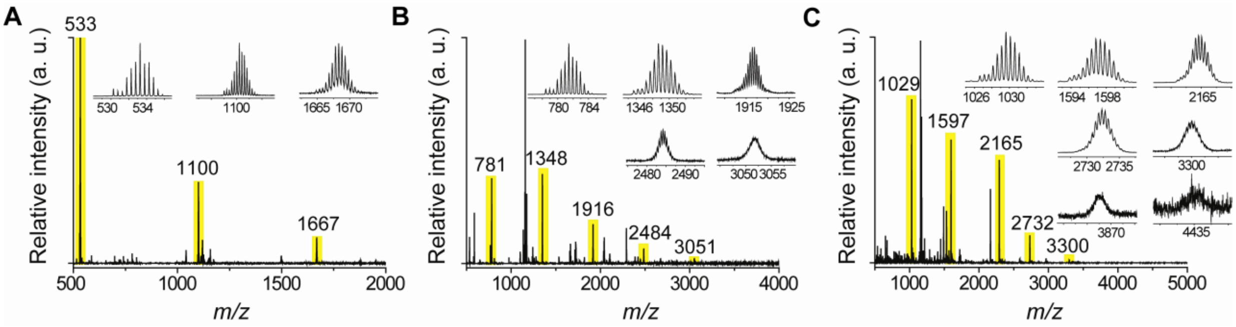

Figure 2. ESI mass spectra of (A) RuCD2 **5**, (B) RuCD4 **6**, and (C) RuCD6 **7**. Peaks corresponding to doubly charged ions of assembled, partially disassembled, and fully disassembled complexes are highlighted with yellow bars, marked with corresponding *m/z* values, and magnified (see insets).

Figure 2A shows the full-scan of the RuCD2 **5** sample. The positive-ion mass spectrum of fully assembled complex **5** clearly reveals a doubly-charged ion $[RuCD_2]^{2+}$ with a mass-to-charge ratio (*m/z*) of approximately 1668. A broad isotope distribution due to the presence of Ru^{2+} is in agreement with the theoretically calculated isotope pattern (Figure 3).

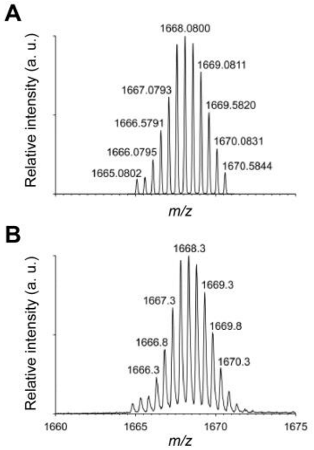

Figure 3. (A) Simulated isotopic distribution of the doubly charged ions of the fully assembled RuCD2 **5** along with (B) the zoom-ins of the respective peaks from the measured spectra. The disagreement between the theoretical and experimental peak positions are due to the systematic error of mass calibration and errors of the peak detection algorithm.

No Ru-containing ions with higher *m/z* values were detected in the mass spectrum, indicating the absence of non-specific aggregates of βCD molecules and Ru-containing ligand either in the electrospray plume or inside the mass spectrometer.12 The peaks at *m/z* around 1100 and 533 corresponding to $[RuCD]^{2+}$ and $[Ru]^{2+}$ ions, respectively, were also detected. The presence of these ion peaks in the mass spectrum indicated partial dissociation of complex **5**. Acceleration and collision of the analyte ions with neutral gas molecules during the electrospray ionization process caused the observed dissociation of the supramolecular complex, and could even have led to covalent bond cleavage under different conditions.[15]

The highlighted peaks in the full-scan mass spectrum of **6** (Figure 2B) correspond to ions from fully-assembled $[RuCD_4]^{2+}$ (*m/z* 3050) and the partially-assembled supramolecular complexes $[RuCD_3]^{2+}$ (*m/z* 2483), $[RuCD_2]^{2+}$ (*m/z* 1916), $[RuCD]^{2+}$ (*m/z* 1349), and $[Ru]^{2+}$ (*m/z* 781). No non-specific aggregates of Ru ligand and βCD were evident in the higher *m/z* range. Although a peak corresponding to the doubly-charged ion of fully assembled RuCD4 complex **6** was detectable, the resolution was not high enough to correctly resolve the individual isotope peaks (Figure 4).

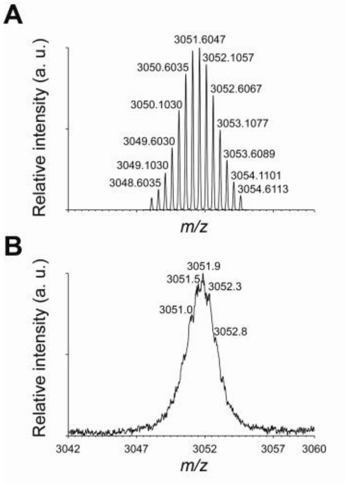

Figure 4. (A) Simulated isotopic distribution of the doubly charged ions of the fully assembled RuCD4 **6** along with (B) the zoom-ins of the respective peaks from the measured spectra. The disagreement between the theoretical and experimental peak positions are due to the systematic error of mass calibration and errors of the peak detection algorithm.

A full-scan mass spectrum of RuCD6 **7** is shown in Figure 2C. Since the $[RuCD_6]^{2+}$ ion has a *m/z* value of approximately 4432, relatively high acceleration voltages were applied to the ion guides to facilitate ion transport. High acceleration of ions resulted in collision-activated dissociation of non-covalent complexes. Nevertheless, signals from ions of partially-assembled RuCD6 complexes such as $[RuCD_5]^{2+}$ (*m/z* 3865), $[RuCD_4]^{2+}$ (*m/z* 3298), $[RuCD_3]^{2+}$ (*m/z* 2731), $[RuCD_2]^{2+}$ (*m/z* 2164), $[RuCD]^{2+}$ (*m/z* 1597), and $[Ru]^{2+}$ (*m/z* 1030) were detected in the mass spectrum (Figure 5).

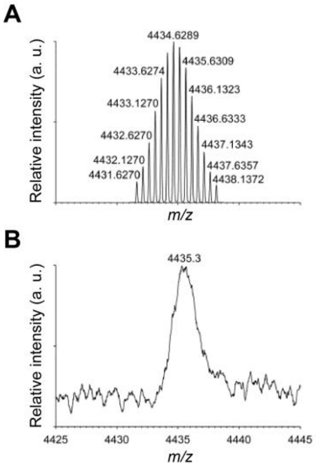

Figure 5. (A) Simulated isotopic distribution of the doubly charged ions of the fully assembled RuCD6 **7** along with (B) the zoom-ins of the respective peaks from the measured spectra.

After the initial failure to measure the fully assembled complex **7** with conventional ESI and nano-ESI sources, different electrospray-based soft ionization methods, such as electrosonic spray ionization (ESSI) and cold-spray were employed. These measurements resulted in signals from $[RuCD6]^{2+}$ above the detection limit and differences in ion yields for assembled, partially, and fully disassembled complexes were observed.

Overall, nano-ESI mass spectrometry-based analysis of the RuCD complexes **5–7** confirmed the existence of complete supramolecular assembly. Stabilizing forces such as dispersion interactions between adamantyl moieties of the Ru(II)-containing ligands and the cavity of the cyclodextrins were insufficient to preserve the complexes from collision-activated dissociation, thus resulting in the presence of partially assembled complexes.

2.4. NMR Study of the Supramolecular Complexes

To confirm that the supramolecular assemblies are anchored by adamantyl groups acting as hosts in the cyclodextrin guests, NMR was employed. Unfortunately, comparative measurements were complicated by the fact that some of the complexes (**2–4**) were only soluble in methanol, whereas others (**5–10**) were only soluble in water. ^{1}H NMR spectra were inconclusive in determining whether the inclusion complex between adamantyl moieties and native βCD or βCDMan occurred for each adamantyl group. Different chemical shift patterns of the adamantyl protons were observed when comparing the ^1H NMR of different complexes and may have resulted only from solvent effects rather than supramolecular assembly.

Nuclear Overhauser effect spectroscopy (NOESY) experiments definitively illustrated the proximity of the adamantyl groups to cyclodextrin. Cross peaks arising from the proximity of the adamantyl moiety and cyclodextrin *via* NOESY analysis of solutions of **5**, **6** and **7** in D_2O were observed (Figure 6A–C).[16]

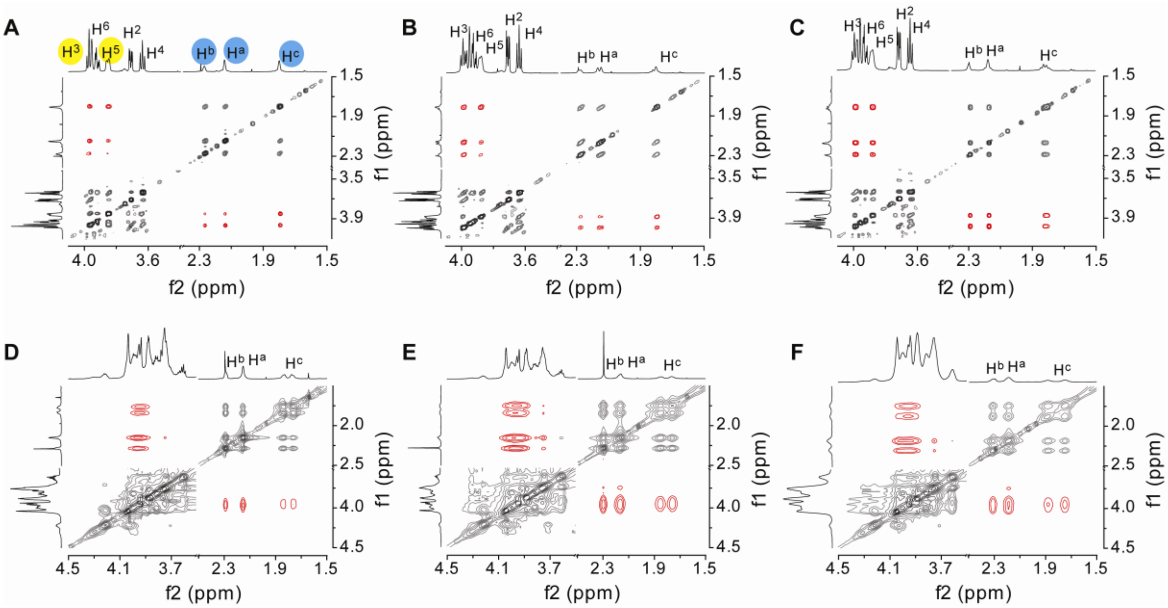

Figure 6. Significant cross peaks from the NOE spectra of (A) RuCD2 **5**, (B) RuCD4 **6** and (C) RuCD6 **7** and of (D) RuCDMan2 **8**, (E) RuCDMan4 **9** and (F) RuCDMan6 **10**. Cross peaks between H^3 and H^5 of βCD or βCDMan and H^a, H^b and H^c of adamantyl are emphasized in red in the spectra (Figure 7).

The cross peaks indicate strong interactions between H^3 and H^5 of βCD with all adamantyl protons (H^a, H^b and H^c) throughout the RuCD complexes (Figure 7).

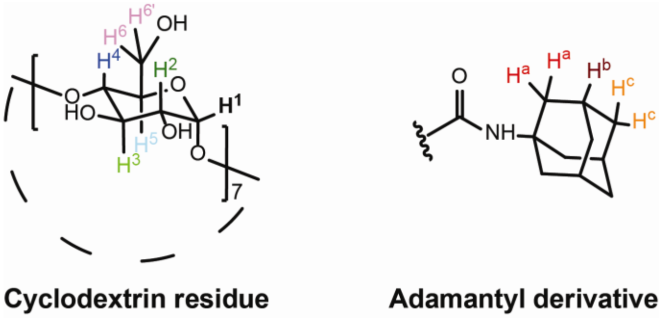

Figure 7. Proton designation of the relevant peaks of the molecule involved in the supramolecular assembly.

Thus, it was confirmed that the adamantyl derivative penetrated completely into the βCD core. Since H^2 and H^4 of βCD are localized outside the cavity, they do not interact with adamantyl protons. All βCD protons in the ^1H NMRs (complexes **5–7**) were shifted in comparison to the peaks of native βCD in D_2O, and proton signals signifying free native βCD were absent (Table 2). All βCD and adamantyl units observed by NMR appear to be involved in supramolecular inclusion, indicating that all complexes were fully assembled.

Table 2. ^1H NMR (in D_2O) chemical shifts of C-H protons from native βCD and from Ru(II)-complexed βCD in the RuCD-series **5–7**.

Entry	Proton shift (ppm)					
	H^1	H^2	H^3	H^4	H^5	H^6
βCD	4.68	3.26	3.58	3.19	3.47	3.49
RuCD2 **5**	5.12	3.71	3.99-3.90	3.64	3.85	3.99-3.90
RuCD4 **6**	5.13	3.71	4.00	3.64	3.89	3.98-3.91
RuCD6 **7**	5.13	3.71	4.02-3.90	3.64	3.88	4.02-3.90

Figure 6D–F show the cross peaks observed from NOESY experiments for solutions of **8**, **9** and **10** in D_2O. Due to the very complex ^1H NMR between 4.2 and 3.6 ppm, it was difficult to identify the H^3 and H^5 of βCDMan and assign changes after supramolecular assembly. Instead, we focused our attention on the protons of the adamantyl moiety and observed a strong NOE interaction with protons from the βCDMan region. As described above for complexes **5–7**, three defined cross-coupling peaks appeared to result from the interaction between βCDMan and three different protons of the adamantyl moiety (H^a, H^b and H^c). In comparison, for complexes **8–10**, the outermost protons of the adamantyl group (H^c) probably split due to the larger steric environment of βCDMan (attributable to the seven mannose residues).[17] Overall, the results from the NOESY experiments clearly indicate that the inner βCD and βCDMan protons are in close proximity to the adamantyl moieties, confirming the presence of fully assembled complexes in the RuCD- and RuCDMan-series **5–10**.

Overall, the combination of photophysical and spectroscopic structural analyses provided a near-complete analytical characterization of complexes **2–10**. Functional studies were conducted to determine binding behavior of the multivalent RuCDMan complexes **8–10**.

2.5. SPR Analysis of the Mannosylated Supramolecular Complexes

SPR is a valuable tool for analyzing protein–carbohydrate complex formation in real time, and for providing insights into the kinetics and mechanics of binding.[18] To understand the influence of mannose density of the RuCDMan complexes upon lectin binding at the surface, the interaction of complexes **8–10** with the mannose-specific plant lectin Con A was investigated.

SPR and kinetic analyses were based on a 1:1 interaction model.[19] Two different concentrations of Con A were covalently bound to a polycarboxylated sensor chip generating low (Con A-LD), and high (Con A-HD) density surfaces. Con A has four mannose binding sites. Immobilizing the lectin at low and high densities was intended to distinguish whether the presence of more mannose-binding sites would stabilize bound complexes, or whether binding site clustering would inhibit this interaction.

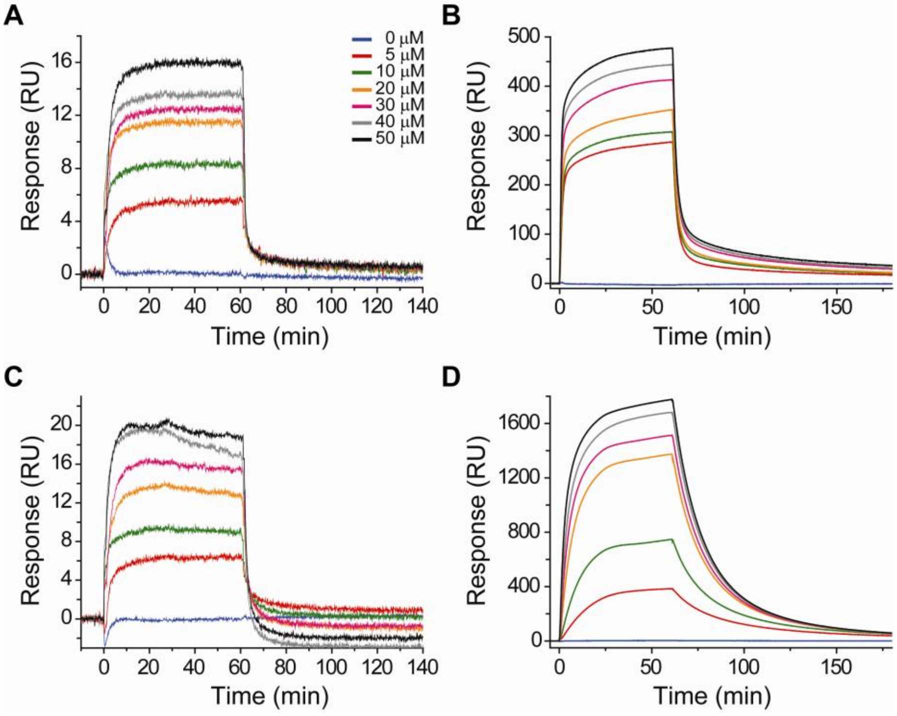

Figure 8. SPR sensorgrams of RuCDMan2 **8** and RuCDMan4 **9** at different concentrations (indicated). Graphs (A) and (B) show binding of RuCDMan2 **8** to Con A-LD and Con A-HD, respectively. Graphs (C) and (D) show binding of RuCDMan4 **9** to Con A-LD and Con A-HD, respectively.

The SPR analyses of ConA–RuCDMan2 **8** and ConA–RuCDMan4 **9** (Figure 8 and Table 3) indicate that both complexes **8** and **9** strongly prefer to bind Con A-HD over Con A-LD indicating that more mannose residues stabilize the binding interaction. This trend correlates well with the prior characterization of Con A binding to mannose.[20] Closer examination shows that **9** binds to Con A-HD more efficiently than **8**, and also that **8** dissociates from Con A much faster than **9** (Figure 8B, D). For the Con A-LD–complex interactions, the K_d for **8** is lower than for **9**. The slight difference in the specific K_d values is most likely attributable to the generally weak binding of the complexes to Con A-LD than to the individual binding capacity of **8** and **9**. Interestingly, complex **10** did not bind to Con A. The binding curves obtained for the interaction between **10** and Con A-HD, as well as Con A-LD were comparable to the results obtained using only 4-(2-hydroxyethyl)-1-piperazineethanesulfonic acid (HEPES) buffer as a negative control. This outcome is not entirely surprising since similar results have been reported for highly multivalent probes.[21] In this case, the addition of two βCDMan units (the structural difference between complexes **9** and **10**) impeded binding with Con A, despite the greater number of mannose residues available for the interaction. One explanation for this finding is that the inherent bulkiness of **10** may prevent the formation of stable interactions between mannose and Con A. Additionally, the spatial arrangement of the mannose-bearing cyclodextrins is important: in the case of **10**, the mannose pattern may represent a non-ideal setup for interacting with surface-immobilized Con A. Together, these results show that in the context of a multivalent platform, the strength of the binding interaction between Con A and mannose directly correlates with the number of participating mannose residues. Nonetheless, there is an upper limit to that number and the sugar structural presentation. Beyond this limit, binding efficiency declines.

Table 3. Equilibrium constants, K_d, of RuCDMan2 **8** and RuCDMan4 **9**.

Entry	K_d (mM)	
	Con A-HD	**ConA-LD**
RuCDMan2 **8**	48.00	17.78
RuCDMan4 **9**	13.88	12.18
RuCDMan6 **10**	No binding	No binding

2.6. Confocal Microscopy with the Mannosylated Supramolecular Complexes

Since the binding capacity of complex **10** was unable to be assessed by SPR, an alternative strategy was devised using the outer surface of bacteria as the target for lectin recognition and binding. Two *E. coli* strains, ORN178 and ORN208, were used.[22] Both strains produce type 1 pili but differ in their expression of the pilus-component FimH, a mannose-specific adhesin. While ORN178 expresses wild-type FimH, ORN208 carries a mutation in the fimH gene which renders the pili unable to bind mannose. Each bacterial strain was incubated with either complex **10** or the negative control –complex **7** that does not contain mannose– and confocal microscopy was then used to visualize the interaction between the complexes and the bacterial pili. The Ru(II)-containing complexes were observable by virtue of their inherent red fluorescence, and the bacteria by using blue 4',6-diamidino-2-phenylindole (DAPI) stain.

Binding was only evident between mannosylated complex **10** and ORN178 (Figure 9A, B). Binding did not occur between complex **10** and ORN208 strain as anticipated due to the mutation in fimH (Figure 9D).[23] Other controls were performed to prove the specificity of the complex towards ORN178. As expected, complex **7** failed to bind to both ORN178 (Figure 9C) and ORN208 (Figure 9E).

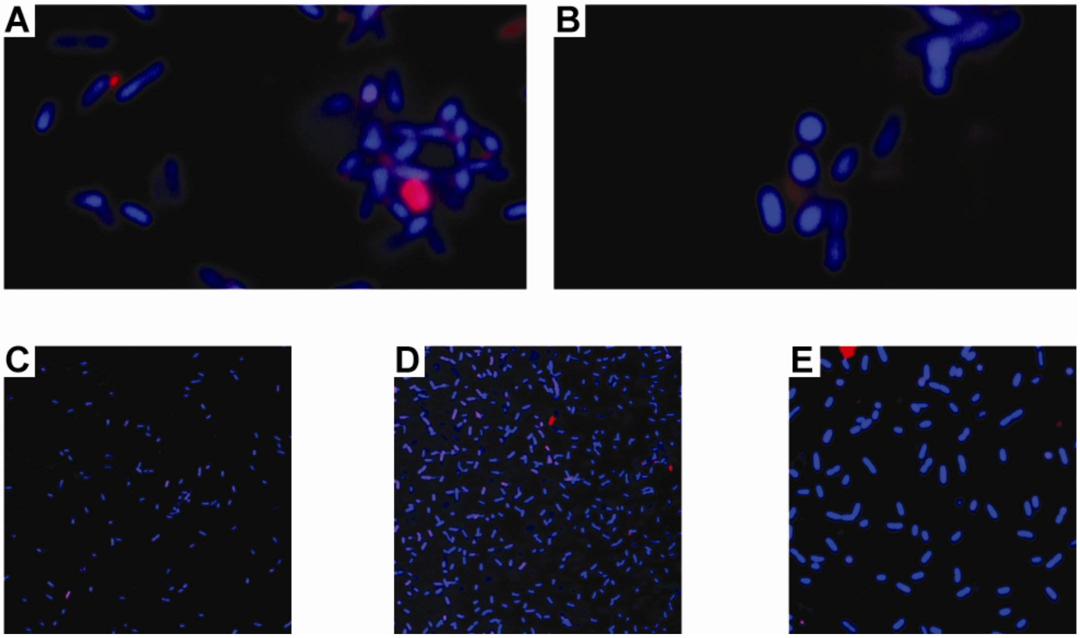

Figure 9. Confocal laser scanning microscopy images for (A), (B) the incubation of bacteria *E. coli* strain ORN178 with RuCDMan6 **10**. Incubation of (C) ORN178 with RuCD6 **7**, (D) ORN208 with RuCDMan6 **10**, and (E) ORN208 with RuCD6 **7** as negative controls.

The images obtained by confocal microscopy show the Ru core as red fluorescent spots that decorate the lateral end of the bacteria along the pili. This implies that complex **10** is attached to the mannose-binding lectin FimH at this site. The molecular interaction between complex **10** and *E. coli* strain ORN178 was both specific and easily detectable, giving rise to the idea that this new fluorescent and highly multivalent system may be adapted to detect bacteria.

Star-shaped clusters of bacteria were produced during incubation with **10** (Figure 9A, B) and may be attributable to the specific arrangement of this octahedral ruthenium complex. This arrangement will be the subject of future investigations.

3. Conclusion

In the chapter 3, I described the synthesis of three different templates that ultimately generate three new scaffolds for the presentation of multiple multivalent carbohydrate ligands by supramolecular assembly. The multivalent complexes self-assemble and display carbohydrates with unique spatial orientation. In addition, binding interactions between the carbohydrate epitopes and lectins were investigated by SPR. Previously, multivalent probes, such as supramolecular and conductive glycopolymers, carbohydrate-capped gold nanoparticles, and quantum dots have been used as probes to identify specific *E. coli* strains or other cell lines.[24]

Taking advantage of the fluorescent properties of Ru(II), distinct interactions between mannosylated complex **10** and *E. coli* strain ORN178 were observed using confocal microscopy. The simplicity of this screen highlights the potential of using these complexes as adaptable and user-friendly bacterial sensing tools. The significance of another property of multivalent complexes was also illustrated by incubating complex **10** with ORN178: the bacterial clusters that formed around the complex were distinctive and star shaped. Therefore, it is likely that the spatial arrangement of the ligands on the multivalent complex ultimately restrict the orientation of the lectins.

Consequently, it may be possible to construct nanostructures that will interact with multiple target binding sites on bacterial cells or proteins in a shape-dependent manner, providing an easy visual read-out of a particular molecular interaction. Application of the multivalent probes to explore other carbohydrate–lectin interactions will be facilitated by the flexible architecture of this system: the mannosylated cyclodextrins are interchangeable with any glycosylated βCD. Simple interchange of the carbohydrate epitopes will also greatly streamline generating collections of multivalent probes.

4. Experimental Part

4.1. Chemical Synthesis

4.1.1. General Experimental Details

Commercial grade reagents and solvents were used without further purification except as indicated below. Deionized water was obtained from an in-house purification system (Millipore). The term "concentrated under reduced pressure" refers to the removal of solvents and other volatile material using a rotary evaporator while maintaining a water bath temperature around 40 °C. The compounds purified by flash chromatography are further concentrated by the removal of residual solvent under high vacuum (< 0.2 mbar). Room temperature (r.t.) refers to the ambient temperature (20–25 °C).

4.1.2. Physical Properties and Spectroscopic Measurements

^{1}H NMR and ^{13}C NMR spectra were measured with a Varian 400-MR, Varian 600-MR, Bruker ECP 400, Bruker AC 500, or Bruker AC 700 spectrometer. The residual proton signal of solvent at δ 7.26 ppm for $CDCl_3$, 3.34 ppm for CD_3OD, and 4.79 ppm for D_2O was used as an internal reference for ^{1}H spectra. For ^{13}C spectra, the chemical shifts are reported relative to the δ 77.36 ppm for $CDCl_3$ and 49.86 ppm for CD_3OD. Coupling constants (*J*) are reported in Hertz (Hz). Multiplicities are given as: *s* (singlet); *d* (doublet); *t* (triplet); *dd* (doublets of doublet); *ddd* (doublets of doublets of doublet); *q* (quartet); *m* (multiplet) or *td* (triplets of doublet). High-resolution mass spectra (HRMS) analyses were performed by the mass service of the Free University Berlin. ESI mass spectra were run on an Agilent 6210 ESI-TOF mass spectrometer. Analytical thin layer chromatography (TLC) was performed on Kieselgel 60 F_{254} glass plates precoated with a 0.25 mm thickness of silica gel. The TLC plates were visualized with UV light and by staining with Hanessian solution (ceric sulfate and ammonium molybdate in aqueous sulfuric acid) or potassium permanganate solution (potassium permanganate in basic aqueous solution). Column chromatography was performed using Kieselgel 60 (230–400 mesh) silica gel with a typical 50–100:1 weight ratio of silica gel to crude product.

4.1.3. Synthesis

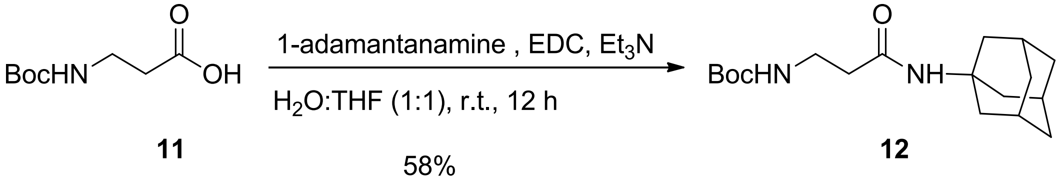

tert-Butyl (3-((3s,5s,7s)-adamantan-1-ylamino)-3-oxopropyl)carbamate (12)

1-Adamantylamine (1.60 g, 10.57 mmol) and 3-(*tert*-butoxycarbonylamino)propanoic acid **11** (2.0 g, 10.57 mmol) were dissolved in a mixture of H_2O:THF (1:1, 40 mL) at r.t. EDC (2.63 g, 13.74 mmol) was then added, followed by the addition of drops of Et_3N to reach pH 8. The reaction mixture was stirred over 12 h at r.t. The product was then extracted with EtOAc (50 mL) and the organic layer was washed with H_2O (2×40 mL). The resulting organic layer was then dried over $MgSO_4$, filtered, concentrated, and the crude was purified by flash column chromatography (silica gel, DCM:MeOH 19:1) and dried under *high vacuo* to give the product **12** (1.96 g, 58%) as a white foam.

R_f 0.72 (DCM:MeOH 19:1). ^{1}H NMR (700 MHz, $CDCl_3$) δ 5.30 (*s*, 1H), 5.23 (*s*, 1H), 3.35 (*dd*, *J* = 12.1 Hz, *J* = 6.1 Hz, 2H), 2.30 (*t*, *J* = 5.9 Hz, 2H), 2.06 (*s*, 3H), 1.97 (*d*, *J* = 3.0 Hz, 6H), 1.66 (*t*, *J* = 3.0 Hz, 6H), 1.42 (*s*, 9H). ^{13}C NMR (176 MHz, $CDCl_3$) δ 170.8. 156.3. 79.3, 52.2, 41.7, 37.2, 36.9, 36.4, 29.5, 28.5. HRMS (ESI, positive mode) calcd. for $C_{18}H_{30}N_2O_3Na$ $[M+Na]^+$: 345.2154, found: 345.2154.

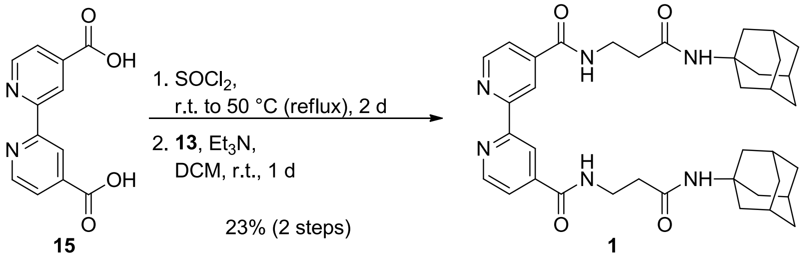

1,1'-(2,2'-Bipyridine-4,4'-diyl)bis-3-β-ethane-(adamantane) (1)

Under an Ar atmosphere, 2,2'-bipyridine-4,4'-dicarboxylic acid **15** (38 mg, 0.16 mmol) and $SOCl_2$ (2.0 mL, 27.40 mmol) were mixed together at r.t. to give a white suspension. The reaction mixture was then heated under reflux over 2 d at 50 °C to give a clear green solution. Excess of

$SOCl_2$ was removed by vacuum distillation at 70 °C and the crude was dried under *high vacuo* to give 2,2'-bipyridine-4,4'-dicarbonyl dichloride as a green solid which was then dissolved in dry DCM (5 mL) under N_2 atmosphere, followed by the addition of adamantyl derivative **13** (138 mg, 0.621 mmol). The resulting mixture was stirred for 5 min at r.t. and then treated dropwise with Et_3N to reach pH 8. The solution turned to rose and was stirred over 1 d at r.t. The solvent was then removed under reduced pressure and the residue was then purified by flash column chromatography (silica gel, DCM:MeOH 19:1 to 9:1), and dried under *high vacuo* to give **1** (23 mg, 23%) as a white solid.

R_f 0.45 (DCM:MeOH 9 : 1). ^{1}H NMR (700 MHz, $CDCl_3$) δ 8.71 (*t*, *J* = 4.8 Hz, 2H), 8.63 (*s*, 2H), 7.67 (*s*, 2H), 6.39 (*s*, 2H), 3.59–3.53 (*m*, 4H), 3.29 (*s*, 2H), 2.38 (*t*, *J* = 5.9 Hz, 4H), 1.97 (*s*, 6H), 1.90 (*s*, 12H), 1.58 (*s*, 12H). ^{13}C NMR (176 MHz, $CDCl_3$) δ 171.2, 166.4, 156.3, 150.0, 142.8, 121.8, 118.7, 52.2, 41.3, 36.7, 36.4, 36.3, 29.7. HRMS (ESI, positive mode) calcd. for $C_{38}H_{48}N_6O_4Na$ $[M+Na]^+$: 675.3629, found: 675.3646.

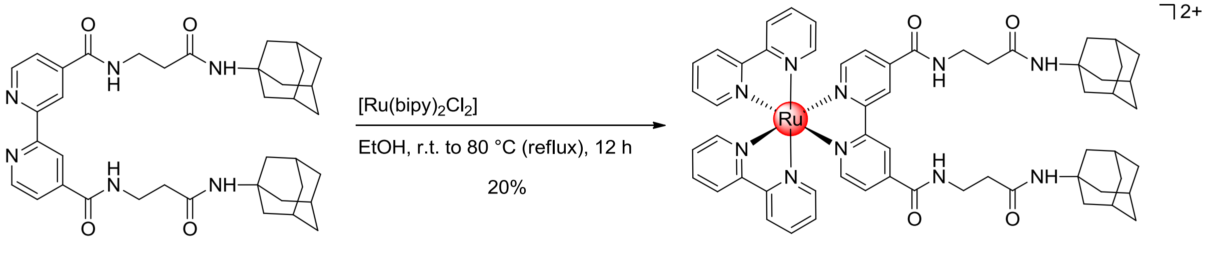

1

2 - Ru2

Ru-diadamantyl Ru2 (2)

Ligand **1** (67.0 mg, 103.0 μmol) was dissolved in EtOH (15 mL) at r.t. followed by the addition of $[Ru(bipy)_2]Cl_2$ hydrate (64.6 mg, 133.0 μmol) to give a dark purple suspension. The reaction mixture was then heated under reflux over 12 h at 80 °C. The solvent was then removed under reduced pressure and the residue was then dissolved in MeCN (2 mL). The crude was purified by flash column chromatography (silica gel, MeCN:sat. solution of KNO_3 97:3 to 8:2). The collected fractions were dried under reduced pressure, dissolved in a minimum of MeCN, and filtered to remove salts. The precipitation was repeated three times to ensure complete removal of salt and the filtrate was then dried under *high vacuo* to give the product **2** (21.4 mg, 20%) as a red solid.

R$_f$ 0.30 (MeCN:sat. solution of KNO_3 9:1). ^{1}H NMR (700 MHz, CD_3OD) δ 9.21 (*d*, *J* = 1.6 Hz, 2H), 8.74 (*dd*, *J* = 8.2, 4.7 Hz. 4H), 8.16 (*ddd*, *J* = 16.1, 8.3, 1.4 Hz, 4H), 8.02 (*d*, *J* = 5.9 Hz, 2H), 7.87–7.82 (m, 6H), 7.55–7.49 (*m*, 4H), 3.69 (*t*, *J* = 6.9 Hz, 4H), 2.52 (*t*, *J* = 7.0 Hz. 4H), 2.03 (*s*, 6H), 2.02 (*s*, 12H), 1.70 (*q*, *J* = 12.3 Hz, 12H). ^{13}C NMR (176 MHz, CD_3OD) δ 172.7, 172.7, 165.5, 165.5, 159.0, 158.4, 158.3, 153.5, 152.8, 152.6, 144.1, 139.6, 129.1, 126.6, 125.8, 123.4, 52.9, 49.5, 47.9, 42.3, 38.3, 37.5, 37.2, 30.9, 30.7, 9.2. HRMS (ESI, positive mode) calcd. for $C_{58}H_{64}N_{10}O_4Ru$ $[M]^{2+}$: 533.2080, found: 533.2092.

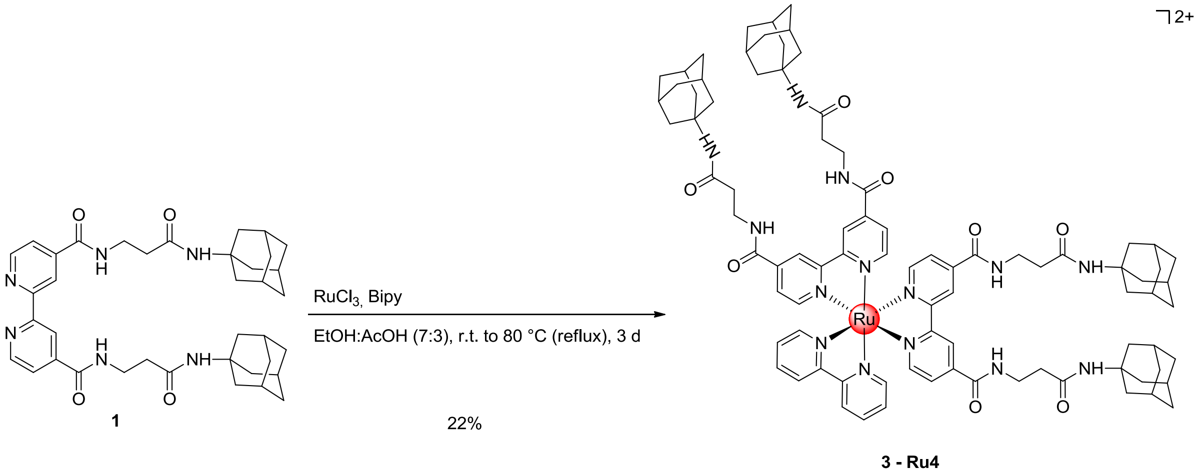

Ru-tetraadamantyl Ru4 (3)

Ligand **1** (120 mg, 180.0 μmol) and $RuCl_3$ trihydrate (11 mg, 40.0 μmol) were dissolved in a mixture of EtOH:AcOH (7:3, 20 mL) at r.t. The reaction mixture was heated under reflux at 80 °C. After 1 d, 2,2'-biypridine (28.0 mg, 180.0 μmol) was then added, and the reaction mixture was stirred under reflux at 80 °C for 3 h. The solvent was then removed under reduced pressure and the residue was then purified by flash column chromatography (silica gel, DCM:MeOH 75:25) to afford the product **3** (11.0 mg, 22%) as a red solid.

R$_f$ 0.48 (DCM:MeOH 3:1). ^{1}H NMR (400 MHz, CD_3OD) δ 9.15 (*s*, 4H), 8.73 (*d*, *J* = 8.3 Hz, 2H), 8.16 (*td*, *J* = 8.0, 1.4 Hz, 2H), 7.99 (*dd*, *J* = 7.4, 5.9 Hz, 4H), 7.83 (*ddd*, *J* = 10.7, 5.9, 1.8 Hz, 4H), 7.53–7.48 (*m*, 2H), 7.45 (*d*, *J* = 1.6 Hz, 2H), 3.66 (*td*, *J* = 6.8, 2.6 Hz, 8H), 2.49 (*td*, *J* = 6.8, 3.3 Hz, 8H), 2.13–1.92 (*m*, 36H), 1.76–1.61 (*m*, 24H). ^{13}C NMR (101 MHz, CD_3OD) δ 158.8, 158.8, 158.2, 153.7, 153.4, 152.8, 144.4, 144.4, 139.8, 129.2, 126.7, 125.8, 123.5, 106.4, 52.9, 47.9, 42.3, 38.3, 37.5, 37.2, 30.9, 9.2. HRMS (ESI, positive mode) calcd. for $C_{86}H_{104}N_{14}O_8Ru$ $[M]^{2+}$: 781.3609, found: 781.3635.

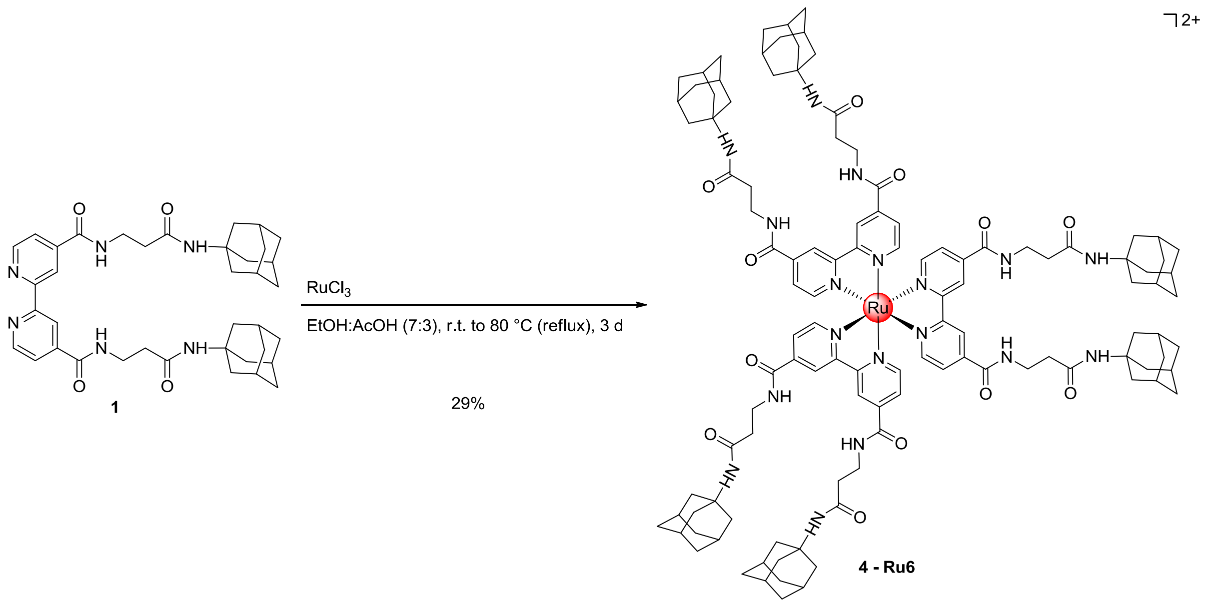

Ru-hexaadamantyl Ru6 (4)

Ligand **1** (120 mg, 180.0 μmol) and $RuCl_3$ trihydrate (11 mg, 40.0 μmol) were dissolved in a mixture of EtOH:AcOH (7:3, 20 mL) at r.t. The reaction mixture was heated under reflux at 80 °C. After 1 d. 2.2'-biypridine (28.0 mg, 180.0 μmol) was then added and the reaction mixture was stirred under reflux at 80 °C for again 3 h. The solvent was then removed under reduced pressure and the residue was then purified by flash column chromatography (silica gel, DCM:MeOH 85:15) to afford the product **4** (9.0 mg, 29%) as a red solid.

R_f 0.40 (DCM:MeOH 85:15). ^1H NMR (400 MHz, CD_3OD) δ 9.26 (*s*, 1H), 8.00 (*d*, *J* = 5.8 Hz, 1H), 7.85 (*d*, *J* = 6.0 Hz, 1H), 3.67 (*t*, *J* = 6.6 Hz, 2H), 2.50 (*t*, *J* = 6.8 Hz, 2H), 2.09–1.90 (*m*, 6H), 1.69 (*q*, *J* = 14.2 Hz, 4H). ^{13}C NMR (101 MHz, CD_3OD) δ 172.7, 165.1, 158.7, 153.7, 144.6, 126.9, 123.7, 106.4, 52.9, 42.3, 38.3, 37.5, 37.1, 30.9. HRMS (ESI, positive mode) calcd. for $C_{114}H_{144}N_{18}O_{12}Ru$ $[M]^{2+}$: 1029.5137, found: 1029.5180.

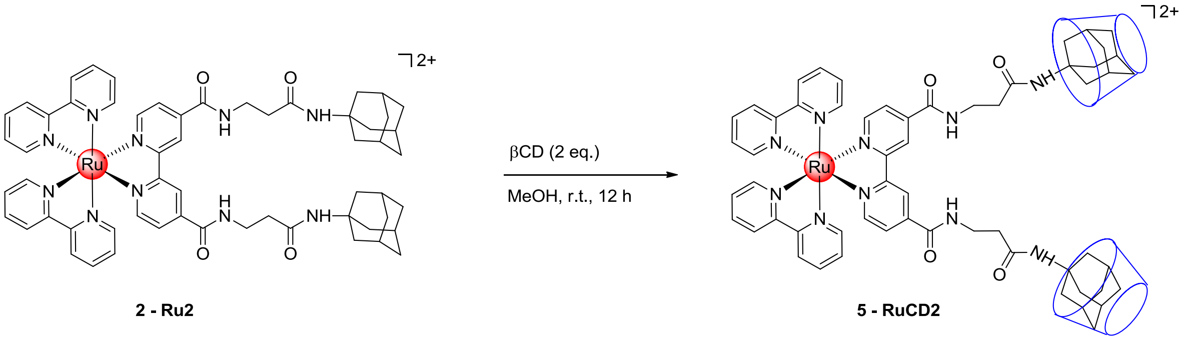

Ru-diadamantyl-dicyclodextrin RuCD2 (5)

To a solution of complex **2** (3.6 mg. 3.4 μmol) in MeOH (3 mL) was added native βCD (8.1 mg, 7.1 μmol) and the reaction mixture was kept at r.t. for 12 h. The solvent was then removed under reduced pressure and dried under *high vacuo*. The product was then dissolved in H_2O (3 mL) and lyophilized to afford the product **5** as a red solid.

^1H NMR (700 MHz, D_2O) δ 8.99 (*s*, 2H), 8.63 (*d*, *J* = 8.3 Hz, 4H), 8.16 (*dd*, *J* = 17.3, 9.0 Hz, 4H), 8.09 (*d*, *J* = 5.8 Hz, 2H), 7.85 (*dd*, *J* = 12.0, 6.0 Hz, 4H), 7.73 (*d*, *J* = 6.1 Hz, 2H), 7.47 (*dd*, *J* = 13.4, 6.7 Hz, 4H), 5.12 (*d*, *J* = 3.6 Hz, 14H), 3.99–3.90 (*m*, 42H), 3.85 (*d*, *J* = 10.3 Hz, 14H), 3.77–3.73 (*m*, 4H), 3.71 (*dd*, *J* = 9.9, 3.5 Hz, 14H), 3.64 (*t*, *J* = 9.5 Hz, 14H), 2.65 (*t*, *J* = 6.8 Hz, 4H), 2.27 (*s*, 6H), 2.17–2.11 (*m*, 12H), 1.83–1.76 (*m*, 12H).

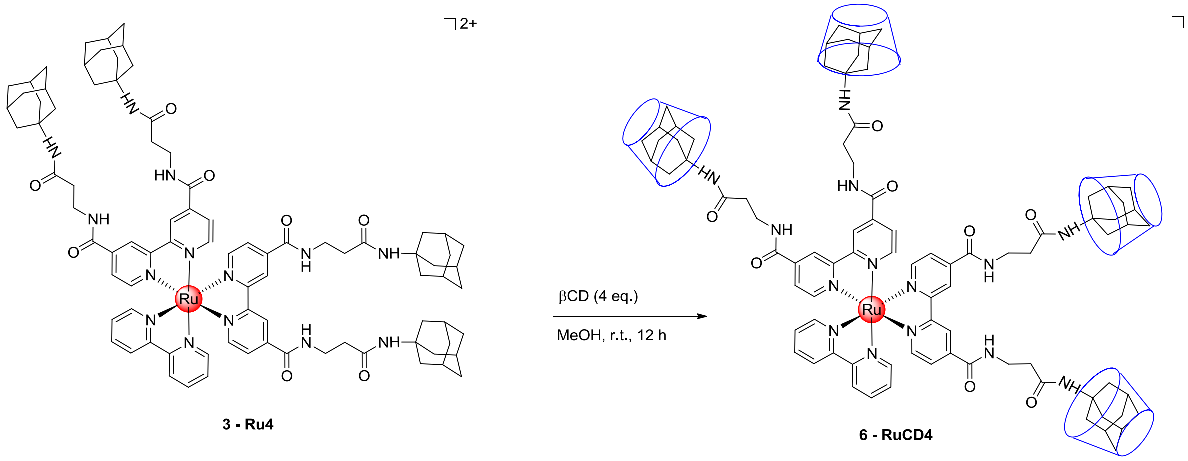

Ru-tetraadamantyl-tetracyclodextrin RuCD4 (6)

To a solution of complex **3** (5.9 mg, 3.8 μmol) in MeOH (4 mL) was added native βCD (18.0 mg, 16.0 μmol) and the reaction mixture was kept at r.t. for 12 h. The solvent was then removed under reduced pressure and dried under *high vacuo*. The product was then dissolved in H_2O (3 mL) and lyophilized to afford the product **6** as a red solid.

^{1}H NMR (700 MHz, D_2O) δ 9.03 (*s*, 4H), 8.65 (*d*, *J* = 8.5 Hz, 2H), 8.24–8.17 (*m*, 2H), 8.09–8.05 (*m*, 4H), 7.83–7.75 (*m*, 4H), 7.54–7.50 (*m*, 2H), 7.47 (*s*, 2H), 5.13 (*d*, *J* = 3.7 Hz, 28H), 4.00 (*t*, *J* = 9.5 Hz, 28H), 3.98–3.91 (*m*, 56H), 3.89 (*d*, *J* = 7.9 Hz, 28H), 3.80–3.73 (*m*, 4H), 3.71 (*dd*, *J* = 9.9, 3.6 Hz, 28H), 3.64 (*t*, *J* = 9.5 Hz, 28H), 2.65 (*t*, *J* = 6.7 Hz, 8H), 2.32–2.25 (*m*, 12H), 2.16 (*d*, *J* = 15.3 Hz, 24H), 1.86–1.77 (*m*, 24H).

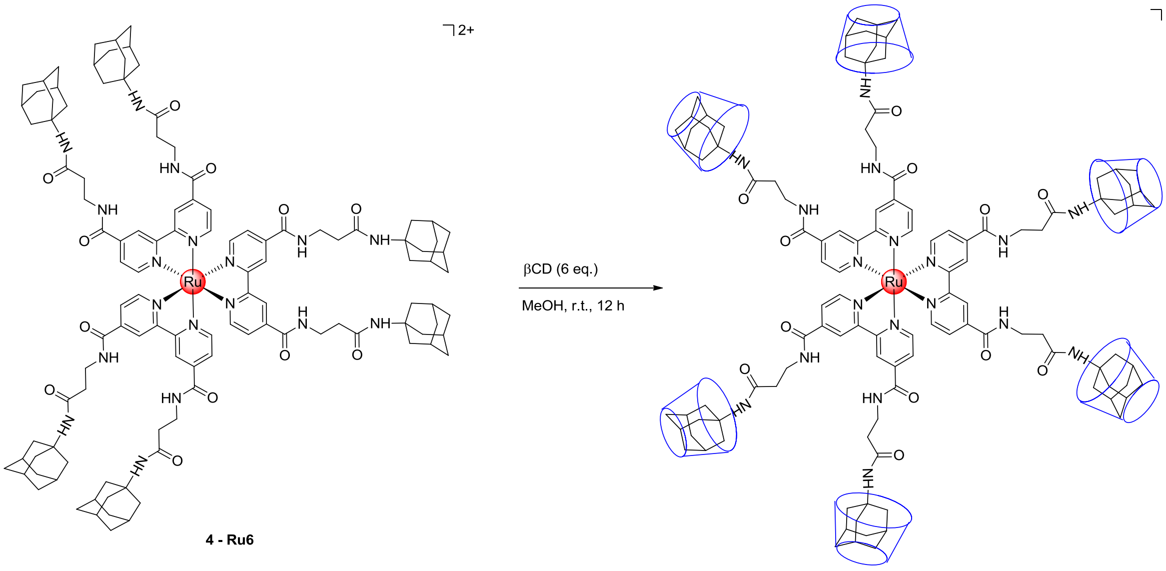

4 - Ru6

7 - RuCD6

Ru-hexaadamantyl-hexacyclodextrin RuCD6 (7)

To a solution of complex **4** (3.8 mg, 1.9 μmol) in MeOH (4 mL) was added native βCD (13.2 mg, 12.0 μmol) and the reaction mixture was kept at r.t. for 12 h. The solvent was then removed under reduced pressure and dried under *high vacuo*. The product was then dissolved in H_2O (3 mL) and lyophilized to afford the product **7** as a red solid.

^{1}H NMR (700 MHz, D_2O) δ 9.06 (*s*, 6H), 8.06–8.00 (*m*, 6H). 7.86-7.80 (*m*, 6H), 5.13 (*d*, *J* = 3.6 Hz, 42H), 4.02–3.90 (*m*, 126H), 3.88 (*d*, *J* = 6.4 Hz, 42H), 3.78–3.75 (*m*, 12H), 3.71 (*dd*, *J* = 9.9, 3.5 Hz, 42H), 3.64 (*t*, *J* = 9.4 Hz, 42H), 2.66 (*dd*, *J* = 6.2, 4.1 Hz, 12H), 2.30 (*d*, *J* = 2.2 Hz, 18H), 2.22–2.13 (*m*, 36H), 1.82 (*dd*, *J* = 24.0, 12.3 Hz, 36H).

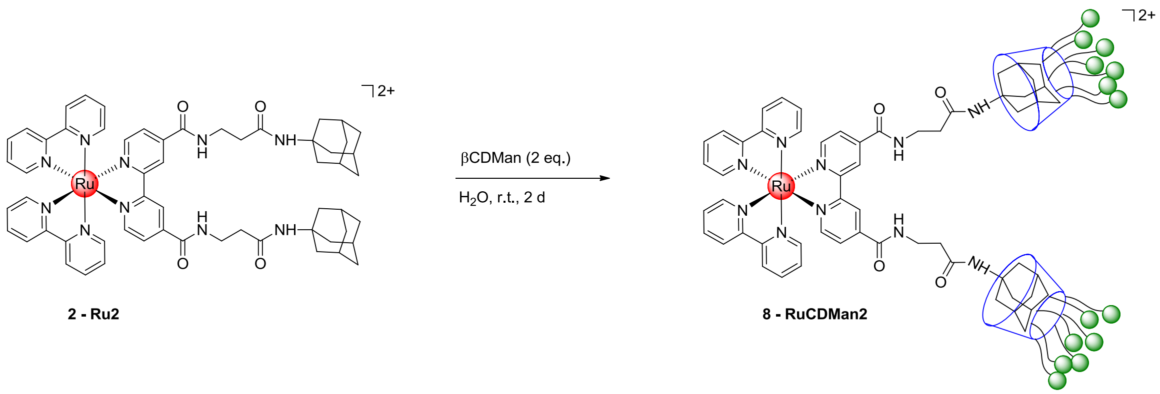

Ru-diadamantyl-dicyclodextrin mannosylated RuCDMan2 (8)

To the complex **3** (2.9 mg, 2.7 μmol) was added a solution of βCDMan (15.4 mg, 5.7 μmol) in H_2O (2.5 mL) and the reaction mixture was kept at r.t. for 2 d. The mixture was then lyophilized to afford the product **8** as a red solid.

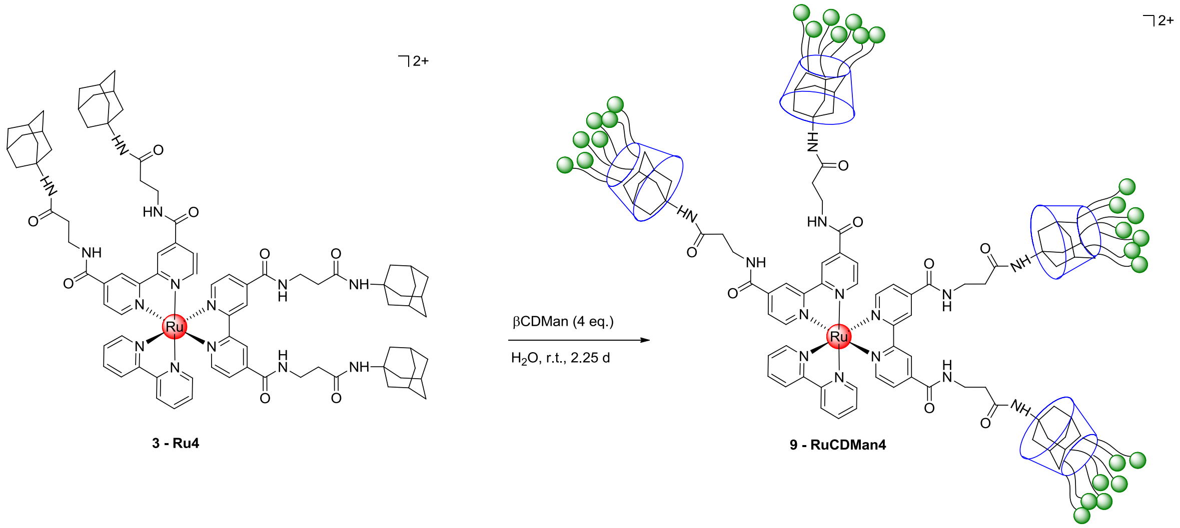

Ru-tetraadamantyl-tetracyclodextrin mannosylated RuCDMan4 (9)

To the complex **4** (2.9 mg, 1.8 μmol) was added a solution of βCDMan (20.6 mg, 7.7 μmol) in H_2O (3.3 mL) and the reaction mixture was kept at r.t. for 2 d and at 35 °C for 6 h. The mixture was then lyophilized to afford the product **9** as a red solid.

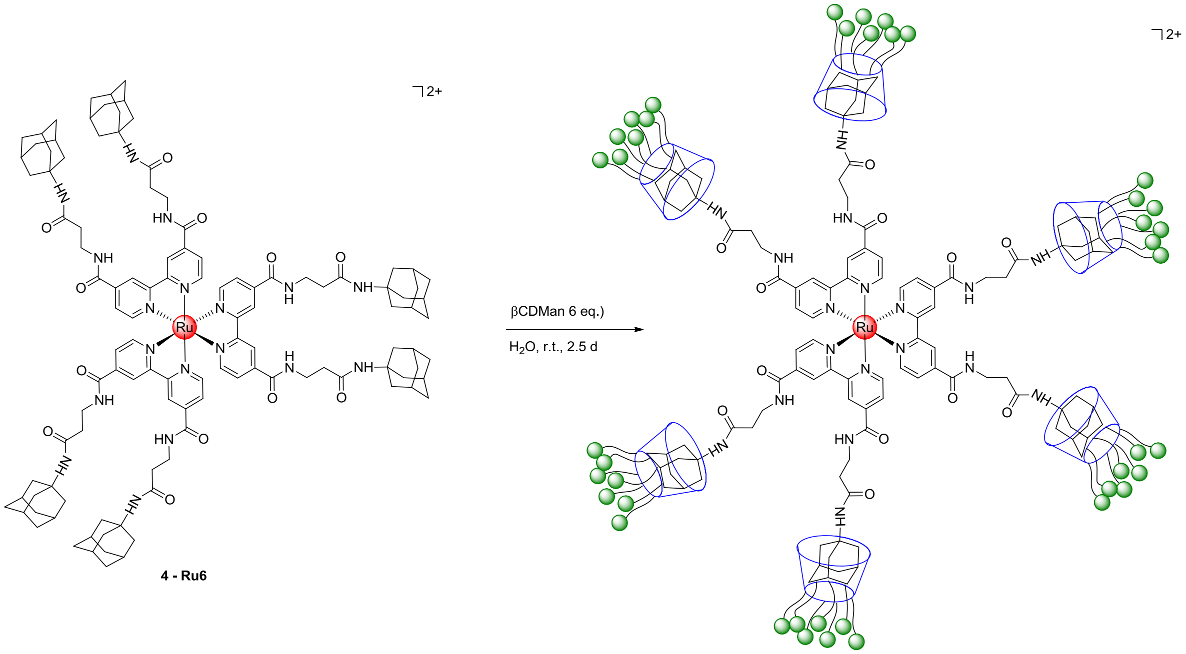

4 - Ru6

10 - RuCDMan6

Ru-hexaadamantyl-hexacyclodextrin mannosylated RuCDMan6 (10)

To the complex **4** (3.2 mg. 1.6 μmol) was added a solution of βCDMan (26.3 mg, 9.8 μmol) in H_2O (4.2 mL) and the reaction mixture was kept at r.t. for 2 d and at 35 °C for 12 h. The mixture was then lyophilized to afford the product **10** as a red solid.

4.2. Materials and Methods

4.2.1. Photophysical Properties

UV-vis spectra (extinction spectra) were recorded with an Ultrospec 6300 pro UV-visible Spectrophotometer (GE Healthcare, Amersham Biosciences, Piscataway, NJ, USA). Emission spectra (fluorescence spectra) were recorded with a LS 55 Fluorescence Spectrometer (Perkin Elmer, MA, USA). Measurements were performed in ultra-pure water or in methanol (HPLC grade, VWR, Darmstadt, Germany).

4.2.2. Mass Spectrometry Study

Samples of supramolecular complexes (RuCD2 **5**, RuCD4 **6** and RuCD6 **7**) were dissolved in ultra-pure water to give a final concentration of 10–100 μM. Mass spectra measurements were performed on the hybrid quadrupole-time of flight instrument (Q-TOF Ultima, Micromass, Manchester, UK) equipped with the Z-spray interface (Waters, Manchester, UK). Automated chip-based nano-electrospray ionization (ESI) robot (Nanomate model 100, Advion Biosciences, Ithaca, NY, USA) was used to generate ions. A high voltage of 1.3–1.5 kV was applied to the nano-ESI chip, 5 bar back pressure was used to assist sample flow. The distance to the sampling cone was adjusted to optimize the electrospray. The ion source temperature was kept at 60 °C. Sampling cone and the first ion guide (RF1 lens) voltages were optimized in the range of 100–150 V and 150–200 V, consistently, in order to achieve the most efficient transmission of desired ions. The quadrupole transmission mode was tuned to cover the *m/z* range of 300–8000. Collision-induced dissociation inside a hexapole collision cell was used in MS/MS experiments. Ar was used as a collision gas. The collision energy offset was varied in the range of 10–50 V. CsI clusters generated from the infusion of the 2 $g \cdot L^{-1}$ solution of CsI (puriss, Fluka Chemie AG, Buchs, Switzerland) in 50% aqueous isopropanol (HPLC grade ≥ 99.9%) were used for mass calibration. Mass spectra were managed and processed in the MassLynx 4.0 (Waters, Manchester, UK). A single scan accumulation time of 1 s was used, and a total of 100 scans were accumulated to obtain a representative mass spectrum with a good signal-to-noise ratio. Savitzky-Golay smoothening filter (k = 2) was employed to remove high-frequency noise from the spectra.

4.2.3. NMR Study

^{1}H, ^{13}C and NOESY (mixing time: 300 ms) spectra of the compounds were recorded by using Avance III 700 MHz (Bruker, Germany) instrument. The solvent signal was used for internal calibration.[25]

4.2.4. SPR Study

Con A was purchased from Sigma-Aldrich (Munich, Germany). The CM5 chip was obtained from GE Healthcare Life Science (Freiburg, Germany). The immobilization reagents and running buffer (0.1 M HEPES-EP: 1.5 M NaCl, 30 mM EDTA, 0.5% v/v Surfactant P20) were purchased from Biacore AB (Uppsala, Sweden). Methyl-α-D-mannopyranoside was purchased from Acros Organics (Geel, Belgium). All SPR experiments were performed using Biacore T100 (GE Healthcare Europe GmbH, Freiburg, Germany).

For the preparation of Con A-coated surfaces, Con A was immobilized at high (Con A-HD) and low (Con A-LD) densities at a flow rate of 10 µL·min^{-1}. The CM5 chip was activated by injection of a mixture of EDC and *N*-hydroxysuccinimide (NHS) for 10 min and functionalized by injecting 100 µg·mL^{-1} and 10 µg·mL^{-1} Con A in acetate buffer pH 5.5 for Con A-HD and Con A-LD, respectively, for 7 min. The remaining activated carboxyl groups were then capped by injection of 1 M ethanolamine for 10 min. Control flow cells were treated with EDC/NHS followed by ethanolamine as described.

Concentration gradients of 5–10 (5 µM, 10 µM, 20 µM, 30 µM, 40 µM, and 50 µM) were injected over the Con A-functionalized surfaces at 10 µL·min^{-1}, allowing 60 s for contact and 300 s for dissociation times, followed by regeneration using 100 mM methyl-α-D-mannopyranoside at 30 µL·min^{-1} for 30 s. Experimental data were analyzed using Biacore T100 Evaluation Software. Kinetic analyses based on a 1:1 interaction model were performed using Scrubber2 (BioLogic Software, Campbell, Australia).

4.2.5. Confocal Laser Scanning Microscopy

A bacterial strain bearing a mannose-binding protein (ORN178) and a mutant strain lacking the mannose binding domain (ORN208) were grown to logarithmic phase. Bacteria were harvested and washed three times with phosphate buffered saline (PBS). Bacteria were resuspended in 225 mL of PBS containing 1 mM $CaCl_2$ and 1 mM $MnCl_2$. A solution of either **7** or **10** in H_2O (25 mL, 10 mM) was added to the bacteria and the mixture was incubated at room temperature (22 °C) with robotic shaking for 30 min. The cells were washed three times in PBS and resuspended in 25 mL PBS. For microscopy, 1 mL of a DAPI solution was added to the cell suspension and incubated at r.t. for 5 min. The cells were washed three times with PBS and then visualized on a confocal microscope LSM700 (Zeiss, Leipzig, Germany).

5. Abbreviations

a. u.	arbitrary unit
abs. u.	absorbance unit
abs.	absorbance
AcOH	acetic acid
bipy	bipyridine
calcd.	calculated
Con A	Concanavalin A
CrO_3	chromium trioxide
d	day(s)
d	doublet
DAPI	4',6-diamidino-2-phenylindole
DCM	dichloromethan
dd	doublets of doublet
ddd	doublets of doublets of doublet
E. coli	*Escherichia coli*
EDC	*N*-ethyl-*N*'-(diethylaminopropyl)-carbodiimide
EDTA	ethylenediaminetetraacetic acid
em.	emission
ESI	electrospray ionization
ESSI	electrosonic spray ionization
Et_3N	triethylamine
EtOH	ethanol
h	hour(s)
H_2SO_4	sulfuric acid
HD	high density
HEPES	4-(2-hydroxyethyl)-1-piperazineethanesulfonic acid
HPLC	high-performance liquid chromatography
HRMS	high-resolution mass spectrometry

Hz	Hertz
J	coupling constant
K_d	dissociation equilibrium constant
KNO_3	potassium nitrate
LD	low density
m	multiplet
m/z	mass-to-charge ratio
MeCN	acetonitrile
MeOH	methanol
min	minute(s)
MS	mass spectrometry
NHS	*N*-hydroxysuccinimide
NMR	nuclear magnetic resonance
NOESY	Nuclear Overhauser effect spectroscopy
PBS	phosphate buffered saline
ppm	parts-per-million
q	quartet
RU	response unit
Ru	ruthenium
s	second(s)
s	singlet
SPR	surface plasmon resonance
t	triplet
td	triplets of doublet
TFA	trifluoroacetic acid
THF	tetrahydrofuran
TLC	thin layer chromatography
βCD	native β-cyclodextrin
βCDMan	heptamannosylated β-cyclodextrin

δ	chemical shift

6. Acknowledgments

I would like to thank here the people that contributed in a way or another to the work presented in this chapter. It would not have been possible to publish nicely this work without their relevant contribution.

I would like to thank Dr. Raghavendra Kikkeri for his precious help in the design of the experiments, the synthesis of the supramolecular structures, as well as for their consistent help in resolving organic synthetic challenges and Dr. Mayeul Collot for providing the mannosylated cyclodextrins.

Dr. Konstantin Barylyuk from Professor Zenobi's group at the Swiss Federal Institute of Technology (Zürich, Switzerland) extensively studied the supramolecular complexes using mass spectrometry. Dr. Martin Schäfer from the analytical service of the Free University (Berlin, Germany) helped me to analyze and interpret the supramolecular assembly using two-dimensional NMR. Ms. Maha Maglinao performed the sensing experiments using surface plasmon resonance. Professor Paul E. Orndorff from North Carolina State University (Raleigh, North Carolina, USA) provided the *E. coli* strains. Dr. Faustin Kamena gave valuable assistance on the confocal microscopy experiments.

7. References

---

[1] (a) Drickamer, K.; Taylor, M. E. *Ann. Rev. Cell Biol.* **1993**, *9*, 237-264. (b) Liu, F. T. *Clin. Immunol.* **2000**, *97*, 79-88. (c) Konstantinov, K. N.; Robbins, B. A.; Liu, F. T. *Am. J. Pathol.* **1996**, *148*, 25-30. (d) Pilobello, K. T.; Slawek, D. E.; Mahal, L. K. *Proc. Natl. Acad. Sci. USA* **2007**, *104*, 11534-9 (e) Bertozzi, C. R.; Kiessling, L. L. *Science* **2001**, *291*, 2357-2364. (f) Lis, H.; Sharon, N. *Chem. Rev.* **1998**, *98*, 637-674.

[2] (a) Kikkeri, R.; Hossain, L. H.; Seeberger, P. H. *Chem. Comm.* **2008**, 2127. (b) De Paz, J. L., Noti, C., Boehm, F., Werner, S. and Seeberger, P. H. *Chem. Biol.* **2007**, 14, 879. (c) Wolfenden, E. K.; Cloninger, M. J. *J. Am. Chem. Soc.* **2005**, *127*, 12168. (d) Roy, R.; Kim, J. M. *Angew. Chem., Int. Ed.* **1998**, *38*, 369. (e) Woller, E. K.; Walter, E. D.; Morgan, J. R.; Singel, D. J.; Cloninger, M. J. *J. Am. Chem. Soc.* **2003**, *125*, 8820. (f) Kikkeri, R.; Liu, X. Y.; Adibekian, A.; Tsai, Y. H.; Seeberger, P. H. *Chem. Comm.* **2010**, *46*, 2197. (g) Lepenies, B.; Yin, J.; Seeberger, P. H. *Curr. Opin. Chem. Biol.* **2010**, *14*, 404. (h) Bernardes, G. J. L.; Kikkeri, R.; Maglinao, M.; Laurino, P.; Collot, M.; Hong, S. Y.; Lepenies, B.; Seeberger, P. H. *Org. Biomol. Chem.* **2010**, *8*, 4987. (i) Disney, M. D.; Zheng, J.; Swager, T. M.; Seeberger, P. H. *J. Am. Chem. Soc.* **2004**, *126*, 13343. (j) Yang, W.; Pan, C. Y.; Luo, M. D.; Zhang, H. B. *Biomacromolecules* **2010**, *11*, 1840. (k) Gestwicki, J. E.; Kiessling, L. L. *Nature* **2002**, *415*, 81. (l) Sasaki, K.; Nishida, Y.; Tsurumi, T.; Uzawa, H.; Kondo, H.; Kobayashi, K. *Angew. Chem., Int. Ed.* **2002**, *41*, 4463. (m) Cario, C. W.; Gestwicki, J. E.; Kanai, M.; Kiessling, L. L. *J. Am. Chem. Soc.* **2002**, *124*, 1615. (n) Laurino, P.; Kikkeri, R.; Azzouz, N.; Seeberger, P. H. *Nano Lett.* **2011**, *11*, 73. (o) Gentsch, R.; Pippig, F.; Nilles, K.; Theato, P.; Kikkeri, R.; Maglinao, M.; Lepenies, B.; Seeberger, P. H.; Börner, H. G. *Macromolecules* **2010**, *43*, 9239-9247. (p) Ryu, J. H.; Lee, E.; Lim, Y. B.; Lee, M. *J. Am. Chem. Soc.* **2007**, *129*, 4808-4814. (q) Kikkeri, R.; Laurino, P.; Odedra, A.; Seeberger, P. H. *Angew. Chem.-Int. Edit.* **2010**, *49*, 2054. (r) Huang, C.-C., Chen, C.-T., Shiang, Y.-C., Lin, Z.-H.; Chang, H.-T. *Anal. Chem.* **2009**, *81*, 875. (s) Lin, C.-C., Yeh, Y.-C., Yang, C.-Y., Chen, C.-L., Chen, G.-F., Chen, C.-C. and Wu, Y.-C. *J. Am. Chem. Soc.* **2002**,*124*, 3508. (t) Gomez-Garcia, M.; Benito, J. M.; Rodriguez-Lucena, D.; Yu, J.-X.; Chmurski, K.; Mellet, C. O.; Gallego, R. G.; Maestre, A.; Defaye, J. and Fernandez, J. M. G. *J. Am. Chem. Soc.* **2005**,*127*, 7970. (u) Benito, J. M., Gomez-Garcia, M., Ortiz Mellet, C., Baussanne, I., Dafaye, J.; Fernandez, J. M.G. *J. Am. Chem. Soc.* **2004**, *126*, 10355. (v) Mellet, C. O., Defaye, J.; Fernandez, J. M. G. *Chem.−Eur. J.* **2002**, *8*, 1982. (w) Fulton, D. A. and Stoddart, J. F. *Bioconjugate Chem.* **2001**, *12*, 655. (x) Baldini, L; Casnati, A.; Sansone, F.; Ungaro R. *Chem. Soc. Rev.* **2007**, *36*, 254. (y) Badjic, J. D.; Nelson, A.; Cantrill, S. J.; Turnbull, W. B.; Stoddart, J. F. *Acc. Chem. Res.* **2005**, *38*, 723. (z) Kikkeri, R.; Kamena, F.; Gupta, T.; Hossain, L. H.; Boonyarattanakalin, S.; Gorodyska, G.; Beurer, E.; Coullerez, G.; Textor, M.; Seeberger, P. H. *Langmuir* **2010**, *26*, 1520. (a') Dai, Z., Kawde, A.-N., Xiang, Y., La Belle, J. T., Gerlach, J., Bhavanandan, V. P., Joshi, L. and Wang, J. *J. Am. Chem. Soc.***2006**, *128*, 10018. (b') Kikkeri, R.; Grünstein, D.; Seeberger, P. H. *J. Am. Chem. Soc.* **2010**, *132*, 10230. (c') Otsuka, H., Akiyama, Y., Nagasaki, Y. and Kataoka, K. *J. Am. Chem. Soc.* **2001**, *123*, 8226. (d') Kikkeri, R., Lepenies, B., Adibekian, A., Laurino, P. and Seeberger, P. H., *J. Am. Chem. Soc.* **2009**, *131*, 2110.

[3] Rosenzweig, B. A.; Ross, N. T.; Tagore, D. M.; Jayawickramarajah, J.; Saraogi, I.; Hamilton, A. D. *J. Am. Chem. Soc.* **2009**, *131*, 5020.

---

[4] (a) Fan, E. K.; Zhang, Z. S.; Minke, W. E.; Hou, Z.; Verlinde, C.; Hol, W. G. J. *J. Am. Chem. Soc.* **2000**, *122*, 2663. (b) Zhang, Z. S.; Merritt, E. A.; Ahn, M.; Roach, C.; Hou, Z.; Verlinde, C.; Hol, W. G. J.; Fan, E. *J. Am. Chem. Soc.* **2002**, *124*, 12991.

[5] Ohta, T.; Miura, N.; Fujitani, N.; Nakajima, F.; Niikura, K.; Sadamoto, R.; Guo, C. T.; Suzuki, T.; Suzuki, Y.; Monde, K.; Nishimura, S. I. *Angew. Chem.-Int. Edit.* **2003**, *42*, 5186.

[6] Garcia-Barrientos, A.; Garcia-Lopez, J. J.; Isac-Garcia, J.; Ortega-Caballero, F.; Uriel, C.; Vargas-Berenguel, A.; Santoyo-Gonzalez, F. *Synthesis* **2001**, 1057.

[7] Kikkeri, R.; Garcia-Rubio, I.; Seeberger, P. H. *Chem. Comm.* **2009**, 235.

[8] Hahn, U.; Vogtle, F.; De Paoli, G.; Staffilani, M.; De Cola, L. *Eur. J. Inorg. Chem.* **2009**, 2639.

[9] Issberner, J.; Vogtle, F.; De Cola, L.; Balzani, V. *Chem.-Eur. J.* **1997**, *3*, 706.

[10] (a) Faiz, J. A.; Kyllonen, L. E. P.; Contreras-Carballada, P.; Williams, R. M.; De Cola, L.; Pikramenou, Z. *Dalton Trans.* **2009**, 3980. (b) Felici, M.; Contreras-Carballada, P.; Vida, Y.; Smits, J. M. M.; Nolte, R. J. M.; De Cola, L.; Williams, R. M.; Feiters, M. C. *Chem.-Eur. J.* **2009**, *15*, 13124.

[11] (a) Wrighton, M.; Morse, D. L. *J. Am. Chem. Soc.* **1974**, *96*, 998. (b) Innocenzi, P.; Kozuka, H.; Yoko, T. *J. Phys. Chem. B* **1997**, *101*, 2285.

[12] Hernandez, H.; Robinson, C. V. *Nat. Prot.* **2007**, *2*, 715.

[13] (a) Fenn, J. B.; Mann, M.; Meng, C. K.; Wong, S. F.; Whitehouse, C. M. *Science* **1989**, *246*, 64. (b) Kebarle, P.; Verkerk, U. H. *Mass Spect. Rev.* **2009**, *28*, 898.

[14] Wilm, M.; Mann, M. *Anal. Chem.* **1996**, *68*, 1.

[15] Gabelica, V.; De Pauw, E. *Mass Spect. Rev.* **2005**, *24*, 566.

[16] Schneider, H. J.; Hacket, F.; Rudiger, V.; Ikeda, H. *Chem. Rev.* **1998**, *98*, 1755.

[17] Jing, B.; Chen, X.; Zhao, Y. R.; Wang, X. D.; Cai, J. G.; Qiu, H. Y. *J. Phys. Chem. B* **2008**, *112*, 7191.

[18] Rich, R. L.; Myszka, D. G. *J. Mol. Recognit.* **2006**, *19*, 478.

[19] Hardman, K. D.; Ainswort, C. F. *Biochemistry* **1972**, *11*, 4910.

[20] Munoz, E. M.; Correa, J.; Fernandez-Megia, E.; Riguera, R. *J. Am. Chem. Soc.* **2009**, *131*, 17765.

[21] (a) Dhayal, M.; Ratner, D. A. *Langmuir* **2009**, *25*, 2181. (b) Schlick, K. H.; Cloninger, M. J. *Tetrahedron* **2010**, *66*, 5305.

[22] Kim, B. S.; Hong, D. J.; Bae, J.; Lee, M. *J. Am. Chem. Soc.* **2005**, *127*, 16333.

[23] (a) Jones, C. H.; Pinkner, J. S.; Roth, R.; Heuser, J.; Nicholes, A. V.; Abraham, S. N.; Hultgren, S. *J. Proc. Natl. Acad. Sci. U.S.A.* **1995**, *92*, 2081. (b) Choudhury, D.; Thompson, A.; Stojanoff, V.; Langermann, S.; Pinker, J.; Hultgren, S. J.; Knight, S. D. *Science* **1999**, *285*, 1061. (c) Harris, S. L.; Spears, P. A.; Havell, E. A.; Hamrick, T. S.; Horton, J. R.; Orndorff, P. E. *J. Bacteriol.* **2001**, *183*, 4099.

[24] (a) Hahan, M. A.; Tabb, J. S.; Krauss, T. D. *Anal. Chem.* **2005**, *77*, 4861. (b) Mukhopadhyay, B.; Martins, M. B.; Karamanska, R.; Russell, D. A.; Field, R. A. *Tetrahedron Lett.* **2009**, *50*, 886. (c) Wang, C.; Irudayaraj, J. *Small* **2008**, *4*, 2204. (d) Huang, P. J.; Tay, L. L.; Tanha, J.; Ryan, S.; Chau, L. K. *Chem.-Eur. J.* **2009**, *15*, 9330. (e) Su, Y. L.; Li, J. R.; Jiang, L.; Cao, J. *J. Colloid Interface Sci.* **2005**, *284*, 114. (f) Li, Y.; Ma, B.; Fan, Y.; Kong, X.; Li, J. *Anal. Chem.* **2002**, *74*, 6349. (g) Gottschaldt, M.; Schubert, U. S.; Rau, S.; Yano, S.; Vos, J. G.; Kroll, T.; Clement, J.; Hilger, I. *Chembiochem* **2010**, *11*, 649.

---

[25] Carrazana, J.; Jover, A.; Meijide, F.; Soto, V. H.; Tato, J. V. *J. Phys. Chem. B* **2005**, *109*, 9719.

Chapter 4

Functionalized Fullerenes Reduce Infarct Volume and Cerebral Inflammation after Ischemic Stroke in Rat Models

---

The results reported in this chapter have been partially published in:

Fluri, F.; Grünstein, D.; Cam, E.; Ungethuem, U.; Hatz, F.; Schäfer, J.; Moch, H.; Schaeren-Wiemers, N.; Zeis, T.; Seeberger, P.H. in preparation.

Table of Contents

Abstract

Ischemic stroke remains an enormous therapeutic challenge. Thrombolysis with recombinant tissue plasminogen activator (rtPA) is the only approved beneficial therapy but is limited to fewer than 5% of stroke patients.

Among therapeutic approaches targeting the ischemic cascade, agents with anti-inflammatory properties may offer unique therapeutic advantages. Water soluble fullerenol (polyhydroxylated fullerenes $C_{60}(OH)_{34-36}$) exerts neuroprotective effects by scavenging oxygen radicals and reducing glutamate excitotoxicity. However, fullerenols had not been investigated for their ability to reduce cerebral inflammation after ischemic stroke.

Since glucosamine (GlcN) attenuates cerebral inflammation after ischemic stroke, we hypothesized that covalent GlcN-fullerene conjugates, such as $C_{60}(GlcN)_{12}$ might potentiate possible anti-inflammatory effects.

In the present study, $C_{60}(OH)_{34-36}$ was administered intravenously in normotensive Kyoto-Wistar rats (WKY) subjected to transient middle cerebral artery occlusion (tMCAO) for 60 min. Both $C_{60}(OH)_{34-36}$ and $C_{60}(GlcN)_{12}$ were also injected in spontaneously hypertensive rats (SHR), since arterial hypertension is the most important risk factor for stroke.

Five days after tMCAO, magnetic resonance imaging (MRI) revealed a significant reduction of infarct volume in $C_{60}(OH)_{34-36}$-treated WKY and SHR and in $C_{60}(GlcN)_{12}$-treated SHR. Treated rats showed improved neurological assessments when compared to placebos. Both agents, $C_{60}(OH)_{34-36}$ and $C_{60}(GlcN)_{12}$, preserved neurons after ischemic stroke in the perilesional area of WKY and SHR and reduced the density of macrophages/microglia infiltration in WKY and SHR. $C_{60}(OH)_{34-36}$ also down-regulated interleukine-1β (IL-1β) and Toll-like receptor 4 (TLR 4) in WKY.

Reduction of the cellular and humoral immune responses after ischemic stroke due to treatment with $C_{60}(OH)_{34-36}$ and $C_{60}(GlcN)_{12}$ may constitute an attractive therapeutic approach. Translation of these encouraging findings to humans is currently being prepared.

1. Introduction

A stroke is a sudden interruption in the blood supply of the brain. According to the World Health Organization, 15 million people suffer strokes worldwide each year. Of these, five million die and another five million are permanently disabled. The most common type of stroke, the ischemic stroke, accounts for almost 87% of all strokes, while the other 13% are hemorrhagic strokes.[1]

Ischemic stroke occurs when an artery to the brain is blocked. When an artery is obstructed, the blood supply to an area of brain stopped, leading to ischemia (lack of oxygen) and eventually necrosis (death of the tissue). If the artery remains blocked for more than a few minutes, the brain cells die *via* a series of events, the so-called ischemic cascade. Therefore, immediate medical treatment is absolutely critical.

The only approved treatment for ischemic stroke in the acute phase is intravenous thrombolysis with rtPA that is able to dissolve thrombotic clots.[2] However, the therapeutic window of this treatment is less than 4.5 h and thus, its application is limited to fewer than 5% of all stroke patients.[3] Moreover, the clot-dissolving drug is not active on the mechanistic issues of the ischemic cascade: radical formation and inflammation due to further immune system activation.

Another potential therapeutic approach consists of targeting the radical formation and inflammatory processes that are associated with all stages of the ischemic cascade by developing neuroprotectants. Indeed, lack of oxygen causes the neuron's normal adenosine triphosphate (ATP) transport pumps to fail. Cells become depolarized, allowing calcium-ions (Ca^{2+}) to flow into the cell. Excess of Ca^{2+} overexcites cells causing the generation of harmful chemicals like free radicals and reactive oxygen species that lead to cell necrosis. Damage-associated molecular patterns from cell death activate the immune system and promote inflammation processes.[4] Ischemic cell death leads to the activation of TLR 4 expressed on microglia.[5] TLR4 –a signalling receptor– activates nuclear factor κB (NF-κB) and pathways linked to the transcription of many pro-inflammatory genes that encode cytokines such as IL-1β and tumor necrosis factor-α (TNF-α), chemokines, and proteins of the complement system.[6] The effects of the proteins involved in this signalling cascade on ischemic stroke have been studied: TLR 4-deficient mice have minor infarcts and less inflammatory response after cerebral ischemia.[7] IL-1β exerts toxic effects in ischemic stroke and blocking its action reduces ischemic brain damage.[8] TNF-α probably has a noxious effect, but its role remains controversial.[9] Complement component C3 mediates inflammatory injury following focal cerebral ischemia and its deletion reduced infarct volume and neurological deficit score.[10] However, anti-inflammatory agents have not been effective in clinical trials since post-ischemic inflammation acts through multiple pathways that cannot be effectively suppressed by blocking a single cytokine or adhesion molecule.[11]

Fullerenes, molecules in the shape of a hollow sphere of 60 carbon atoms exhibit properties that make them promising candidates for biomedical applications and controlled drug delivery. When appropriately modified and in certain conditions [i.e. blood brain barrier (BBB) disruption], fullerenes can migrate through the BBB.[12]

Hydroxylated fullerenes, also called fullerenols, possess neuroprotective properties by scavenging free radicals *in vitro* but also *in vivo*. Indeed, the remaining carbon double bonds present in the C_{60} structure are able to accept free radicals.[13] Furthermore, fullerenols inhibit glutamate channels that lower glutamate-induced increase of intracellular Ca^{2+} concentration, a critical mechanism of excitotoxicity in neurons.[14] Until now, the efficacy of fullerenols on cerebral inflammation after ischemic stroke has not been investigated (Figure 1A).

To potentiate a possible anti-inflammatory effect of fullerene, GlcN was covalently attached. Since GlcN inhibits the NF-κB to reduce the humoral and cellular immune response, we created GlcN-fullerene conjugates to test the effects the molecule (Figure 1A).[15]

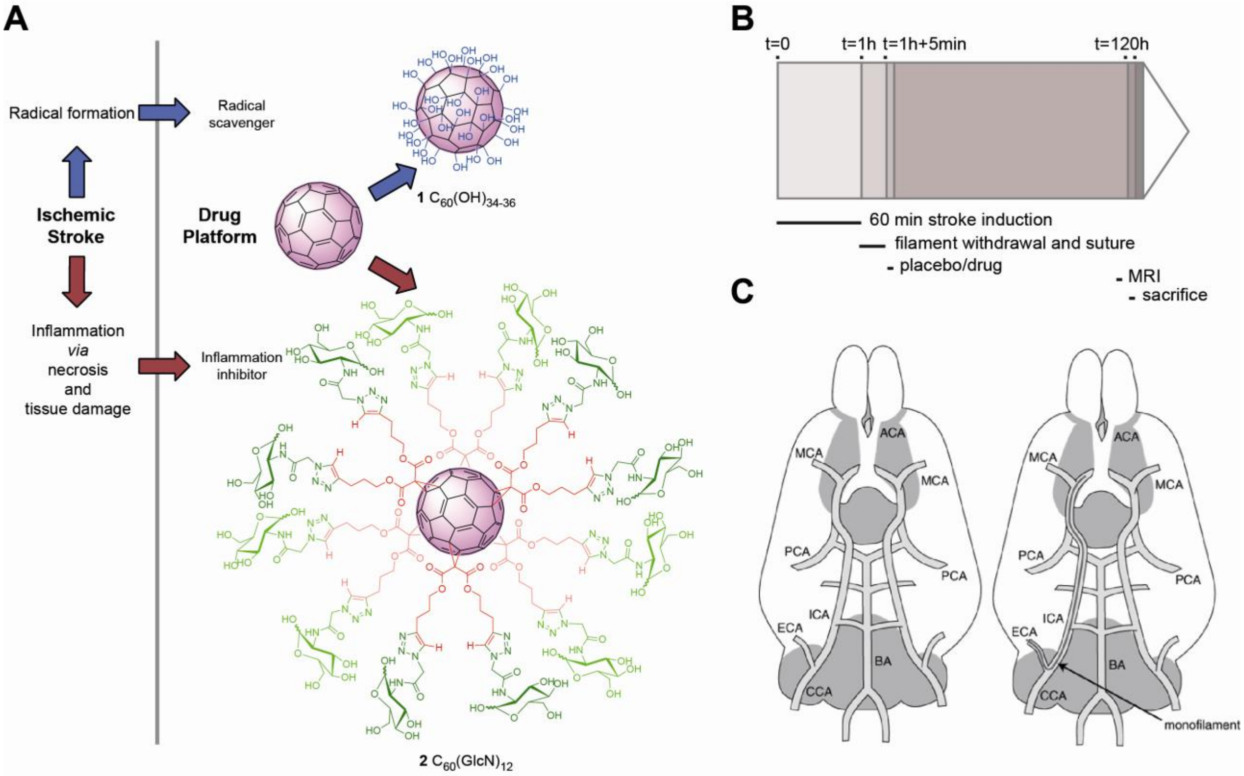

Figure 1. (A) Explicative scheme of the experiment rationale. Radical formation and inflammation are consequences of ischemic stroke. $C_{60}(OH)_{34\text{-}36}$ (radical scavenger) and $C_{60}(GlcN)_{12}$ (a potent anti-inflammatory agent) were prepared to address these problems. (B) Timeline of experiments: placebo/drug administration and MRI experiments. (C) Illustration of the intraluminal monofilament model of cerebral ischemia.[16] Carotid and cerebral arteries in the rat before (left) and after (right) insertion of the intraluminal monofilament. ACA, anterior cerebral artery; BA, basilar artery; CCA, common carotid artery; ECA, external carotid artery; ICA, internal carotid artery; MCA, middle cerebral artery; PCA, posterior cerebral artery.

Here, we report that cerebral infarct volume and post-stroke inflammation are reduced in WKY and SHR treated with $C_{60}(OH)_{34\text{-}36}$ and in SHR treated with $C_{60}(GlcN)_{12}$ compared to placebos after tMCAO, an animal model of ischemic stroke using an intraluminal thread that is inserted to occlude the internal carotid of the rat. (Figure 1B, C)

2. Results and Discussion

2.1. Chemical Synthesis

2.1.1. Synthesis of Fullerenols $C_{60}(OH)_{34\text{-}36}$

Many methods have been established for the preparation of fullerenols.[17] We synthesized hydroxylated fullerenes using an alkaline reaction. To a fullerene solution in toluene was added aqueous sodium hydroxide (NaOH) followed by the catalyst, tetrabutylammonium hydroxide (TBAH) (Scheme 1).[18] After the removal of toluene, water was added to complete the reaction. The aqueous phase was then evaporated and a brown sludge precipitated upon the addition of methanol (MeOH). The precipitate was intensively washed with MeOH to remove traces of TBAH and NaOH to obtain **1** as a brownish powder after drying.

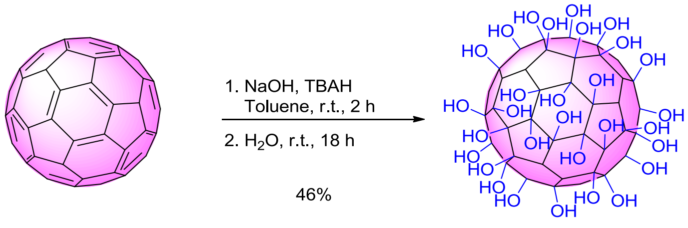

3 **1**

Scheme 1. Synthesis of $C_{60}(OH)_{34\text{-}36}$ **1**.

Fullerenol **1** was characterized by means of UV-vis- and infrared (IR)-spectroscopy. Its dissociation behavior was investigated under matrix assistant time-of-flight mass spectrometer (MADLI-TOF-MS) conditions (Figure 2). The UV-vis absorption spectra of **1** in water was taken and compared with pristine C_{60} in toluene (Figure 2A). Fullerenols are almost transparent below 400 nm, implying their decreased π-conjugation due to the introduction of hydroxyl groups on the double bounds. The IR spectrum of fullerenol **1** is shown in Figure 2B along with the spectrum of the starting material **3**. A broad band at 3400 cm^{-1} is characteristic of the O–H bond vibration that clearly differs from the fullerene signal. The spectra shows also three other specific bands at 1620, 1370, and 1080 cm^{-1} that are assigned for ν(C=C), δ_s(C–O–H), and ν(C–O) absorption, respectively. The small peak around 1720 cm^{-1} implies the existence of either a carboxylic group, which might have formed either by further oxidation of the hydroxyl group *via* oxidation of an hydroxyl group associated with a C–C bond cleavage of C_{60} core or by a carbonyl group formed through pinacol rearrangement of a vicinal hydroxyl group.[19] The result of laser-induced dissociation of **1** is shown in Figure 2C. The spectrum indicates that fullerenol dissociation occurred *via* a successive elimination of C_2 moieties. The dissociation behavior of **1** represented by its fragmentation pattern yielded C_{60}, C_{58}, C_{56}, and C_{54} fragments. This data was comparable with analogous measurements done with different fullerenols of various hydroxyl numbers, suggesting that the relative stability of fullerenols depends on their hydroxyl numbers.[20]

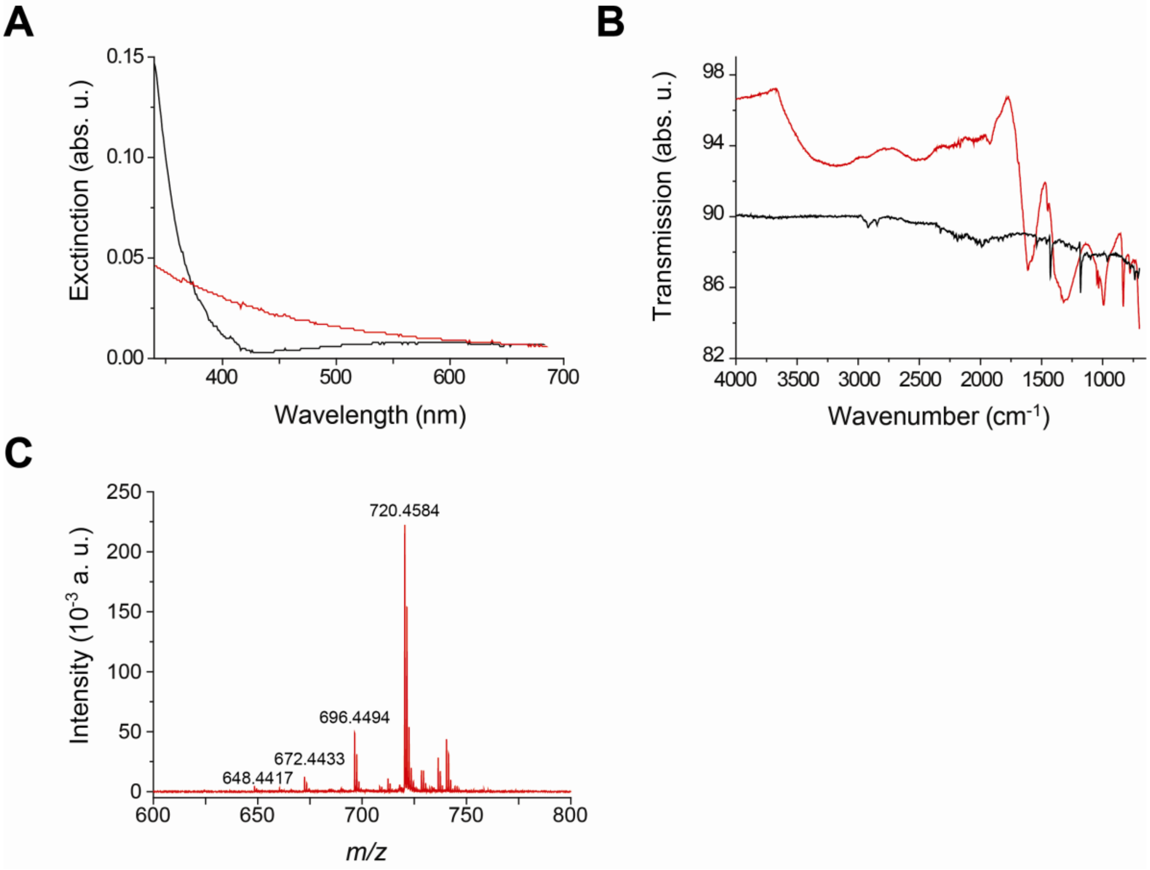

Figure 2. (A) UV-vis spectra of fullerenol $C_{60}(OH)_{34\text{-}36}$ in water (red line) and pristine C_{60} in toluene (black line) measured at concentrations of 3.33 $mg\cdot mL^{-1}$. (B) IR spectra of fullerenol $C_{60}(OH)_{34\text{-}36}$ (black line) and fullerene C_{60} (red line). (C) TOF mass spectra of a direct laser-induced dissociation of $C_{60}(OH)_{34\text{-}36}$ measured with the negative ion and a reflect modes (without matrix). Instability of fullerenols in the ionization stage is shown in the fragmentation *via* successive elimination of C_2 moieties: [$\Delta(m/z) = 24$].

In order to determine exactly the number of hydroxyl groups that append the C_{60} core, we performed an elemental analysis. The formula $C_{60}H_{34.87 \pm 0.28}O_{34.87 \pm 0.28}$ was found. Therefore, we estimated the number of hydroxyl residues between 34 and 36. For sake of presentation, hereafter, fullerenol is written $C_{60}(OH)_{34\text{-}36}$.

2.1.2. Synthesis of GlcN-fullerene Conjugate $C_{60}(GlcN)_{12}$

Nierengarten *et al.* have reported pioneering work in the design and synthesis of dodecavalent fullerene-based glycoclusters.[21] C_{60} hexakisadducts with a T_h-symmetrical octahedral structure are molecules with a spherical architecture. We synthesized a C_{60} hexakisadduct derivative bearing twelve alkyne groups and used the copper-mediated Huisgen 1,3-dipolar cycloaddition to append the twelve GlcN moieties on the C_{60} periphery.

The synthesis of the C_{60} hexakisadduct **8** bearing twelve alkynes is described in Scheme 2. The reaction of malonyl chloride **4** with the alcohol **5** in the presence of a base afforded the manolate ester **6**. The hexakisadduct was readily synthesized *via* carbene insertion into six double bounds of the C_{60} core. The cyclopropanation on the fullerene was carried out using tetrabromocarbon (CBr_4), 1,8-diazabicyclo [5.4.0]undec-7-ene (DBU), and the manolate **6** in *o*-dichlorobenzene (ODCB). Compound **7** was then desilylated using tetrabutylammonium fluoride (TBAF) to afford the corresponding product **8** with twelve terminal alkyne units.

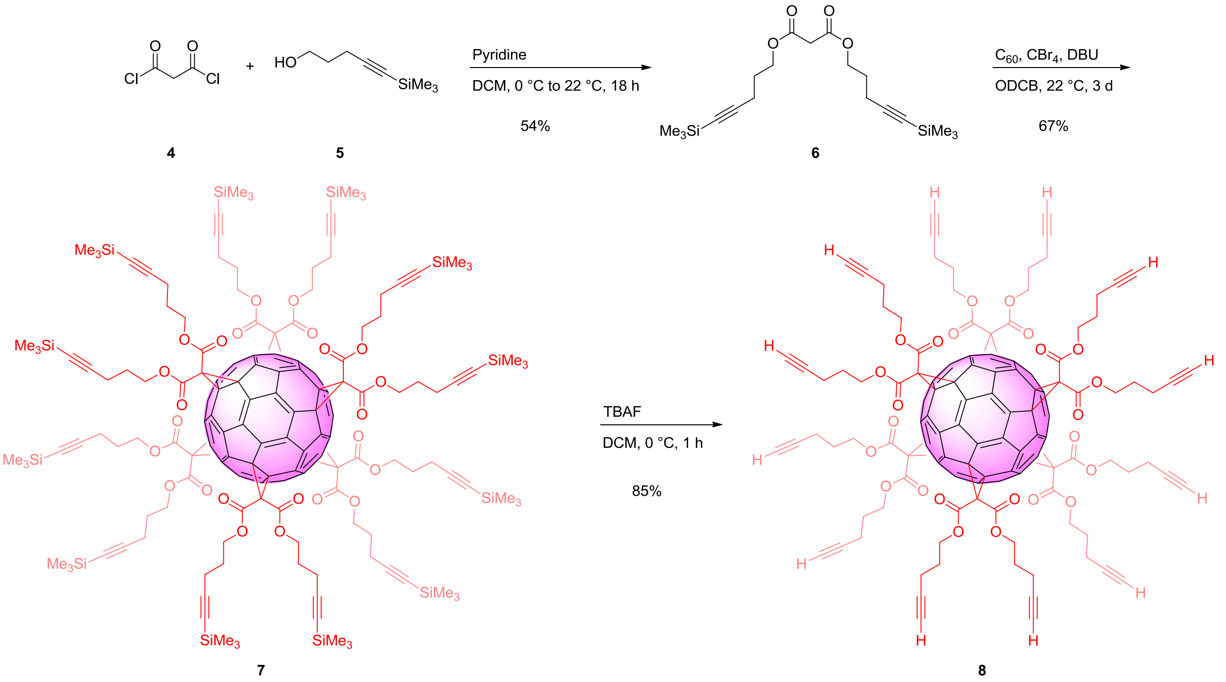

Scheme 2. Synthesis of the C_{60} hexakisadduct **8** bearing twelve alkynes.

The chemical structure of **8** was confirmed by means of high resolution mass spectrometry, ^{1}H and ^{13}C NMR spectra. The ^{13}C NMR spectrum was in full agreement with the T_h-symmetrical structure and showed the three expected fullerene resonances: δ 145.8 and 141.2 for the two different sp^2 carbon atoms and δ 69.2 attributed to the sp^3 carbon of the C_{60} core (Figure 3).

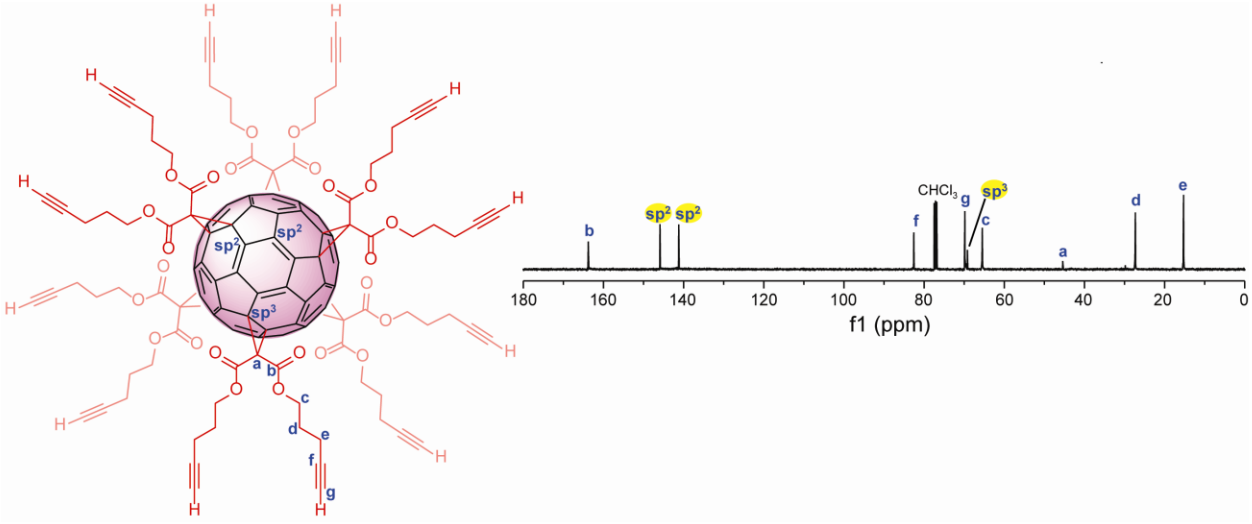

Figure 3. Annotated ^{13}C NMR spectra of **8** highlighting in particular the three characteristic resonances of the T_h-symmetrical structure on the C_{60} core.

The GlcN moiety modified with an azido linker **12** was synthesized starting from glucosamine hydrochloride **9**.[22] Monosaccharide **9** was deprotonated with sodium methoxide (NaOMe), followed by acylation with chloroacetic anhydride to furnish **10**. Sodium azide (NaN_3) was then used to displace the halide. Peracetylation with acetic anhydride (Ac_2O) of the deprotected sugar was done to allow for proper column chromatography purification in order to get **11** as a mixture of α and β isomers. The final product **12** was then obtained as a mixture of isomers after acetyl deprotection with NaOMe.

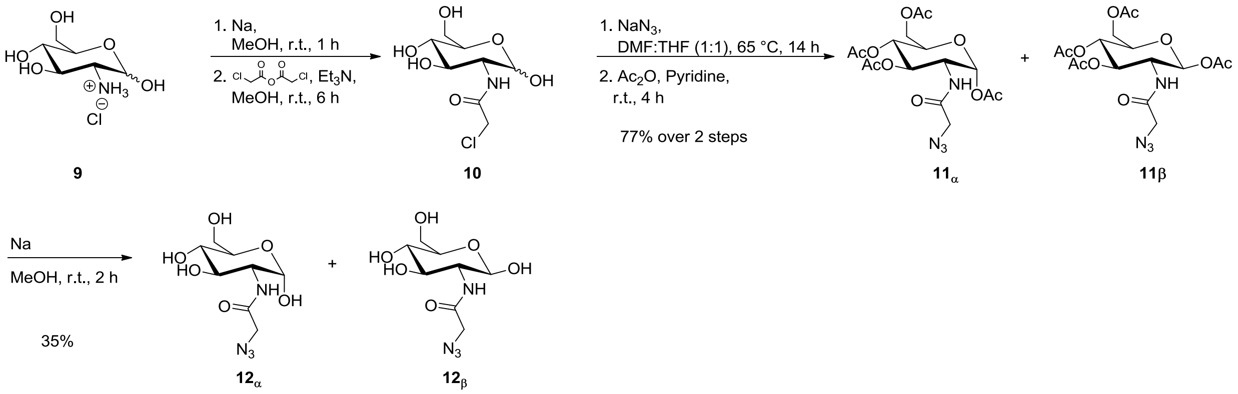

Scheme 3. Synthesis the GlcN synthon **12** bearing an azido linker.

The copper catalyzed azide-alkyne cycloaddition was used in an effort to attach twelve azide units of **12** on to the template fullerene **8** with twelve alkynes resulting in the dodecavalent fullerene bearing twelve GlcN residues. The synthesis of compound **2** is depicted in Scheme 4. Reaction of **8** with **12** in the presence of copper sulfate ($CuSO_4$) and sodium ascorbate in dimethyl sulfoxide (DMSO) gave the functionalized fullerene **2** in 47% yield with twelve 1,2,3-triazoles.

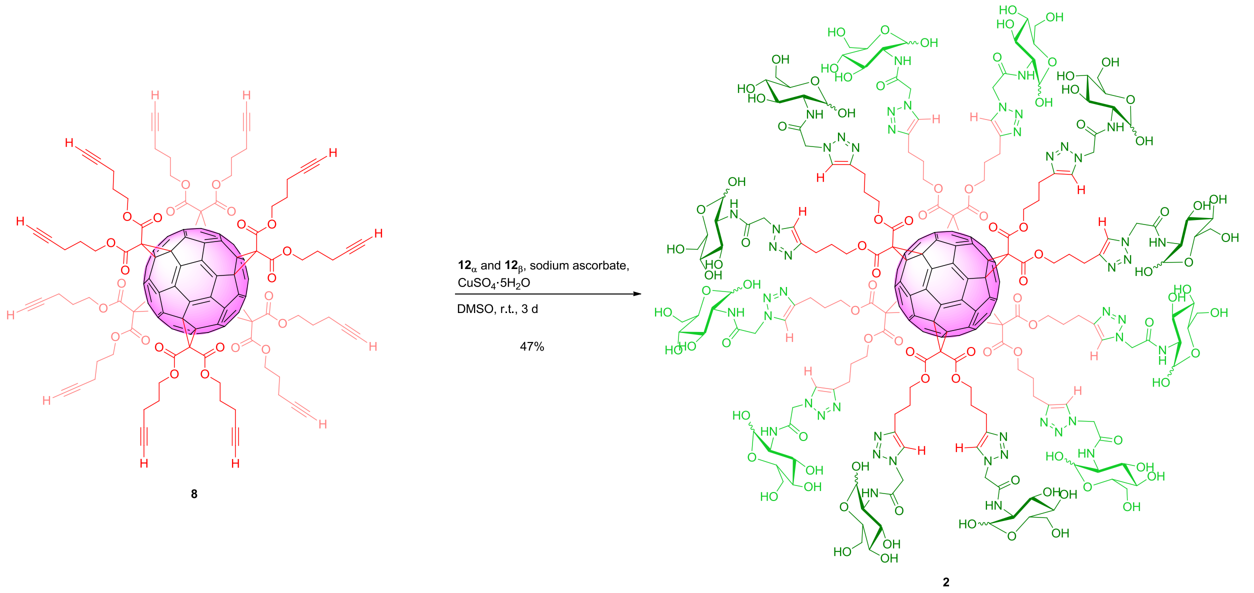

Scheme 4. Synthesis of GlcN-fullerene conjugate $C_{60}(GlcN)_{12}$ **2**.

Mass spectra of **2** was recorded. Despite the high-level of fragmentation, we observed the expected molecular peak *m/z* 1780.5359 $[M+3Na]^{3+}$. Compound **2** was further characterized by means of ^{1}H and ^{13}C NMR spectra and compared with previous spectra of analogous compound to validate its chemical structure.[23] The ^{13}C NMR spectrum also indicated that all alkynes underwent cycloaddition (Figure 4).

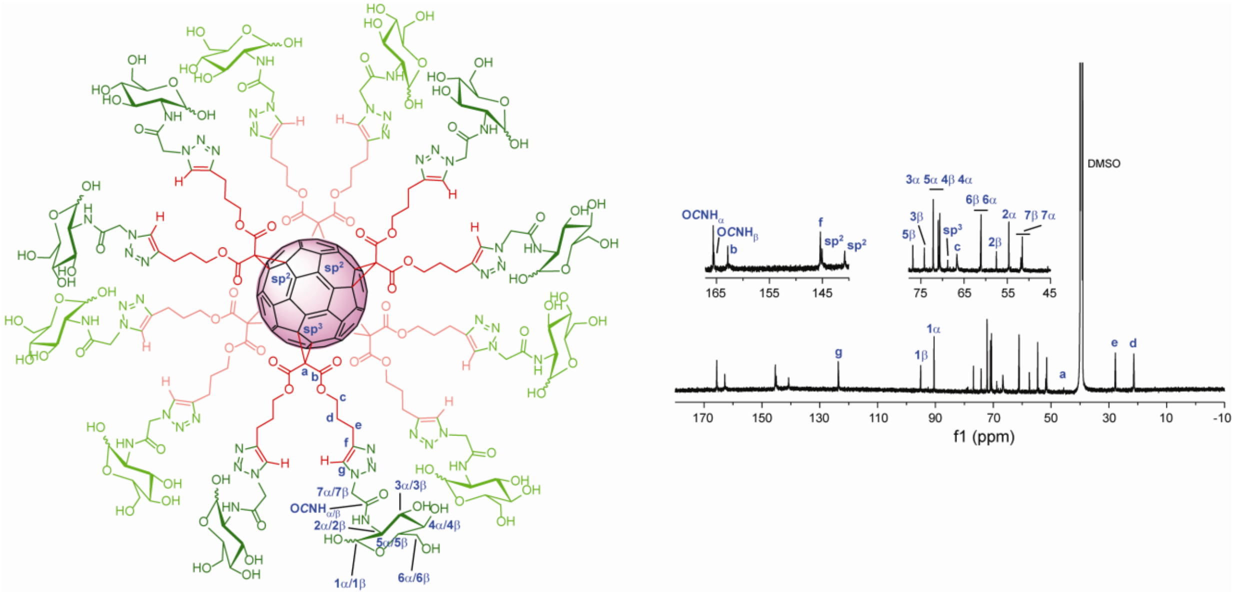

Figure 4. Annotated ^{13}C NMR spectra of **2**.

2.1.3. Synthesis of HCPAMP-GlcN-fullerene Conjugate C_{60}(HCPAMP)(GlcN)$_{11}$

Pharmacokinetics is a branch of pharmacology dedicated to the determination of the fate of substances administered externally to a living organism. To forestall potential medical applications of **2**, we developed a slight modified version to enable *in vivo* imaging and further pharmacokinetic study of C_{60}(GlcN)$_{12}$. Thus, **2** with twelve sugar units was modified to get compound **19** bearing eleven sugars and a bifunctional chelator that binds technetium-99m-metal (^{99m}Tc), a radioisotope used in single photon emission computed tomography (SPECT). The radiolabelled compound **21** was then prepared for further *in vivo* imaging studies.

Firstly, to the bifunctional tidentate chelator 2-[[(2-hydroxy-5-carboxyphenyl)amino] methyl]pyridin (HCPAMP), that would simultaneously coordinate the ^{99m}Tc-metal core and tether the potential drug, was attached an azido linker **14**, that was readily synthesized from the commercially available salt **13**.[24] The azido linker **14** was then conjugated to the preactivated and protected chelator **16** to form the amide **17**. Further silyl deprotection using TBAF afforded then compound **18** (Scheme 5).[25]

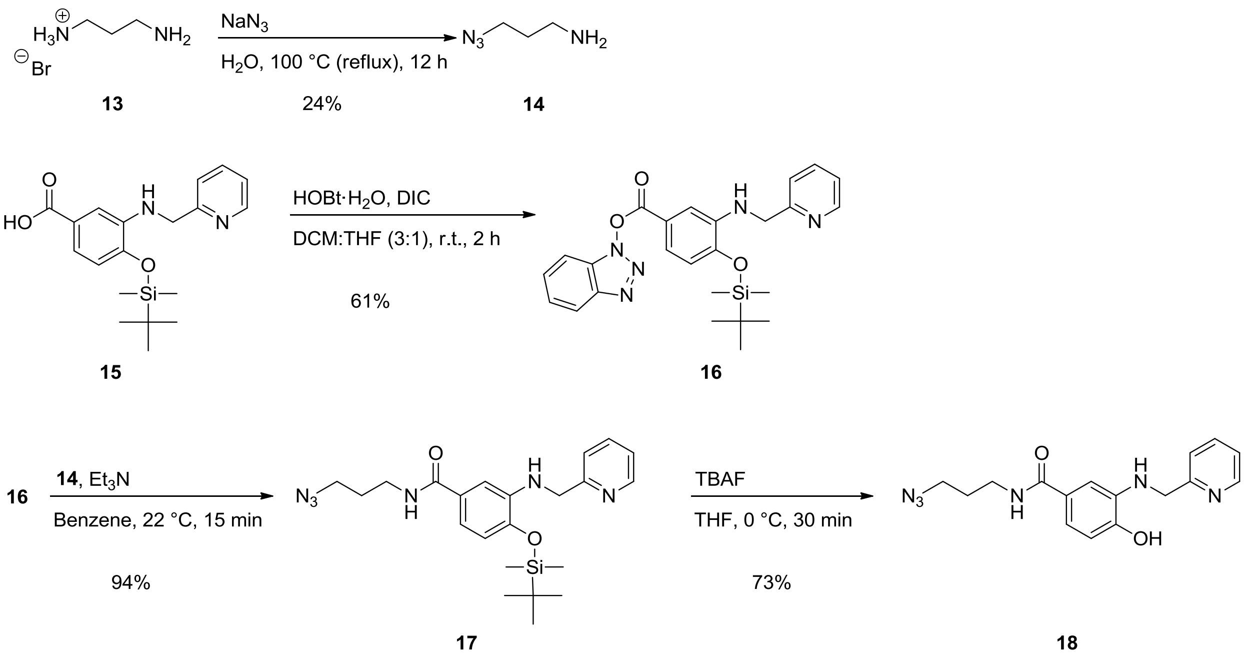

Scheme 5. Synthesis the bifunctional tridentate chelator **18** bearing an azido linker.

The bifunctional tridentate chelator **18** was then reacted with **8** to afford a mixture of fullerene substituted one to three times with the chelator. This mixture was purified by column chromatography to afford **19** bearing a single 1,2,3-triazole unit. The remaining eleven alkyne residues underwent copper catalyzed azide-alkyne cycloaddition with **12** to get the multimodal target C_{60}(HCPAMP)(GlcN)$_{11}$ **20** bearing eleven sugar units and the chelator (Scheme 6).

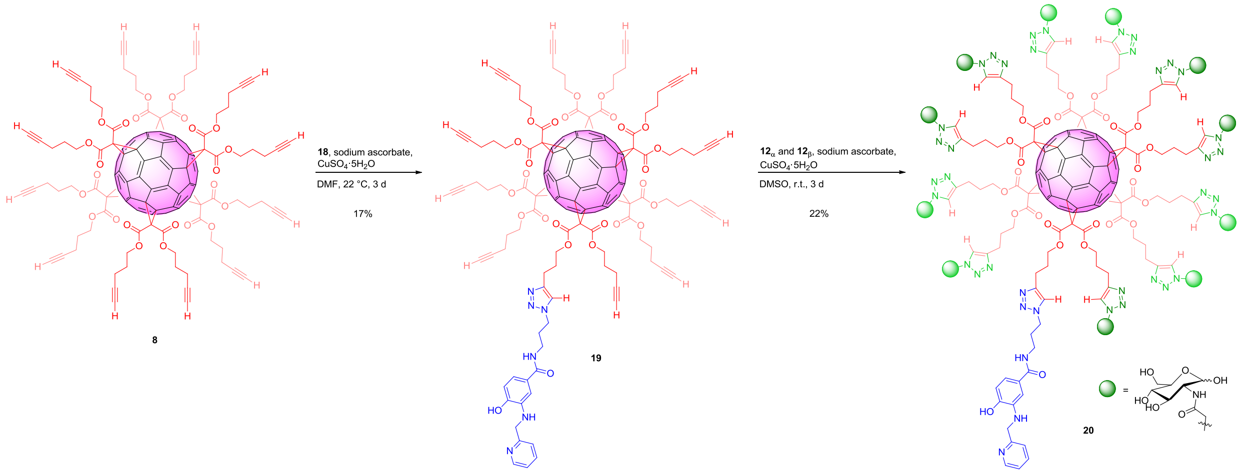

Scheme 6. Synthesis of the multimodal compound C_{60}(HCPAMP)(GlcN)$_{11}$ **20**.

In anticipation of potential clinical applications, radiolabeling of C_{60}(HCPAMP)(GlcN)$_{11}$ **20** was performed in a single step, using a “kit-like” approach, by adapting the procedure for the synthesis of the [^{99m}Tc(H_2O)$_3$(CO)$_3$]$^+$ precursor developed by Alberto *et al.*[26] A solution of [^{99m}Tc(H_2O)$_3$(CO)$_3$]$^+$ was adjusted to pH 7–8 by dropwise addition of aqueous hydrochloric acid (HCl) and phosphate buffer saline (PBS) solution prior to the radiolabeling process.[27] The ^{99m}Tc-labeled compounds **21** was synthesized by the reaction of [^{99m}Tc(H_2O)$_3$(CO)$_3$]$^+$ with a solution of **20** in a mixture of DMSO and water at pH 7.5–8 and 45 °C (Scheme 7).

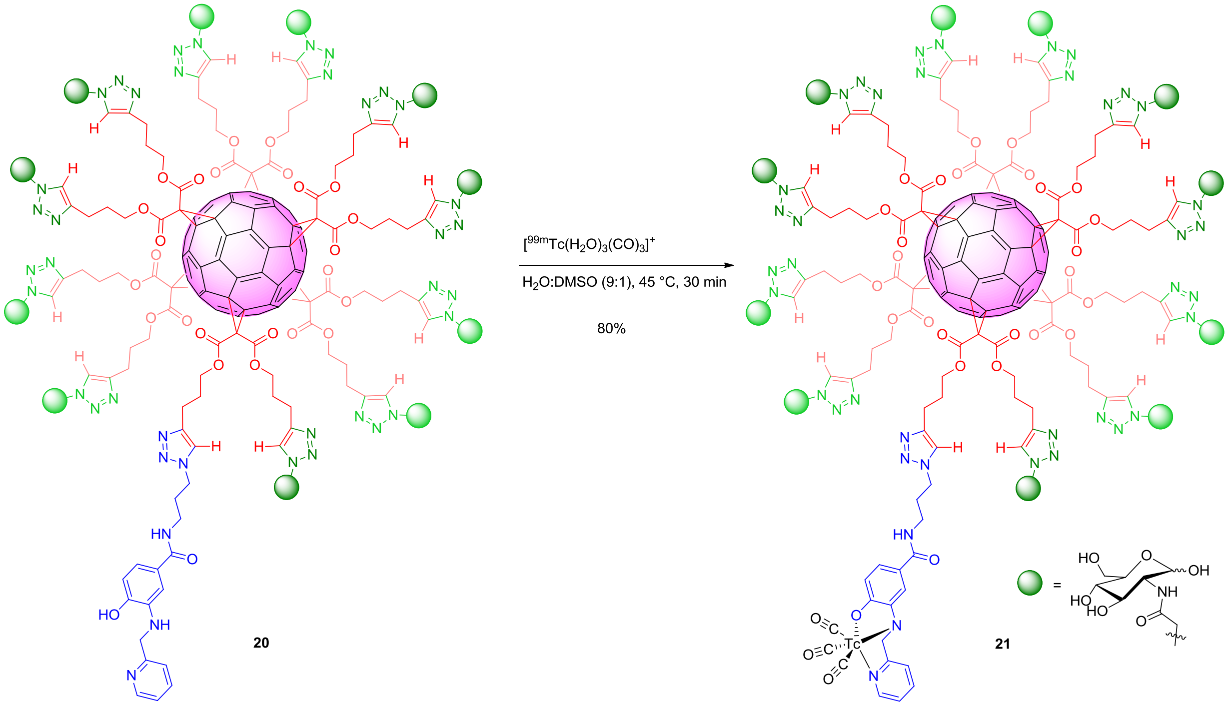

Scheme 7. ^{99m}Tc-radiolabeling of HCPAMP-GlcN-fullerene conjugate C_{60}(HCPAMP)(GlcN)$_{11}$ **20** to form radiolabelled compound **21**.

Radiochemical yield and purity of [^{99m}TcC_{60}(HCPAMP)(GlcN)$_{11}$] **21** was then verified by HPLC analysis (Figure 5). The radiolabelling occurred with 80% yield and the ^{99m}Tc-labeling product could be collected for readily *in vivo* applications.

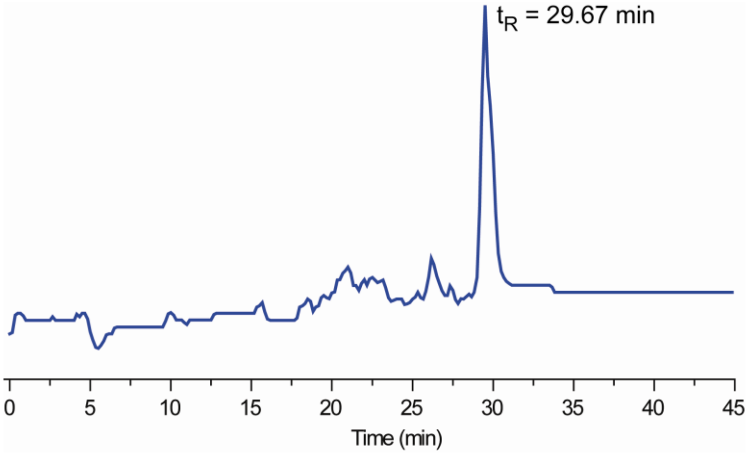

Figure 5. HPLC trace for the complex **21** detected with a γ-detector.

2.2. Biological and Medical Studies

2.2.1. Infarct Volume after $C_{60}(OH)_{34\text{-}36}$- and $C_{60}(GlcN)_{12}$-treatment in WKY and SHR

To assess the effect of $C_{60}(OH)_{34\text{-}36}$ on infarct volume in the tMCAO model, WKY and SHR were treated with $C_{60}(OH)_{34\text{-}36}$ (0.5 $mg \cdot kg^{-1}$). Infarct volume was determined by T2 weighted (T2w) MRI five days after tMCAO (Figure 6A). In control WKY (0.9% NaCl), infarction was detected in the left caudoputamen and partly in the cortex, whereas in most treated WKY, infarction was restricted to the left caudoputamen only. WKY treated with $C_{60}(OH)_{34\text{-}36}$ exhibited a significant reduction of 67% in infarct volume compared to placebo (Figure 6B).

In both, the control and treated SHR, infarction was observed in the left caudoputamen and the cortex fed by the ipsilateral middle cerebral artery (MCA). $C_{60}(OH)_{34\text{-}36}$-treatment (0.5 $mg \cdot kg^{-1}$) in SHR resulted in 26% reduction of in infarct volume (Figure 6C). Treatment with $C_{60}(OH)_{34\text{-}36}$ (0.5 $mg \cdot kg^{-1}$) reduced the infarct volume in WKY more than in SHR.

To investigate whether infarct reduction in SHR was dose-dependent, $C_{60}(OH)_{34\text{-}36}$ was intravenously administered immediately after tMCAO at two additional doses: a middle-dose group (1.0 $mg \cdot kg^{-1}$) and a high-dose group (2.0 $mg \cdot kg^{-1}$). Comparison of the infarct volume reduction with the low-dose group (0.5 $mg \cdot kg^{-1}$) showed no particular improvement upon higher dosage administration. Infarct volume reduction of the middle-dose group and high-dose group were 23% and 30% reduction, respectively. However, discomfort was more severe in SHR treated with higher dosages. Moreover, two animals died within 48 h, whereas in the low-dose group all ten animals survived. Therefore, further experiments were only conducted using 0.5 mg·kg^{-1} of $C_{60}(OH)_{34\text{-}36}$.

In SHR treated animals with $C_{60}(GlcN)_{12}$ (0.5 mg·kg^{-1} or 5.0 mg·kg^{-1}), infarction was observed both in the left caudoputamen and partly in the cortex. Compared to placebo, $C_{60}(GlcN)_{12}$ administration led to a dose-dependent reduction of infarct volume with 19% in infarct reduction with 0.5 mg·kg^{-1} and 34% reduction with 5.0 mg·kg^{-1} (Figure 6D). We conducted the next experiments using the high-dose of 5.0 mg·kg^{-1}.

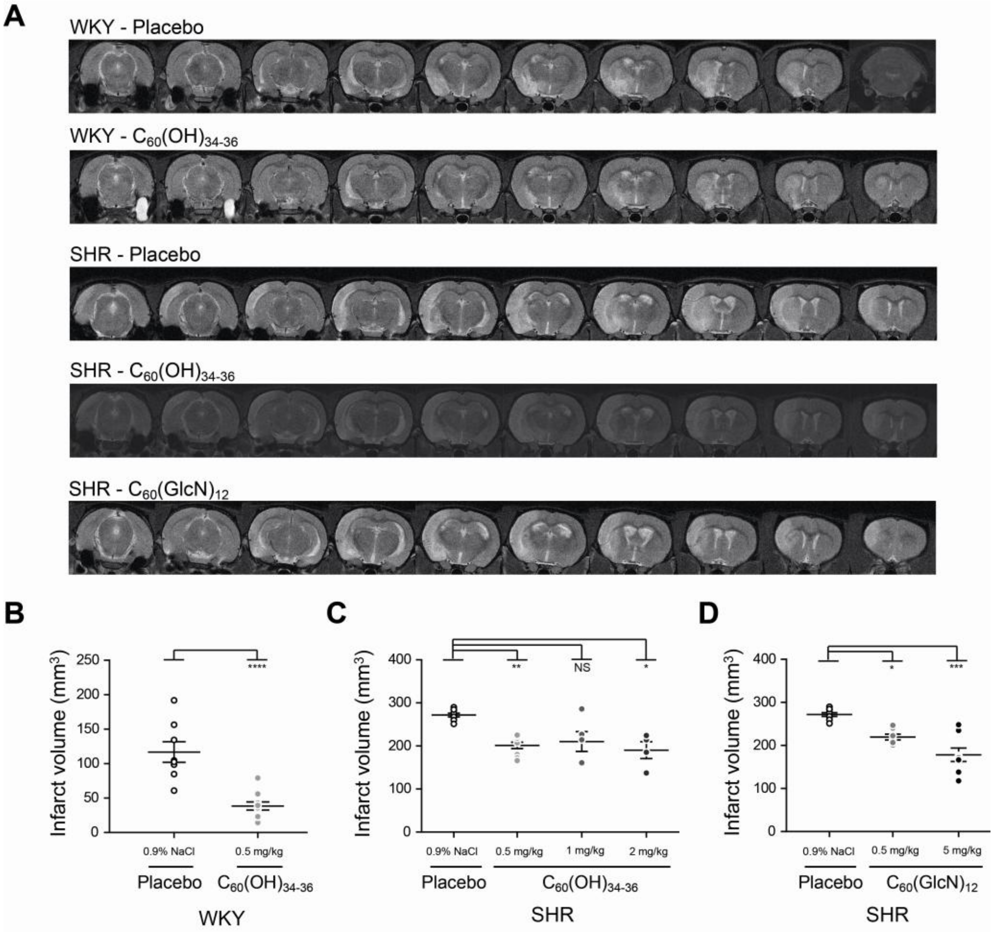

Figure 6. Treatment with $C_{60}(OH)_{34\text{-}36}$ or $C_{60}(GlcN)_{12}$ attenuates infarct volume in WKY or SHR subjected to tMCAO. (A) Representative T2w images of strokes incurred in placebos (0.9% NaCl) and treated animals with $C_{60}(OH)_{34\text{-}36}$ or $C_{60}(GlcN)_{12}$ five days after tMCAO. (B)–(D) Quantitative analysis of infarct volumes five days after tMCAO in (B) WKY rats and in (C), (D) SHR rats. Different dosages were used in SHR strain. Aligned dot plot of values. Bars and error bars in indicate means of N = 8 [WKY; Placebo], N = 10 [WKY; 0.5 mg·kg^{-1} $C_{60}(OH)_{34\text{-}36}$], N = 9 [SHR; Placebo], N = 10 [SHR; 0.5 mg·kg^{-1} $C_{60}(OH)_{34\text{-}36}$], N = 5 [SHR; 1 mg·kg^{-1} $C_{60}(OH)_{34\text{-}36}$], N = 4 [SHR; 2.0 mg·kg^{-1} $C_{60}(OH)_{34\text{-}36}$], N = 7 [SHR; 0.5 mg·kg^{-1} $C_{60}(GlcN)_{12}$], N = 8 [SHR; 5.0 mg·kg^{-1} $C_{60}(GlcN)_{12}$] per group ± standard error of mean (S.E.M.). (B) Mann-Whitney U test; (C), (D) Kruskall-Wallis statistic. NS = non-significant; $*P < 0.05$; $**P < 0.01$; $***P < 0.001$; $****P < 0.0001$.

2.2.2. Neurological assessment after treatment with $C_{60}(GlcN)_{12}$ and $C_{60}(OH)_{34\text{-}36}$

To determine neurological deficits at day 1 and day 5 after tMCAO, a 5-point score was used according to Menzies *et al.* methodology for neurological assessment. These studies were also performed by Dr. Felix Fluri.[28] Compared to placebo, treatment with $C_{60}(OH)_{34\text{-}36}$ in WKY and SHR ameliorated neurological scores at day 1 and 5. SHR treated with $C_{60}(GlcN)_{12}$ showed less neurological deficit after day 1 and 5 compared to placebo. Nevertheless, no improvement was observed between day 1 and 5 with GlcN-fullerene conjugates (Figure 7).

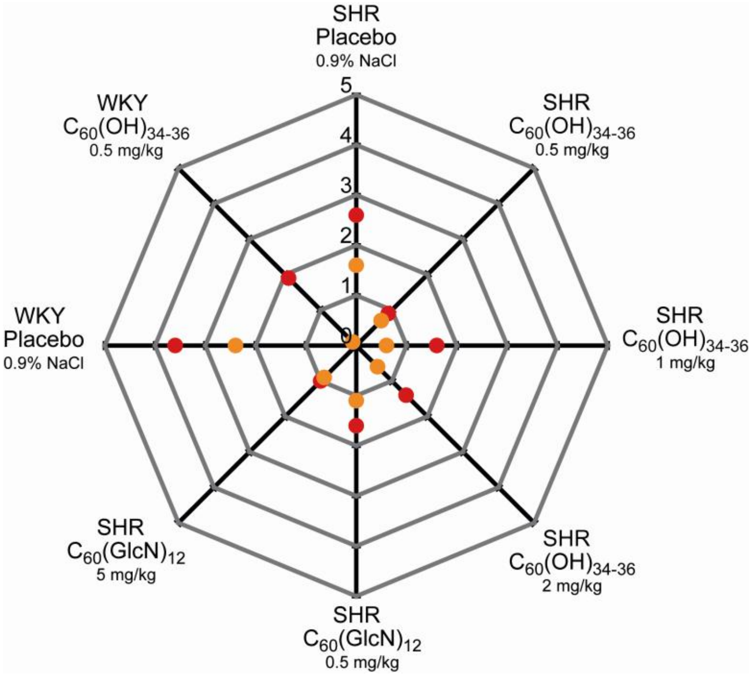

Figure 7. Neurological scores one day (red spots) and five days (orange spots) after tMCAO in animals treated either with placebo, $C_{60}(OH)_{34\text{-}36}$ or $C_{60}(GlcN)_{12}$. The assessment is summarized in a Spider chart form whereby 0 = no neurologic deficits, 1 = contralateral forelimb flexion, 2 = contralateral circling after tail pull, 3 = spontaneously contralateral circling, 4 = falling to the right, 5 = no spontaneous walking. Symbols indicate means of N = 8 [WKY; Placebo], N = 10 [WKY; 0.5 mg·kg^{-1} $C_{60}(OH)_{34\text{-}36}$], N = 9 [SHR; Placebo], N = 10 [SHR; 0.5 mg·kg^{-1} $C_{60}(OH)_{34\text{-}36}$], N = 5 [SHR; 1 mg·kg^{-1} $C_{60}(OH)_{34\text{-}36}$], N = 4 [SHR; 2.0 mg·kg^{-1} $C_{60}(OH)_{34\text{-}36}$], N = 7 [SHR; 0.5 mg·kg^{-1} $C_{60}(GlcN)_{12}$], N = 8 [SHR; 5.0 mg·kg^{-1} $C_{60}(GlcN)_{12}$] per group.

2.2.3. Effects of $C_{60}(OH)_{34\text{-}36}$ and $C_{60}(GlcN)_{12}$ on Cerebral Inflammation

To investigate anti-inflammatory properties of $C_{60}(OH)_{34\text{-}36}$ and $C_{60}(GlcN)_{12}$, quantitative real-time polymerase chain reaction (qRT PCR) for IL-1β, TNF-α, complement C3 and TLR-4 was performed. Cellular inflammation was visualized by CD68 immunostaining. CD68 is a glycoprotein expressed on macrophages and is therefore an indicator of inflammation.

In WKY, treatment with $C_{60}(OH)_{34\text{-}36}$ led to a down-regulation of C3, TLR-4, IL-1β, and TNF-α expression compared to placebo. In SHR, treatment of $C_{60}(OH)_{34\text{-}36}$ or $C_{60}(GlcN)_{12}$ did not significantly affect the expression of C3, TLR-4, IL-1β, and TNF-α (Figure 8).

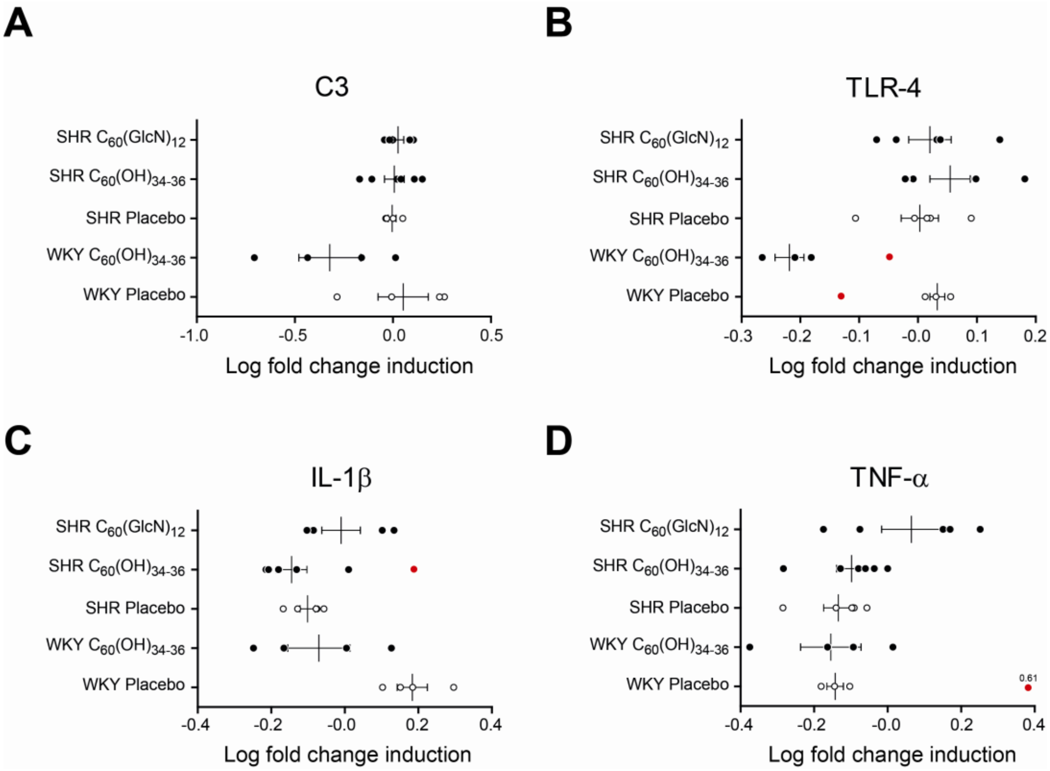

Figure 8. Induction of pro-inflammatory components. qRT PCR analysis of changes in gene expression represented as log-fold change induction. Representative gene expression fold changes in WKY and SHR treated with either placebo, $C_{60}(OH)_{34\text{-}36}$ or $C_{60}(GlcN)_{12}$ for (A) complement C3, (B) TLR-4, (C) IL-1β, and (D) TNF-α. Aligned dot plot of values. Bars and error bars in indicate means of N = 4 [WKY; Placebo], N = 4 [WKY; $C_{60}(OH)_{34\text{-}36}$], N = 5 [SHR; Placebo] (C3: N = 4), N = 6 [SHR; $C_{60}(OH)_{34\text{-}36}$], N = 5 [SHR; $C_{60}(GlcN)_{12}$] per group. Red points are discarded. No P values were determined due to the small N.

$CD68^+$ cells were significantly decreased in WKY treated with $C_{60}(OH)_{34\text{-}36}$ compared to placebos (44% reduction). In SHR treated with $C_{60}(OH)_{34\text{-}36}$, no significant reduction of $CD68^+$ cells was observed; however, $C_{60}(GlcN)_{12}$ treatment revealed a very significant reduction of these cells in SHR (40% reduction) (Figure 9).

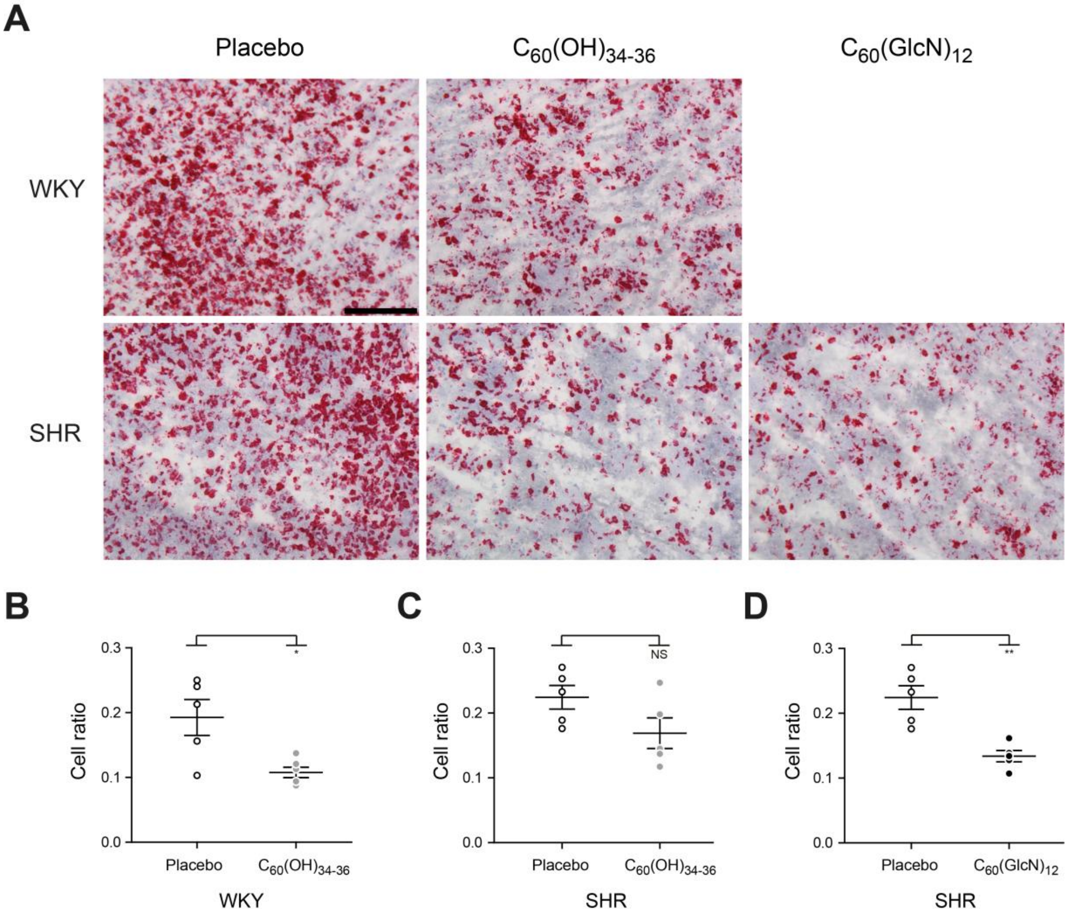

Figure 9. Treatment with $C_{60}(OH)_{34\text{-}36}$ or $C_{60}(GlcN)_{12}$ reduces $CD68^+$ expressed on monocytes and macrophages in the subcortical lesion. (A) Representative $CD68^+$ staining images of WKY and SHR treated with either placebo, $C_{60}(OH)_{34\text{-}36}$ or $C_{60}(GlcN)_{12}$. Scale bar: 200 μm. (B)–(D) Quantitative immunohistochemical analysis of $CD68^+$ in (B) WKY rats and in (C), (D) SHR rats. Results are expressed as ratios of $CD68^+$ per field of view. Aligned dot plot of values. Bars and error bars in indicate means of N = 6 [WKY; $C_{60}(OH)_{34\text{-}36}$] or N = 5 per group ± S.E.M. (B) Mann-Whitney U test; (C), (D) Kruskall-Wallis statistic. NS = non-significant; *$P < 0.05$; **$P < 0.01$.

2.2.4. Neuronal Survival after $C_{60}(OH)_{34\text{-}36}$- and $C_{60}(GlcN)_{12}$-treatment

Neuronal nuclei (NeuN) is a marker for neurons and reacts with most neuronal cell types throughout the nervous system. The staining is primarily localized in the nucleus of the neurons (Figure 10). In $C_{60}(OH)_{34\text{-}36}$-treated WKY, significantly more NeuN positive cells were detected in the subcortical area than in the control WKY (47%) (Figure 10B). SHR treated with $C_{60}(GlcN)_{12}$ showed significantly more $NeuN^+$ cells in the subcortical area compared to the placebos SHR (45% increase) (Figure 10D).

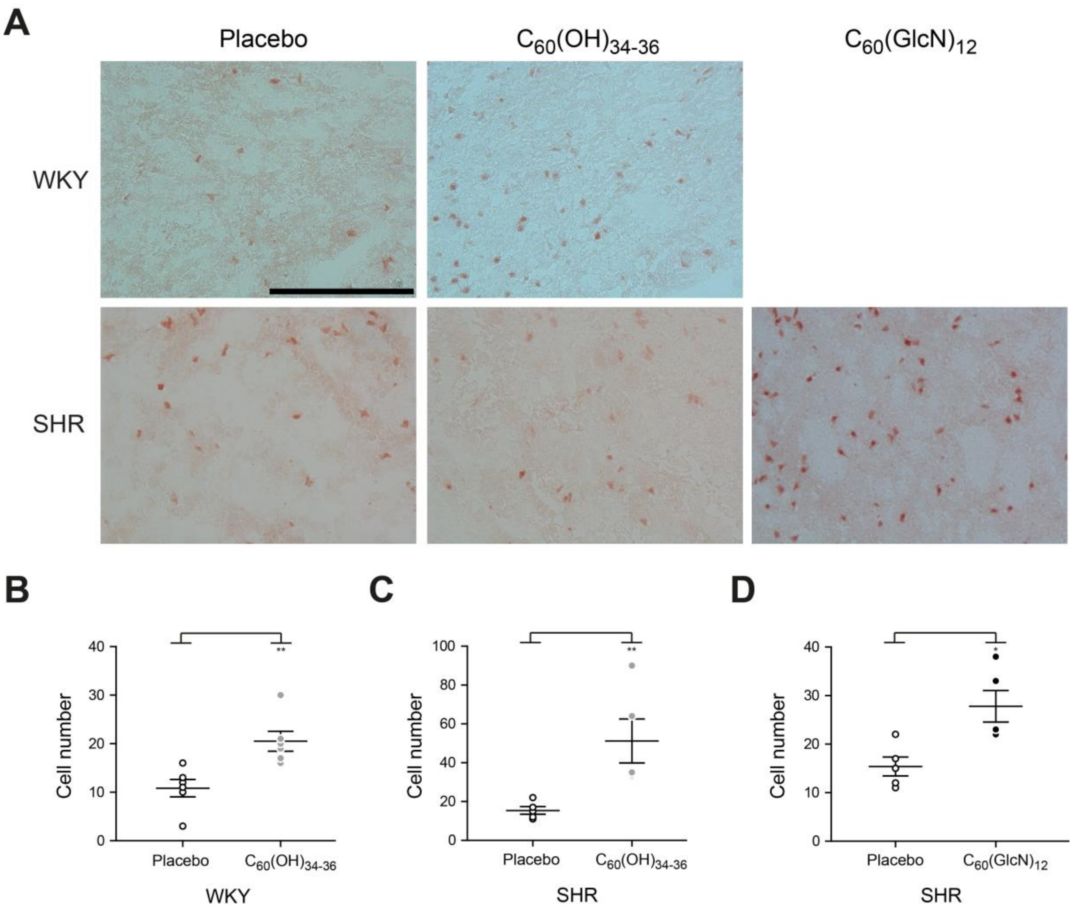

Figure 10. Treatment with $C_{60}(OH)_{34\text{-}36}$ or $C_{60}(GlcN)_{12}$ improves neuron-specific nuclear protein NeuN expressed on neurons in the perilesional area. (A) Representative $NeuN^+$ cells staining images of WKY and SHR treated with either placebo, $C_{60}(OH)_{34\text{-}36}$ or $C_{60}(GlcN)_{12}$. Scale bar: 200 μm. (B)–(D) Quantitative immunostaining analysis of $NeuN^+$ cells in (B) WKY rats and in (C), (D) SHR rats. Results are expressed as $NeuN^+$ cells per field of view. Aligned dot plot of values. Bars and error bars in indicate means of N = 6 [WKY], N = 5 [SHR; Placebo], N = 3 [SHR; $C_{60}(OH)_{34\text{-}36}$], N = 4 [SHR; $C_{60}(GlcN)_{12}$] per group ± S.E.M. (B) Mann-Whitney U test; (C), (D) Kruskall-Wallis statistic. $^*P < 0.05$; $^{**}P < 0.01$.

Ki-67 is cellular marker for proliferation. Ki-67 protein is present during all active phases of the cell cycle and is consequently an excellent marker to determine the growth fraction of a given cell population (Figure 11). Upon Ki-67 staining, $C_{60}(OH)_{34\text{-}36}$-treated WKY and $C_{60}(GlcN)_{12}$-treated SHR showed a clear tendency to have more positive Ki-67 cells than controls (32% and 26%, respectively) (Figure 11C, D).

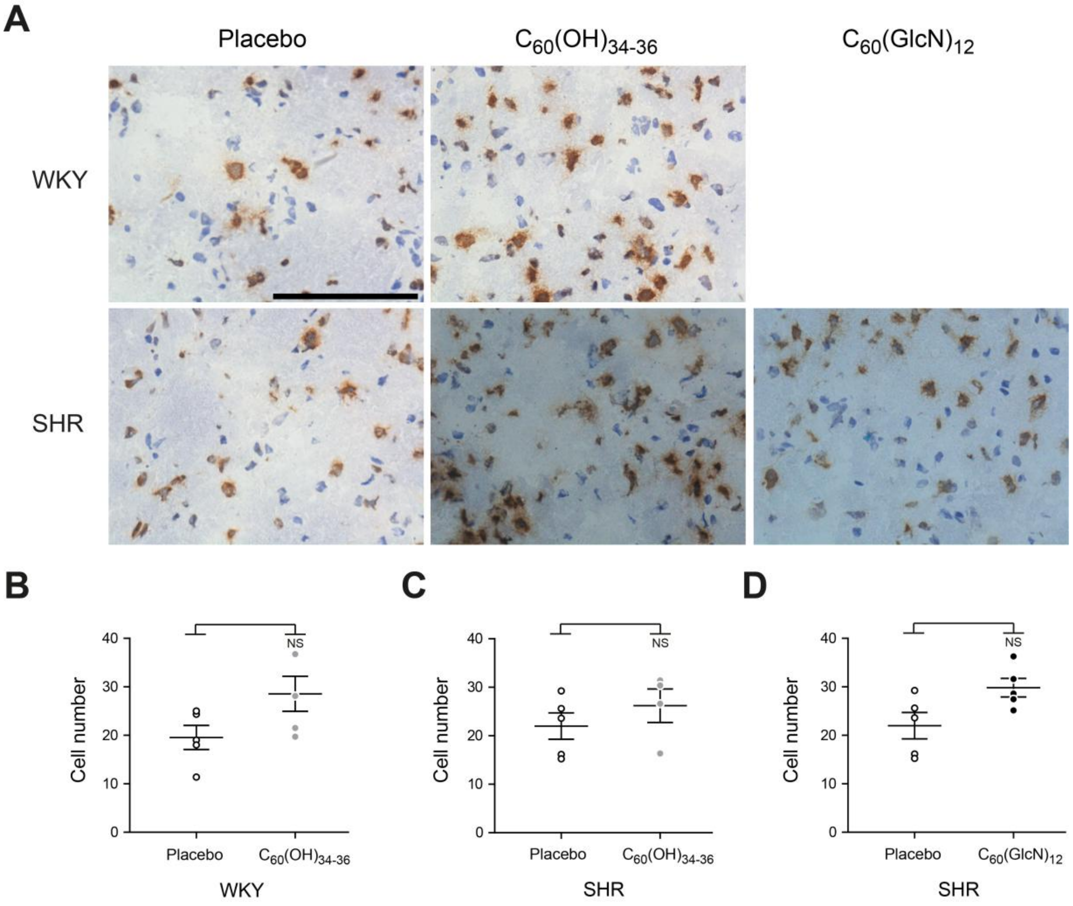

Figure 11. Treatment with $C_{60}(OH)_{34-36}$ or $C_{60}(GlcN)_{12}$ improves cell proliferation. (A) Representative Ki-67 positive cells staining images of WKY and SHR treated with either placebo, $C_{60}(OH)_{34-36}$or $C_{60}(GlcN)_{12}$. Scale bar: 100 µm. (B)–(D) Quantitative immunostaining analysis of Ki-67 positive cells in (B) WKY rats and in (C), (D) SHR rats. Results are expressed as Ki-67 positive cells per field of view. Aligned dot plot of values. Bars and error bars in indicate means of N = 5 [WKY], N = 5 [SHR; Placebo], N = 4 [SHR; $C_{60}(OH)_{34-36}$], N = 5 [SHR; $C_{60}(GlcN)_{12}$] per group ± S.E.M. (B) Mann-Whitney U test; (C), (D) Kruskall-Wallis statistic. NS = non-significant.

2.3. Discussion

Inflammation plays a key role in the pathophysiology of cerebral ischemia by exerting deleterious effects on the progression of tissue damage and therefore, remains an attractive target for therapeutic intervention.[29] In this chapter, I report that the radical scavenging activity of fullerenol $C_{60}(OH)_{34-36}$ and anti-inflammatory effects GlcN-fullerene conjugates $C_{60}(GlcN)_{12}$ attenuate cerebral inflammation after ischemic stroke and reduce infarct size in normotensive and hypertensive rats.

Intravenously administration of $C_{60}(OH)_{34-36}$ reduced significantly infarct volume and inflammatory response in normotensive WKY. The reduction of infarct volume might be due to

(1) antioxidant and free radical scavenger properties of $C_{60}(OH)_{34\text{-}36}$, since the remaining double bonds of the C_{60} structure accept free radicals, (2) due to inhibition of glutamate receptors by binding of the hydroxyl groups to the positive charge residues near or at the glutamate receptor resulting in steric hindrance by the bulky molecule and (3) due to anti-inflammatory properties.

According to the Stroke Therapy Academic Industry Roundtable (STAIR) preclinical recommendations, the efficacy of neuroprotective agents should be investigated in animals with comorbidity, since most stroke patients show at least one vascular risk factor such as diabetes or arterial hypertension.[30] We chose SHR since arterial hypertension is the most important vascular risk factor for stroke.[31] Interestingly, the same dose of $C_{60}(OH)_{34\text{-}36}$ led to a smaller reduction of infarct volume and cerebral inflammation after ischemic stroke in SHR compared to WKY. Furthermore, the infarct volume in SHR did not change upon increasing the fullerenol dose from 0.5 to 2 $mg \cdot kg^{-1}$. A lack of a dose-dependent response on infarct volume in SHR seems to indicate that mechanisms other than oxidative stress are involved in the development of ischemic infarct in SHR. Arterial hypertension has been shown to be associated with a slightly chronic inflammation in the brain of SHR.[32]

We hypothesized that post-stroke inflammation might play a more important role in SHR when compared to WKY in respect to infarct evolution. Therefore, we intended to potentiate the effects of C_{60} by adding a molecule such as glucosamine with known anti-inflammatory properties. GlcN has been suggested to reduce significantly infarct volume in experimental stroke and to suppress microglia activation and macrophage accumulation in the post-ischemic brain. In addition, GlcN was reported to suppress the induction of pro-inflammatory markers such as IL-1β and TNF-α.[33] Administration of $C_{60}(GlcN)_{12}$ in two different doses (i. e. 0.5 and 5.0 $mg \cdot kg^{-1}$) did not reduce infarct volume significantly more than treatment with fullerenol; however the mechanisms that led to that reduction appears to differ from $C_{60}(OH)_{34\text{-}36}$ treatment. Therefore, injection of a combination of both drugs in order to test combinatorial effects of $C_{60}(OH)_{34\text{-}36}$ and $C_{60}(GlcN)_{12}$ is of significant interest for future studies.

Anatomical and morphological differences of the cerebral vasculature of WKY and SHR might be more important in the evolution of ischemic infarction than oxidative stress or cerebral inflammation. Hypertensive rats have less collateral arteries compared to normotensive strains. Furthermore, the middle cerebral artery in normotensive rats has been shown to develop compensatory mechanisms, comprising enhanced distensibility and decreased myogenic tone, an increase in wall stiffness, and wall thickness that counteracts the effect of ischemia-reperfusion damage. These compensatory mechanisms are lost in hypertension.[34] Compared to normotensive rats, SHR have a smaller penumbra –the portion of ischemic brain surrounding the infarcted core– that is potentially salvageable if an appropriate treatment is administered.[35] Furthermore, the perfusion deficit in hypertensive rats increases over time. Thus, SHR rats present a priori less salvageable tissue compared to WKY. Nevertheless, $C_{60}(OH)_{34\text{-}36}$ and $C_{60}(GlcN)_{12}$ appear to have a strong neuroprotective effect even in SHR compared to the neuroprotective NXY-059. This phenylbutynitrone exerted in normotensive rat a remarkable infarct volume reduction of 48%; however the equivalent drug dose however did not reduce significantly infarct volume in SHR.[36]

The reduced infarct volume and ameliorated neurological score observed in the present study after $C_{60}(OH)_{34\text{-}36}$ and $C_{60}(GlcN)_{12}$ treatment might be due to the reduction of microglia and macrophages in the infarcted area of WKY and SHR. This effect had not been observed previously. Additionally, suppression of IL-1β and TLR-4 was observed in fullerenol-treated WKY. Inflammatory processes are involved already in the early post-ischemic period and have a deleterious effect that amplifies ischemic injury.[37] Within the first hours of stroke, a rapid activation of resident microglia and production of pro-inflammatory cytokines including IL-1β and TNF-α takes place.[38] IL-1β exerts ischemia-induced brain damage by inducing the synthesis of cyclooxygenase-2 and nitric oxide synthase as well as by activating NF-κB signaling pathways.[39] TLR-4, a signaling receptor of the innate immunity that recognize host-derived molecules released from injured cells is also expressed in microglia as well as in astrocytes and neurons after cerebral ischemia.[40] TLR-4 activates NF-κB signaling pathways linked to the transcription of many pro-inflammatory genes. Down-regulation of IL-1β and TLR-4 in $C_{60}(OH)_{34\text{-}36}$ treated WKY is probably due to the reduced microglia of the infarcted zone. The role of TNF-

α in stroke is not clear since both noxious and beneficial effects have been reported. Surprisingly, TNF-α which is also produced by microglia, was almost not changed in fullerenol-treated WKY compared to placebos. TNF-α is increased 3 h after stroke and persists for 24 h, and therefore a probable difference is no longer detectable five days after tMCAO.[41] Although complement C3 mediates inflammatory cerebral injury after brain ischemia, this compound was not influenced by $C_{60}(OH)_{34-36}$ in WKY in all animals.

In the present study, $C_{60}(GlcN)_{12}$ reduced the number of microglia/macrophages in SHR. The dose of 5 $mg \cdot kg^{-1}$ $C_{60}(GlcN)_{12}$ probably leads only to an increase of cell accumulation but is not strong enough to suppress the activity of these cells and attenuate the synthesis of pro-inflammatory cytokines. Hwang and coworkers have reported that suppression of pro-inflammatory mRNAs was observed using at least a dose of 50 $mg \cdot kg^{-1}$ in rats.[15] However, experiments in the aforementioned study were conducted only in normotensive animals. SHR have increased endothelial macrophage infiltration and inflammatory marker expression.[32] This cerebrovascular inflammation might be protective by promoting anti-inflammatory responses and producing neuroprotective molecules leading to a form of preconditioning. A preconditioning stimulus has suggested triggering first the TLR/cytokine inflammatory pathways, resulting not only in cerebral inflammation but also in simultaneous up-regulation of feedback inhibitors of inflammation.

Administration of $C_{60}(OH)_{34-36}$ in WKY and $C_{60}(GlcN)_{12}$ in SHR preserved neurons in the perilesional zone of the caudoputamen, underlining the neuroprotective effect of these agents. These observations corroborate the findings of another study, where functionalized fullerenes prevent neuronal death. This cytoprotective effect is probably based on the ability of fullerenes to interfere in different phases of the ischemic cascade including oxidative stress, glutamate toxicity or inflammation.

As a novel finding, $C_{60}(GlcN)_{12}$ treatment was associated with a tendency of cell proliferation when compared to placebo. $C_{60}(OH)_{34-36}$ also showed a tendency toward cell proliferation. Therefore, it remains to be determined whether GlcN promotes cell proliferation in the same manner as fullerenols do.

The finding that treatment with functionalized fullerenes is associated with an increase of neurons indicates that these compounds are not neuronotoxic, even when the cells are in a vulnerable state as is the case under ischemic conditions. The acute toxicity of fullerenol is low: while mice showed symptoms of discomfort and some weight loss after a single intraperitoneal injection at 200–500 mg·kg^{-1} doses of fullerenol, all of them survived. The LD_{50} value of polyhydroxylated fullernes was estimated to be 1.2 g·kg^{-1} intraperitoneally in mice.[42] The reduced acute cytotoxicity of functionalized fullerenes is probably due to the fact that these molecules can hardly penetrate the lipid bilayer (i.e. cell wall) and remain at the bilayer/water interface.[43] Interestingly, oral administration of C_{60} dissolved in olive oil (0.8 mg·mL^{-1}) at repeated doses (1.7 mg·kg^{-1}) to rats does not entail chronic toxicity, but in contrast almost doubles their lifespan.[44] After repeated oral administration of C_{60} during 29 days, C_{60} were not detected in the liver, spleen or kidney.[45]

3. Conclusion

To date, more than one thousand neuroprotective agents that appeared promising in animal experiments failed to show promising results in stroke patients. Although the reasons for these failures are manifold, one contributing feature is that most agents focused on a single aspect of the complex ischemic cascade.[46]

Functionalized fullerenes exert a potent oxygen scavenging activity, reduce glutamate excitotoxicity by binding to glutamate receptors decreased nitric oxide and recovery of glutathione.[47]

In the present study, we demonstrated anti-inflammatory effects of functionalized fullerenes. Therefore, this molecule interferes in different aspects of the ischemic cascade, rendering functionalized fullerenes a promising molecule for stroke treatment. Efforts to translate these findings to humans will commence following further preclinical evaluations.

4. Experimental Part

4.1. Chemical Synthesis

4.1.1. General Experimental Details

Commercial grade reagents and solvents were used without further purification except as indicated below. Deionized water was obtained from an in-house purification system (Millipore). The term “concentrated under reduced pressure” refers to the removal of solvents and other volatile material using a rotary evaporator while maintaining a water bath temperature around 40 °C. The compounds purified by flash chromatography are further concentrated by the removal of residual solvent under high vacuum (< 0.2 mbar). Room temperature (r.t.) refers to the ambient temperature (20–25 °C).

4.1.2. Physical Properties and Spectroscopic Measurements

^{1}H NMR and ^{13}C NMR spectra were measured with a Varian 400-MR, Varian 600-MR, Bruker ECP 400, Bruker AC 500, or Bruker AC 700 spectrometer. The residual proton signal of solvent at δ7.26 ppm for $CDCl_3$, 3.34 ppm for CD_3OD, 2.50 ppm for DMSO, and 4.79 ppm for D_2O was used as an internal reference for ^{1}H spectra. For ^{13}C spectra, the chemical shifts are reported relative to the δ77.36 ppm for $CDCl_3$, 49.86 ppm for CD_3OD, and 39.51 ppm for DMSO. Coupling constants (*J*) are reported in Hertz (Hz). Multiplicities are given as: *s* (singlet); *d* (doublet); *t* (triplet); *dd* (doublets of doublet); *bs* (broad singlet); *m* (multiplet); *tt* (triplets of tiplet); *dt* (doublets of triplet); *td* (triplets of doublet); *q* (quartet); *ddd* (doublets of doublets of doublet) or *p* (pentet). High-resolution mass spectra (HRMS) analyses were performed by the mass service of the Free University Berlin. High resolution matrix-assisted laser desorption/ionisation (MALDI) and electrospray ionization (ESI) mass spectra were run on Bruker Autoflex Speed mass spectrometer and on an Agilent 6210 ESI-TOF mass spectrometer, respectively. Elemental analysis was performed on an ICP-Mass Spectrometry (Thermo Fischer Element 2). Infrared (IR) spectra were recorded on a Spectrum 100 FTIR spectrophotometer (Perkin-Elmer). UV-vis spectra (extinction spectra) were recorded with an Ultrospec 6300 pro UV-visible Spectrophotometer (GE Healthcare, Amersham Biosciences, Piscataway, NJ, USA). Analytical thin layer chromatography (TLC) was performed on Kieselgel 60 F_{254} glass plates precoated with a 0.25 mm thickness of silica gel. The TLC plates were visualized with UV light and by staining with Hanessian solution (ceric sulfate and ammonium molybdate in aqueous sulfuric acid) or potassium permanganate solution (potassium permanganate in basic aqueous solution). Column chromatography was performed using Kieselgel 60 (230–400 mesh) silica gel with a typical 50–100:1 weight ratio of silica gel to crude product.

4.1.3. Compound Characterization

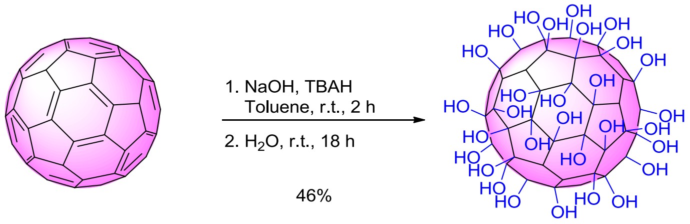

3 1

Fullerenol (1)

Fullerene **3** (80 mg, 0.111 mmol) was dissolved in toluene (60 mL) followed by the addition of aqueous NaOH (1 g·mL^{-1}, 2 mL) und vigorous stirring. TBAH (1 mL, 40% in H_2O) was then added, and the reaction mixture was stirred at r.t. in an open flask for 2 h. The toluene solution, originally deep violet, turned colorless, and a brown sludge precipitated. After removal of toluene by decantation and evaporation under reduced pressure, the sludge and remaining aqueous solution was stirred with additional water (10 mL) for 18 h. Further water (20 mL) was then, and the clear reddish brown aqueous solution was filtered. The filtrate was concentrated to about 5 mL of water and MeOH (50 mL) was added to produce a brown precipitate. The precipitate was centrifuged and the supernatant was discarded. The precipitation process was repeated 5 times to ensure complete removal of TBAH and NaOH. The precipitate was then extensively washed with MeOH (100 mL) and dried under *high vacuo* to give fullerenol **1** (66 mg, 46%) as a brownish powder.

EA calcd. for $C_{60}H_{33}O_{33}$: C, 56.22; H, 2.59; O, 41.19, found: C, 56.56 ± 0.09; H, 2.685 ± 0.069. HRMS (MALDI, negative mode, no matrix) 4 fragmental species C_{60}: 720.456; C_{58}: 696.449; C_{56}: 672.441; C_{54}:648.439.

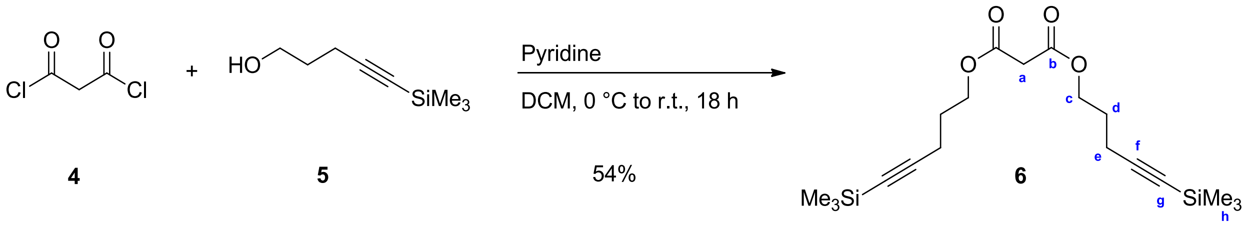

Bis(5-(trimethylsilyl)pent-4-yn-1-yl) malonate (6)

Malonyl dichloride **4** (1.07 mL, 11.00 mmol) was added to a solution of **5** (3.45 g, 22.07 mmol) and pyridine (1.79 mL, 22.13 mmol) in DCM (150 mL). The reaction mixture was allowed to stir at 0 °C under N_2 atmosphere. After 1 h, the mixture warmed up to r.t., and then stirred for another 18 h. The reaction mixture was then filtered, and the filtrate coevaporated with DCM (3×50 mL). The crude was purified by column chromatography (silica gel, DCM:hexane 1:1) to give **6** (2.26 g, 54%) as a colorless oil.

^{1}H NMR (400 MHz, $CDCl_3$) δ 4.24 (*t*, *J* = 6.3 Hz, 4H, *H$_c$*), 3.38 (*s*, 2H, *H$_a$*), 2.32 (*t*, *J* = 7.0 Hz, 4H, *H$_e$*), 1.86 (*p*, *J* = 6.7 Hz, 4H, *H$_d$*), 0.14 (*s*, 18H, *H$_h$*).

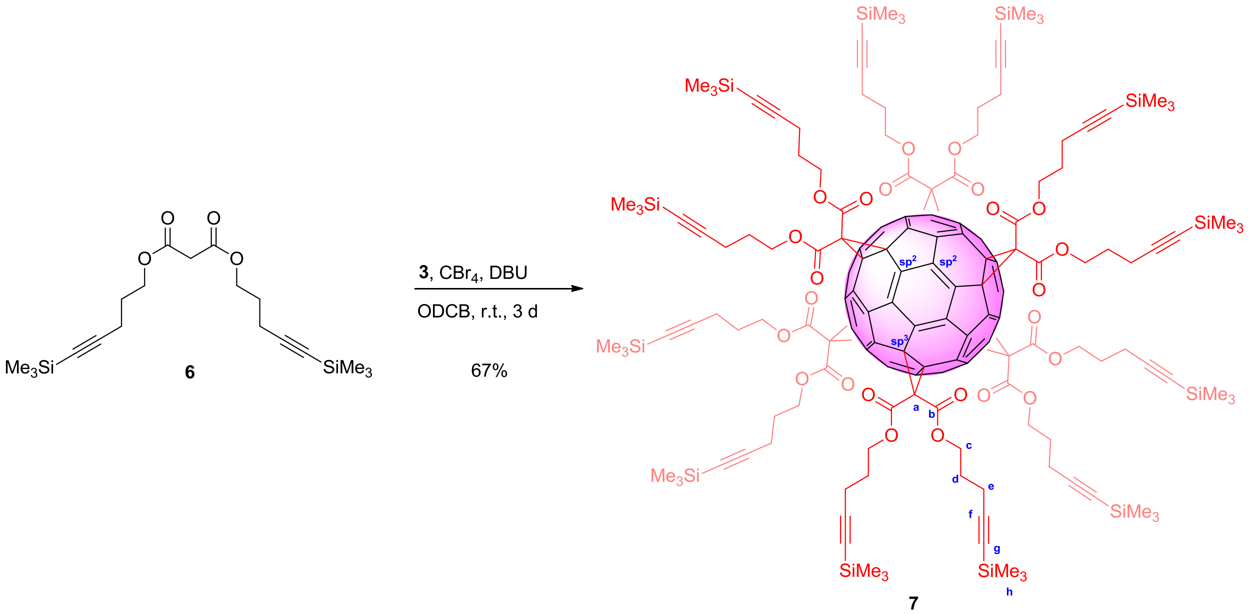

Dodecatrimethylsilylalkyne-fullerene (7)

CBr_4 (17.42 g, 52.5 mmol), **6** (2.0 g, 5.25 mmol), and DBU (1.58 mL, 10.48 mmol) were added successively to a solution of fullerene **3** (0.38 g, 0.527 mmol) in ODCB (100 mL). The mixture was stirred for 3 d and the solvent was evaporated. The crude was purified by column chromatography (silica gel, toluene:EtOAc 100:0 to 97:3) to give **7** (1.06 g, 67%) as a red glassy oil.

^{1}H NMR (400 MHz, $CDCl_3$) δ 4.37 (*t*, *J* = 6.5 Hz, 24H, H_c), 2.32 (*t*, *J* = 7.0 Hz, 24H, H_e), 1.92 (*tt*, *J* = 11.5, 5.7 Hz, 24H, H_d), 0.15 (*s*, 108H, H_e).

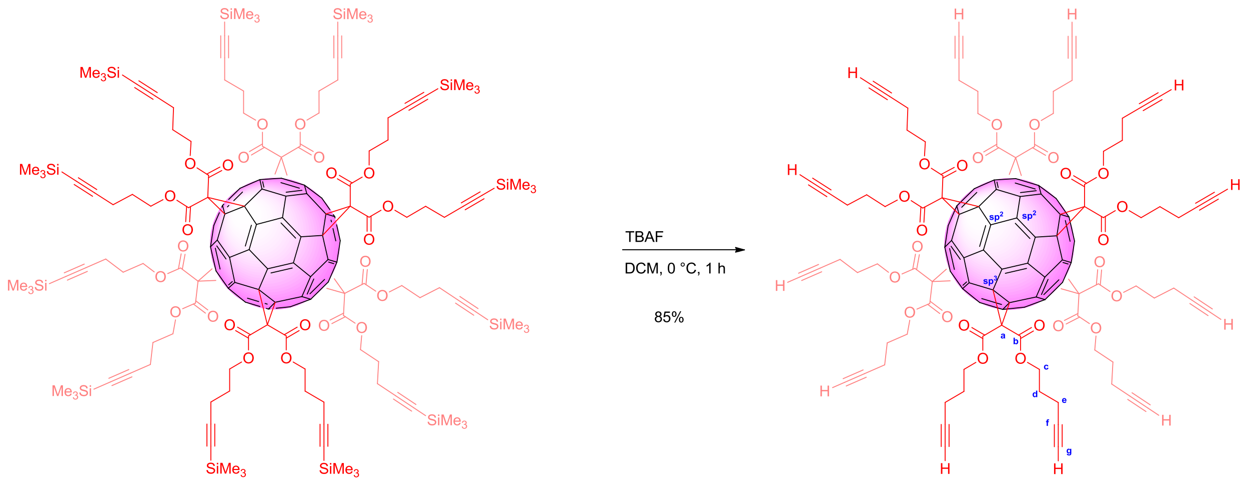

7 **8**

Dodecaalkyne-fullerene (8)

A solution of TBAF in THF (1 M, 1.17 mL) was added to **7** (250 mg, 0.083 mmol) in DCM (10 mL) at 0 °C. After 1h stirring, the organic layer was diluted with DCM (10 mL), washed with H_2O (20 mL), dried over $MgSO_4$, filtered, and concentrated under reduced pressure. The crude was purified by column chromatography (silica gel, DCM:cyclohexane:MeOH 88:10:2) to afford **8** (152 mg, 85%) as an orange glassy oil.

^{1}H NMR (400 MHz, $CDCl_3$) δ 4.39 (*t*, *J* = 6.3 Hz, 24H, H_c), 2.28 (*td*, *J* = 6.9, 2.6 Hz, 24H, H_e), 2.00 (*t*, *J* = 2.6 Hz, 12H, H_g), 1.97–1.88 (*m*, 24H, H_d). ^{13}C NMR (100 MHz, $CDCl_3$) δ 163.7 (C_b), 145.8 (C_{sp2}), 141.2 (C_{sp2}), 82.5 (C_f), 69.8 (C_g), 69.2 (C_{sp3}), 65.4 (C_c), 45.4 (C_a), 27.2 (C_d), 15.2 (C_e). HRMS (MALDI, positive mode, CHCA as matrix) calcd. for $C_{138}H_{94}NO_{24}$ $[M+NH_4]^+$: 2148.6166, found: 2148.697.

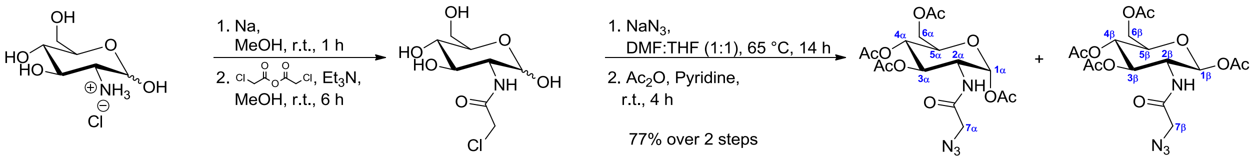

9 **10** **11_{α}** **11_{β}**

***O*-Acetyl azidoglucosamine (11_{α} and 11_{β})**

Glucosamine hydrochloride **9** (0.2 g, 0.928 mmol) was dissolved in MeOH (5 mL) under N_2 atmosphere. Na (21 mg, 0.928 mmol) was then added. The reaction mixture was stirred at r.t. for 1 h at which point Et_3N (133 μL, 0.955 mmol) and chloroacetic anhydride (810 mg, 4.74 mmol) were added. The reaction mixture was stirred for a further 6 h at r.t. Removal of solvent provided crude **10** which was then partially purified by column chromatography (silica gel, $CHCl_3$:MeOH 9:1 to 7:3). The resulting oil was dissolved in DMF (4 mL) and THF (4 mL). NaN_3 (1.22 g, 18.77 mmol) was added, and the reaction mixture was heated to 65 °C for 14 h. Upon cooling to r.t., the inorganics were discarded upon filtration, and the solvents were removed under reduced pressure. The residue was redissolved in pyridine (5 mL, 61.8 mmol) and Ac_2O (2.5 mL, 26.5 mmol). After stirring 4 h at r.t., the reaction mixture was poured into DCM (100 mL). The organic layer was washed with aqueous HCl (1 M, 2×40 mL), saturated aqueous solution of $NaHCO_3$ (2×40 mL), H_2O (2×40 mL), brine (2×40 mL), and dried over anhydrous $MgSO_4$, filtered, concentrated, and the crude obtained was purified by column chromatography (silica gel, hexane:EtOAc 4:1 to 3:2) to afford **11_{α}** and **11_{β}** (mixture of α:β 2.5:1) (309 mg, 77%) as a white powder.

^1H NMR (600 MHz, $CDCl_3$) δ 6.55 (*d*, *J* = 9.3 Hz, 1H, NH_{β}), 6.44 (*d*, *J* = 8.8 Hz, 2.5H, NH_{α}), 6.19 (*d*, *J* = 3.7 Hz, 2.5H, $H_{1\alpha}$), 5.78 (*d*, *J* = 8.7 Hz, 1H, $H_{1\beta}$), 5.31–5.23 (*m*, 3.5H, $H_{3\alpha}$ and $H_{3\beta}$), 5.20 (*t*, *J* = 9.8 Hz, 2.5H, $H_{4\alpha}$), 5.12 (*t*, *J* = 9.6 Hz, 1H, $H_{4\beta}$), 4.44 (*ddd*, *J* = 10.9, 8.9, 3.7 Hz, 2.5H, $H_{2\alpha}$), 4.29–4.19 (*m*, 4.5H, $H_{6\beta}$, $H_{6\alpha}$ and $H_{2\beta}$), 4.14–4.04 (*m*, 3.5H, $H_{6\beta}$ and $H_{6\alpha}$), 4.01 (*ddd*, *J* = 10.2, 3.9, 2.5 Hz, 2.5H, $H_{5\alpha}$), 3.92 (*s*, 5H, $H_{7\alpha}$), 3.89 (*d*, *J* = 1.2 Hz, 2H, $H_{7\beta}$), 3.83 (*ddd*, *J* = 9.9, 4.6, 2.3 Hz, 1H, $H_{5\beta}$), 2.19 (*s*, 7.5H, $OCCH_{3\alpha}$), 2.10 (*s*, 3H, $OCCH_{3\beta}$), 2.08 (*s*, 8.5H, $OCCH_{3\alpha}$ and $OCCH_{3\beta}$), 2.04 (*s*, 7.5H, $OCCH_{3\alpha}$), 2.04 (*s*, 7.5H, $OCCH_{3\alpha}$), 2.03 (*s*, 3H, $OCCH_{3\beta}$), 2.03 (*s*, 3H, $OCCH_{3\beta}$). ^{13}C NMR (150 MHz, $CDCl_3$) δ 171.6 ($OCCH_{3\alpha}$), 170.9 ($OCCH_{3\beta}$), 170.7 ($OCCH_{3\alpha}$), 170.7 ($OCCH_{3\beta}$), 169.4 ($OCCH_{3\beta}$), 169.3 ($OCCH_{3\beta}$), 169.2 ($OCCH_{3\alpha}$), 168.7 ($OCCH_{3\alpha}$), 167.2 ($OCNH_{\beta}$), 167.0 ($OCNH_{\alpha}$), 92.3 ($C_{1\beta}$), 90.3 ($C_{1\alpha}$), 72.9 ($C_{5\beta}$), 72.2 ($C_{3\beta}$), 70.4 ($C_{3\alpha}$), 69.9 ($C_{5\alpha}$), 67.8 ($C_{4\beta}$), 67.5 ($C_{4\alpha}$), 61.7 ($C_{6\beta}$), 61.6

($C_{6\alpha}$), 53.2 ($C_{2\beta}$), 52.7 ($C_{7\beta}$), 52.5 ($C_{7\alpha}$), 51.3 ($C_{2\alpha}$), 21.0 (OC$CH_{3\alpha}$), 20.9 (OC$CH_{3\beta}$), 20.8 (OC$CH_{3\beta}$), 20.7 (OC$CH_{3\alpha}$ and OC$CH_{3\alpha}$), 20.7 (OC$CH_{3\beta}$), 20.6 (OC$CH_{3\beta}$), 20.6 (OC$CH_{3\alpha}$). HRMS (ESI, positive mode) calcd. for $C_{16}H_{22}N_4NaO_{10}$ $[M+Na]^+$: 453.1234, found: 453.1232.

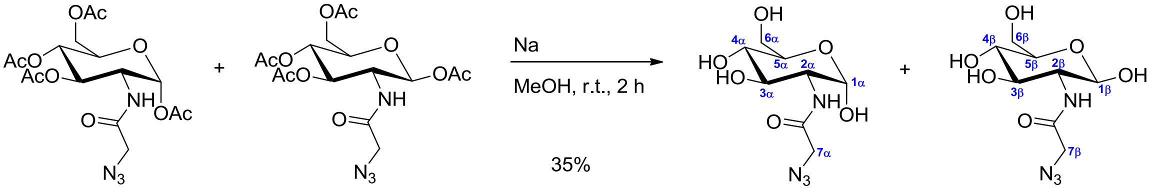

$\mathbf{11_\alpha}$ $\mathbf{11_\beta}$ $\mathbf{12_\alpha}$ $\mathbf{12_\beta}$

Azidoglucosamine ($\mathbf{12_\alpha}$ and $\mathbf{12_\beta}$)

Compounds $\mathbf{11_\alpha}$ and $\mathbf{11_\beta}$ (165 mg, 0.383 mmol) were dissolved in MeOH (2 mL). NaOMe (25 mg, 0.463 mmol) was then added. The reaction mixture was stirred for 2 h at r.t. and neutralized with Amberlite 120 (H^+) resin. The resin was filtered, washed with MeOH, and the filtrate was evaporated under reduced pressure. The residue was then purified on Sep-pax C18 column (H_2O:MeOH 1:0 to 8:2) to afford $\mathbf{12_\alpha}$ and $\mathbf{12_\beta}$ (mixture of α:β 1.8:1) (35 mg, 35%) as white powder.

^{1}H NMR (600 MHz, D_2O) δ 5.24 (*d*, *J* = 3.3 Hz, 1.8H, $H_{1\alpha}$), 4.79 (*s*, *J* = 7.7 Hz, 1H, $H_{1\beta}$), 4.10 (*s*, 5.6H, $H_{7\alpha}$ and $H_{7\beta}$), 3.99–3.85 (*m*, 6.4H, $H_{2\alpha}$, $H_{3\alpha}$, $H_{6\alpha}$ and $H_{6\beta}$), 3.84–3.72 (*m*, 5.6H, $H_{2\beta}$, $H_{5\alpha}$, $H_{6\alpha}$ and $H_{6\beta}$), 3.62 (*dd*, *J* = 9.5, 8.5 Hz, 1H, $H_{3\beta}$), 3.54–3.48 (*m*, 3.8H, $H_{5\beta}$, $H_{4\alpha}$ and $H_{4\beta}$). ^{13}C NMR (150 MHz, D_2O) δ 170.9 (OCNH$_\beta$), 170.6 (OCNH$_\alpha$), 94.5 ($C_{1\beta}$), 90.7 ($C_{1\alpha}$), 75.9 ($C_{5\beta}$), 73.5 ($C_{3\beta}$), 71.5 ($C_{3\alpha}$), 70.5 ($C_{5\alpha}$), 69.9 ($C_{4\alpha}$), 69.8 ($C_{4\beta}$), 60.6 ($C_{6\beta}$), 60.5 ($C_{6\alpha}$), 56.7 ($C_{2\beta}$), 54.04 ($C_{2▯}$), 51.9 ($C_{7\beta}$), 51.6 ($C_{7\alpha}$). HRMS (ESI, positive mode) calcd. for $C_8H_{14}N_4NaO_6$ $[M+Na]^+$: 285.0811, found: 285.0793.

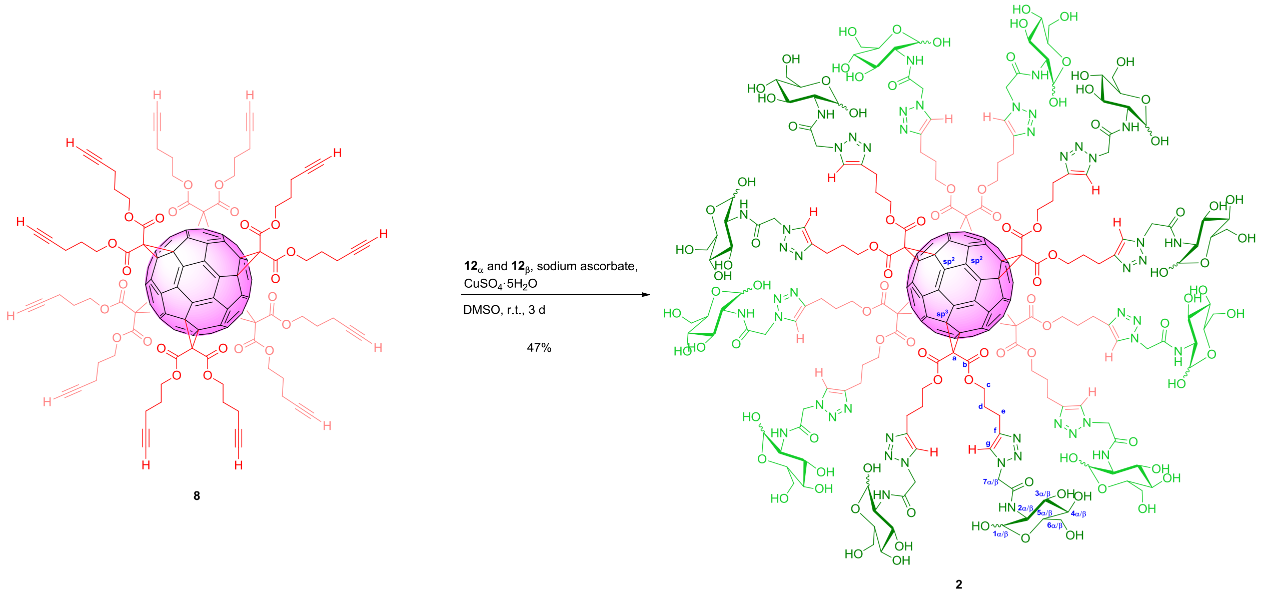

Dodecaglucosamine-fullerene (2)

Compound **8** (11 mg, 5.17 µmol), **12_α** and **12_β** (mixture of α:β 1.8:1) (30 mg, 0.114 mmol) were dissolved in DMSO (2 mL) under N_2 atmosphere. Sodium ascorbate (2.56 mg, 0.013 mmol) and $CuSO_4 \cdot 5H_2O$ (1 mg, 3.88 µmol) were then added to the reaction mixture. The reaction was stirred for 3 days at r.t. The product was then precipitated by the addition of MeOH (5 mL), and centrifuged in MeOH (3×50 mL). The crude was then redissolved in water and purified by Sephadex G-25 (water:EtOH 95:5) to afford $C_{60}(Gln)_{12}$ **2** (12.7 mg, 47%) as brownish powder.

^{1}H NMR (600 MHz, DMSO) δ 8.21 (*bs*, 24H, NH_α and NH_β), 7.78 (*bs*, 12H, H_g), 6.62 (*bs*, 5H, O$H_{1\beta}$), 6.57 (*bs*, 7H, O$H_{1\alpha}$), 5.05 (*bs*, 24H, $H_{7\alpha}$ and $H_{7\beta}$), 5.03–4.92 (*m*, 28H, $H_{1\alpha}$ and O*H*), 4.84 (*bs*, 7H, O*H*), 4.55 (*bs*, 5H, O*H*), 4.47 (*bs*, 15H, $H_{1\beta}$ and O*H*), 4.34 (*bs*, 24H, H_c), 3.72–3.27 (*m*, $H_{2\alpha}$, $H_{3\alpha}$, $H_{5\alpha}$, $H_{2\beta}$, $H_{3\beta}$, $H_{6\alpha}$, $H_{6\beta}$ and O*H*), 3.22–3.02 (*m*, 19H, $H_{4\beta}$, $H_{4\alpha}$ and $H_{5\beta}$), 2.63 (*bs*, 24H, H_d), 1.98 (*bs*, 24H, H_e). ^{13}C NMR (150 MHz, DMSO) δ 165.6 (O*C*NH$_\alpha$), 165.4 (O*C*NH$_\beta$), 162.8 (C_b), 145.3 (C_f), 145.0 (C_{sp2}), 140.7 (C_{sp2}), 123.6 (C_g), 95.0 ($C_{1\beta}$), 90.4 ($C_{1\alpha}$), 76.8 ($C_{5\beta}$), 74.1 ($C_{3\beta}$), 72.1 ($C_{3\alpha}$), 70.9 ($C_{5\alpha}$), 70.6 ($C_{4\beta}$), 70.6 ($C_{4\alpha}$), 68.7 (C_{sp3}), 66.6 (C_c), 61.1 ($C_{6\beta}$), 61.0 ($C_{6\alpha}$), 57.5 ($C_{2\beta}$), 54.6 ($C_{2\alpha}$), 51.8 ($C_{7\beta}$), 51.5 ($C_{7\alpha}$), 45.6 (C_a), 27.7 (C_e), 21.3 (C_d). HRMS (ESI, positive mode) calcd. for $C_{234}H_{252}N_{48}O_{96}Na_3$ $[M+3Na]^{3+}$: 1780.5359, found: 1780.5267.

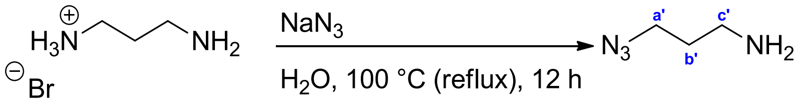

13 24% **14**

3-Azidopropan-1-amine (14)

To a solution of **13** (3.2 g, 14.62 mmol) in H_2O (10 mL) was slowly added NaN_3 (3.2 g, 49.2 mmol) in H_2O (15 mL). The resulting solution was allowed to stir at reflux (100 °C) overnight. After cooling to r.t., about two third of the water was removed by evaporation and the remaining residue diluted with ether (50 mL). The biphasic mixture was cooled to 0 °C, and KOH pellets (4.0 g) were slowly added. The phases were separated and the aqueous layer was extracted with ether (2×30 mL). All organics were combined, dried over $MgSO_4$, filtered, and concentrated under reduced pressure to afford **14** (352 mg, 24%) as a yellow oil.

^1H NMR (400 MHz, $CDCl_3$) δ 3.35 (*t*, *J* = 6.7 Hz, 2H, $H_{a'}$), 2.78 (*t*, *J* = 6.8 Hz, 2H, $H_{c'}$), 1.71 (*p*, *J* = 6.7 Hz, 2H, $H_{b'}$), 1.39 (*s*, 2H, NH_2).

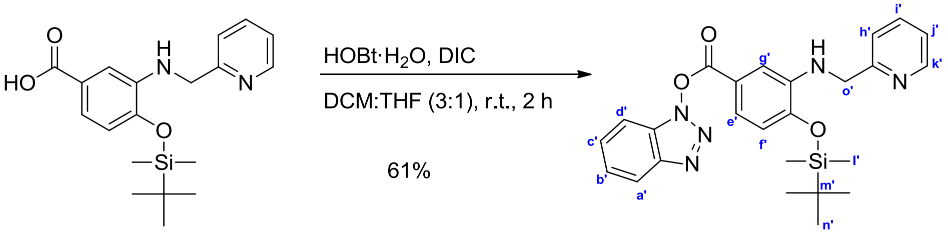

15 **16**

Protected activated chelator HCPAMP (16)

The acid **15** (0.3 g, 0.837 mmol) was dissolved in a DCM:THF mixture (4 mL, 3:1 mL) followed by the addition of HOBt·H_2O (170 mg, 1.11 mmol) and DIC (130 μL, 0.837 mg). The reaction mixture was stirred for 2 h at r.t. Hexane (2 mL) was then added and the urea was filtered. The filter was washed with a hexane:EtOAc mixture (1:1, 2.5 mL). The orange solution was concentrated to dryness and purified by column chromatography (silica gel, hexane:EtOAc 8:2) to afford **16** (243 mg, 61%) as a pale yellow powder.

^1H NMR (600 MHz, $CDCl_3$) δ 8.58 (*dd*, *J* = 7.1, 6.6 Hz, 1H, $H_{k'}$), 8.09–8.07 (*m*, 1H, $H_{d'}$), 7.71 (*td*, *J* = 7.7, 1.7 Hz, 1H, $H_{i'}$), 7.62 (*dt*, *J* = 7.8, 2.1 Hz, 1H, $H_{e'}$), 7.55–7.51 (*m*, 1H, $H_{b'}$), 7.47 (*dt*, *J* = 8.4, 0.9 Hz, 1H, $H_{a'}$), 7.44–7.40 (*m*, 1H, $H_{c'}$), 7.39 (*d*, *J* = 2.2 Hz, 1H, $H_{g'}$), 7.34 (*d*, *J* = 7.8 Hz, 1H, $H_{h'}$), 7.24 (*dd*, *J* = 7.0, 5.3 Hz, 1H, $H_{j'}$), 6.89 (*d*, *J* = 8.2 Hz, 1H, $H_{f'}$), 4.56 (*s*, 2H, $H_{o'}$), 1.09 (*s*, 9H, $H_{n'}$), 0.35 (*s*, 6H, $H_{l'}$). ^{13}C NMR (150 MHz, CDCl$_3$) δ 163.1 (O*C*O), 156.8 (C$_{\mathrm{e'}}$*C*NH), 149.4 (C$_{\mathrm{g'}}$*C*NH), 148.6 ($C_{k'}$), 143.6 (C$_{\mathrm{d'}}$*C*NH), 140.6 (C$_{\mathrm{e'}}$*C*C$_{\mathrm{g'}}$), 137.3 ($C_{i'}$), 129.0 (C$_{\mathrm{a'}}$*C*N), 128.6 ($C_{b'}$), 124.8 ($C_{c'}$), 122.6 ($C_{j'}$), 121.9 ($C_{h'}$), 121.1 ($C_{e'}$), 120.5 ($C_{d'}$), 117.8 (C$_{\mathrm{f'}}$*C*O), 117.1 ($C_{f'}$), 111.6 ($C_{g'}$), 108.7 ($C_{a'}$), 48.1 ($C_{o'}$), 25.8 ($C_{n'}$), 18.4 ($C_{m'}$), -4.0 ($C_{l'}$).

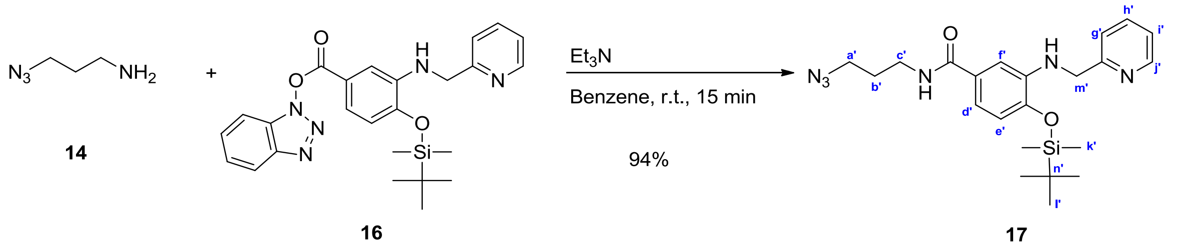

Protected azido chelator HCPAMP (17)

The activated carboxylic acid **16** (49 mg, 0.103 mmol) was dissolved in benzene (1 mL) under N$_2$ atmosphere. **14** (11.35 mg, 0.113 mmol) in benzene (1.3 ml) was then added followed by the addition of Et$_3$N (14.36 µL, 0.103 mmol). The reaction mixture was stirred for 15 min at r.t. Solvent was evaporated and excess of 3-azidopropan-1-amine (11.35 mg, 0.113 mmol) was evaporated under *high vacuo*. The product was extracted with EtOAc (2 mL) and washed twice with water (2×2 mL). The organic phase was dried over MgSO$_4$, filtered and evaporated. The crude was purified by column chromatography (silica gel, hexane:EtOAc 2:1 to 1:1) to afford **17** (42.6 mg, 94%) as a white solid.

^{1}H NMR (600 MHz, CDCl$_3$) δ 8.53 (*d*, *J* = 4.8 Hz, 1H, $H_{j'}$), 7.63 (*td*, *J* = 7.6, 1.0 Hz, 1H, $H_{h'}$), 7.28 (*d*, *J* = 7.8 Hz, 1H, $H_{g'}$), 7.19–7.15 (*m*, 1H, $H_{i'}$), 7.07 (*d*, *J* = 1.6 Hz, 1H, $H_{f'}$), 6.97 (*dd*, *J* = 8.1, 1.8 Hz, 1H, $H_{d'}$), 6.71 (*d*, *J* = 8.0 Hz, 1H, $H_{e'}$), 6.52 (*t*, *J* = 5.5 Hz, 1H, N*H*), 4.47 (*s*, 2H, $H_{m'}$), 3.47 (*q*, *J* = 6.4 Hz, 2H, $H_{c'}$), 3.37 (*t*, *J* = 6.6 Hz, 2H, $H_{a'}$), 1.84 (*p*, *J* = 6.6 Hz, 2H, $H_{b'}$), 1.04 (*s*, 9H, $H_{l'}$), 0.25 (*s*, 6H, $H_{k'}$). ^{13}C NMR (150 MHz, CDCl$_3$) δ 168.2 (O*C*NH), 157.6 (C$_{\mathrm{m'}}$*C*N), 148.7 ($C_{j'}$), 145.8 (C$_{\mathrm{f'}}$*C*N), 140.1 (C$_{\mathrm{d}}$*C*C$_{\mathrm{f}}$), 136.9 ($C_{h'}$), 127.9 (C$_{\mathrm{e'}}$*C*O), 122.2 ($C_{i'}$), 121.8 ($C_{g'}$), 116.8 ($C_{e'}$), 115.5 ($C_{d'}$), 109.5 ($C_{f'}$), 49.6 ($C_{a'}$), 48.5 ($C_{m'}$), 37.7 ($C_{c'}$), 28.9 ($C_{b'}$), 25.8 ($C_{l'}$), 18.3 (Si*C*C$_{\mathrm{k'}}$), -4.1 ($C_{k'}$). HRMS (ESI, positive mode) calcd. for $C_{22}H_{33}N_6O_2Si$ [M+H]$^+$: 441.2434, found: 441.2432.

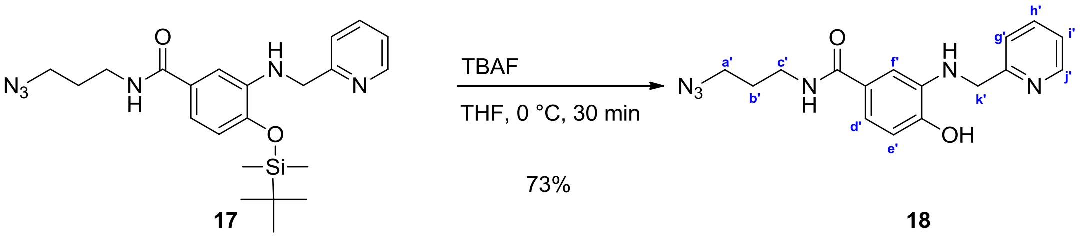

17 **18**

Azido chelator HCPAMP (18)

Compound **17** (21 mg, 0.048 mmol) was dissolved in THF (3 mL) and cooled to 0 °C. TBAF in THF (1 M, 0.095 mL) was then added and the reaction mixture was allowed to stir for 30 min at 0 °C under N_2 atmosphere. The mixture was then diluted with EtOAc (3 mL), washed with aqueous NH_4Cl (3 mL), and extracted with EtOAc (2×3 mL). The organic phase was then washed with water (2×5 mL). The organic phase were combined and dried over $MgSO_4$, filtered, and concentrated. The crude was then purified by column chromatography (silica gel, DCM:MeOH 98:2 to 96:4) to afford **18** (11.3 mg, 73%) as a colorless oil.

^{1}H NMR (400 MHz, CD_3OD) δ 8.51 (*d*, *J* = 4.5 Hz, 1H, $H_{j'}$), 8.19 (*s*, 1H, N*H*), 7.77 (*td*, *J* = 7.7, 1.7 Hz, 1H, $H_{h'}$), 7.47 (*d*, *J* = 7.9 Hz, 1H, $H_{g'}$), 7.29 (*dd*, *J* = 6.8, 5.3 Hz, 1H, $H_{i'}$), 7.06 (*dd*, *J* = 8.1, 2.1 Hz, 1H, $H_{d'}$), 6.99 (*d*, *J* = 2.0 Hz, 1H, $H_{f'}$), 6.74 (*d*, *J* = 8.1 Hz, 1H, $H_{e'}$), 4.53 (*s*, 2H, $H_{k'}$), 3.42–3.32 (*m*, 4H, $H_{a'}$ and $H_{c'}$), 1.83 (*p*, *J* = 6.8 Hz, 2H, $H_{b'}$). ^{13}C NMR (100 MHz, CD_3OD) δ 170.8 (O*C*NH), 160.7 ($C_{k'}$*C*N), 149.6 ($C_{j'}$), 149.3 ($C_{f'}$*C*N), 138.7 ($C_{h'}$), 138.1 (C_d*C*C_f), 127.0 ($C_{e'}$*C*O), 123.6 ($C_{i'}$), 123.0 ($C_{g'}$), 118.1 ($C_{d'}$), 113.7 ($C_{f'}$), 110.4 ($C_{e'}$), 50.2 ($C_{k'}$ and $C_{a'}$), 38.2 ($C_{c'}$), 29.8 ($C_{b'}$). HRMS (ESI, positive mode) calcd. for $C_{16}H_{19}N_6O_2$ $[M+H]^+$: 327.1569, found: 327.1562.

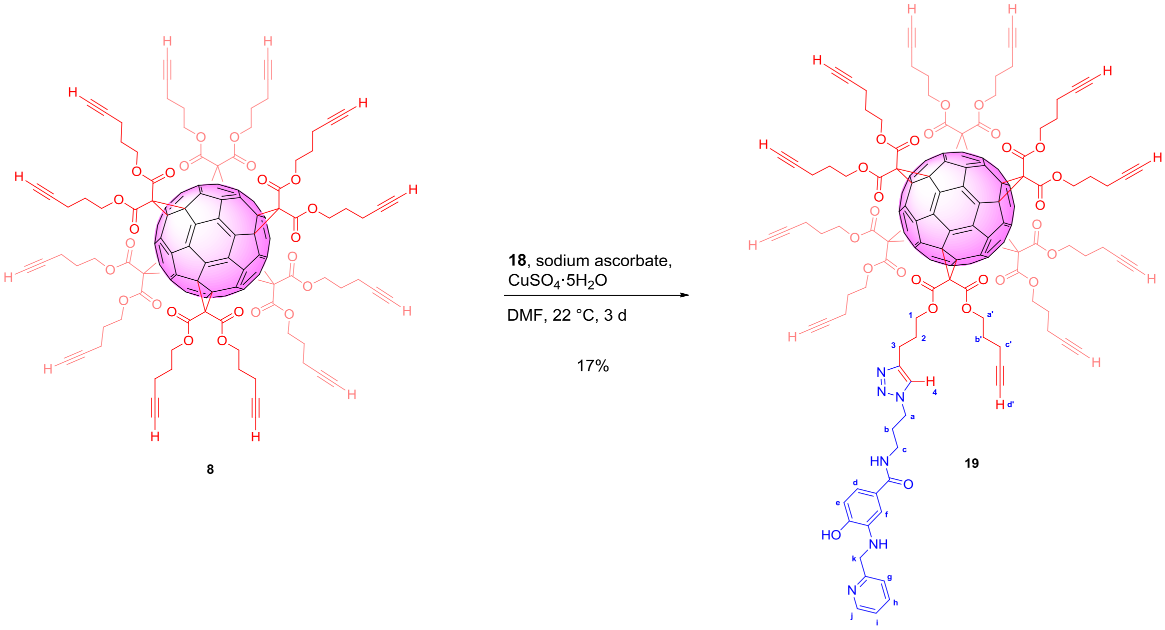

Undecaalkyne HCPAMP-fullerene (19)

Compounds **8** (26.6 mg, 0.013 mmol) and **18** (5.72 mg, 0.018 mmol) were dissolved in DMF (1.5 mL) under N_2 atmosphere. Sodium ascorbate (0.744 mg, 3.75 µmol) and $CuSO_4 \cdot 5H_2O$ (0.312 mg, 1.251 µmol) were then added in water (0.4 mL). The reaction was stirred for 3 d at r.t. The reaction mixture was diluted with $CHCl_3$ (10 mL), and the $CHCl_3$ layer washed with water (2×10 mL). The product was then extracted. The organic phase was dried over $MgSO_4$, filtered, and evaporated. The crude was purified by column chromatography (silica gel, $CHCl_3$:hexane:MeOH 89.5:10:0.5 to 5:0:95) to afford **19** (5.2 mg, 2.12 µmol, 17%) as an orange glassy oil.

^{1}H NMR (600 MHz, $CDCl_3$) δ 8.57 (*d*, *J* = 2.7 Hz, 1H, H_j), 7.72–7.67 (*m*, 1H, H_h), 7.35 (*d*, *J* = 7.5 Hz, 1H, H_g), 7.25–7.20 (*m*, 1H, H_i), 7.10 (*s*, *J* = 11.7 Hz, 1H, H_d), 6.98 (*d*, *J* = 6.6 Hz, 1H, H_f), 6.73 (*d*, *J* = 4.6 Hz, 1H, H_e), 6.35 (*s*, 1H, N*H* or O*H*), 5.49–5.27 (*m*, 1H, H_4), 4.60 (*s*, N*H* or O*H*), 4.54–4.27 (*m*, 26H, H_1, $H_{a'}$ and H_k), 3.53–3.43 (*m*, 2H, H_c), 3.42–3.38 (*m*, 2H, H_a), 2.39–2.20 (*m*, 24H, $H_{c'}$ and H_2), 2.03–1.84 (*m*, 37H, H_3, $H_{d'}$, H_b and $H_{b'}$).[i] HRMS (ESI-MS, positive mode) calcd. for $C_{154}H_{103}N_6O_{26}$ $[M+H]^+$: 2452.6949, found: 2452.6918.[ii, iii]

---

[i] Integrals were adjusted.

[ii] Many other peaks appeared on ESI spectra probably due to high rate of fragmentations.

[iii] ^{13}C NMR was not taken due to the amount of material available but HSQC showed clearly the presence of the product with the appearance of Carbon correlation of H_4 at {5.35; 129.88}.

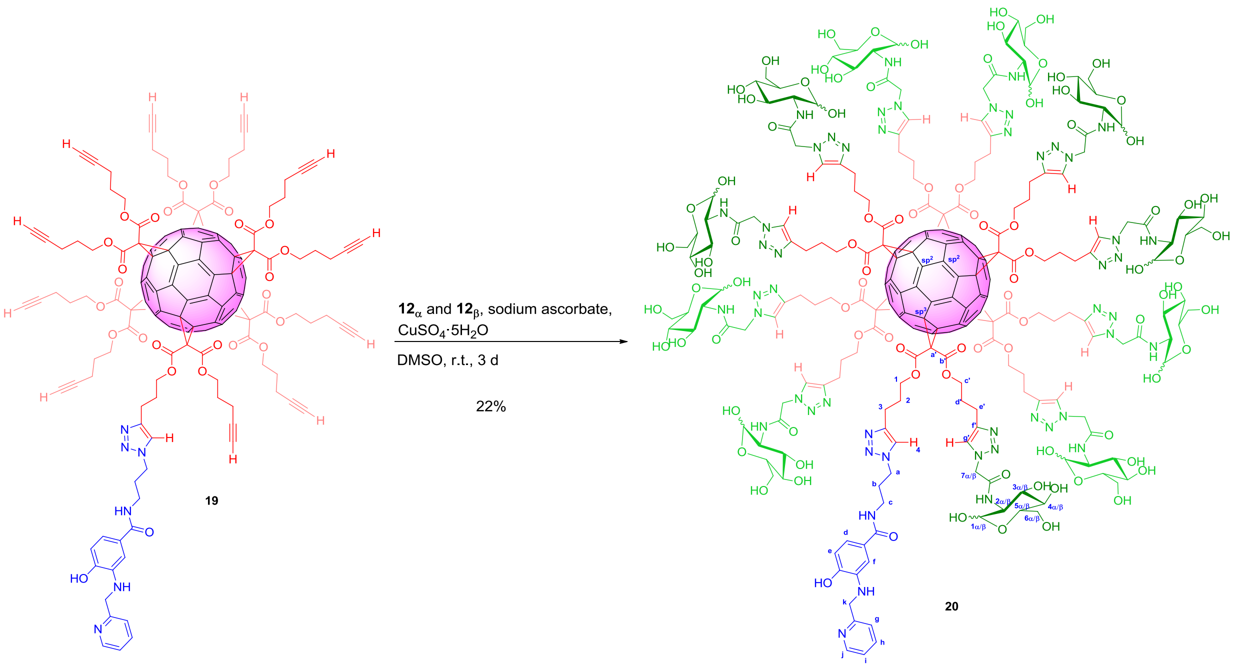
12_{α} and 12_{β}, sodium ascorbate, $CuSO_4{\cdot}5H_2O$

DMSO, r.t., 3 d

22%

19

20

Undecaglucosamine HCPAMP-fullerene (20)

Compounds **19** (5.2 mg, 2.120 µmol), $\mathbf{12_{\alpha}}$ and $\mathbf{12_{\beta}}$ (mixture of α:β 1.8:1) (13.9 mg, 0.053 mmol) were dissolved in DMSO (1.5 mL) under N_2 atmosphere. Sodium ascorbate (1.05 mg, 5.30 µmol) and $CuSO_4{\cdot}5H_2O$ (0.397 mg, 1.590 µmol) were then added in DMSO (0.5 mL). The reaction was stirred for 3 d at r.t. The product was precipitated in $CHCl_3$ (5 mL), centrifuged 5 times (3×15 mL $CHCl_3$ and 2×15 mL MeOH). The crude was then redissolved in DMSO:MeOH (1:1, 1 mL) and purified by Sephadex LH-20 (DMSO:MeOH 1:1) to afford **20** (2.5 mg, 22%) as brownish solid.

^{1}H NMR (600 MHz, DMSO) δ 8.53 (*bs*, H_j), 8.41 (*bs*, H_h), 8.21 (*bs*, NH_{Gln}), 8.02 (*bs*, H_4 and $H_{g'}$), 7.78 (*bs*, H_g), 7.62 (*bs*, H_i), 7.54 (*bs*, H_d), 7.34 (*s*, H_f), 7.19 (*s*, H_e), 6.80–6.50 (*m*, $OH_{1\alpha}$ and $OH_{1\beta}$), 5.35–4.66 (*m*), 4.66–3.96 (*m*, H_k, $H_{c'}$ and H_1), 3.78–3.06 (*m*), 2.65 (*bs*, $H_{d'}$ and H_2), 2.18–1.82 (*m*, $H_{e'}$ and H_3).[i]

---

[i] Only ^{1}H NMR could be taken due to the amount of material available. The ^{1}H NMR is easily comparable to the ^{1}H NMR of **2**, with slight differences in the aromatic region showing the presence of the ligand.

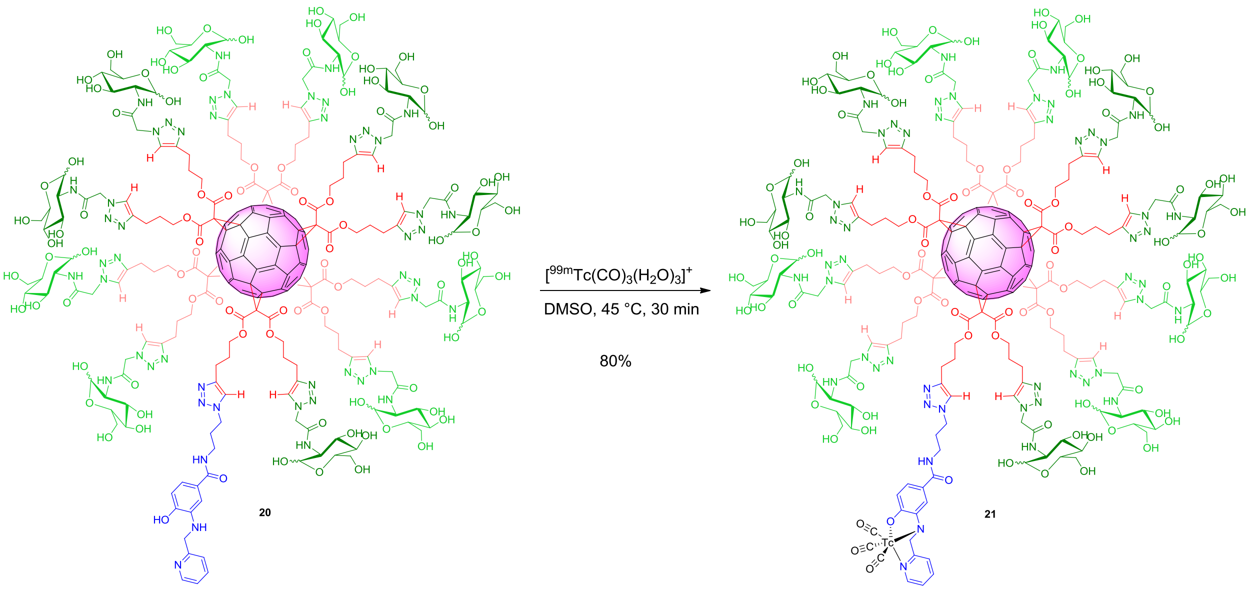

Undecaglucosamine ^{99m}Tc-HCPAMP-fullerene (21)

$[^{99m}TcO_4]^-$ (1 mL 0.9% NaCl solution, 1 GBq) was poured into the carbonylation kit (C-Kit) and heated in a preheated water bath (95–98 °C) for 15 min. The reaction mixture was cooled in an ice bath (0 °C) for 5 min. To the resulting solution, PBS (0.1 mL, 10x) was added and the pH was adjusted to 7.5–8 by dropwise addition of 1 M HCl solution. Thereafter, a solution of **22** (150 µL, 28 nmol) in DMSO was added and the reaction mixture was headed to 45 °C for 30 min. The resulting pale yellow solution was then cooled to 22 °C and was injected to HPLC C-18 [water:MeCN (0.1% TFA)]. The product eluted at t_R = 29.67 min with 80% labelling.

4.2. Materials and Methods

4.2.1. Analytical Purification

Analytical HPLC analyses were carried out on a Merck-Hitachi L6200 system equipped with an UV-detector (Merck Hitachi L-4250) and γ radiation-detector (Beckmann, 171 radioisotope detector). The separation was performed on a C-18 (AA 137) column (Knauer GmbH, Berlin, Germany) and all compounds were eluted with a linear gradient of water:MeCN:0.1% TFA. Preparative HPLC was performed using an Agilent 1200 HPLC apparatus with Prep C-18 column, and a mixture of water:MeCN:0.1% TFA. UV signals were detected at wavelengths of 220, 230, 245 and 280 nm.

4.2.2. Animals

All animal experiments were approved by the Veterinäramt Zürich (approval number 148/2009). Male SHR (Charles River, Sulzfeld, Germany) weighing 250–300 g and WKY (Charles River, Germany) weighing 250–300 g were used throughout this study. Animals were acclimatized in an animal facility (3 rats per cage) for 1 week before the start of the experiment. They were housed in a room with controlled temperature (24 ± 1 °C) under a 12:12 h light-dark cycle. They were allowed free access to food and water.

4.2.3. Anesthesia and General Preparation

Rats were anesthetized with 2.5% isoflurane in 70% N_20:30% O_2 during the surgery. Rectal temperature was maintained at 37 ± 0.5 °C by a feedback-controlled heating system (Doccol PID temperature controller WS1500B, Doccol Co., Redlands, CA, USA). The left femoral artery was cannulated with a PE-50 polyethylene catheter (Helix Medical, Carpenteria, CA, USA) for continuous monitoring of heart rate (HR) and mean arterial blood pressure (MBP) was measured using a CyberSense monitor (Model BPM01 CyQ 302, Nicholasville, KY, USA). Blood gas analyses [$p(CO_2)$, $p(O_2)$] and pH were measured using an ABL 5 blood gas analyzer (Radiometer ApS, Danmark). Results of weight changes, HR, MBP and blood gas analyses can be found at the end of the chapter (Table 1–Table 3).

4.2.4. tMCAO Model

Temporary focal cerebral ischemia was induced by occlusion of the left MCA according to the method of Longa *et al*.[48] Briefly, under a surgical microscope, a middle incision was made in the neck and the left external carotid artery (ECA) was exposed and dissected. A silicone rubber coated monofilament nylon suture with a diameter of 0.37 mm and 30 mm in length (Doccol Co., Redlands, CA, USA) was inserted through the left ECA into the internal carotid artery (ICA) and advanced along the ICA to the extent of 20 mm from the bifurcation until a moderate resistance was felt occluding the left MCA. After 60 minutes of ischemia, the suture was withdrawn for reperfusion. The animals were then allowed to recover from anesthesia. They were euthanized 5 days after tMCAO for histological analyses. Animals without infarction, detected 24 h after tMCAO were excluded from the study.

4.2.5. Application of $C_{60}(OH)_{34\text{-}36}$ and $C_{60}(GlcN)_{12}$ in Animals

Each agent [$C_{60}(OH)_{34\text{-}36}$ or $C_{60}(GlcN)_{12}$] was dissolved in aqueous NaCl (0.9%, 2.5 mL). In all groups, the agent was given by bolus injection in the penil vein immediately after recirculation. Animals receiving an equivalent volume of NaCl 0.9% solution by intravenous bolus injection in the penil vein immediately after recirculation served as control group. The injection rate for each agent and NaCl 0.9% was 0.5 $mL \cdot min^{-1}$.

In a first series, $C_{60}(OH)_{34\text{-}36}$ (0.5 $mg \cdot kg^{-1}$) was administered in WKY (N = 10) and the effect of this agent was compared to control WKY (N = 10) in respect to infarct volume, anti-inflammatory and neuroprotective properties.

Since assessment of drug efficacy is recommended to investigate in another rat strain or species rats with arterial hypertension (SHR) were chosen for further experiments. $C_{60}(OH)_{34\text{-}36}$ (0.5 $mg \cdot kg^{-1}$) was injected in SHR (N = 10) and infarct volume was compared to control SHR (N = 10). A dose-response curve for $C_{60}(OH)_{34\text{-}36}$ was established in SHR, encompassing (1) the investigated low-dose $C_{60}(OH)_{34\text{-}36}$ group (0.5 $mg \cdot kg^{-1}$), (2) a middle-dose $C_{60}(OH)_{34\text{-}36}$ group (1.0 $mg \cdot kg^{-1}$; N = 7) and (3) a high-dose $C_{60}(OH)_{34\text{-}36}$ group (2.0 $mg \cdot kg^{-1}$; N = 7).

In a further series, the effect of $C_{60}(Gln)_{12}$ was evaluated. Firstly, the effect of $C_{60}(Gln)_{12}$ (0.5 $mg \cdot kg^{-1}$; N = 7) was studied. Because less fullerene is contained in $C_{60}(Gln)_{12}$ than in the equivalent dose of fullereol, $C_{60}(Gln)_{12}$ was also administered at a dose of 5.0 $mg \cdot kg^{-1}$.

4.2.6. Neurological Score

Neurological evaluation was performed 1 day and 5 days after tMCAO induction and scored as follows: 0 = no neurologic deficits, 1 = contralateral forelimb flexion, 2 = contralateral circling after tail pull, 3 = spontaneously contralateral circling, 4 = falling to the right; 5 = no spontaneous walking.

4.2.7. MRI Protocol

Five days after tMCAO, MRI was conducted with a 4.7 T/16 cm BrukerPharmaScan tomograph (BrukerBioSpin AG, Fällanden, Switzerland) using a linear polarized volume resonator. Rats were placed into a plastic holder and connected to the same breathing anesthesia system as for the surgery. Rapid acquisition with relaxation enhancement (RARE) sequences [9 continuous slices, 2 mm thickness, repetition time (TR) = 2500 ms, echo time (TE) = 33 ms] were used to verify symmetric positioning of the rat brain. T2w spin-echo imaging was used to map lesion and hemispheric volumes. 17 continuous coronal slices (thickness: 1 mm, inter-slice distance: 1 mm) were acquired with a field of view (FOV) of 3.5 cm^2 and a matrix size of 384×384 (TR = 3000 ms; echo time 1 and 2 = 30 ms; 3 averages, total acquisition time: 14 min and 24 s).

4.2.8. Measurement of Lesion Volume

Hemispheric volumes were determined on T2w using ImageJ Analysis Software 1.45 s [National Institutes of Health, USA; (http://rsb.info.nih.gov/ij/)]. After enlargement and optimal adjustment of brightness and contrast, the hemispheres were traced manually on each slice. The position of the midline was determined with the use of the following neuroanatomic landmarks: falx cerebri, corpus pineale, fissura longitudinalis, infudibulum, aqueductus cerebri and third ventricle. The areas were then summed and multiplied by the slice thickness.[49]

4.2.9. Immunohistochemistry

After deep anesthesia, rats were euthanized by decapitation, the brains were removed rapidly, and immediately frozen by -80 °C. Coronal sections (8 μm thick) were cut at 400 μm intervals using a cryostat (Hyrax C60, Zeiss, Switzerland) and mounted on Superfrost Plus slides (Menzel, Braunschweig, Germany). Sections were fixed for 10 min in acetone at r.t.

For NeuN immunostaining, sections were treated with 0.3% hydrogen peroxide and blocked with blocking buffer (1% non-gel sieving, 2% Fish skin gelatin, 0.15% Triton). Thereafter, sections were incubated with anti-NeuN (1:500, Millipore, Zug, Switzerland) overnight at 4 °C. Secondary biotinylated antibodies were applied for 1 h at room temperature followed by the ABC complex reagent (Vector Labs) for 1 h. Color reaction was performed with AEC (3-Amino-9-ethylcarbazole). Slides were mounted with Kaiser's glycerin gelatin.

For Ki-67 immunostaining, the slides were contra-fixed with acetone for 10 min. and thereafter, endogenous peroxidases were blocked for 30 min., using blocking solution (The Blocking Solution, Candor Bioscience GmbH, Wangen, Germany). The primary antibody (1:100; LabForce

AG, Nunningen, Switzerland) was incubated for 1 h at 37 °C. After washing in PBS, Secondary PO goat anti-rabbit antibodies (1:200) (N-Histofine Simple Stain Mouse MAX PO; Biosystems, Nunningen, Switzerland) were applied for 30 min at r.t. After rinsing in PBS, the immunoreactivity was visualized with DAB (Dako, Baar/Switzerland) as a chromogen and then contra-staining was performed with Mayer's hemalaun. Slides were dehydrated and mounted with Eukitt (Erne-Chemie, Dällikon/Switzerland).

For CD68 immunostaining, the slides were contra-fixed with acetone for 10 min. The primary antibody (1:250) was incubated for 30 min at 37 °C. Detection was performed using Leica-AP-Refine-Kit according to the manufacturer's guideline.

Sections were imaged with a microscope (Olympus, BX61, Volketswil, Switzerland) equipped with an Olympus camera. Visual assessment and densitometric measurement were performed using Olympus cell^P (Olympus Professional Imaging Software, Gloor Instruments, Uster, Switzerland).

4.2.10. Immunohistochemical Evaluation

To determine the cell count of NeuN-stained sections, a magnification of ×20 was chosen. Cell count of NeuN positive cells was performed in 5 randomly selected areas of the perilesional zone of the caudaputamen of three consecutive sections. Because the density of Ki-67 positive cells per field of view was high, a magnification of ×40 was used to count the positive cells in the perilesional zone of the caudoputamen of 10 randomly selected areas. In CD68 immunostaining, cell density was measured (magnification ×10) in the lesional zone of the caudoputamen of 10 randomly selected areas. Analyses were done in 5 animals of each treatment group and in 5 control animals of each strain (i.e. WKY and SHR).

4.2.11. Tissue Homogenization

In order to select brain tissue, brains were mounted in a cryostat and coronal sections were made, until the level of the bregma was reached. Samples were then taken using a sample corer (inner diameter 1 mm, outer diameter 1.8 mm, length 1 mm, Fine Science Tools, Heidelberg/Germany) and kept frozen until RNA extraction.

Upon thawing on ice, each sample was transferred to a 1.5 mL Eppendorf tube and homogenized in a Mixer-Mill MM 301 (Retsch, Haan/Germany) at 30 Hz for 2 min in the presence of a 3 mm stainless metal bead (Retsch) and 0.5 mL Qiazol (Qiagen, Hombrechtikon, Switzerland). Following 5 min incubation at r.t., 140 µL $CHCl_3$ was added to the sample. Following vortexing full speed for 15 s, incubation at r.t. for 3 min, spinning for 15 min at 4 °C, aqueous phase was mixed with an equal volume of 70% EtOH and loaded directly on an RNeasy column provided in the miRNeasy Mini Kit (Qiagen). Default recommendations were followed to isolate total RNA. High quality RNA was quality-checked using the RNA Nano 6000 Chip on 2100 Bioanalyzer (Agilent, Basel, Switzerland).

4.2.12. cDNA Target Synthesis

Target synthesis was led starting from 200 ng total RNA using the WT Expression kit (Ambion, Life Technologies, Zug, Switzerland) following standard recommendations, except that 12 µg cRNA was used instead of 10 µg for entering the second reverse-Transcription. Fragmentation and labeling of amplified cDNA were performed using the WT Terminal Labeling Kit (Affymetrix, Santa Clara, CA, USA).

4.2.13. qRT PCR

qRT PCR of IL-1β, TNF-α, complement C3, and TLR-4 was performed according to the manufacturer's protocol (Applied Biosystems, Life Technologies Europe, Zug, Switzerland). RNA amounts were calculated with relative standard curves for all mRNAs of interest. 60s ribosomal protein L13A and β2-microglobulin (B2M) was used for normalization.

4.2.14. Statistical Analysis

Comparisons of vital parameters [MBP, HR, pH, $p(CO_2)$, and $p(O_2)$], infarct volumes, mRNA fold inductions, infarct size, and immunostaining were performed using non-parametric t-test with correction for non-Gaussian distributions (Mann-Whitney U test) for 2 groups comparisons and non-parametric one-way ANOVA with correction for non-Gaussian distributions (Kruskal-Wallis test) for 3 groups comparisons. For immunostaining, a mean value of all cell counts/area of one individual animal was calculated, before statistical analysis for the group was done.

Table 1. Mean blood pressure and heart rate of treated and control groups before, during and after tMCAO.

Strain	Treatment	Dosage (mg·kg^{-1})	Blood pressure (mmHg)			Heart rate (Hz)		
			Pre-tMCAO	**tMCAO**	**Post-tMCAO**	**Pre-tMCAO**	**tMCAO**	**Post-tMCAO**
WKY	Placebo	0.9% NaCl	80 ± 4	76 ± 11	69 ± 8	323 ± 18	343 ± 42	333 ± 24
	$C_{60}(OH)_{34-36}$	0.5	79 ± 10	73 ± 8	60 ± 9	312 ± 18	340 ± 33	313 ± 13
SHR	Placebo	0.9% NaCl	153 ± 3	142 ± 6	147 ± 3	384 ± 18	415 ± 6	396 ± 11
	$C_{60}(OH)_{34-36}$	0.5	154 ± 14	145 ± 9	150 ± 1	390 ± 15	416 ± 1	381 ± 11
		1.0	151 ± 4	141 ± 5	153 ± 3	380 ± 21	404 ± 39	406 ± 8
		2.0	160 ± 4	143 ± 6	160 ± 9	383 ± 30	393 ± 33	355 ± 10
	$C_{60}(GlcN)_{12}$	0.5	151 ± 15	144 ± 5	149 ± 1	388 ± 10	402 ± 23	356 ± 91
		5	160 ± 10	147 ± 4	162 ± 6	381 ± 44	388 ± 48	362 ± 76

Table 2. Mean weight changes of treated and control groups before, during and after tMCAO

Strain	Treatment	Dosage (mg·kg^{-1})	Weight (kg)		Weight loss (kg)	Weight loss (%)
			Pre-tMCAO	**Post-tMCAO**		
WKY	Placebo	0.9% NaCl	300	251	49	16.6
	$C_{60}(OH)_{34-36}$	0.5	289	252	42	14.4
SHR	Placebo	0.9% NaCl	280	228	53	18.96
	$C_{60}(OH)_{34-36}$	0.5	280	253	28	9.8
		1.0	281	249	32	11.2
		2.0	281	248	34	12.0
	$C_{60}(GlcN)_{12}$	0.5	288	249	40	13.7
		5	287	263	24	8.4

Table 3. Blood gas analyses [pH, $p(CO_2)$ and $p(O_2)$] of treated and control groups before, during and after tMCAO.

Strain	Treatment	Dosage ($mg \cdot kg^{-1}$)	pH			Partial pressure in CO_2 (kPa)			Partial pressure in O_2 (kPa)		
			Pre-tMCAO	**tMCAO**	**Post-tMCAO**	**Pre-tMCAO**	**tMCAO**	**Post-tMCAO**	**Pre-tMCAO**	**tMCAO**	**Post-tMCAO**
WKY	Placebo	0.9% NaCl	7.44 ± 0.01	7.45 ± 0.02	7.44 ± 0.01	5.1 ± 0.35	4.76 ± 0.27	4.73 ± 0.38	21.6 ± 2.6	20.6 ± 3.24	20.3 ± 2.8
	$C_{60}(OH)_{34\text{-}36}$	0.5	7.44 ± 0.03	7.45 ± 0.01	7.43 ± 0.03	5.23 ± 0.19	5.1 ± 0.42	4.98 ± 0.21	21.0 ± 1.7	20.4 ± 1.89	21.0 ± 2.0
SHR	Placebo	0.9% NaCl	7.45 ± 0.03	7.46 ± 0.01	7.43 ± 0.01	5.12 ± 0.18	5.02 ± 0.16	5.02 ± 0.37	21.1 ± 1.1	20.9 ± 1.9	22.1 ± 3.1
	$C_{60}(OH)_{34\text{-}36}$	0.5	7.45 ± 0.03	7.45 ± 0.02	7.44 ± 0.02	5.10 ± 0.60	5.01 ± 0.36	5.04 ± 0.21	20.5 ± 2.2	20.3 ± 2.2	20.4 ± 3.2
		1.0	7.44 ± 0.02	7.45 ± 0.03	7.43 ± 0.02	5.2 ± 0.16	5.10 ± 0.36	5.1 ± 0.21	21.7 ± 2.2	21.7 ± 1.7	22.1 ± 3.05
		2.0	7.45 ± 0.01	7.45 ± 0.02	7.44 ± 0.01	5.2 ± 0.25	5.13 ± 0.20	5.0 ± 0.24	22.8 ± 1.0	21.8 ± 1.4	21.6 ± 2.1
	$C_{60}(GlcN)_{12}$	0.5	7.45 ± 0.03	7.46 ± 0.01	7.46 ± 0.02	5.3 ± 0.13	5.22 ± 0.17	5.1 ± 0.29	22.1 ± 0.70	21.8 ± 1.17	22.0 ± 1.8
		5	7.44 ± 0.07	7.45 ± 0.15	7.43 ± 0.03	5.0 ± 0.26	4.73 ± 0.43	4.8 ± 0.29	22.0 ± 2.2	21.1 ± 0.70	20.2 ± 1.9

5. Abbreviations

abs. u.	absorbance unit
Ac_2O	acetic anhydride
ANOVA	analysis of variance
ATP	adenosine triphosphate
B2M	β2-microglobulin
BBB	blood brain barrier
bs	broad singlet
C_{6o}	fullerene
Ca^{2+}	calcium ion
calcd.	calculated
CBr_4	tetrabromocarbon
CHCA	α-Cyano-4-hydroxycinnamic acid
$CuSO_4$	copper sulfate
d	day(s)
d	doublet
DBU	1,8-diazabicyclo[5.4.0]undec-7-ene
DCC	dicyclohexylcarbodiimide
DCM	dichloromethane
dd	doublets of doublet
ddd	doublets of doublets of doublet
DMF	*N*,*N*'-dimethylformamide
DMSO	dimethyl sulfoxide
DNA	deoxyribonucleic acid
dt	doublets of triplet
EA	elemental analysis
ECA	external carotid artery
ESI	electrospray ionization
Et_3N	triethylamine

EtOAc	ethyl acetate
EtOH	ethanol
FOV	field of view
GlcN	glucosamine
h	hour(s)
HCl	hydrochloric acid
HCPAMP	2-[[(2-hydroxy-5-carboxyphenyl)amino]methyl]pyridin
HOBt	hydroxybenzotriazole
HPLC	high-performance liquid chromatography
HR	hear rate
HRMS	high-resolution mass spectrometry
Hz	Hertz
ICA	internal carotid artery
IL-1β	interleukine-1β
IR	infrared
KOH	potassium hydroxide
LD_{50}	lethal dose, 50%
m	multiplet
m/z	mass-to-charge ratio
MALDI	high resolution matrix-assisted laser desorption/ionisation
MBP	mean arterial blood pressure
MCA	middle cerebral artery
MeCN	acetonitrile
MeOH	methanol
min	minute(s)
MRI	magnetic resonance imaging
MS	mass spectrometry
Na	sodium
NaCl	sodium chloride

NaN_3	sodium azide
NaOH	sodium hydroxide
NaOMe	sodium methoxide
NF-κB	nuclear factor κB
NH_4Cl	ammonium chloride
NMR	nuclear magnetic resonance
ODCB	*o*-dichlorobenzene
p	pentet
PBS	phosphate buffered saline
ppm	parts-per-million
q	quartet
qRT PCR	quantitative real-time polymerase chain reaction
r.t.	room temperature
RARE	rapid acquisition with relaxation enhancement
RNA	ribonucleic acid
ROI	region of interest
rtPA	recombinant tissue plasminogen activator
s	singlet
SHR	spontaneously hypertensive rats
SPECT	single photon emission computed tomography
STAIR	Stroke Therapy Academic Industry Roundtable
t	triplet
T2w	T2 weighted
TBAF	tetrabutylammonium fluoride
TBAH	tetrabutylammonium hydroxide
Tc	technetium
td	triplets of doublet
THF	tetrahydrofuran
TLC	thin layer chromatography

TLR-4	Toll-like receptor 4
tMCAO	transient middle cerebral artery occlusion
TNF-α	tumor necrosis factor-α
TOF	time-of-flight
t_R	retention time
tt	triplets of tiplet
WKY	Kyoto-Wistar rats
δ	chemical shift

6. Acknowledgments

First of all, I place on record my sincere gratitude to Dr. Felix Fluri from the Universitätsspital (Zürich, Switzerland) for the invitation to participate to this challenging and interdisciplinary project. We have work in a close relationship together over the past two years to design the project first, then to conduct the experiments, and finally to interpret the result of our research. I would also like to thank Dr. Felix Fluri for the intensive work input he made on animal experiments and all the efforts he did to turn out the scientific work into a scientific publication. The medical work as well as all biological experiments presented in this chapter would have not been possible without his relevant contribution.

I want to express also my sincere appreciation to Dr. Sung-You Hong. He introduced me to the fullerene chemistry. It helped me a lot for the synthesis of the various compounds made for that work.

Finally, I take also the opportunity to thank Dr. Ali Barandov for the help he delivered in the synthesis and characterization of the radioactive compound.

7. References

---

[1] The Internet Stroke Center, http://www.strokecenter.org.

[2] Adams, H. P.; del Zoppo, G.; Alberts, M. J.; Bhatt, D. L.; Brass, L.; Furlan, A.; Grubb, R. L.; Higashida, R. T.; Jauch, E. C.; Kidwell, C.; Lyden, P. D.; Morgenstern, L. B.; Qureshi, A. I.; Rosenwasser, R. H.; Scott, P. A.; Wijdicks, E. F. M. *Circulation* **2007**, *115*, E478.

[3] Fonarow, G. C.; Smith, E. E.; Saver, J. L.; Reeves, M. J.; Bhatt, D. L.; Grau-Sepulveda, M. V.; Olson, D. M.; Hernandez, A. F.; Peterson, E. D.; Schwamm, L. H. *Circulation* **2011**, *123*, 750.

[4] (a) Moskowitz, M. A.; Lo, E. H.; Iadecola, C. *Neuron* **2010**, *67*, 181. (b) Lipton, P. *Physiol. Rev.* **1999**, *79*, 1431. (c) Caso, J.R.; Pradillo, J.M.; Hurtado, O.; Lorenzo, P.; Moro, M.A.; Lizasoain, I. *Circulation* **2007***, 115,* 1599. (d) Caso, J.R.; Pradillo, J.M.; Hurtado, O.; Leza, J.C.; Moro, M.A.; Lizasoain, I. *Stroke* **2008***, 39,* 1314. (e) Brea, D.; Blanco, M.; Ramos-Cabrer, P.; Moldes, O.; Arias, S.; Pérez-Mato, M.; Leira, R.; Sobrino, T.; Castillo, J. *J. Cerebral Blood Flow & Metabolism* **2011***, 31,* 1424. (f) Iadecola, C.; Anrather, J. *Nature Medicine* **2011***, 17,* 796.

[5] (a) Olson, J. K.; Miller, S. D. *J. Immunol.* **2004**, *173*, 3916. (b) Jack, C. S.; Arbour, N.; Manusow, J.; Montgrain, V.; Blain, M.; McCrea, E.; Shapiro, A.; Antel, J. P. *J. Immunol.* **2005**, *175*, 4320.

[6] Medzhitov, R.; PrestonHurlburt, P.; Janeway, C. A. *Nature* **1997**, *388*, 394.

[7] Caso, J. R.; Pradillo, J. M.; Hurtado, O.; Lorenzo, P.; Moro, M. A.; Lizasoain, I. *Circulation* **2007**, *115*, 1599.

[8] (a) Allan, S. M.; Tyrrell, P. J.; Rothwell, N. J. *Nat. Rev. Immunol.* **2005**, *5*, 629. (b) Boutin, H.; LeFeuvre, R. A.; Horai, R.; Asano, M.; Iwakura, Y.; Rothwell, N. J. *J. Neurosci.* **2001**, *21*, 5528. (c) Loddick, S. A.; Rothwell, N. J. *J. Cereb. Blood Flow Metab.* **1996**, *16*, 932. (d) Mulcahy, N. J.; Ross, J.; Rothwell, N. J.; Loddick, S. A. *Br. J. Pharmacol.* **2003**, *140*, 471.

[9] (a) Hallenbeck, J. M. *Nat. Med.* **2002**, *8*, 1363. (b) McCoy, M. K.; Tansey, M. G. *J. Neuroinflamm.* **2008**, *5*.

[10] (a) Yanamadala, V.; Friedlander, R. M. *Trends Mol. Med* **2010**, *16*, 69. (b) Mocco, J.; Mack, W. J.; Ducruet, A. F.; Sosunov, S. A.; Sughrue, M. E.; Hassid, B. G.; Nair, M. N.; Laufer, I.; Komotar, R. J.; Holland, M. C. H.; Pinsky, D. J.; Connolly, E. S. *Circ.Res.* **2006**, *99*, 209.

[11] del Zoppo, G. J. *Neuroinflammation in Stroke* **2004**; *47*, 155.

[12] (a) Bosi, S.; Da Ros, T.; Spalluto, G.; Prato, M. *Eur. J. Med. Chem.* **2003**, *38*, 913. (b) Partha, R.; Conyers, J. L. *Int. J. Nanomed.* **2009**, *4*, 261. (c) Satoh, M.; Takayanag, I. *J. Pharmacol. Sci.* **2006**, *100*, 513. (d) Bakry, R.; Vallant, R. M.; Najam-Ul-Haq, M.; Rainer, M.; Szabo, Z.; Huck, C. W.; Bonn, G. K. *Int. J. Nanomed.* **2007**, *2*, 639. (e) Yamago, S.; Tokuyama, H.; Nakamura, E.; Kikuchi, K.; Kananishi, S.; Sueki, K.; Nakahara, H.; Enomoto, S.; Ambe, F. *Chem. Biol.* **1995**, *2*, 385.

[13] (a) Chiang, L. Y.; Lu, F. J.; Lin, J. T. *J. Chem. Soc.-Chem. Commun.* **1995**, 1283. (b) Krusic, P. J.; Wasserman, E.; Keizer, P. N.; Morton, J. R.; Preston, K. F. *Science* **1991**, *254*, 1183. (c) Lai, H.-S.; Chen, W.-J.; Chang, L.-Y. *World J. Surg.* **2000**, *24*, 450. (d) Yin, J.-J.; Lao, F.; Fu, P.P.; Wagmer, W.G.; Zhao, Y.; Wang, P.C.; Qiu, Y.; Sun, B; Xing, G.; Dong, J.; Liang, X.-J.; Chen, Chunying *Biomaterials* **2009**, *30*, 611.

[14] Jin, H.; Chen, W. Q.; Tang, X. W.; Chiang, L. Y.; Yang, C. Y.; Schloss, J. V.; Wu, J. Y. *J. Neurosci. Res.* **2000**, *62*, 600.

[15] (a) Hwang, S. Y.; Shin, J. H.; Hwang, J. S.; Kim, S. Y.; Shin, J. A.; Oh, E. S.; Oh, S.; Kim, J. B.; Lee, J. K.; Han, I. O. *Glia* **2010**, *58*, 1881. (b) Shaunak, S.; Thomas, S.; Gianasi, E.; Godwin, A.; Jones,

---

E.; Teo, I.; Mireskandari, K.; Luthert, P.; Duncan, R.; Patterson, S.; Khaw, P.; Brocchini, S. *Nature Biotech.* **2004***, 22,* 977. (c) Yang, Z.; Liang, G.; Ma, M.; Abbah, A. S.; Lu, W. W.; Xu, B. *Chem. Comm.* **2007***,* 843.

[16] O'Neill, M. J.; Clemens, J. A. *Current Protocols in Neuroscience* **2001**, *9.6*, 1.

[17] (a) Chiang, L. Y.; Upasani, R. B.; Swirczewski, J. W. *J. Am. Chem. Soc.* **1992**, *114*, 10154. (b) Chiang, L. Y.; Upasani, R. B., Swirczewski, J. W.; Soled, S. *J. Am. Chem. Soc*. **1993**, *115*, 5453. (c) Chiang, L. Y.; Wang, L. Y.; Tseng, S. M.; Wu, J. S.; Hsieh, K. H. *J. Chem. Soc., Chem. Commun*. **1994**, 2675. (d) Chiang, L. Y.; Wang, L. Y.; Tseng, S. M.; Wu, J. S.; Hsieh, K. H. *Synth Met*. **1995**, *70*, 1477. (e) Chiang, L. Y.; Lu, F.-J.; Lin, J.-T. *J. Chem. Soc., Chem. Commun*. **1994**, 1283. (f) Ros, D. T.; Prato, M. *Chem. Commun*. **1999**, 663. (g) Mikawa, M.; Kato, H.; Okumura, M.; Narazaki, M.; Kanazawa, Y.; Miwa, N.; Shinohara, H. *Bioconjugate Chem*. **2001**, *12*, 510.

[18] Adnađević, B; Gigov, M.; Adnađević, T.; Jovanovića, J. *J. Braz. Chem. Soc.* **2010**, *21*, 476.

[19] Li, J.; Takeuchi, A.; Ozawa, M.; Li, X. H.; Saigo, K.; Kitazawa, K. *J. Chem. Soc.-Chem. Commun.* **1993**, 1784.

[20] Xing, G.; Zhang, J.; Zhao, Y.; Tang, J.; Zhang, B.; Gao, X.; Yuan, H.; Qu, L.; Cao, W.; Chai, Z.; Ibrahim, K.; Su, R. *J. Phys. Chem. B* **2004***, 108,* 11473.

[21] (a) Iehl, J.; Nierengarten, J. F. *Chem.-Eur. J.* **2009**, *15*, 7306. (b) Iehl, J.; de Freitas, R. P.; Delavaux-Nicot, B.; Nierengarten, J. F. *Chem. Commun.* **2008**, 2450. (c) Compain, P.; Decroocq, C.; Iehl, J.; Holler, M.; Hazelard, D.; Barragan, T. M.; Mellet, C. O.; Nierengarten, J. F. *Angew. Chem.-Int. Edit.* **2010**, *49*, 5753. (d) Sigwalt, D.; Holler, M.; Iehl, J.; Nierengarten, J. F.; Nothisen, M.; Morin, E.; Remy, J. S. *Chem. Commun.* **2011**, *47*, 4640.

[22] Saxon, E.; Luchansky, S.J.; Hang, H.C.; Yu, C.; Lee, S.C.; Bertozzi, C.R. *J. Am. Chem. Soc* **2002**, *124*, 14893.

[23] Cecioni, S.; Oerthel, V.; Iehl, J.; Holler, M.; Goyard, D.; Praly, J. P.; Imberty, A.; Nierengarten, J. F.; Vidal, S. *Chem.-Eur. J.* **2011**, *17*, 3252.

[24] Lampkins, A. J.; O'Neil, E. J.; Smith, B. D. *J. Org. Chem.* **2008**, *73*, 6053.

[25] Barandov, A.; Grünstein, D.; Apostolova, I.; Roger, M.; Buchert, R.; Abram, U.; Brenner, W.; Seeberger, P.H. *submitted*.

[26] Alberto, R.; Ortner, K.; Wheatley, N.; Schibli, R.; Schubiger, P. A. *J. Am. Chem. Soc.* **2001**, *123*, 3135.

[27] Garayoa, E. G.; Ruegg, D.; Blauenstein, P.; Zwimpfer, M.; Khan, I. U.; Maes, V.; Blanc, A.; Beck-Sickinger, A. G.; Tourwe, D. A.; Schubiger, P. A. *Nucl. Med. Biol.* **2007**, *34*, 17.

[28] Menzies, S. A.; Smith, R. R.; Hoff, J. T.; Betz, A. L. *Neurosurgery* **1992**, *31*, 100.

[29] del Zoppo, G. J. *Neuroscience* **2009**, *158*, 972.

[30] Fisher, M.; Feuerstein, G.; Howells, D. W.; Hurn, P. D.; Kent, T. A.; Savitz, S. I.; Lo, E. H.; Grp, S. *Stroke* **2009**, *40*, 2244.

[31] (a) Dubow, J.; Fink, M. E. *Curr. Atherosclerol. Rep.* **2011**, *13*, 298. (b) Lawes, C. M. M.; Bennett, D. A.; Feigin, V. L.; Rodgers, A. *Stroke* **2004**, *35*, 776.

[32] Liu, Y.; Liu, T. N.; McCarron, R. M.; Spatz, M.; Feuerstein, G.; Hallenbeck, J. M.; Siren, A. L. *Am. J. Physiol.-Heart Circul. Physiol.* **1996**, *270*, H2125.

[33] Gouze, J. N.; Bianchi, A.; Becuwe, P.; Dauca, M.; Netter, P.; Magdalou, J.; Terlain, B.; Bordji, K. *FEBS Lett.* **2002**, *510*, 166.

---

[34] (a) Cipolla, M. J.; Curry, A. B. *Stroke* **2002**, *33*, 2094. (b) Coulson, R. J.; Chesler, N. C.; Vitullo, L.; Cipolla, M. J. *Am. J. Physiol.-Heart Circul. Physiol.* **2002**, *283*, H2268. (c) Cipolla, M. J.; Binder, N. D.; Osol, G. *Am. J. Obstet. Gynecol.* **1997**, *177*, 215. (d) Jimenez-Altayo, F.; Martin, A.; Rojas, S.; Justicia, C.; Briones, A. M.; Giraldo, J.; Planas, A. M.; Vila, E. *Am. J. Physiol.-Heart Circul. Physiol.* **2007**, *293*, H628.

[35] (a) McCabe, C.; Gallagher, L.; Gsell, W.; Graham, D.; Dominiczak, A. F.; Macrae, I. M. *Stroke* **2009**, *40*, 3864. (b) Fisher, M. *Cerebrovasc. Dis.* **2004**, *17*, 1.

[36] (a) Macleod, M. R.; van der Worp, H. B.; Sena, E. S.; Howells, D. W.; Dirnagl, U.; Donnan, G. A. *Stroke* **2008**, *39*, 2824. (b) Zhao, Z. G.; Cheng, M. S.; Maples, K. R.; Ma, J. Y.; Buchan, A. M. *Brain Res.* **2001**, *909*, 46.

[37] (a) Iadecola, C.; Anrather, J. *Nat. Med.* **2011**, *17*, 796. (b) Fassbender, K.; Rossol, S.; Kammer, T.; Daffertshofer, M.; Wirth, S.; Dollman, M.; Hennerici, M. *J. Neurol. Sci.* **1994**, *122*, 135.

[38] (a) Gelderblom, M.; Leypoldt, F.; Steinbach, K.; Behrens, D.; Choe, C. U.; Siler, D. A.; Arumugam, T. V.; Orthey, E.; Gerloff, C.; Tolosa, E.; Magnus, T. *Stroke* **2009**, *40*, 1849. (b) Huang, J.; Upadhyay, U. A.; Tamargo, R. J. *Surg. Neurol.* **2006**, *66*, 232.

[39] (a) Collaco-Moraes, Y.; Aspey, B.; Harrison, M.; deBelleroche, J. *J. Cereb. Blood Flow Metab.* **1996**, *16*, 1366. (b) Iadecola, C.; Zhang, F. Y.; Casey, R.; Nagayama, M.; Rose, M. E. *J. Neurosci.* **1997**, *17*, 9157. (c) Dinarello, C. A. *Blood* **1996**, *87*, 2095.

[40] (a) Bowman, C. C.; Rasley, A.; Tranguch, S. L.; Marriott, I. *Glia* **2003**, *43*, 281. (b) Tang, S. C.; Arumugam, T. V.; Xu, X. R.; Cheng, A. W.; Mughal, M. R.; Jo, D. G.; Lathia, J. D.; Siler, D. A.; Chigurupati, S.; Ouyang, X.; Magnus, T.; Camandola, S.; Mattson, M. P. *Proc. Natl. Acad. Sci. U. S. A.* **2007**, *104*, 13798.

[41] Berti, R.; Williams, A. J.; Moffett, J. R.; Hale, S. L.; Velarde, L. C.; Elliott, P. J.; Yao, C. P.; Dave, J. R.; Tortella, F. C. *J. Cereb. Blood Flow Metab.* **2002**, *22*, 1068.

[42] Ueng, T. H.; Kang, J. J.; Wang, H. W.; Cheng, Y. W.; Chiang, L. Y. *Toxicol. Lett.* **1997**, *93*, 29.

[43] (a) Sayes, C. M.; Fortner, J. D.; Guo, W.; Lyon, D.; Boyd, A. M.; Ausman, K. D.; Tao, Y. J.; Sitharaman, B.; Wilson, L. J.; Hughes, J. B.; West, J. L.; Colvin, V. L. *Nano Lett.* **2004**, *4*, 1881. (b) Isakovic, A.; Markovic, Z.; Todorovic-Markovic, B.; Nikolic, N.; Vranjes-Djuric, S.; Mirkovic, M.; Dramicanin, M.; Harhaji, L.; Raicevic, N.; Nikolic, Z.; Trajkovic, V. *Toxicol. Sci.* **2006**, *91*, 173. (c) Qiao, R.; Roberts, A. P.; Mount, A. S.; Klaine, S. J.; Ke, P. C. *Nano Lett.* **2007**, *7*, 614.

[44] Baati, T.; Bourasset, F.; Gharbi, N.; Njim, L.; Abderrabba, M.; Kerkeni, A.; Szwarc, H.; Moussa, F. *Biomaterials* **2012**, *33*, 4936.

[45] Takahashi, M.; Kato, H.; Doi, Y.; Hagiwara, A.; Hirata-Koizumi, M.; Ono, A.; Kubota, R.; Nishimura, T.; Hirose, A. *J. Toxicol. Sci.* **2012**, *37*, 353.

[46] O'Collins, V. E.; Macleod, M. R.; Donnan, G. A.; Horky, L. L.; van der Worp, B. H.; Howells, D. W. *Ann. Neurol.* **2006**, *59*, 467.

[47] Lai, H. S.; Chen, Y.; Chen, W. J.; Chang, K. J.; Chiang, L. Y. *Transplant. Proc.* **2000**, *32*, 1272.

[48] Longa, E. Z.; Weinstein, P. R.; Carlson, S.; Cummins, R. *Stroke* **1989**, *20*, 84.

[49] Gerriets, T.; Stolz, E.; Walberer, M.; Muller, C.; Kluge, A.; Bachmann, A.; Fisher, M.; Kaps, M.; Bachmann, G. *Stroke* **2004**, *35*, 566.

Chapter 5

Localized Surface Plasmon Resonance Transducers for Studying Carbohydrate–Protein Interactions

---

The results reported in this chapter have been partially published in:

Bellapadrona, G.; Tesler, A. B.; Grünstein, D.; Hossain, L. H.; Kikkeri, R.; Seeberger, P. H.; Vaskevich, A.; Rubinstein, I. *Anal. Chem.* **2012**, *84*, 232. G.B., A.B.T., and D.G. contributed equally to this work.
(DOI: 10.1021/ac202363t – The original article is available at: http://pubs.acs.org/doi/abs/10.1021/ac202363t)

Table of Contents

Abstract

Noble metal nanostructures supporting localized surface plasmons (SPs) have been widely applied to chemical and biological sensing. Changes in the effective refractive index in the vicinity of the nanostructures affect the intensity and wavelength of the SP extinction band, thus making localized surface plasmon resonance (LSPR) spectroscopy a convenient tool for studying biological interactions.

Carbohydrate–protein interactions are of major importance in living organisms. Therefore, the construction of biosensors is crucial for understanding biological processes mediated by protein–sugar interaction, diagnostics, and drug development.

Here, LSPR transducers based on gold (Au) island films prepared by evaporation on glass and annealing were optimized for monitoring the specific interaction between Concanavalin A (Con A) and mannose. The sugar was modified with a polyethylene glycol (PEG)-thiol linker and immobilized on the Au islands.

Sensing assays were performed under stationary and flow conditions, the latter providing kinetic parameters for protein binding and dissociation. Ellipsometry and Fourier transform infrared spectroscopy (FTIR) data, as well as scanning electron microscope (SEM) imaging of fixated and stained samples, furnished independent evidence for the protein–sugar recognition.

Enhanced response and visual detection of protein binding was demonstrated using Au nanoparticles (AuNPs) stabilized with the linker-modified mannose molecules. Mannose-coated transducers display an excellent selectivity toward Con A in the presence of a large excess of bovine serum albumin (BSA).

1. Introduction

In recent years, developing optical transducers for the study of interactions between biological molecules has become a prime objective in materials chemistry. Despite the central role of surface plasmon resonance (SPR) as the major technique used for this purpose in life sciences, the number of applications of LSPR has increased progressively, primarily due to the lower cost and higher flexibility with respect to SPR.[1]

Much effort has been invested in finding optimal metal nanostructures for LSPR biosensing applications, producing a variety of examples ranging from noble metal nanoparticles (NPs), through more complex systems such as nanorods, nanoholes and nanocages, to nanostructured metal films deposited on solid transparent supports.[2] The common experimental scheme for LSPR sensing consists of immobilization of a receptor layer on the nanostructured metal surface of the transducer, and monitoring local changes in the refractive index occurring upon binding of the biological analyte.[3]

The difference between propagating and localized surface plasmons is illustrated below.[4] In the case of surface plasmon polaritons used in SPR, plasmons can be excited on thin metal films using grating or prism couplers and they propagate in the x- and y-directions along the metal-dielectric interface, for distances on the order of tens to hundreds of microns, and exponentially decay evanescently in the z-direction (Figure 1).[5]

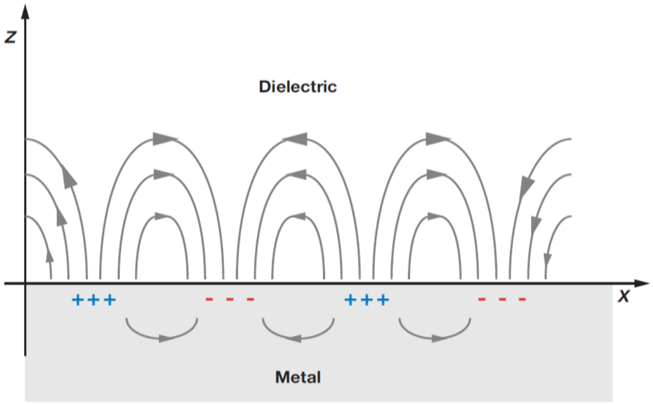

Figure 1. Schematic diagram illustrating a SP polariton (or propagating plasmon).

The interaction between the metal surface-confined electromagnetic wave and a molecular surface layer of interest leads to shifts in the plasmon resonance condition, which can be observed in three modes: angle resolved, wavelength shift, and imaging.

In the case of localized surface plasmons, light interacts with particles much smaller than the incident wavelength (Figure 2). This leads to a plasmon that oscillates locally around the nanoparticle with a frequency known as the LSPR that depends on the size, shape, composition, and local dielectric environment. Similar to the SPR, the LSPR is sensitive to changes in the local dielectric environment.[6] This latter property has been exploited for label-free optical sensing where adsorbate-induced refractive index changes near or on plasmonic nanostructures are used to monitor binding events in real time.

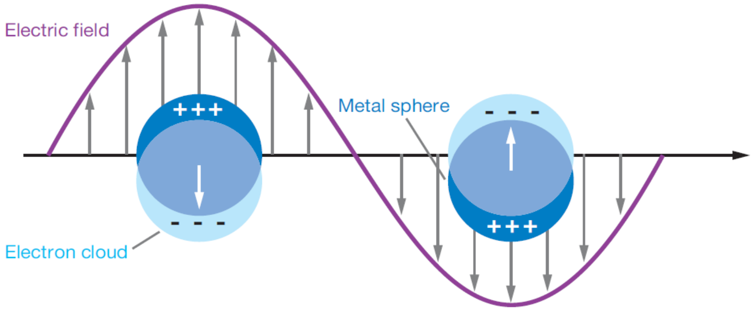

Figure 2. Schematic diagram representing a localized surface plasmon.

I have studied LSPR transducers based on random discontinuous (island-type) gold films prepared by evaporation on transparent substrates (mostly glass slides) followed by annealing in air. These systems were shown to be suitable for gas sensing, as well as for detecting biological interactions such as specific antigen-antibody recognition.[7]

In this chapter, I demonstrate the utility of Au nano-island based LSPR transducers in the characterization of carbohydrate–protein interactions. In the field of biomolecular recognition, carbohydrate–protein and carbohydrate–carbohydrate interactions represent a relatively unexplored area, despite their major importance in a myriad of biological systems. Carbohydrate–protein interactions are predominant in many fundamental biological processes, such as cell to cell adhesion and communication, host–pathogen interactions, fertility and development, and cancer.[8] Study of such interactions is therefore crucial for the understanding of basic biological processes as well as for the development of biosensors, primarily for diagnostics and drug development. An automated method for the synthesis of carbohydrates has opened new possibilities in this research direction.[9]

To illustrate the approach, the specific recognition between the lectin Con A from *Canavalia ensiformis* and the sugar mannose was selected. Lectins are carbohydrate-binding proteins endowed with a remarkably different affinity for different carbohydrates, thus representing a suitable model system for establishing the specificity and sensitivity of our LSPR transducers in such applications.[10] Au island transducers were derivatized with PEG-thiol linker **1,** PEG-thiol modified mannose **2** and galactose **3** (Scheme 1), to obtain LSPR transducers for monitoring, quantification, and imaging of mannose–Con A interactions.

Optimization of the system for Con A detection was demonstrated using a series of transducers with increasing average island dimensions, enabling achievement of maximal sensitivity. The performance of these transducers was critically evaluated by comparison with results obtained by other techniques.[11] AuNPs stabilized with the same linker-mannose molecules are used to decorate Con A bound to the Au island surface, providing enhanced LSPR signal as well as convenient imaging of Con A recognition. Separation of the SP bands of the Au islands and the AuNP was achieved by choice of transducers comprising large, single-crystalline Au islands, providing, in addition, superior imaging of the carbohydrate functionalized AuNPs (Carb@AuNPs) on the Au islands.

2. Results and Discussion

2.1. Chemical Synthesis

Linker **1** was assembled from a hexaethyleneglycol segment and bromoundecene. The terminal double bound was then converted to a terminal thiol group. Mannose and galactose were covalently bound to the same linker segment to yield molecules **2** and **3**, respectively (Scheme 1).

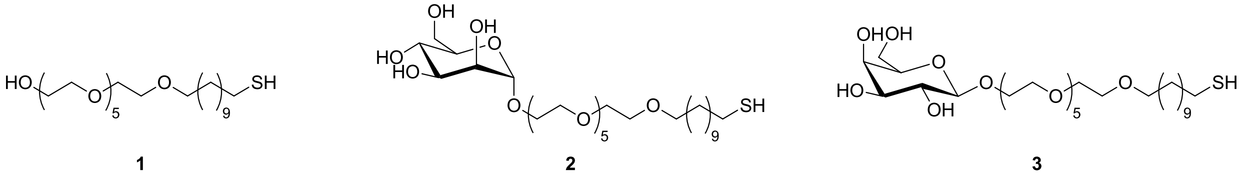

Scheme 1. Molecules used for the formation of the self-assembled monolayers on the Au surfaces: linker **1**, linker-modified mannose **2**, and linker-modified galactose **3**.

The synthesis of **1** was carried out by using hexaethyleneglycol **4**, bromoundec-11-ene **5**, and sodium hydride (NaH), to afford desired compound **6**. Functionalization of the terminal double bond of **6** was achieved using thioacetic acid (AcSH) and azobisisobutyronitrile (AIBN), furnishing thioacetate **7**. Hydrolysis of the thioacetate was then carried out under basic conditions, to afford **1** (Scheme 2).

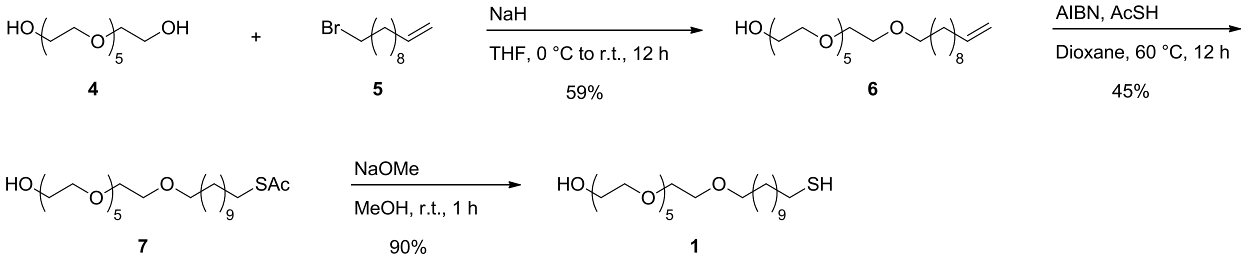

Scheme 2. Synthesis of linker **1**.

Mannose **8** was treated with acetic anhydride (Ac_2O) and pyridine to afford the peracetylated product, which was then treated with hydrazine to remove the anomeric acetate ester. Installation of the trichloroacetimidate (TCA) group in the presence of 1,8-diazabicyclo[5.4.0]undec-7-ene (DBU) afforded the desired compound **9**. A glycosylation using excess of boron trifluoride diethyl etherate ($BF_3{\cdot}Et_2O$) and linker **6**, followed by the functionalization of the terminal double bond gave the thioaceate **11**. Global deprotection of the acetates in the presence of sodium methoxide (NaOMe) yielded the desired compound **2** (Scheme 3).

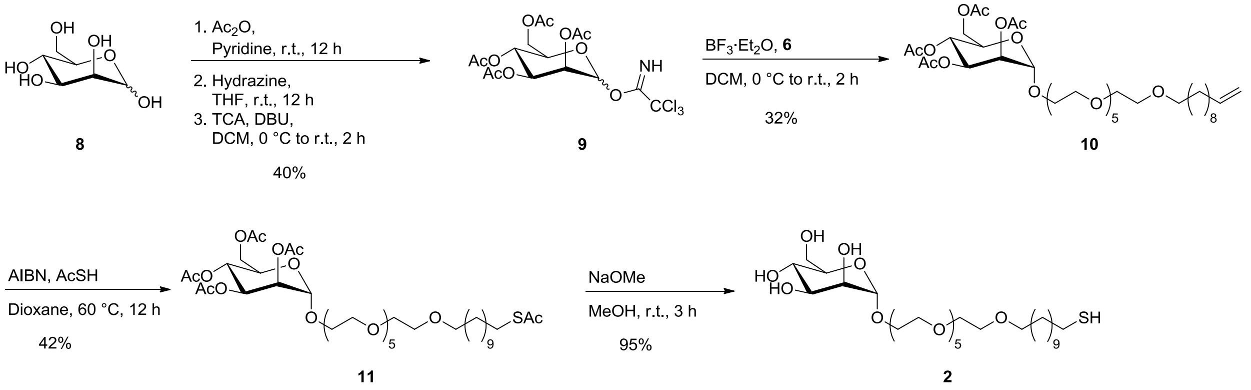

Scheme 3. Synthesis of linker-modified mannose **2**.

A similar strategy was used for the synthesis of **3**. Peracetylation of galactose was carried out using Ac_2O and pyridine. The anomeric acetate ester was selectively cleaved and the TCA leaving group was installed, affording **13** (from Dr. Laila H. Hossain). Glycosylation with the linker **6** followed, furnishing the desired compound **14**. Functionalization of the terminal double bond with AcSH and AIBN, followed by global deprotection with NaOMe yielded the desired compound **3** (Scheme 4).

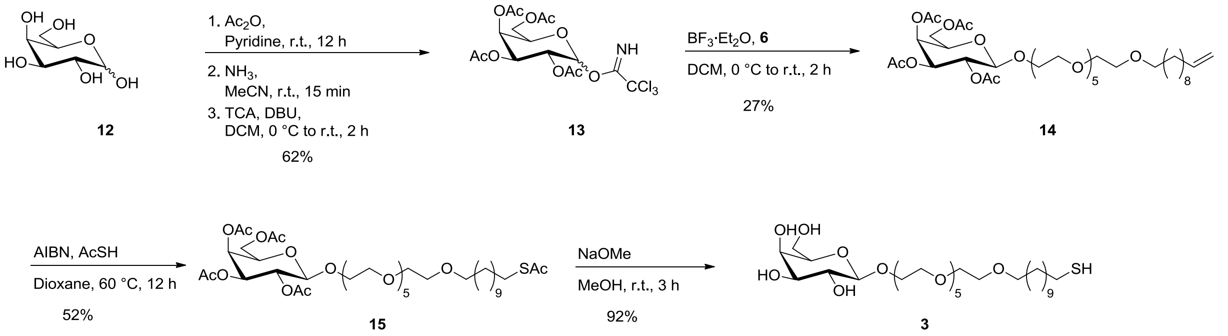

Scheme 4. Synthesis of linker-modified galactose **3**.

2.2. Self-assembly of Carbohydrate Monolayers on Gold and Con A Recognition

Thermally stabilized 1.5–15 nm Au island LSPR transducers were prepared as detailed in the experimental part and analyzed by high-resolution scanning electron microscopy (HRSEM) (Figure 3).[12]

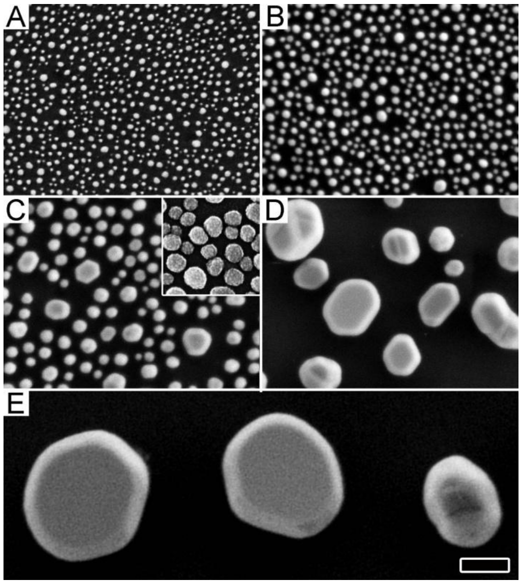

Figure 3. HRSEM images of 1.5, 2.5, 5.0, 10, and 15 nm nominal thickness [(A)–(D), respectively] Au island films, evaporated on glass and annealed 10 h at 570 °C. The inset in (C) shows the 5.0 nm film covered with 3 nm sputtered chromium. Scale bar: 100 nm.

Immediately before use, each sample was pretreated by UV-ozone and ethanol dip.[13] The transducers were then reacted with PEG-silane to form a blocking PEG layer on the bare glass surface between the islands, thus preventing spurious adsorption on the glass.

Slight changes in the LSPR spectrum observed upon formation of the PEG-silane layer (Figure 4A) are related to an increase in the refractive index of the environment surrounding the perimeter of the Au islands. In the present system, the PEG-silane molecules bind selectively to the glass and not to the Au islands, hence the PEG-silane treatment has a minimal effect on subsequent formation of self-assembled monolayers (SAMs) of thiolated molecules on the Au islands. The orthogonal nature of the binding of PEG-silane and thiolated molecules to the island system is further evidenced by differential LSPR spectra showing order-of-magnitude difference in the response to PEG-silane and PEG-thiol **1** adsorption (Figure 4A, right). Moreover, polarization-modulation infrared reflection-absorption spectroscopy (PM-IRRAS) measurements (Figure 4B, C) showed no adsorption of PEG-silane on 100 nm continuous Au film, while the incubation with the thiolated PEG molecules –indicating formation of a SAM– were confirmed by the presence of the C–O and C–C stretching vibrations of the PEG molecules at 1043 cm^{-1}.

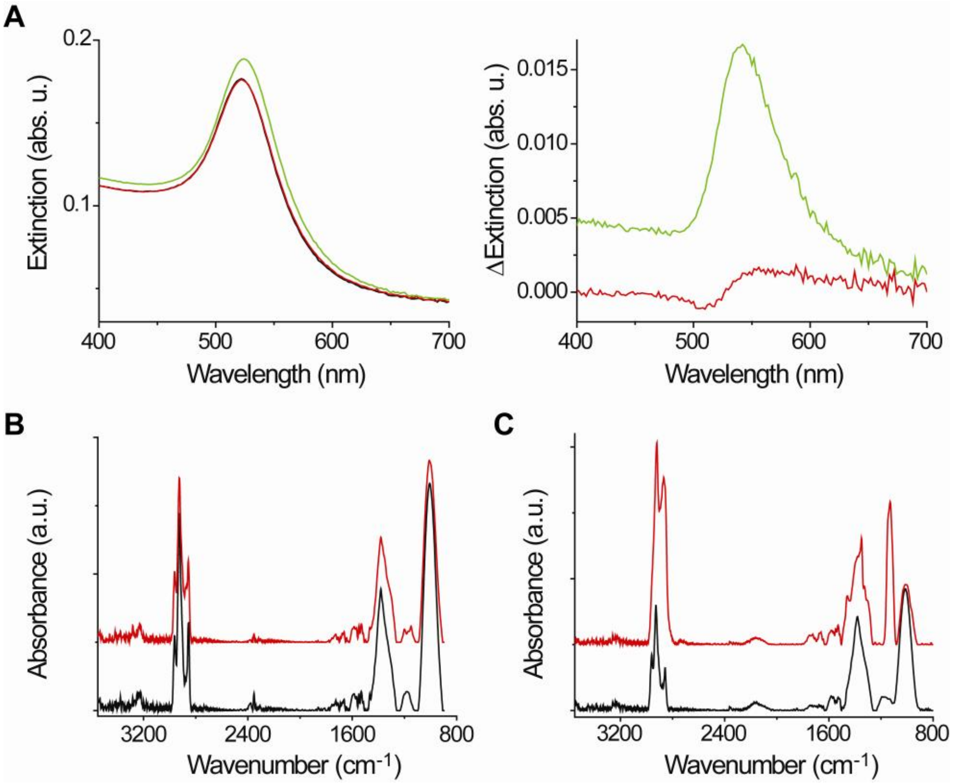

Figure 4. (A) Transmission UV-vis spectra (left) and corresponding difference spectra (right) of a 5.0 nm Au island film, before (black line) and after sequential incubation with PEG-silane (red lines) and linker **1** (green lines). (B), (C) PM-IRRAS spectra of two 100 nm continuous Au films, before (black lines) and after (red lines) incubation with PEG-silane (B) or linker **1** (C).

To demonstrate specific recognition between Con A and mannose immobilized on the Au islands, a series of experiments were performed (Figure 5). These included specific interaction of Con A with a SAM of mannose **2** (Figure 5A), as well as three controls, i.e., no SAM (Figure 5B), a SAM of linker **1** (Figure 5C), and a SAM of the non-specific binder galactose **3** (Figure 5D). SAMs composed of **1–3** were assembled on 1.5, 2.5, 5.0, 10, and 15 nm (nominal thickness) Au island films (Figure 3) for LSPR measurements, as well as on 100 nm continuous Au substrates for obtaining ellipsometry and FTIR data. Self-assembly was accomplished by wetting the Au surfaces with 1 mM ethanolic solution of the respective thiol compound, as detailed in the experimental section. The response of the differently prepared surfaces to Con A was assayed by incubation with Con A (1 µM) in tris(hydroxymethyl)aminomethane hydrochloride (Tris-HCl) buffer solution (10 mM, pH 7.4) containing NaCl (0.1 M), $CaCl_2$ (1 mM) and $MnCl_2$ (1 mM), a solution in which the protein is assembled in its active tetrameric form (hereafter referred to as the buffer solution).

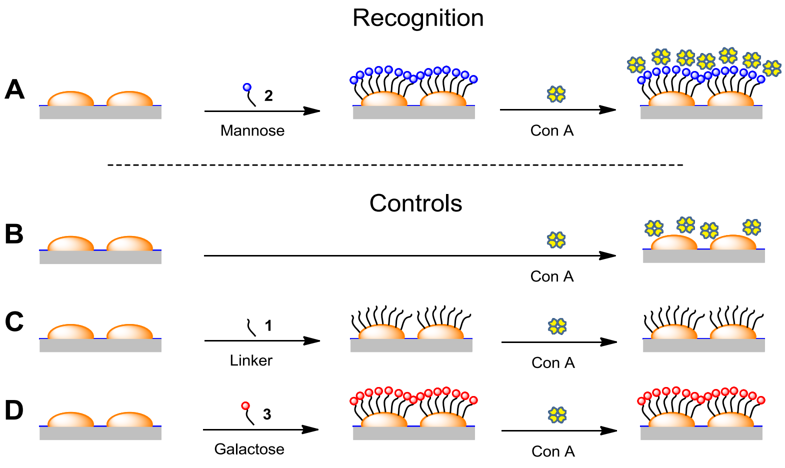

Figure 5. Schematic presentation of the recognition and control experiments with Au island transducers. (A) Specific binding of Con A to a SAM of **2** (mannose); (B) non-specific adsorption of Con A on bare Au; (C), (D) non-specific interaction of Con A with SAMs of **1** (linker) and **3** (galactose), respectively.

Transmission spectra for the series of experiments described in Figure 5 are shown for 5.0 nm (Figure 6) and 10 nm (Figure 7) Au island films, using for convenience the same A–D notation as in Figure 5. Formation of the respective SAMs on the Au island films is indicated by the increase in intensity and red-shift of the SP band observed following incubation of the transducers with molecules **1–3** (Figure 6A, C, D and Figure 7A, C, D).

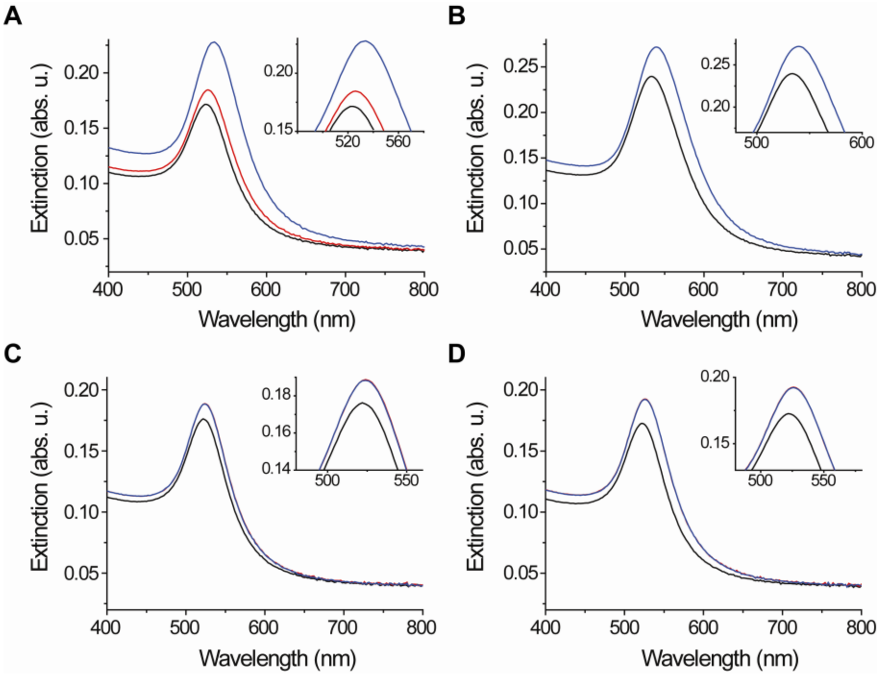

Figure 6. LSPR spectra of 5.0 nm Au island films. (A)–(D) correspond to the experiments depicted in Figure 5. The different spectra were recorded after PEG-silane modification (black lines), formation of a carbohydrate or linker SAM (red lines), and incubation with Con A (blue lines). Note that in (C) and (D) the red and blue lines coincide.

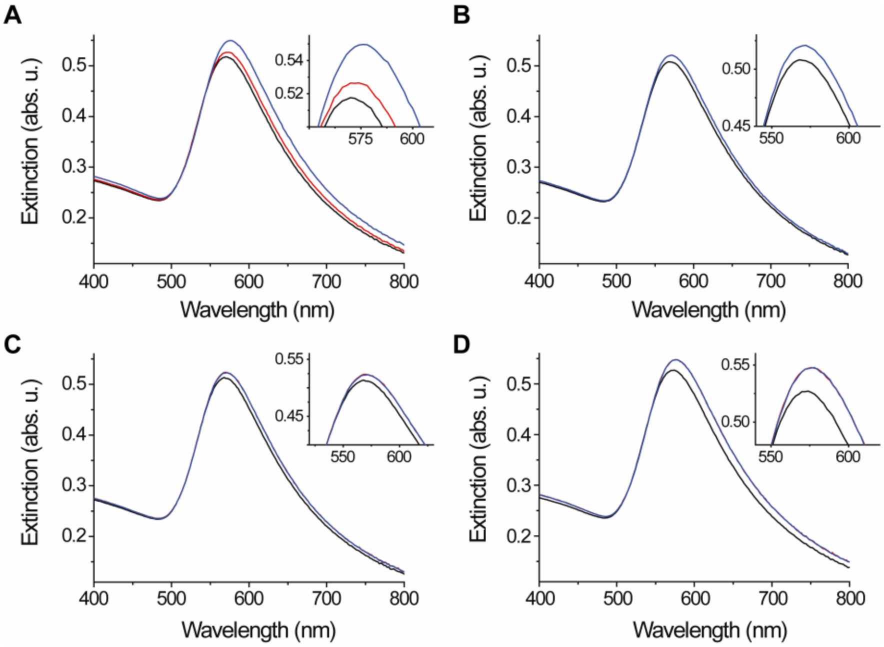

Figure 7. LSPR spectra of 10 nm Au island films. (A)–(D) correspond to the experiments depicted in Figure 5. The different spectra were recorded after PEG-silane modification (black lines), formation of a carbohydrate or linker SAM (red lines), and incubation with Con A (blue lines). Note that in (C) and (D) the red and blue lines coincide.

A marked response to specific binding of Con A to the mannose SAM is evident as a distinct increase in the maximum intensity and a red-shift of the plasmon band position for both transducers (Figure 6A and Figure 7A). Control experiments with no SAM show adsorption of Con A on the bare Au (Figure 6B and Figure 7B). On the other hand, when Au island transducers were coated with a linker SAM (negative control) or a galactose SAM (non-specific control), no response to Con A was observed (Figure 6C, D and Figure 7C, D). The changes in the maximum extinction and plasmon position accompanying the different steps, summarized in Figure 8, clearly show the LSPR response to specific binding of Con A to mannose immobilized on the Au island surface. The response of 5.0 nm transducers is considerably higher than that of 10 nm transducers, a point further discussed below.

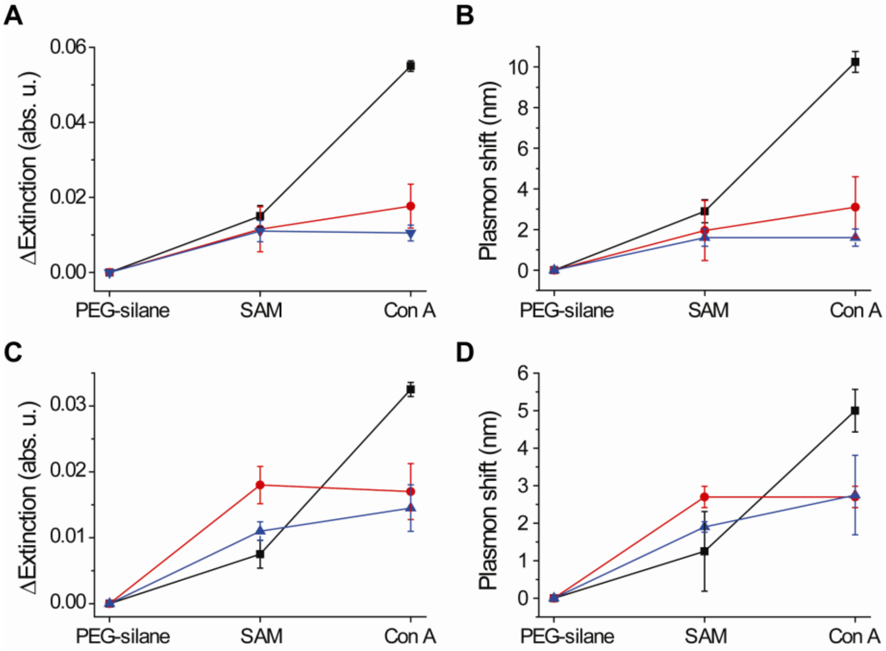

Figure 8. Summary of the optical response of 5.0 nm mannose (black lines), galactose (red lines), and linker (blue lines) LSPR transducers [(A) and (B), data extracted from Figure 6] and 10 nm LSPR transducers [(C) and (D), data extracted from Figure 7], presented as changes in maximum extinction (left) and plasmon wavelength (right). Symbols and error bars indicate means of N = 3 per measurement ± standard deviation (S.D.).

The LSPR results are supported by ellipsometric and PM-IRRAS data obtained with 100 nm continuous Au films (Figure 9). SAM formation on the continuous Au is indicated by the decrease in the ellipsometric Δ [Figure 9A, C, D (left) and Table 1] as well as by the presence of a peak at 1043 cm^{-1} in the PM-IRRAS spectra [Figure 9A, C, D (right)], attributed to C–O and C–C stretching vibrations of the linker segment. Specific binding of Con A to the mannose SAM is manifested by a decrease in the ellipsometric Δ and a respective increase in the bound layer thickness [Figure 9A (left) and Table 1], as well as C=O stretching vibrations (1651 cm^{-1} and 1666 cm^{-1}), N–H bending vibrations (1543 cm^{-1} and 1545 cm^{-1}) and H-bonded O–H stretching vibrations (3288 cm^{-1}), characteristic of proteins adsorbed on surfaces [Figure 9A, B (right)], absent in the non-specific cases [Figure 9C, D (right)].[14]

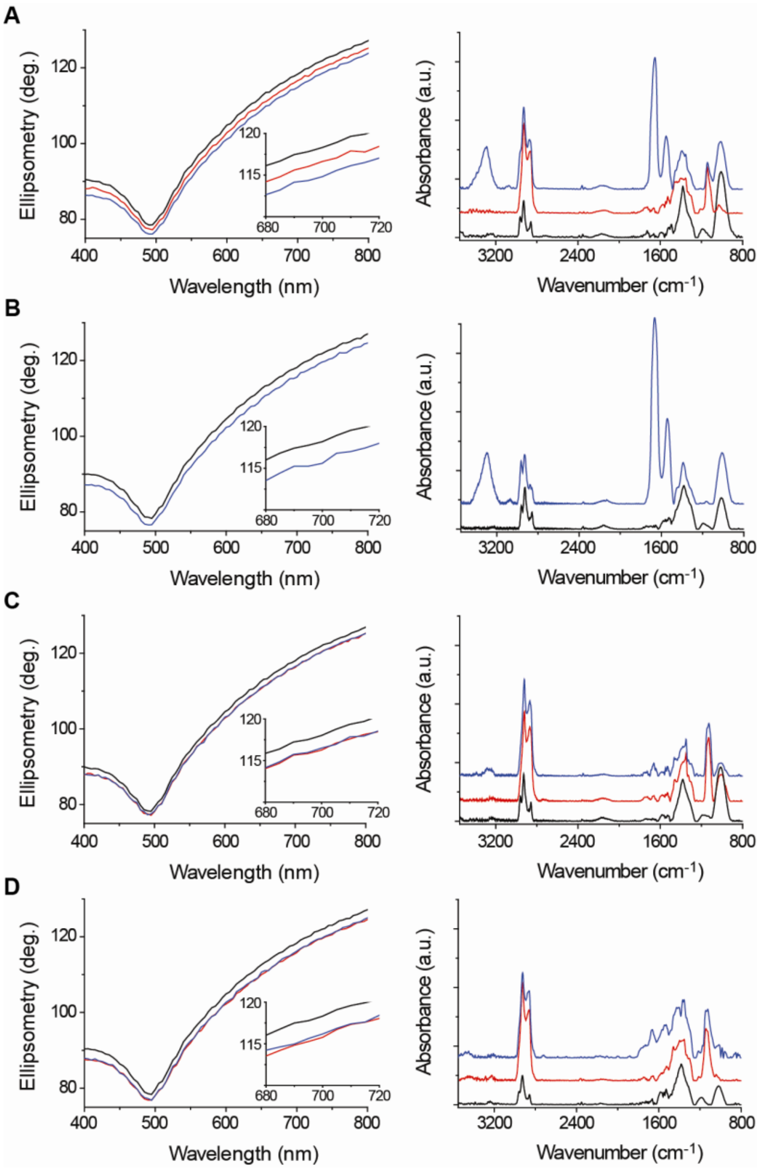

Figure 9. Spectroscopic ellipsometry (left) and PM-IRRAS (right) results. (A)–(D) correspond to the experiments depicted in Figure 5, using a continuous Au substrate. The different spectra were recorded after UV-ozone + ethanol treatment (black lines), formation of a carbohydrate or linker SAM (red lines), and incubation in Con A solution (blue lines). Note that in (C) and (D) the red and blue lines overlap.

Table 1. Ellipsometric thicknesses measured on continuous Au films under conditions corresponding to experiments (A)–(D) in Figure 5.

Experiment	SAM	Monolayer thickness (nm)	Thickness after incubation with Con A (nm)
A	Mannose	2.7	4.1
B	No SAM	-	3.4
C	Linker	2.4	2.4
D	Galactose	3.2	3.0

Visual evidence for specific mannose–Con A binding is obtained using HRSEM imaging of samples which underwent fixation, staining and coating with 3 nm sputtered chromium (Cr) (Figure 10). The grainy texture results from the Cr layer (Figure 3C, inset). Binding of Con A to the mannose SAM is clearly seen as an added layer on the Au islands (Figure 10B) with a distinctly different morphology, whereas the images corresponding to the linker and galactose SAMs exposed to Con A (Figure 10D, F) appear identical to the bare Au islands.

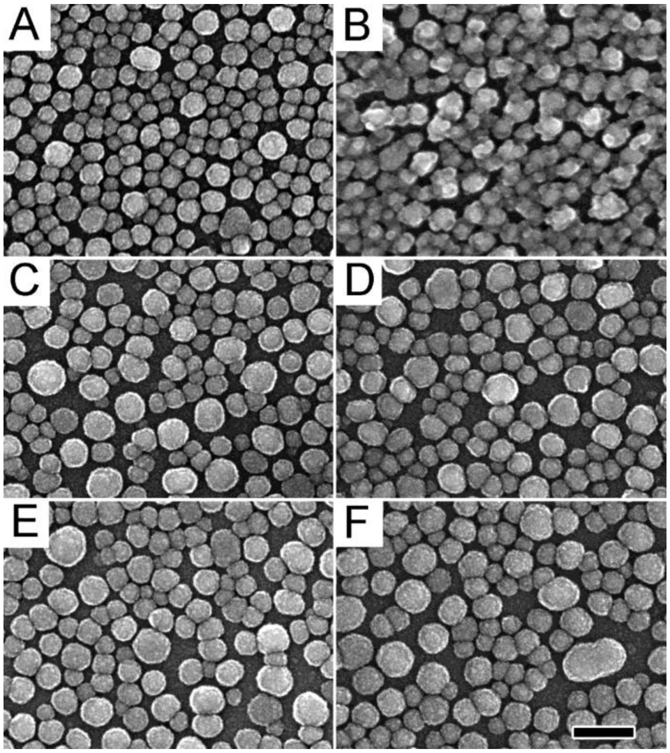

Figure 10. HRSEM images of 5.0 nm Au island films after formation of SAMs of (A) **2** (mannose); (C) **1** (linker); (E) **3** (galactose). (B), (D), and (F) are respective images after incubation with Con A. All samples were fixated, stained and coated with 3 nm sputtered Cr. Scale bar: 100 nm.

2.3. Optimization of the LSPR Transducer Response

The response of LSPR transducers is determined by two basic parameters characteristic of a given transducer, i.e., the refractive index sensitivity (RIS) and the decay length of the plasmon evanescent field. When attempting to maximize the optical response to a specific analyte, it is desirable to pick a transducer with a high RIS and a decay length that matches the dimensions of the analyte and recognition interface. However, these requirements are often contradicting, as the RIS and decay length are correlated.[15] For the island systems studied here, both parameters increase upon increasing the Au nominal thickness, reaching decay length values considerably greater than the recognition interface and Con A dimensions. Maximal response can be achieved by choosing a transducer with an optimal combination of RIS and decay length that best matches the given biological system.

To optimize the response to Con A, Au island films of 1.5, 2.5, 5.0, and 10 nm (Figure 3) were treated with PEG-silane, derivatized with mannose-linker and incubated with Con A (Figure 5A). The optical response to the sequence of treatments was measured and changes in the spectral parameters accompanying Con A binding (i.e., the last step in Figure 5A) were compared for the different transducers.

The data in Figure 8 indicates that both the wavelength shift and extinction change of the LSPR band maximum can be used in actual sensing. It is known that differential LSPR spectra display a maximum at a wavelength red-shifted from the maximum of the LSPR band (Figure 11).[16] Hence, measurement of the extinction change at a constant wavelength near the maximum of the difference spectrum presents a more sensitive as well as a simpler sensing mode, particularly suitable for kinetics studies.

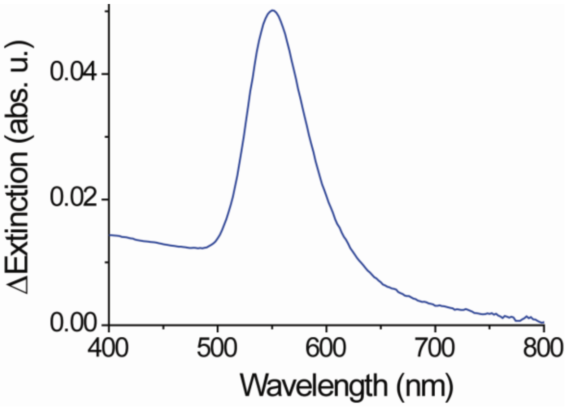

Figure 11. Difference spectrum for a 5.0 nm Au island film, corresponding to the change in the LSPR spectrum accompanying Con A binding to a mannose SAM (last step in Figure 5A) obtained by subtracting the spectrum recorded after formation of the mannose SAM from the spectrum after binding of Con A. Maximum differential extinction was observed at $\lambda_{max} \approx 545$ nm for 5.0 nm Au island films.

Plasmon extinction change at a constant wavelength (chosen for each transducer) and plasmon peak shift values are summarized in Figure 12. Generally, the response in terms of both extinction intensity and wavelength shift shows a maximum for Au island films of intermediate thickness (2.5 and 5.0 nm). These Au transducers represent a combination of RIS and decay length that best fits the analyte and recognition layer dimensions in the present system.

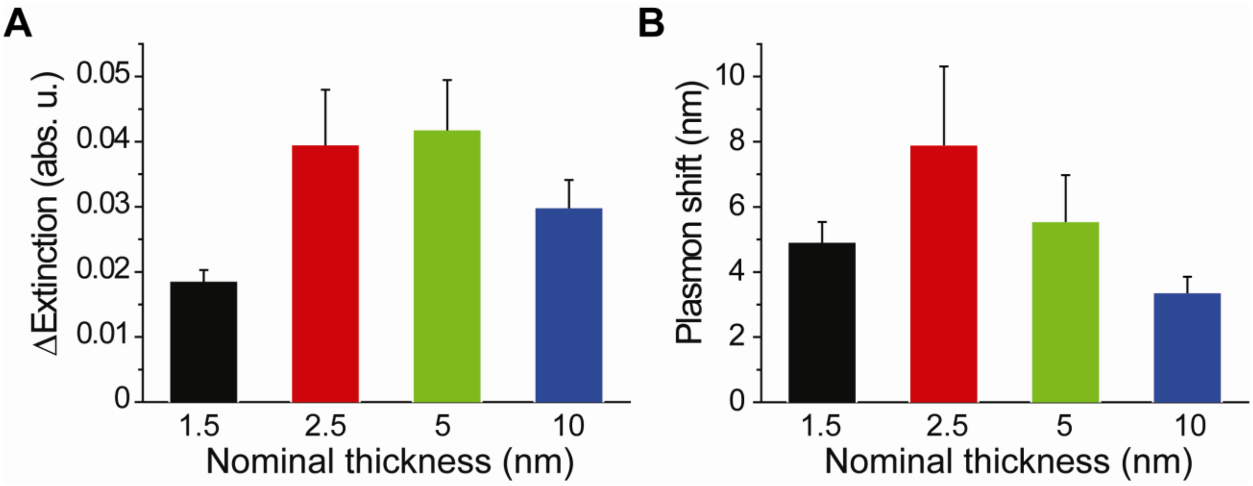

Figure 12. Optimization of the LSPR transducer response using Au island films of different nominal thicknesses (1.5, 2.5, 5.0, and 10 nm). Changes in extinction at a constant wavelength (A) and in plasmon wavelength (B) are shown for binding of Con A to mannose-modified transducers. The constant wavelengths in (A), chosen near the maximum differential extinction, were 545, 554, 545 and 609 nm for Au transducers of 1.5, 2.5, 5.0 and 10 nm, respectively. Bars and error bars indicate means of N = 3 per measurement ± S.D.

2.4. Con A Binding Kinetics

The kinetics of Con A binding to a mannose SAM were monitored in a flow configuration (Figure 13) using 5.0 nm Au island films, chosen to provide a high sensitivity (Figure 12). Measurements of Con A binding to the different SAMs (linker, mannose and galactose) were carried out by monitoring the extinction change at a constant wavelength of 545 nm, in the vicinity of the maximum differential extinction (Figure 11). A solution of Con A (0.5 µM) in buffer was pumped at 50 µL·min^{-1} through the cell, initially filled with pure buffer solution, and the LSPR transducer response was measured (Figure 14A). A sizeable extinction increase, indicating specific binding, was recorded when Con A was injected over the mannose-coated LSPR transducer, followed by a slow release upon change to buffer solution. On the other hand, essentially no response was detected upon injection of Con A over the linker-coated transducer, while a weak response was observed for the non-specific binding of Con A to the galactose-coated transducer.

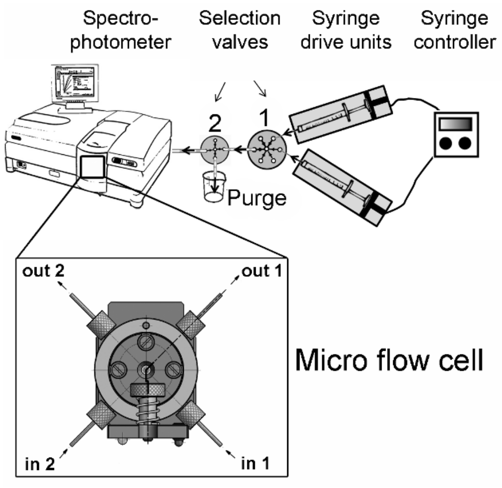

Figure 13. Schematic presentation of the flow system and the micro flow cell (60 µL internal volume) used for kinetic experiments.

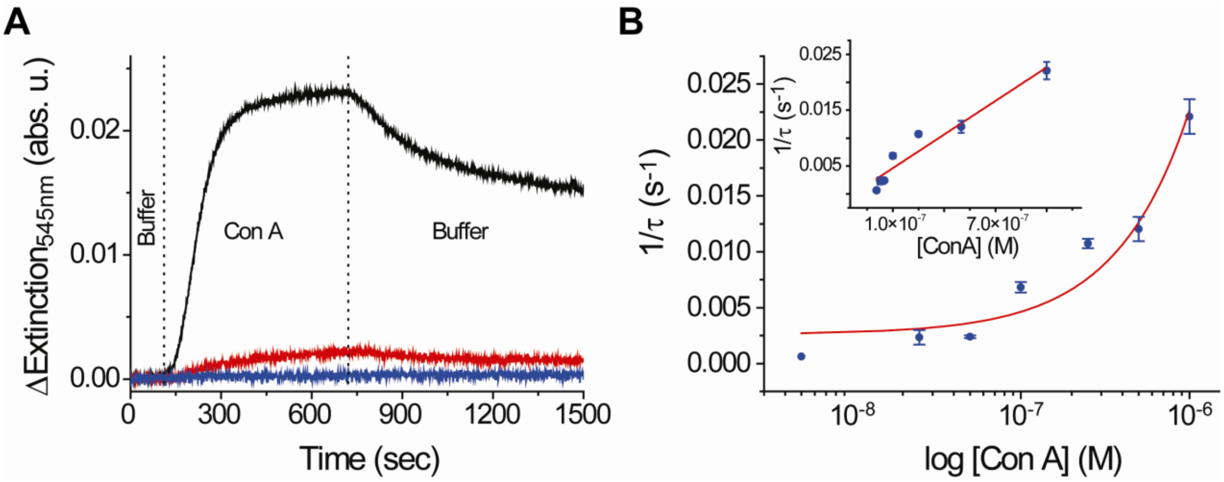

Figure 14. (A) Con A association and dissociation kinetics measured with 5 nm Au island transducers, recorded as change in the extinction at a constant wavelength of 545 nm in the micro flow cell. The flow sequence included buffer solution, 0.5 µM Con A in buffer, and buffer solution again. The transducers were modified with SAMs of **2** (black line), **1** (blue line), and **3** (red line). (B) Determination of the binding affinity of Con A to a mannose SAM; data extracted from Figure 15. Treatment of the results according to Equation 4 is shown on logarithmic and linear scales. Symbols and error bars indicate means of N = 3 per measurement ± S.D.

The kinetics of Con A binding to the mannose-coated transducer were measured as a function of the protein concentration in order to determine the kinetic parameters of the interaction between Con A and mannose (Figure 15A, B). In kinetic terms, the formation of a [Con A–mannose] complex can be described by:

$$[\text{Con A}]_{(\text{solution})} + [\text{mannose}]_{(\text{surface})} \underset{k_{\text{off}}}{\overset{k_{\text{on}}}{\rightleftharpoons}} [\text{Con A– mannose}]_{(\text{surface})} \tag{1}$$

where the association (k_{on}) and dissociation (k_{off}) rate constants determine the surface concentration of [Con A–mannose] complex at each time, given by:

$$[\mathrm{Con\ A\text{–}\ mannose}]_{(t)} = [\mathrm{Con\ A\text{–}\ mannose}]_{\infty} \times [1 - e^{-t}\ \tau] \qquad (2)$$

As noted above, the functional form of Con A is a tetramer having four carbohydrate binding sites. This implies that the protein can bind more than one mannose molecule on the surface; however, the LSPR signal is sensitive only to the first binding event, in support of the use of the simple model.[17]

It is assumed that changes in the extinction are directly proportional to the surface concentration of the complex, hence:

$$\Delta_{\mathrm{ext(t)}} = \Delta_{\mathrm{ext(\infty)}} \times [1 - e^{-t}\ \tau] \qquad (3)$$

and

$$\frac{1}{\tau} = k_{\mathrm{on}} \times \ \mathrm{Con\ A}\ + k_{\mathrm{off}} \qquad (4)$$

The kinetic data were analyzed according to equation 4 (Figure 14B). The slope and intercept were obtained by linear fitting of the (1/τ) vs. [Con A] data, giving the values $k_{on} = 2.0 \cdot 10^{4}\ M^{-1} \cdot s^{-1}$ and $k_{off} = 2.6 \cdot 10^{-3}\ s^{-1}$ for the association and dissociation rate constants, respectively. The apparent association (K_a) and dissociation (K_d) equilibrium constants were calculated to give: $K_a = k_{on}/k_{off} = 7.7 \cdot 10^{-6}$ M and $K_d = 1/K_a = 1.3 \cdot 10^{5}\ M^{-1}$.

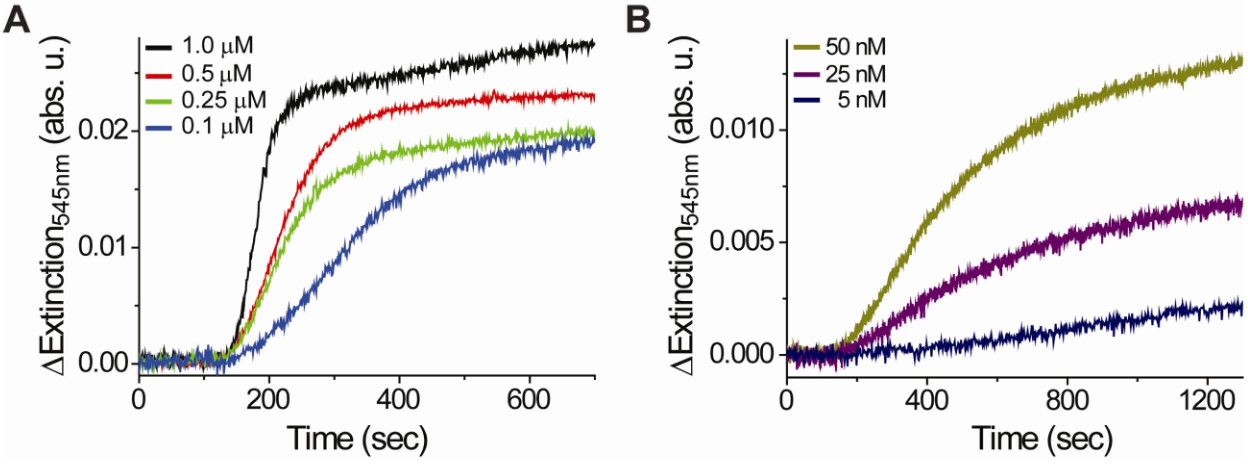

Figure 15. Con A binding kinetics. Curves in (A) and (B) were obtained as in Figure 14, using mannose-coated 5.0 nm Au island transducers and different Con A concentrations (indicated).

The kinetic values were compared with literature data for the interaction between Con A and mannose derivatives, obtained using a variety of techniques (Table 2). The wide variability in the literature values ($10^3 < k_{on} < 10^5$ $M^{-1}\cdot s^{-1}$; $10^{-2} < k_{off} < 10^{-4}$ s^{-1}) suggests a marked dependence on the experimental conditions and the technique used. The LSPR-derived k_{on} and k_{off} fit well within the range of published values.

Table 2. Kinetic parameters for the interaction between Con A and mannose derivatives, obtained using a variety of techniques [SPR, quartz crystal microbalance (QCM), and LSPR].

Method	k_{on} ($M^{-1}\cdot s^{-1}$)	k_{off} (s^{-1})	Reference
SPR	$5.72\cdot10^4$	$2.48\cdot10^{-4}$	11b
SPR	$1.07\cdot10^5$	$4.47\cdot10^{-3}$	11e
QCM	$(4 \pm 1)\cdot10^4$	$(1.2 \pm 0.2)\cdot10^{-2}$	11g
QCM	$(1.4 \pm 0.2)\cdot10^5$	$(7 \pm 2)\cdot10^{-3}$	11g
LSPR	$5.2\cdot10^3$	$2.2\cdot10^{-3}$	11f
LSPR	$7.4\cdot10^3$	$1.0\cdot10^{-3}$	11f
LSPR	$2.0\cdot10^4$	$2.6\cdot10^{-3}$	Present work

2.5. Binding of Carb@AuNPs

The tetrameric functional form of the lectin Con A has four active sites for carbohydrate binding. When the protein is bound to a two-dimensional recognition interface (i.e., the mannose SAM on the Au surface), part of the active sites remain free as a result of their three-dimensional distribution in the tetrameric structure, and can be exploited for further binding with additional mannose molecules. For this purpose 16 nm AuNPs were synthesized, stabilized with mannose-linker **2** (Man@AuNPs) or galactose-linker **3** (Gal@AuNPs), the latter for use as control (Figure 16). Binding of Man@AuNP labels to Con A on the transducer surface in a sandwich configuration may serve to visualize the protein binding, as well as enhance the sensor response and signal-to-noise by means of a dual-recognition scheme.

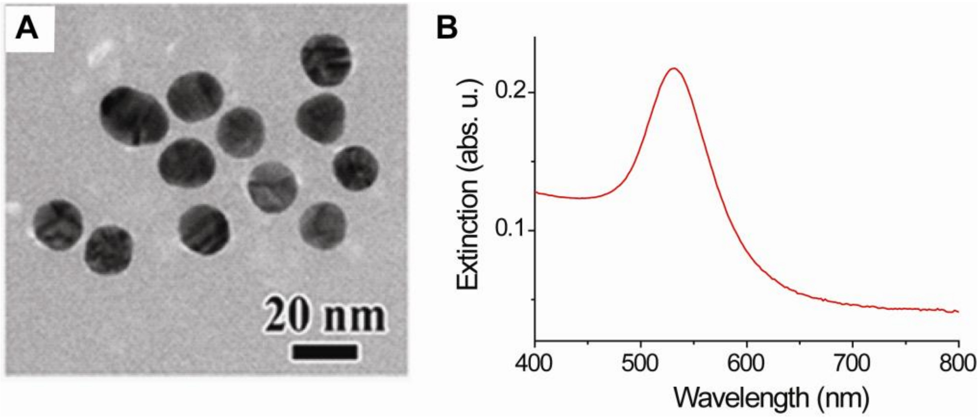

Figure 16. Transmission electron microscope (TEM) image (A) and transmission spectrum in solution (B) of Man@AuNPs.

Binding of Man@AuNPs was assayed using 5.0 nm and 15 nm Au island films. UV-vis spectra corresponding to the preparation of the recognition interface and the binding of Con A followed by Man@AuNPs were recorded *in situ* in a cuvette filled with the buffer, to eliminate the effect of drying-induced NP aggregation on the spectra. Binding of Man@AuNPs was evident as a major change in the spectra of the Au films studied (Figure 17, left panels).

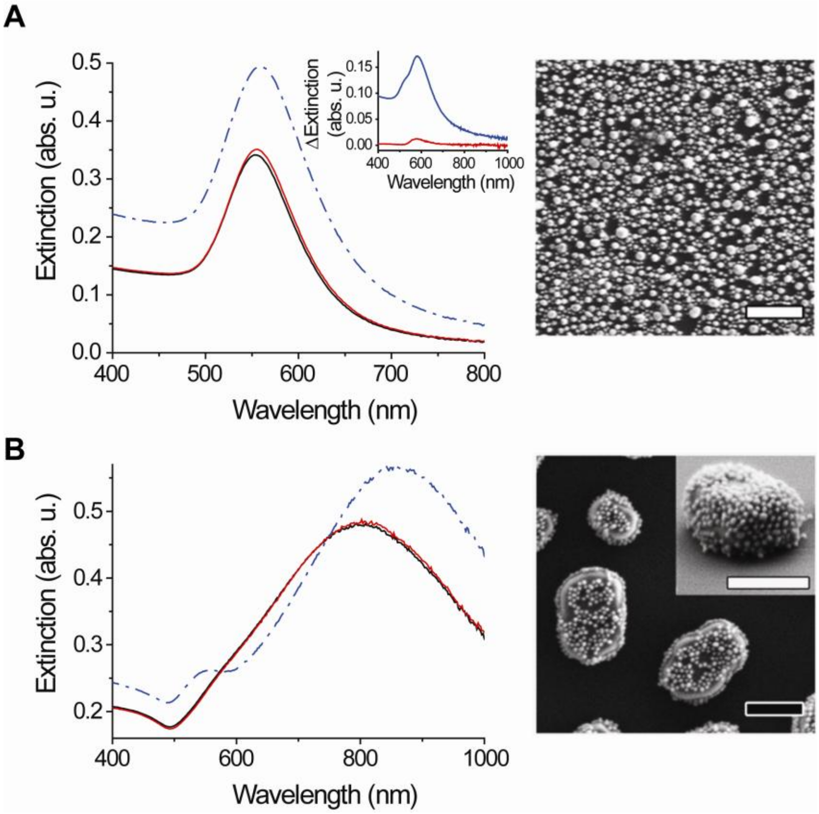

Figure 17. UV-vis spectra (left) and HRSEM images (right) corresponding to the binding of Man@AuNPs to Con A bound to mannose-modified 5.0 nm (A) and 15 nm (B) Au films. Spectra were recorded in solution after formation of a mannose SAM (black lines), binding of Con A from a Con A solution (1 µM) (red lines), and incubation with Man@AuNPs (blue dashed-dotted lines). Inset in (A): difference spectra obtained by subtracting the spectrum recorded after formation of the mannose SAM from the spectrum after binding of Con A (red line) and the spectrum after binding of the Man@AuNPs (blue line). Inset in (B): tilted projection of a single island coated with Man@AuNPs. Scale bars: 200 nm.

The 5.0 nm Au film is composed of rather symmetrical, small islands (Feret diameter: 23 ± 9 nm), displaying a SP band around 550 nm. As expected, binding of Con A to the mannose SAM, monitored in solution [Figure 17A (left)], shows a smaller change in the SP band compared to the corresponding measurement in air (Figure 6). Subsequent binding of Man@AuNPs is seen as a significant increase in the intensity (0.16 abs. u.) and a small red-shift (3–4 nm) of the absorption band [Figure 17A (left)]. The optical response reflects change in the SP band of the island film as a results of NP binding as well as the SP extinction of the bound NPs (λ_{max} of the NPs in solution at ≈ 525 nm, Figure 16), which largely overlap. For 15 nm Au islands, the difference spectrum (Figure 17, inset) shows a distinct shoulder in the wavelength range of the SP band of the colloid, evidently corresponding to the absorbance of the bound

NPs. However, the overlap of the two SP bands does not enable effective discerning of the spectral behavior of the islands and the NPs in the case of 5.0 nm Au islands.

The HRSEM image in Figure 17A (right), as well as imaging and statistical analysis of the 5.0 nm transducers before and after binding of Man@AuNPs (Figure 18 and Table 3), provide additional evidences for Man@AuNP binding on the 5.0 nm Au island transducer surface. Note that the NPs are located mainly between islands rather than on the islands, which may be attributed to the effect of drying, a frequent issue.

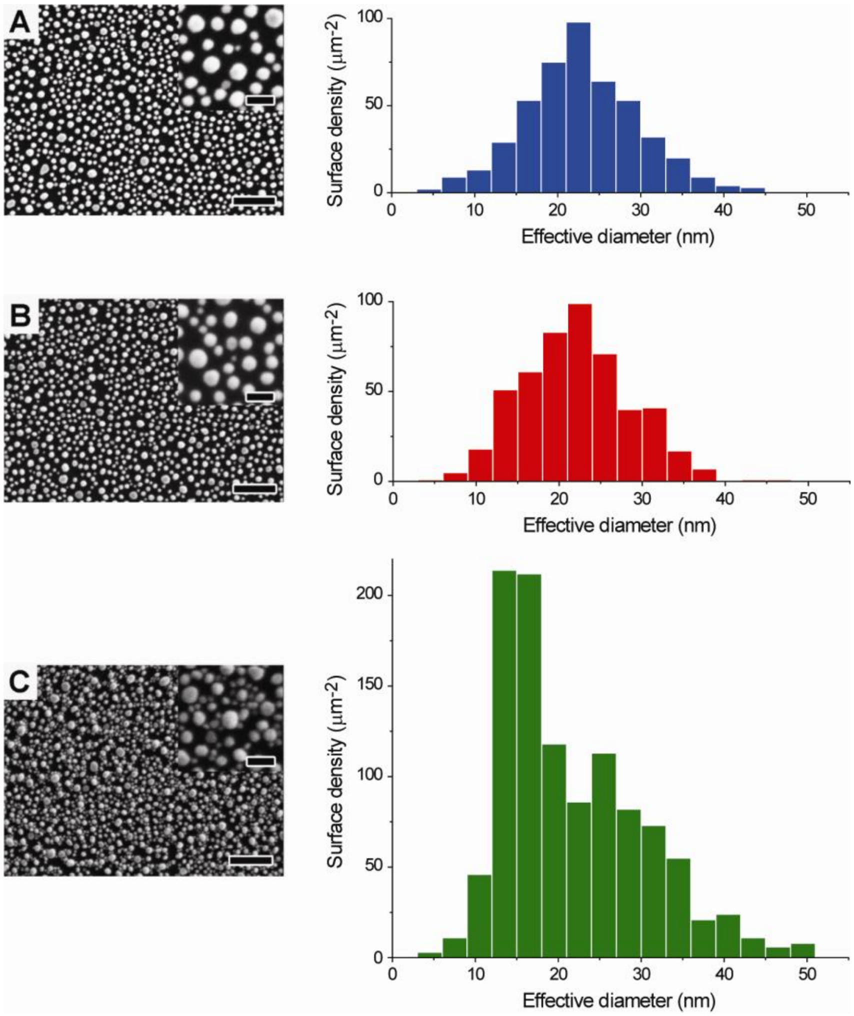

Figure 18. Left: HRSEM imaging of a bare 5.0 nm Au island transducer (A), a similar film after treatment with PEG-silane, mannose SAM and Con A (B), and a film similar to that in (C) after exposure to Man@AuNPs. Scale bars: 200 nm (large images), 50 nm (insets). Right: Statistical distribution of the equivalent particle diameter in the corresponding images (A)–(C).

Table 3. Particle surface density corresponding to images (A)–(C) in Figure 18.

Experiment	**System**	**Particles (cm^{-2})**
A	Bare Au	$(6.6 \pm 0.3)\cdot 10^{10}$
B	PEG-silane, mannose SAM, and Con A	$(6.9 \pm 0.4)\cdot 10^{10}$
C	Man@AuNPs	$(1.0 \pm 0.3)\cdot 10^{11}$

The difficulties associated with the study of NP binding to 5.0 nm islands, both in spectroscopy (overlap of the island and NP SP bands) and in imaging (similar diameter), can be largely alleviated by using 15 nm Au island transducer (Figure 3E). Such films present large, single-crystalline Au islands (major axis: 328 ± 117 nm) while displaying a substantially red-shifted SP band ($\lambda_{max} \approx 805$ nm). Binding of Man@AuNPs leads to a large increase in the intensity (0.09 abs. u.) and a significant red-shift (≈ 50 nm) of the island SP band [Figure 17B (left)], as well as the appearance of a well-defined band around 550 nm, attributed to the bound NPs. The latter directly relates the change in the Au island SP band to binding of the Man@AuNPs.

The spectroscopic data are supported by microscopic evidence [Figure 18B (right)], showing the individual Man@AuNPs attached to the Au islands. Note that a set of control experiments using 15 nm Au island transducers covered with (i) a mannose SAM, no Con A, exposed to Man@AuNPs (Figure 19A); (ii) a galactose SAM + Con A, exposed to Man@AuNPs (Figure 19B); and (iii) a mannose SAM + Con A, exposed to Gal@AuNPs (Figure 19C), provided firm support to the Carb@AuNP results.

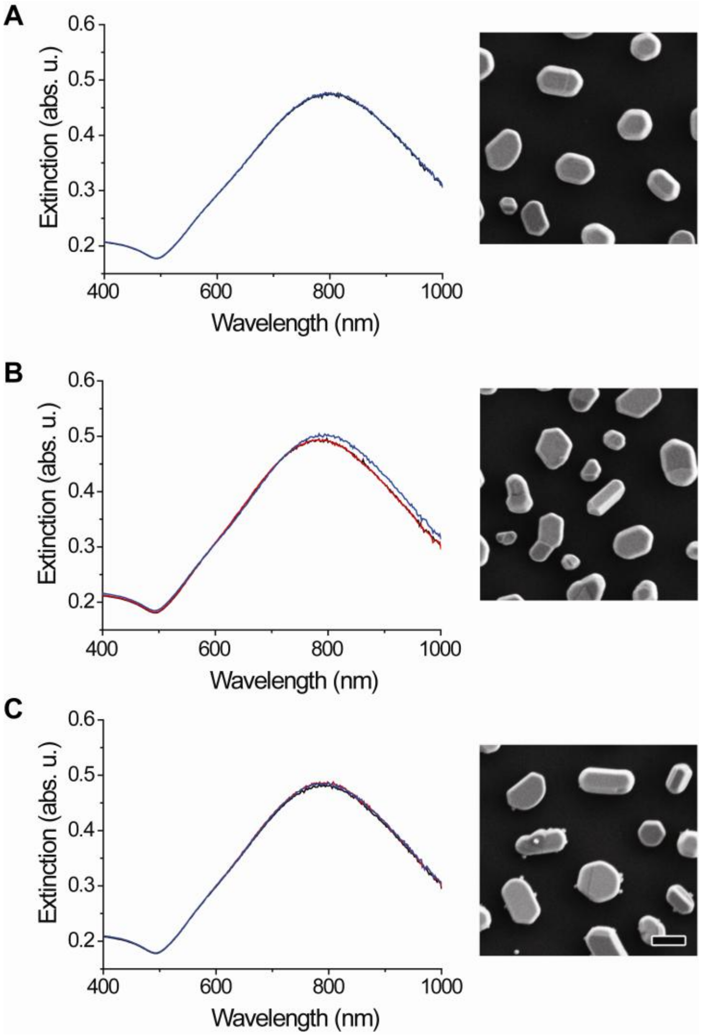

Figure 19. UV-vis spectra (left) and HRSEM images (right) corresponding to control binding assays using Carb@AuNPs on 15 nm Au island films, in the following sequence: (A) Mannose SAM–Man@AuNPs; (B) Galactose SAM–Con A–Man@AuNPs; (C) Mannose SAM–Con A–Gal@AuNPs. Spectra were recorded in solution after formation of a carbohydrate SAM (black lines), incubation with Con A solution (1 µM) (red lines), and incubation with Carb@AuNP solution (100 µL) (blue lines). In all cases the black and red lines nearly overlap. Scale bar: 200 nm.

2.6. Selectivity of Carbohydrate-derivatized Au Island Transducers

Au island transducers to Con A in the presence of excess non-specific protein was tested using BSA as the interfering protein. BSA contains 35 cysteine residues and thus represents an ideal non-specific competitor for binding to gold surfaces. The histogram in Figure 20 (left) presents the response of mannose-modified 5.0 nm Au island transducers to the following two-step procedure: (i) binding of Con A from solutions of different concentrations (0.5 µM, 50 nM, 5 nM) in the presence of a large excess of BSA (1.5 µM); (ii) binding of Man@AuNPs to the

Con A on the surface. The spectra corresponding to the experiments in Figure 20 are shown in Figure 21.

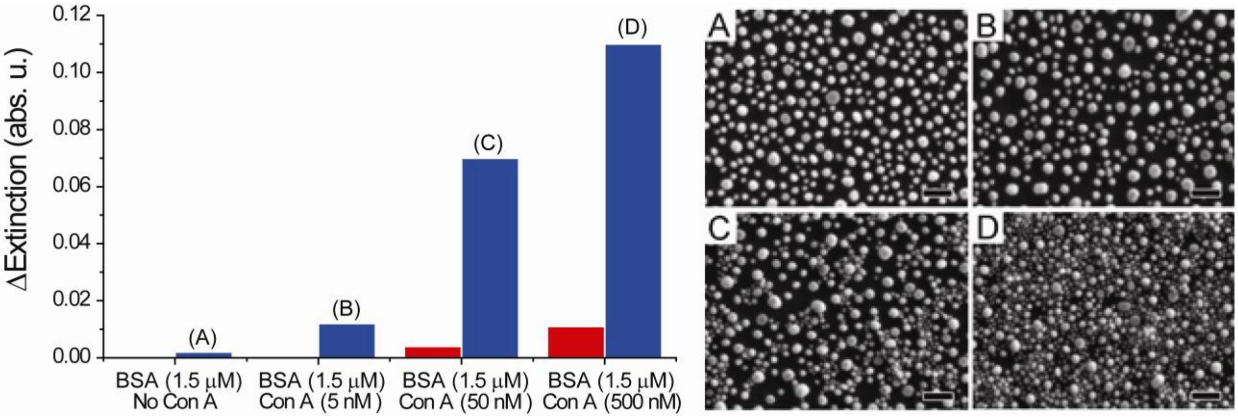

Figure 20. Left: histogram representation of the two-step response of mannose-modified, 5.0 nm Au island transducers to protein binding (red bars) and subsequent incubation with Man@AuNPs (blue bars). Protein solution compositions are indicated. The response is measured as change in maximum extinction. Right: Corresponding HRSEM images, performed after Man@AuNP binding and drying. The (A)–(D) notation corresponds to the steps described on the left. Scale bars: 100 nm.

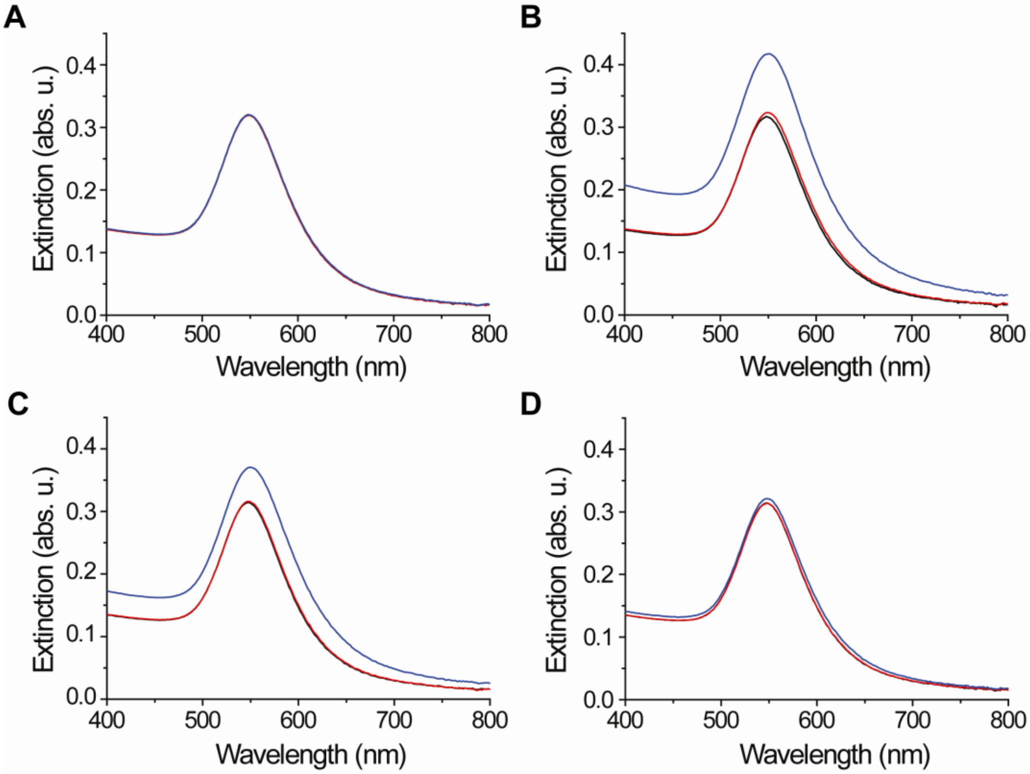

Figure 21. UV-vis spectra recorded in solution for 5.0 nm Au island transducers covered with a mannose SAM (black lines), after protein binding (red lines) and after incubation with Man@AuNPs (blue lines). Protein solution: (A) BSA (1.5 μM); (B) BSA (1.5 μM) + Con A (0.5 μM); (C) BSA (1.5 μM) + Con A (50 nM); (D) BSA (1.5 μM) + Con A (5 nM). In (A) the red and blue lines overlap.

The extinction difference after exposure to BSA alone is within the level of the instrument noise (0.001 abs. u.) (Table 4). Without the NP labels, binding of Con A produces a detectable signal for a Con A concentration of ≈ 50 nM and above. The detection limit goes down to < 5 nM upon application of the Man@AuNP labels, producing a signal of 0.012 abs. u. at a concentration ratio of 300:1 in favor of the non-specific protein. The HRSEM images in Figure 20 (right) show that the enhancement of the optical signal is directly related to the Man@AuNPs bound to the transducer surface. Hence, the mannose LSPR transducers display a high level of selectivity toward Con A.

Table 4. Extinction values corresponding to the results in Figure 20 (left) and Figure 21.

Experiment	**Protein**	**Δ Extinction**	
		Label-free	**Man@AuNPs**
A	BSA (1.5 μM)	Noise level	0.002
B	BSA (1.5 μM) + Con A (0.5 μM)	0.011	0.11
D	BSA (1.5 μM) + Con A (50 nM)	0.004	0.07
C	BSA (1.5 μM) + Con A (5 nM)	Noise level	0.012

3. Conclusion

Ultrathin gold island films prepared by evaporation on glass and annealing were derivatized with synthetic PEG-thiol terminated carbohydrates, to achieve receptor-modified LSPR transducers for monitoring and imaging of carbohydrate–protein interactions. The specific interaction between the monosaccharide mannose and the lectin Con A was used as a model to demonstrate specific recognition, with the non-specific sugar galactose serving as a control. Protein binding was monitored using a variety of techniques, including LSPR spectroscopy, ellipsometry, PM-IRRAS, and direct HRSEM imaging. Our ability to tune the morphology and optical properties of the Au island transducers proved beneficial in optimizing the system to the detected analyte, thereby maximizing the transducer response. When operated in a flow mode, the optimized LSPR system enabled determination of the association (k_{on}) and dissociation (k_{off}) rate constants for the interaction between Con A and immobilized mannose.

The ability of the tetrameric Con A to bind four mannose ligands was exploited for subsequent binding of Man@AuNPs, providing direct visualization of Con A binding as well as enhancement of the signal-to-noise by virtue of a dual-recognition assay in a sandwich configuration. Use of large, single-crystalline, atomically-flat Au islands furnished the possibility of superior SEM imaging of the NP-decorated Au islands, as well as effective separation of the SP bands of the islands and the bound NPs. The latter provided straightforward spectroscopic evidence of the NP binding to the islands. The separation of the SP bands enables effective analysis of the optical behavior of the hybrid system.

The results of this study indicate that carbohydrate-modified Au island films can be optimized and used as effective and sensitive LSPR transducers for studying carbohydrate–protein interactions. Corresponding Carb@AuNP labels modified with the same linker-carbohydrate molecules can serve to enhance the sensitivity in a sandwich configuration. The selectivity of the system was established using Con A assays in the presence of a large excess of the non-specific protein BSA.

Biosensing applications of this system using sugars relevant to pathogenic viruses, parasites or bacteria are underway.

4. Experimental Part

4.1. Chemical Synthesis

4.1.1. General Experimental Details

Commercial grade reagents and solvents were used without further purification except as indicated below. Deionized water was obtained from an in-house purification system (Millipore). The term “concentrated under reduced pressure” refers to the removal of solvents and other volatile material using a rotary evaporator while maintaining a water bath temperature around 40 °C. The compounds purified by flash chromatography are further concentrated by the removal of residual solvent under high vacuum (< 0.2 mbar). Room temperature (r.t.) refers to the ambient temperature (20–25 °C).

4.1.2. Physical Properties and Spectroscopic Measurements

^{1}H NMR and ^{13}C NMR spectra were measured with a Varian 400-MR, Varian 600-MR, Bruker ECP 400, Bruker AC 500, or Bruker AC 700 spectrometer. The residual proton signal of solvent at δ 7.26 ppm for $CDCl_3$, 3.34 ppm for CD_3OD, and 4.79 ppm for D_2O was used as an internal reference for ^{1}H spectra. For ^{13}C spectra, the chemical shifts are reported relative to the δ 77.36 ppm for $CDCl_3$ and 49.86 ppm for CD_3OD. Coupling constants (*J*) are reported in Hertz (Hz). Multiplicities are given as: *s* (singlet); *d* (doublet); *t* (triplet); *dd* (doublets of doublet); *bs* (broad singlet); *m* (multiplet) or *bm* (broad multiplet). High-resolution mass spectra (HRMS) analyses were performed by the mass service of the Free University Berlin. High resolution matrix-assisted laser desorption/ionisation (MALDI) and electrospray ionization (ESI) mass spectra were run on Bruker Autoflex Speed mass spectrometer and on an Agilent 6210 ESI-TOF mass spectrometer, respectively. Analytical thin layer chromatography (TLC) was performed on Kieselgel 60 F_{254} glass plates precoated with a 0.25 mm thickness of silica gel. The TLC plates were visualized with UV light and by staining with Hanessian solution (ceric sulfate and ammonium molybdate in aqueous sulfuric acid) or potassium permanganate solution (potassium permanganate in basic aqueous solution). Column chromatography was performed using Kieselgel 60 (230–400 mesh) silica gel with a typical 50–100:1 weight ratio of silica gel to crude product.

4.1.3. Compound Characterization

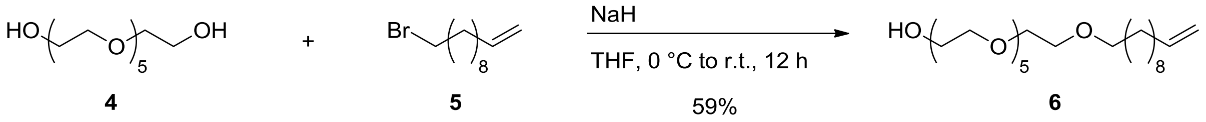

3,6,9,12,15,18-hexaoxanonacos-28-en-1-ol (6)

3,6,9,12,15-Pentaoxaheptadecane-1,17-diol **4** (10.4 mL, 41.4 mmol) and 11-bromoundec-1-ene **5** (3.0 mL, 13.8 mmol) were dissolved in THF (10 mL) under N_2 atmosphere and the reaction mixture was cooled to 0 °C. NaH (60% in mineral oil) (331 mg, 13.8 mmol) was then slowly added. The reaction mixture was warmed to r.t. and allowed to stir for 12 h. Water (10 mL) was then slowly added. The crude was extracted with DCM (25 mL) and the aqueous phase was washed with EtOAc (3×50 mL). The combined organic layers were concentrated under reduced pressure. The crude was then purified by flash column chromatography (silica gel, cyclohexane:EtOAc 1:1 to DCM:MeOH 9:1), dried under reduced pressure and *high vacuo* to give **6** (3.5 g, 59%) as yellowish oil.

Characterization data were consistent with previously reported data.[18]

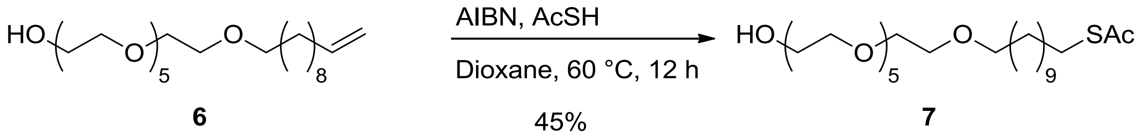

[1-[(Methylcarbonyl)thioundec-11-yl]hexa(ethylene glycol) (7)

To a solution of **6** (150 mg, 345 μmol) and AIBN (283 mg, 1.7 mmol) in dioxane (5 mL) was added AcSH (600 μL, 8.4 mmol). The reaction mixture was then allowed to stir for 12 h at 60 °C under N_2 atmosphere. The solvent was then evaporated and the crude was purified by flash column chromatography (silica gel, cyclohexane:EtOAc 1:1 to 1:9) dried under reduced pressure and *high vacuo* to give **7** (79 mg, 45%) as a yellowish oil.

Characterization data were consistent with previously reported data.[18]

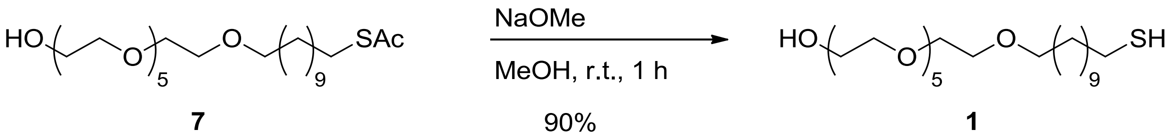

(1-Mercaptoundec-11-yl)hexa(ethylene glycol) (1)

7 (79 mg, 155 μmol) was dissolved in MeOH (5 mL) followed by the addition of NaOMe (42 mg, 773 μmol). The reaction was stirred at r.t. for 1 h. The crude was then neutralized with Amberlite 120 (H^+) resin, filtered, and washed with MeOH (10 mL). The solvent were removed under reduced pressure and the compound was dried under *high vacuo* to give the product **1** (71 mg, 90%) as yellowish oil.

Characterization data were consistent with previously reported data.[18]

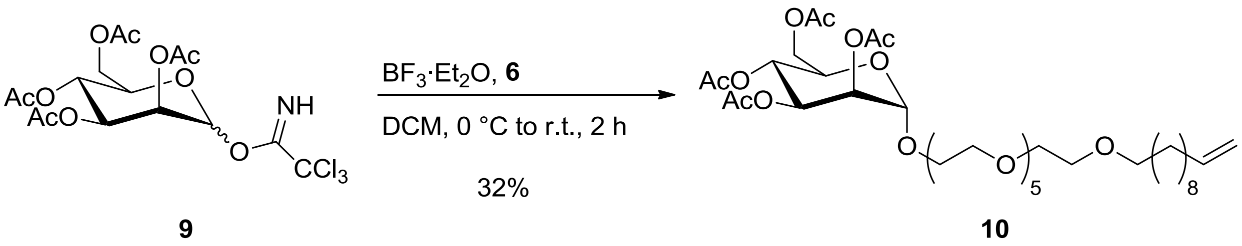

Undec-1-en-11-ylhexa(ethy1eneglycol)-2,3,4,6-penta-*O*-acetyl-α-D-mannopyranoside (10)

To a solution of **9** (330 mg, 670 μmol) and **6** (750 mg, 1.7 mmol) in DCM (5 mL) at 0 °C under N_2 atmosphere, was added $BF_3{\cdot}Et_2O$ (255 μL, 2.0 mmol) and the reaction mixture was allowed to stir for 2 h at 0 °C. The reaction mixture was then quenched with Et_3N (1 mL) and warmed to r.t. The solvent were removed under reduced pressure. The crude was dissolved in EtOAc (10 mL) and washed three times with water (3×10 mL). The organic layer was then dried over $MgSO_4$, filtered and evaporated under reduced pressure. The crude was then purified by column chromatography (silical gel, EtOAc:DCM 3:7 to 1:1), dried under reduced pressure and *high vacuo* to give **10** (163 mg, 32%) as colorless oil.[19]

R_f 0.32 (EtOAc:Hexane 4:1). ^{1}H NMR ($CDCl_3$, 400 MHz) δ 5.80–5.66 (*m*, 1H), 5.31–5.18 (*m*, 2H), 4.94–4.80 (*m*, 2H), 4.26–4.13 (*m*, 1H), 4.05–3.97 (*m*, 1H), 3.77–3.50 (*m*, 26H), 3.37 (*t*, *J* = 6.9 Hz, 2H), 2.08–1.92 (*m*, 12H), 1.52–1.48 (*m*, 2H), 1.32–1.21 (*m*, 12H). ^{13}C NMR ($CDCl_3$, 100 MHz) δ 170.4, 169.8, 169.6, 169.5, 139.0, 113.9, 97.5, 71.3, 70.5, 70.3, 69.8, 69.7, 69.3, 68.9, 67.2, 65.9, 63.4, 62.2, 33.6, 29.4, 29.3, 29.2, 29.1, 28.9, 28.7. HRMS (MALDI, positive mode) calcd. for $C_{37}H_{64}O_{16}Na$ $[M+Na]^+$: 787.4092, found: 787.4099.

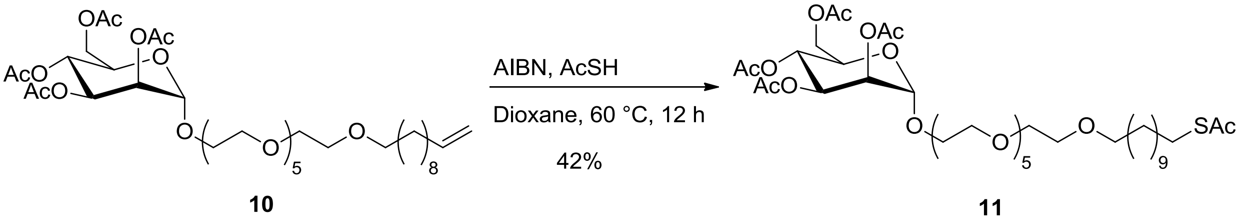

[1-[Methylcarbonyl)thio]undec-11-yl-hexa(ethyleneglycol)-2,3,4,6-*O*-acetyl-α-D-mannopyranoside (11)

To a solution of **10** (138 mg, 180 μmol) and AIBN (148 mg, 902 μmol) in dioxane (5 mL) was added AcSH (300 μL, 4.2 mmol). The reaction mixture was then allowed to stir for 12 h at 60 °C under N_2 atmosphere. The solvent was then evaporated and the crude was purified by flash column chromatography (silica gel, cyclohexane:EtOAc 1:1 to 1:9), dried under reduced pressure and *high vacuo* to give **11** (60 mg, 42%) as a yellowish oil.

R_f 0.32 (EtOAc:Hexane 4:1). ^{1}H NMR ($CDCl_3$, 400 MHz) δ 5.30–5.19 (*m*, 3H), 4.80 (*d*, *J* = 1.6 Hz, 1H), 4.22 (*dd*, *J* = 4.8, 12.1 Hz, 1H), 4.05–3.97 (*m*, 2H), 3.77–3.72 (*m*, 1H), 3.62–3.49 (*m*, 27H), 3.37 (*t*, *J* = 6.8 Hz, 2H), 2.79 (*t*, *J* = 7.4 Hz, 2H), 2.25 (*s*, 3H), 2.10 (*s*, 3H), 2.03 (*s*, 3H), 1.97 (*s*, 3H), 1.92 (*s*, 3H), 1.53–1.45 (*m*, 4H), 1.29–1.19 (*bm*, 17H). ^{13}C NMR ($CDCl_3$, 100 MHz) δ 195.9, 170.6, 169.9, 169.8, 169.7, 97.7, 71.5, 70.7, 70.6, 70.58, 70.56, 70.0, 69.9, 69.6, 69.1, 68.4, 67.4, 66.2, 30.6, 29.6, 29.5, 29.46, 29.43, 29.41, 29.1, 29.0, 28.8, 26.1, 20.8, 20.7, 20.6, 20.6. HRMS (MALDI, positive mode) calcd. for $C_{39}H_{68}O_{17}SNa$ $[M+Na]^+$: 863.4075, found: 863.4053.

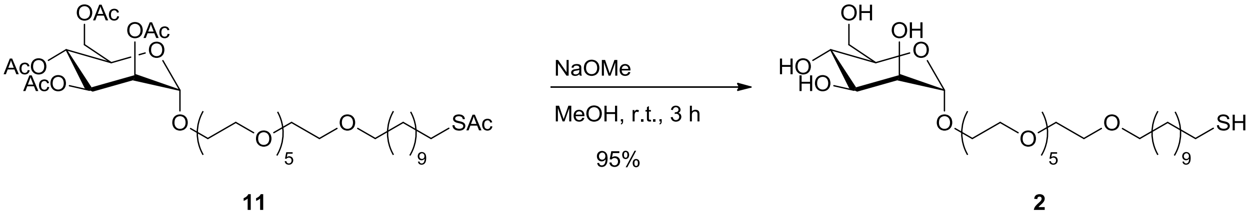

(1-Mercaptoundec-11-yl)hexaethyleneglycol-α-D-mannopyranoside (2)

Compound **11** (60 mg, 73.0 μmol) was dissolved in MeOH (5 mL) followed by the addition of NaOMe (2 mg, 36 μmol). The reaction was then stirred at r.t. After 2 h, NaOMe (1 mg, 17 μmol) was again added and the reaction mixture was then stirred for another 1 h. The crude was then neutralized with Amberlite 120 (H^+) resin, filtered, and the resin washed with MeOH (20 mL). The solvent were evaporated under reduced pressure and *high vacuo* to give the product as mixture of disulfide and thiol (44 mg, 95%) as yellowish oil.

^{1}H NMR (D_2O, 400 MHz) δ 4.79 (*d*, *J* = 1.61 Hz, 1H), 3.86–3.81 (*m*, 3H), 3.73–3.55 (*m*, 34H), 3.46 (*t*, *J* = 6.6 Hz, 2H), 2.68[i] (*t*, *J* = 9.6 Hz, 1H), 2.51–2.46[ii] (*m*, 1H), 1.70–1.52 (*m*, 4H), 1.31 (*bs*, 18H). ^{13}C NMR (D_2O, 100 MHz) δ 103.3, 73.2, 71.1, 70.9, 70.7, 70.2, 70.1, 69.9, 69.7, 67.2, 66.4, 61.5, 38.4, 33.8, 29.28, 29.27, 29.25, 29.23, 29.17, 29.13, 29.11, 29.10, 28.8, 28.76, 28.74, 27.97, 27.94. HRMS (ESI, positive mode) calcd. for $C_{29}H_{58}O_{12}SNa$ $[M+Na]^+$: 652.3450, found: 652.3467.

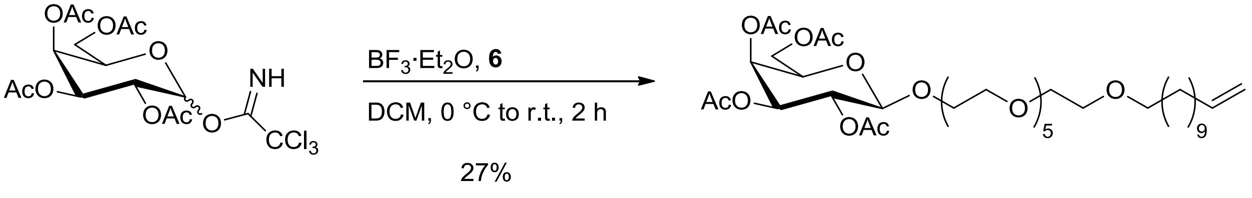

13 **14**

Undec-1-en-11-ylhexa(ethy1eneglycol)-2,3,4,6-penta-O-acetyl-β-D-galactopyrannoside (14)

To a solution of **13** (400 mg, 812 μmol) and **6** (950 mg, 2.2 mmol) in DCM (5 mL) at 0 °C, was added $BF_3 \cdot Et_2O$ (309 μL, 2.4 mmol) and the reaction mixture was allowed to stir for 2 h at 0 °C under N_2 atmosphere. The reaction mixture was then quenched with Et_3N (1 mL) and warmed to r.t. Solvent was then removed under reduced pressure. The crude was dissolved in EtOAc (10 mL) and washed with water (3×10 mL). The organic layer was then dried over $MgSO_4$, filtered and evaporated under reduced pressure. The crude was purified by column chromatography (silical gel, EtOAc:DCM 3:7 to 1:1), dried under reduced pressure and *high vacuo* to give **14** (167 mg, 27%) as colorless oil.[20]

R_f 0.36 (EtOAc). ^{1}H NMR ($CDCl_3$, 300 MHz) δ 5.87–5.85 (*m*, 1H), 5.39 (*dd*, *J* = 0.9, 3.3 Hz, 1H), 5.24–5.17 (*m*, 1H), 5.03–4.90 (*m*, 3H), 4.56 (*dd*, *J* = 8.1 Hz, 1H), 4.20–4.11 (*m*, 1H), 4.00–3.88 (*m*,

---

[i] C(H_2)–S- from disulfide.

[ii] C(H_2)–SH from thiol.

2H), 3.78–3.71 (*m*, 1H), 3.68–3.55 (*m*, 20H), 3.44 (*t*, *J* = 6.6 Hz, 2H), 2.15 (*s*, 3H), 2.10–2.05 (*m*, 6H), 1.98 (*s*, 3H), 1.59–1.53 (*bm*, 2H), 1.39–1.27 (*bm*, 12H). ^{13}C NMR ($CDCl_3$, 75 MHz) δ 170.6, 170.2, 170.1, 139.2, 114.1, 101.4, 71.5, 70.71, 70.68, 70.64, 70.60, 70.5, 70.3, 70.1, 33.8, 29.6, 29.5, 29.46, 29.40, 29.1, 28.9, 26.1, 20.7, 20.7, 20.6, 20.5. HRMS (ESI, positive mode) calcd. for $C_{37}H_{64}O_{16}Na$ $[M+Na]^+$: 787.4087, found: 787.4090.

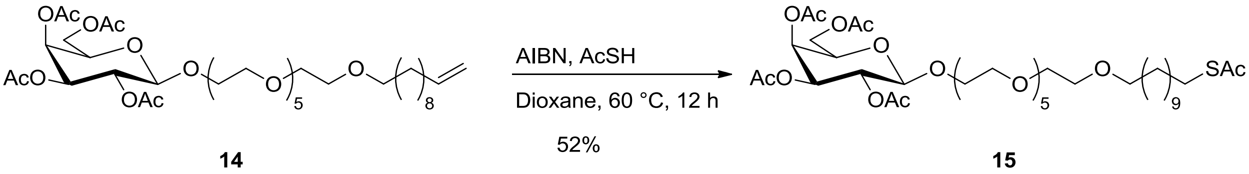

[1-[Methylcarbonyl)thio]undec-11-yl-hexa(ethyleneglycol)-2,3,4,6-O-acetyl-β-D-galactopyrannoside (15)

To a solution of **14** (143 mg, 187 μL) and AIBN (153 mg, 935 μmol) in dioxane (5 mL) was added AcSH (300 μL, 4.2 mmol) under N_2 atmosphere. The reaction mixture was then allowed to stir for 12 h at 60 °C. The solvent was then evaporated and the crude was purified by flash column chromatography (silica gel, cyclohexane:EtOAc 1:1 to 1:9), and dried under *high vacuo* to give **15** (80 mg, 52%) as a yellowish oil.

^{1}H NMR ($CDCl_3$, 400 MHz) δ 5.33 (*dd*, *J* = 3.4, 0.9 Hz, 1H), 5.14 (*dd*, *J* = 10.5, 8.0 Hz, 1H), 4.97 (*dd*, *J* = 10.5, 3.4 Hz, 1H), 4.52 (*d*, *J* = 8.0 Hz, 1H), 4.10 (*dd*, *J* = 6.7, 4.3 Hz, 2H), 3.94–3.85 (*m*, 2H), 3.62–3.55 (*m*, 27H), 3.55–3.48 (*m*, 2H), 3.39 (*t*, *J* = 6.8 Hz, 2H), 2.79 (*t*, *J* = 7.4 Hz, 2H), 2.28 (*s*, 3H), 2.10 (*s*, 3H), 2.02 (*s*, 3H), 1.98 (*s*, 3H), 1.93 (*s*, 3H), 1.53–1.45 (*m*, 4H), 1.29–1.19 (*bm*, 17H).

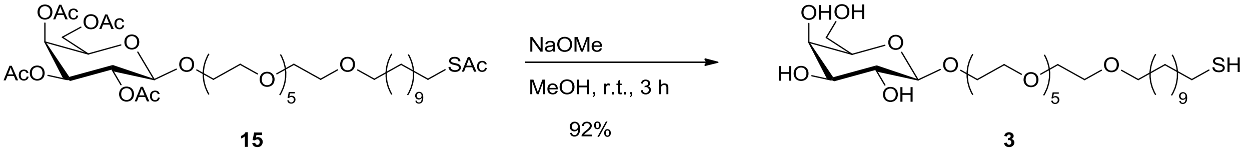

(1-Mercaptoundec-11-yl)hexaethyleneglycol-β-D-galactopyrannoside (3)

Compound **15** (80 mg, 97 μmol) was dissolved in MeOH (5 mL) followed by the addition of sodium methoxide (2.6 mg, 48 μmol) and the reaction was stirred at r.t. After 2 h, sodium methoxide (1.3 mg, 24 μmol) was again added and the reaction mixture was then stirred for another 1 h. The crude was then neutralized with Amberlite 120 (H^+) resin, filtered, and the resin washed with MeOH (15 ml). The solvent were removed under reduced pressure, dried under *high vacuo* to give the product **3** (56 mg, 92%) as yellowish oil.

^{1}H NMR (D_2O, 400 MHz) δ 4.25 (*d*, *J* = 7.2 Hz, 1H), 4.04–3.99 (*m*, 1H), 3.83–3.44 (*m*, 38H), 2.68 (*t*, *J* = 7.2 Hz, 2H), 1.72–1.53 (*m*, 4H), 1.32–1.29 (*m*, 14H). ^{13}C NMR (D_2O, 100 MHz) δ 105.1, 76.7, 74.9, 72.6, 72.4, 71.6, 71.5, 71.2, 70.3, 69.6, 39.9, 30.8, 30.7, 30.65, 30.62, 30.60, 30.3, 30.2, 29.5, 27.2. HRMS (ESI, positive mode) calcd. for $C_{29}H_{58}O_{12}SNa$ $[M+Na]^+$: 652.3463, found: 652.3468.

4.2. Materials and Methods

4.2.1. Preparation of Gold Films

Continuous, 100 nm thick gold films were prepared by evaporation on microscope cover-glass slides (Menzel-Glaser, N^o 5) cut to 22×9 mm^2, at a deposition rate of 0.1 nm·s^{-1}. After deposition, annealing of the Au-coated slides was carried out in air at 200 °C for 20 h in an oven (Ney Vulcan 3-550). The heating rate was 5 °C·min^{-1} and the annealed slides were left to cool in air to r.t. and then stored under dry conditions.

Discontinuous island-type Au films (nominal thickness: 1.5, 2.5, 5.0, 10, and 15 nm) were prepared by evaporation on bare microscope cover-glass slides (Menzel-Glaser, N^{O}3), cut to 22×9 mm^2, at a deposition rate of 0.01 nm·s^{-1}. After deposition, annealing of the Au-coated slides was carried out in air at 570 °C for 10 h in the oven. The heating rate was 5 °C·min^{-1} and the annealed slides were left to cool in air to r.t. and then stored under dry conditions. The long annealing at 570 °C induces partial embedding of the islands in the glass substrate, thereby stabilizing the system.

4.2.2. Au Surface Modification and Interaction with Con A

Au films, either continuous or island-type, were treated 20 min in a UV-ozone cleaning system (UVOCS model T10·10/OES/E), dipped in ethanol for 20 min with stirring and dried under a nitrogen stream. Island-type Au films were then incubated for 2 h in 2 mM PEG-silane in ethanolic solution, washed in ethanol for 20 min with stirring and dried under a N_2 stream.

Self-assembly of the linker **1** or the carbohydrate-modified linker molecules **2** and **3** (Scheme 1) on Au substrates was carried out by wetting the Au surface with an ethanolic solution (50 µL, 1 mM) of the respective compound. Throughout the assembly process the slides were placed in a Petri dish containing an ethanol pool in a closed space to prevent evaporation of the solvent during self-assembly. Following 20 min immersion the samples were washed 20 min in pure ethanol with stirring and dried under a N_2 stream.

Prior to incubation with Con A, each sample was washed 20 min with stirring in 10 mM Tris-HCl buffer (pH 7.4) containing NaCl (0.1 M), $CaCl_2$ (1 mM) and $MnCl_2$ (1 mM). This solution is hereafter referred to as the buffer solution. The buffer wash was followed by extensive rinsing in triply-distilled water and drying under a nitrogen stream. The transducer surface was then wetted with Con A (100 µL, 1 µM) in the buffer solution for 1 h in a Parafilm-sealed Petri dish, washed in the pure buffer for 20 min with stirring, rinsed extensively with triply-distilled water and dried under a N_2 stream.

4.2.3. Preparation of the Carb@AuNPs

Water-soluble, citrate-stabilized AuNPs were prepared according to the method of Turkevich using sodium citrate as the reducing and capping agent.[21] In order to prepare mannose- or galactose-functionalized AuNPs, the citrate-capped AuNP solution (900 µL) were mixed with ethanolic solution of mannose linker **2** or galactose-linker **3** (100 µL, 10 mM) and incubated for 24 h. The solution was then centrifuged 45 min at 14500 rpm in a centrifuge (Eppendorf MiniSpin) until a compact red pellet was formed. The supernatant (900 µL) was removed and replaced with buffer solution (900 µL) and the pellet was resuspended upon vortexing. The procedure was repeated six times in order to completely remove traces of citrate and mannose linker or galactose-linker, and the resulting solution was stored at 4 °C. The mean diameter of the Carb@AuNPs, determined by TEM imaging, was 16.2 ± 3.1 nm (Figure 16).

4.2.4. Binding Assays with Carb@AuNPs

The binding assays were performed using Au island films of 5.0 or 15 nm (nominal thickness), covered with mannose or galactose SAMs, incubated with Con A solution and washed as described above. To achieve maximum NP binding, the transducer surface was wetted either several times, 30 min each, with Carb@AuNPs (50 µL), or in one step by incubation in Carb@AuNPs (100 µL) for 1–3 h or overnight, in a Parafilm-sealed Petri dish, followed by washing in pure buffer for 20 min with stirring. Transmission UV-vis spectra were recorded in a 1 cm quartz cuvette filled with pure buffer. Samples were then rinsed with triply-distilled water, dried under a nitrogen stream and used for HRSEM imaging.

4.2.5. Fixation and Staining of Biological Samples

The specimens underwent fixation and staining according to a common procedure, as detailed previously.[7a]

4.2.6. LSPR Spectroscopy

Transmission UV-vis spectra of Au island films were collected in air or in solution using a Varian CARY 50 spectrophotometer operated at a wavelength resolution of 2 nm and an average acquisition time per point of 0.2 s, with air or buffer as baseline, respectively. Spectra were measured either in air using a specially-designed holder ensuring reproducible position of the analyzed slides, or in solution by placing the slides in a 1 cm (pathlength) quartz cuvette. Measurements at different stages of the experiment were carried out in air after washing with water and drying the sample, or in solution after washing the sample with pure buffer.

4.2.7. Kinetic Experiments

Kinetic experiments were carried out using a flow system consisting of a controlled syringe-based pumping unit (Longer Precision Pump Co.), manual selection valves and a micro flow-cell (Figure 13). The home-made micro flow-cell was designed to accommodate 8×8 mm^2 samples while minimizing the cell volume (60 µL). The solution volume required for performing the kinetic assay was ≈ 0.5 mL. LSPR transducers comprising Au island films (5.0 nm nominal thickness) coated with various SAMs (linker, mannose, galactose) were cut to 8×8 mm^2 pieces and placed in the micro flow-cell. The cell was filled with buffer solution and mounted in the Varian CARY 50 spectrophotometer. The flow rate was set to 50 $\mu L \cdot min^{-1}$ and the flux was maintained constant throughout the experiment. The extinction was measured in the transmission mode at a constant wavelength of 545 nm with 0.3 s integration time and 1 s acquisition time.

4.2.8. Spectroscopic Ellipsometry

Ellipsometric measurements were performed with 100 nm continuous Au films using a spectroscopic ellipsometer (Model PhE 102, Angstrom Advanced, USA). Data were collected at an incident angle of 70° in the spectral range 400–800 nm at a resolution of 5 nm. Measurements were carried out in air at different stages of the experiment after washing with water and drying the sample. The film apparent thickness was obtained by fitting the ellipsometric data by means of Film Wizard software (Scientific Computing International), using Cauchy's equation for approximation of the film refractive index.

4.2.9. PM-IRRAS

PM-IRRAS measurements were carried out with the same samples used for ellipsometry, using a FTIR Bruker Tensor 27 spectrometer with a polarization modulation setup (PMA50), equipped with a photoelastic modulator (PEMTM 100, Hinds Instruments, USA). All spectra were recorded at a resolution of 4 cm^{-1}. The PEM maximum efficiency was set for the half-wave retardation at 2600 cm^{-1} for analysis of the C=O stretching modes (≈ 1650 cm^{-1}) and the NH bending modes (≈ 1545 cm^{-1}). Each spectrum represents an average of 1420 scans collected within a total time of 20 min, with the first 100 scans measured as background. The angle of incident light was set to 85°. PM-IRRAS spectra were collected in air after purging the sample and detector compartments with pure nitrogen, and processed using the OPUS software (Bruker). Spectra were recorded at different stages of the experiment after washing with water and drying the sample.

4.2.10. SEM and HRSEM

SEM and HRSEM imaging was performed using an ULTRA 55 FEG ZEISS microscope. Measurements were carried out at a working distance of 3 mm using an Everhart-Thornley SE detector at an applied voltage of 2 kV. Cr-coated samples were imaged using a high-efficiency in-lens SE detector at an applied voltage of 20 kV. Cr coating was obtained using an EMITECH K575X sputtering apparatus.

4.2.11. TEM

Measurements were performed with a Philips CM-120 transmission electron microscope operating at 120 kV, equipped with a CCD camera (2k×2k, Gatan Ultrascan 1000). TEM samples were prepared by drying a drop of Man@AuNPs solution on copper grids coated with cellulose and carbon.

4.2.12. Size Distribution of Au Nanostructures

Statistical analysis of the distribution of particle diameters (including Au islands and NPs) in HRSEM images was carried out using ImageJ software. An equal area of 0.1785 μm^2 was analyzed in each picture. Four different pictures were analyzed for each histogram.

5. Abbreviations

a. u.	arbitrary unit
abs. u.	absorbance unit
Ac_2O	acetic anhydride
AcSH	thioacetic acid
AIBN	azobisisobutyronitrile
Au	gold
AuNP	gold nanoparticle
$BF_3 \cdot Et_2O$	boron trifluoride diethyl etherate
bm	broad multiplet
bs	broad singlet
BSA	bovine serum albumin
calcd.	calculated
Carb@AuNP	carbohydrate-coated gold nanoparticle
Con A	Concanavalin A
Cr	chromium
d	day(s)
d	doublet
DBU	1,8-diazabicyclo[5.4.0]undec-7-ene
DCM	dichloromethane
dd	doublets of doublet
deg.	degree
ESI	electrospray ionization
Et_3N	triethylamine
EtOAc	ethylacetate
FTIR	Fourier transform infrared spectroscopy
Gal@AuNP	galactose-coated gold nanoparticle
h	hour(s)
HRMS	high

HRSEM	high-resolution mass spectrometry
Hz	Hertz
J	coupling constant
K_a	association equilibrium constant
K_d	dissociation equilibrium constant
k_{off}	dissociation rate constant
k_{on}	association rate constant
LSPR	localized surface plasmon resonance
m	multiplet
MALDI	matrix-assisted laser desorption/ionisation
Man@AuNP	mannose-coated gold nanoparticle
MeOH	methanol
min	minute(s)
N	number of experiment(s)
NaOMe	sodium methoxide
NMR	nuclear magnetic resonance
NP	nanoparticle
PEG	polyethylene glycol
PM-IRRAS	polarization-modulation infrared reflection-absorption spectroscopy
ppm	parts-per-million
QCM	quartz crystal microbalance
r.t.	room temperature
RIS	refractive index sensitivity
s	second(s)
s	singlet
SAM	self-assembled monolayer
S.D.	standard deviation
SEM	scanning electron microscope
SP	surface plasmon

SPR	surface plasmon resonance
t	triplet
TCA	trichloroacetimidate
TEM	transmission electron microscope
THF	tetrahydrofuran
TLC	thin layer chromatography
Tris-HCl	tris(hydroxymethyl)aminomethane hydrochloride
δ	chemical shift

6. Acknowledgments

I was fortunate to collaborate on this project with members of Professor Rubinstein's group at the Weizmann Institute (Re'hovot, Israel). First of all, I wish to express my sincere thanks to Professor Israel Rubinstein, for inviting me for three months in his laboratory as well as for providing me with all the necessary facilities and equipment during my stage in Israel.

I place on record my sincere gratitude to Alexander B. Tesler and Dr. Giuliano Bellapadrona for the intensive work input they made on the sensing experiments. They both have been my tutors on this project and took time to teach me principles of LSPR and how to perform a myriad of experiments related to the project. I fully appreciate their precious help, guidance, and the efforts they made to turn out the scientific work into a scientific publication. Part of the work presented in this chapter would not have been possible without their relevant contribution.

I want to express also my sincere appreciation to Dr. Alexander Vaskevich for the fruitful discussions on biosensing issues and for sharing with me his right and rigorous analysis on scientific matters.

Finally, I take also the opportunity to thank Dr. Laila H. Hossain for initiating the collaborative work with the Weizmann Institute and for the compounds she left behind, but also Dr. Raghavendra Kikkeri for the help and advice he provided on synthetic issues.

7. References

---

[1] (a) Jason-Moller, L.; Murphy, M.; Bruno, J. *Curr. Protoc. Protein Sci.* **2006**, *Chapter 19*, Unit 19-13. (b) Homola, J. *Chem. Rev.* **2008**, *108*, 462. (c) Piliarik, M.; Vaisocherova, H.; Homola, J. *Method. Mol. Biol.* **2009**, 65. (d) Homola, J. *Anal. Bioanal. Chem.* **2003**, *377*, 528. (c) Zhao, J.; Zhang, X. Y.; Yonzon, C. R.; Haes, A. J.; Van Duyne, R. P. *Nanomedicine* **2006**, *1*, 219. (d) Hutter, E.; Fendler, J. H. *Adv. Mater.* **2004**, *16*, 1685.

[2] (a) Marinakos, S. M.; Chen, S. H.; Chilkoti, A. *Anal. Chem.* **2007,** *79*, 5278. (b) Murphy, C. J.; Gole, A. M.; Hunyadi, S. E.; Stone, J. W.; Sisco, P. N.; Alkilany, A.; Kinard, B. E.; Hankins, P. *Chem. Commun.* **2008**, 544. (c) Nusz, G. J.; Curry, A. C.; Marinakos, S. M.; Wax, A.; Chilkoti, A. *ACS Nano* **2009**, *3*, 795. (d) Stuart, D. A.; Haes, A. J.; Yonzon, C. R.; Hicks, E. M.; Van Duyne, R. P. *IEE Proceedings: Nanobiotechnology* **2005**, *152*, 13. (e) Jennings, T.; Strouse, G. Past, present, and future of gold nanoparticles. In *Bio-Applications of Nanoparticles*, Springer-Verlag Berlin: Berlin, 2007; Vol. 620, pp 34. (f) Lu, X. M.; Rycenga, M.; Skrabalak, S. E.; Wiley, B.; Xia, Y. N. *Annu. Rev. Phys. Chem.* **2009**, *60*, 167. (g) Nath, N.; Chilkoti, A. *Anal. Chem.* **2004**, *76*, 5370. (h) Nath, N.; Chilkoti, A. *Anal. Chem.* **2002**, *74*, 504. (i) Sannomiya, T.; Hafner, C.; Voros, J. *J. Biomed. Opt.* **2009**, *14*, 64027. (j) Rindzevicius, T.; Alaverdyan, Y.; Dahlin, A.; Hook, F.; Sutherland, D. S.; Kall, M. *Nano Letters* **2005**, *5*, 2335. (k) Hu, M.; Chen, J. Y.; Li, Z. Y.; Au, L.; Hartland, G. V.; Li, X. D.; Marquez, M.; Xia, Y. N. *Chem. Soc. Rev.* **2006**, *35*, 1084. (l) Dahlin, A.; Zach, M.; Rindzevicius, T.; Kall, M.; Sutherland, D. S.; Hook, F. *J. Am. Chem. Soc.* **2005**, *127*, 5043. (m) Jonsson, M. P.; Jonsson, P.; Dahlin, A. B.; Hook, F. *Nano Letters* **2007**, *7*, 3462. (n) Lahav, M.; Vaskevich, A.; Rubinstein, I. *Langmuir* **2004**, *20*, 7365. (o) Sannomiya, T.; Sahoo, P. K.; Mahcicek, D. I.; Solak, H. H.; Hafner, C.; Grieshaber, D.; Voros, J. *Small* **2009**, *5*, 1889. (p) Szunerits, S.; Praig, V. G.; Manesse, M.; Boukherroub, R. *Nanotechnology* **2008**, *19*, 195712.

[3] (a) Vaskevich, A.; Rubinstein, I., LSPR spectroscopy. In *Handbook of Biosensors and Biochips*, Marks, R.; Cullen, D.; Lowe, C.; Weetall, H. H.; Karube, I. Eds. Wiley: Chichester, **2007**; Vol. 1. (b) Willets, K. A.; Van Duyne, R. P. *Annu. Rev. Phys. Chem.* **2007**, *58*, 267.

[4] (a) Van Duyne, R.P. *Science*, **2004**, *306*, 985. (b) Haes, A.J.; Haynes, C.L.; McFarland, A.D.; Zou, S.; Schatz, G.C.; Van Duyne, R.P. *MRS Bull.*, **2005**, *30*, 368. (d) Kelly, K.L.; Coronado, E.; Zhao, L.; Schatz, G.C. *J. Phys. Chem. B*, **2003**, *107*, 668.

[5] (a) Brockman, J.M.; Nelson, B.P.; Corn, R.M. *Annu. Rev. Phys. Chem.* **2000**, *51*, 41. (b) Knoll, W. *Annu. Rev. Phys. Chem.* **1998**, *49*, 569. (c) Knobloch, H.; Brunner, H.; Leitner, A.; Aussenegg, F.; Knoll, W. *J. Chem. Phys.* **1993**, *98*, 10093.

[6] (a) Miller, M.M.; Lazarides, A.A. *J. Phys. Chem. B*, **2005**, *109*, 21556. (b) Jensen, T.R.; Duval, M.L.; Kelly, L.; Lazarides, A.; Schatz, G.C.; Van Duyne, R.P. *J. Phys.Chem. B.* **1999**, *103*, 9846.

[7] (a) Bendikov, T. A.; Rabinkov, A.; Karakouz, T.; Vaskevich, A.; Rubinstein, I. *Anal. Chem.* **2008**, *80*, 7487. (b) (a) Karakouz, T.; Vaskevich, A.; Rubinstein, I. *J. Phys. Chem. B* **2008**, *112*, 14530.

[8] (a) Rhodes, J. M.; Campbell, B. J.; Yu, L. G. *Biochem. Soc. Trans.* **2008**, *36*, 1482. (b) Sarter, K.; Mierke, C.; Beer, A.; Frey, B.; Fuhrnrohr, B. G.; Schulze, C.; Franz, S. *Autoimmunity* **2007**, *40*, 345. (c) Lloyd, D. H.; Viac, J.; Werling, D.; Rème, C. A.; Gatto, H. *Vet. Dermatol.* **2007**, *18*, 197. (d) Howes, L.; Jones, R. *J. Reprod. Immunol.* **2002**, *53*, 181. (e) Stringer, S. E. *Biochem. Soc. Trans.* **2006**, *34*, 451. (f) Yu, L. G. *Glycoconjugate J.* **2007**, *24*, 411.

[9] Seeberger, P. H.; Werz, D. B. *Nature* **2007**, *446*, 1046.

---

[10] Lis, H.; Sharon, N. *Annu. Rev. Biochem.* **1973**, *42*, 541.

[11] (a) Mann, D. A.; Kanai, M.; Maly, D. J.; Kiessling, L. L. *J. Am. Chem. Soc.* **1998**, *120*, 10575. (b) Nahálková, J.; Svitel, J.; Gemeiner, P.; Danielsson, B.; Pribulová, B.; Petrus, L. *J. Biochem. Bioph. Methods* **2002**, *52*, 11. (c) Smith, E. A.; Thomas, W. D.; Kiessling, L. L.; Corn, R. M. *J. Am. Chem. Soc.* **2003**, *125*, 6140. (d) Yonzon, C. R.; Jeoungf, E.; Zou, S. L.; Schatz, G. C.; Mrksich, M.; Van Duyne R. P. *J. Am. Chem. Soc.* **2004**, *126*, 12669. (e) Vornholt, W.; Hartmann, M.; Keusgen, M. *Biosens. Bioelectron.* **2007**, *22*, 2983. (f) Kitano, H.; Takahashi, Y.; Mizukami, K.; Matsuura, K. *Colloid. Surf. B.* **2009**, *70*, 91. (g) Mori, T.; Toyoda, M.; Ohtsuka, T.; Okahata, Y. *Anal. Biochem.* **2009**, *395*, 211.

[12] (a) Karakouz, T.; Tesler, A. B.; Bendikov, T. A.; Vaskevich, A.; Rubinstein, I. *Adv. Mater.* **2008**, *20*, 3893. (b) Karakouz, T.; Holder, D.; Goomanovsky, M.; Vaskevich, A.; Rubinstein, I. *Chem. Mater.* **2009**, *21*, 5875.

[13] Ron, H.; Matlis, S.; Rubinstein, I. *Langmuir* **1998**, *14*, 1116.

[14] Barth, A. *BBA-Bioenergetics* **2007**, *1767*, 1073.

[15] Kedem, O.; Tesler, A. B.; Vaskevich, A.; Rubinstein, I. *ACS Nano*, **2011**, *5*, 748.

[16] (a) Kalyuzhny, G.; Schneeweiss, M. A.; Shanzer, A.; Vaskevich, A.; Rubinstein, I. *J. Am. Chem. Soc.* **2001**, *123*, 3177. (b) Kalyuzhny, G.; Vaskevich, A.; Schneeweiss, M. A.; Rubinstein, I. *Chem. Eur. J.* **2002**, *8*, 3850.

[17] Kalyuzhny, G.; Vaskevich, A.; Ashkenasy, G.; Shanzer, A.; Rubinstein, I. *J. Phys. Chem. B.* **2000**, *104*, 8238.

[18] Palegrosdemange, C.; Simon, E. S.; Prime, K. L.; Whitesides, G. M. *J. Am. Chem.Soc.* **1991**, *113*, 12.

[19] Kerekgyarto, J.; Kamerling, J. P.; Bouwstra, J. B.; Vliegenthart, J. F. G. *Carbohydr. Res.* **1989**, *186*, 51.

[20] Yu, H.; Chen, X. *Org. Lett.* **2006**, *8*, 2393.

[21] Enüstün, B. V.; Turkevich, J. *J. Am. Chem. Soc.* **1963**, *85*, 3317.

Chapter 6

Conclusion and Outlook

Rapid progress in nanoscience and its potential applications have spurred observers to predict that nanotechnology will be the foremost science of the 21st century. Nanomaterials are beginning to have a major impact on research and applications across the material and life sciences. While wide varieties of nanomaterials have been prepared with proteins, DNA, lipids and polymers, serious limitations arise with the neo-glycoconjugates due to the ambiguous structures and lack of well-defined carbohydrates.

My doctoral work focused on the pragmatic development of useful and relevant carbohydrate-based systems for biology and medicine. Therefore, I have investigated the role of different carbohydrate constructs ranging from monovalent to polyvalent nanoscale materials and their application in molecular diagnostics, biosensing, imaging, and medicine.

In the chapter 1, I summarized different strategies for preparing multivalent carbohydrate probes that have been prepared over the last five years in the Seeberger laboratory and to extensively describe their major applications in molecular diagnostics, biosensing, and imaging. Carbohydrate functionalized architectures (i.e. nanoparticles or surfaces) are meeting an important need for studying the multivalent interactions between carbohydrates and other biomolecules. Innovations in nanomaterials are revolutionizing how these carbohydrate interfaces are studied and highlighting their importance in the case of biochemical interactions. The Seeberger group has developed a myriad of different polyvalent systems with the aim of direct application. This chemistry is at the interface with other disciplines and success in the scientific challenges requires a rational design of the chemical structures conform to the proper intent.

As a first example of direct application of such carbohydrate systems in medical imaging, chapter 2 described the synthesis of a bifunctional chelator construct, that simultaneously coordinate ^{99m}Tc-metal cores and tether biomolecules (i.e. carbohydrates) for selective targeting and imaging of specific organs. Synthesis and subsequent investigation of the *in vivo* characteristics of this novel class of compounds is the focus of ongoing studies. Ultimately, the full potential of this new bifunctional chelator will be realized through conjugation with complex oligosaccharides to take advantage of the high binding affinities of those molecules for certain organ or tumor-specific lectins but also by appending carbohydrate dendritic or nanosized architectures that benefit from the multivalent effect.

In the chapter 3, I described the development of a series of multivalent sensors that self-assemble *via* hydrophobic supramolecular interactions The multivalent complexes self-assemble and display carbohydrates with unique spatial orientation. Binding interactions between the carbohydrate epitopes and lectins were investigated by SPR and, by taking advantage of the fluorescent properties of Ru(II), distinct interactions between the mannosylated complex bearing 42 sugar units and *E. coli* strain ORN178 were observed using confocal microscopy. The simplicity of this screen highlights the potential of using these complexes as adaptable and user-friendly bacterial sensing tools. Application of the multivalent probes to explore other carbohydrate–lectin interactions will be facilitated by the flexible architecture of this system: the mannosylated cyclodextrins are interchangeable with any glycosylated cyclodextrins. Simple interchange of the carbohydrate epitopes will also greatly streamline generating collections of multivalent probes.

The design and synthesis of multivalent structures should involve a rationale whereby the multivalent framework identity as well as the template support should be taken into account with respect to the potential application. Chapter 4 reported the design and synthesis of polyhydroxylated fullerenes and dodecavalent fullerene-based glycoclusters. Both constructs were used as radical scavengers and anti-inflammatory agents in the treatment of ischemic stroke in rats subjected to transient middle cerebral artery occlusion. C_{60} fullerenes exhibit properties that make them promising candidates for biomedical applications and controlled drug delivery applications. When appropriately modified, fullerenes can migrate through the blood brain barrier and be applied for biomedical purposes. To potentiate a possible anti-inflammatory effect of fullerene, glucosamine was covalently attached to the C_{60} core. “Click chemistry” was used as key step to append the glucosamine units on the multivalent central scaffold. Efforts to translate these findings to humans will commence following further preclinical evaluations.

In addition to nanoparticle- and microarray-based structures that are already extensively studied for detecting carbohydrate–lectin interactions, our group has been particularly interested in the development and design of new platforms for measuring these inherently weak interactions. The chapter 5 presented the work that has been done in the development of localized surface plasmon resonance transducers based on Au island films for monitoring the specific interaction between Con A and mannose immobilized on Au islands. Sensing assays were performed under stationary and flow conditions, the latter providing kinetic parameters for protein binding and dissociation. Enhanced response and visual detection of protein binding was demonstrated using Au nanoparticles stabilized with mannose molecules. Biosensing applications of this system using sugars relevant to pathogenic viruses, parasites or bacteria are underway. An automated method for the synthesis of more complex carbohydrates has opened new possibilities in this research direction.

The glycome is vaster than either the genome or proteome and understanding the interactions of carbohydrates that coat the surfaces of most living organisms is critical to understanding disease states and developing novel therapies that can intervene at the interface between carbohydrates and other biomolecules. Known lectins are being exploited as reporters on interactions between carbohydrates and other carbohydrate-binding molecules and novel glycosylated surfaces and particles are being developed to elucidate new interactions that will pertain to important biomedical conditions to enhance our understanding of biochemical signaling and recognition. Nanoscale materials are needed to continue to advance understanding at the interface of carbohydrates with other macromolecules and such tools will further our understanding of the critical role carbohydrates play in so many life processes.